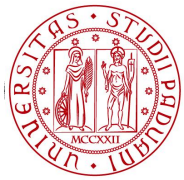

UNIVERSITÀ
DEGLI STUDI
DI PADOVA

Università degli Studi di Padova

Dipartimento di Biologia

SCUOLA DI DOTTORATO DI RICERCA IN BIOSCIENZE E BIOTECNOLOGIE

INDIRIZZO BIOTECNOLOGIE

CICLO XXVII

Human Pluripotent Stem Cell-based Microtechnologies for *in Vitro* Modeling of Cardiac Diseases

Direttore della Scuola: Ch.mo Prof. Giuseppe Zanotti

Coordinatore d'indirizzo: Ch.ma Prof.ssa Fiorella Lo Schiavo

Supervisore: Ch.mo Prof. Nicola Elvassore

Dottorando: Sebastian Martewicz

Table of contents

Appendix C
Cell Culture Analyses Protocols

Sommario

Le cellule pluripotenti umane stanno velocemente emergendo come strumenti fondamentali nella ricerca *in vitro.* In particolare, l'avvento delle cellule pluripotenti indotte ha aperto nuovi orizzonti sullo studio e la modellazione delle malattie umane e lo *screening* di approcci terapeutici. La possibilità di avere in coltura cellule di origine umana provenienti da tessuti da cui è difficile ottenere campioni bioptici, ha permesso di delineare nuove prospettive di studi *in vitro* per tessuti come il cervello, il pancreas o il cuore. Specialmente in quest'ultimo caso, il bisogno di nuovi modelli di studio è esaltato dall'impatto che le malattie cardiache hanno sulla sanità e sull'economia mondiali, a cui i modelli di studio tradizionali non riescono a far fronte in modo efficace.

L'oggetto di studio di questa tesi di dottorato sono i cardiomiociti umani derivati per differenziamento da cellule staminali pluripotenti e la loro applicazione come modello di studio del tessuto cardiaco. In particolar modo, ci si è focalizzati sul loro fenotipo, ritenuto precoce ed immaturo rispetto al cardiomiocita adulto, che limita enormemente il loro impiego in campo medico e scientifico, impedendo il pieno sviluppo del loro potenziale.

Dopo aver introdotto i modelli sperimentali attualmente impiegati nello studio di patologie cardiache, verranno descritte le principali caratteristiche delle cellule pluripotenti umane (hPSC) e dei loro derivati cardiaci (hPSC-CM). Successivamente, l'attenzione verrà focalizzata su due caratteristiche fondamentali che descrivono la fisiologia di un cardiomiocita: l'organizzazione strutturale della cellula legata alla sua funzionalità ed il suo profilo metabolico. In entrambe queste categorie, i hPSC-CM vengono spesso paragonati a cellule

cardiache fetali, lontane in termini di sviluppo dal fenotipo del cardiomiocita adulto.

L'organizzazione ultrastrutturale di una cellula cardiaca è strettamente correlata con la sua capacità funzionale: nei cardiomiociti adulti si assiste ad una perfetta concertazione spazio-temporale di diverse componenti molecolari la cui azione coordinata permette alle cellule del cuore di svolgere l'attività contrattile. Nel Capitolo 2 di questa tesi, vengono impiegati biomateriali e substrati micro-ingegnerizzati per studiare i meccanismi molecolari che promuovono la maturazione strutturale e funzionale dei cardiomiociti umani *in vitro*, rendendoli così più vicini fenotipicamente ad una cellula adulta su cui svolgere studi farmacologici e di modellazione di patologie.

Il metabolismo cardiaco è una caratteristica altrettanto unica e caratterizzante per un cardiomiocita, essendosi adattato ad sostenere un'attività costante ed energicamente dispendiosa com'è la generazione di forza meccanica. Nel Capitolo 3 viene descritto il metabolismo di un cardiomiocita e viene proposta una nuova piattaforma microfluidica da utilizzare per la validazione di protocolli di maturazione metabolica *in vitro*. Con il saggio funzionale messo a punto viene inoltre dimostrato come l'induzione di un metabolismo maturo è possibile attraverso la variazione dei substrati energetici presenti nel mezzo di coltura.

Infine, in prospettiva dell'applicazione dei protocolli di maturazione descritti nei capitoli precedenti a colture cardiache umane, nel Capitolo 4 viene presentato l'allestimento di due modelli cellulari di patologie genetiche: la distrofia muscolare di Duchenne e la cardiomiopatia aritmogena del ventricolo destro. Vengono presentati e caratterizzati cardiomiociti umani derivati per differenziamento da cellule hiPS di pazienti affetti, mostrando come i cardiomiociti in coltura presentino il fenotipo molecolare aberrante caratterizzante le malattie prese in esame. Si fornisce, così, un modello cellulare cardiaco umano che può trovare impiego nella modellazione *in vitro* delle due patologie.

Summary

Human pluripotent stem cells are quickly emerging as a fundamental tool for *in vitro* studies. In particular, the advent of "induced pluripotency" opened completely new horizons for *in vitro* disease modeling and patient-specific disease-on-a-dish therapeutic approach screening. The easy access to cell types of human origin hardly available otherwise, with virtually infinite amounts in a donor-unrestricted manner, unlocked *in vitro* studies for human tissues such as brain, pancreas and the heart. In the latter case, the need for new models of human cardiac physiology and physiopathology is highlighted by the severe fallouts of heart conditions on worldwide health and economy.

The main focus of this thesis are human cardiomyocytes derived through differentiation of pluripotent stem cells, and their application as an *in vitro* model of the human cardiac tissue. In particular, the stress point of the work is their early and immature phenotype, that often limits their application and frustrates the potential of a human heart model in a Petri dish.

After introducing the current scenario of study models for heart diseases and describing the main features of human pluripotent stem cells (hPSCs) and their cardiac derivatives (hPSC-CMs), this thesis will separately focus on the two main aspects of the cardiomyocyte physiology: structural and functional features and metabolic profile. From these perspectives, human cardiomyocytes derived from hPSCs display *in vitro* an early and immature phenotype, closely resembling cardiomyocytes at early stage of the development, such as fetal cardiomyocytes.

Cell ultrastructural organization and functional performance are two strictly related features that find in adult cardiomyocytes perfect synthesis, with a very

specialized function performed through a finely orchestrated sequence of events hugely relying on the right spatial distribution of key molecular components. In Chapter 2, biomaterials and microengineered substrates are employed to address the molecular mechanisms triggering cardiac maturation *in vitro*, in order to provide insight in the process and drive hPSC-CMs towards more adult-like phenotypes, better suiting disease modeling and drug screening.

Cardiac metabolism is likewise a characterizing feature of the tissue supporting in a unique fashion the impressive workload of the heart. In Chapter 3, hPSC-CM metabolism is described and a novel microfluidic technology is developed for metabolic maturation screening of cardiac cultures. With this approach, hPSC-CMs are shown to positively respond to an optimized metabolic maturation protocol, similar to the very rapid fetal-to-adult metabolism switch in hCMs after birth in response to changing metabolite availability.

Finally, in perspective of the maturation approaches previously described and their feasible application to human cardiac cultures, in Chapter 4 are discussed two human genetic diseases affecting the heart muscle. For both Duchenne's muscular dystrophy and arrhythmogenic right ventricular cardiomyopathy/ dysplasia, cardiac cellular models are set up and proven to display *in vitro* the molecular hallmarks of the disease, thus providing the biological substrate for further studies on human cardiomyocyte cultures.

Foreword

The work presented in this thesis was performed at the Department of Industrial Engineering of the University of Padua and at the Venetia Institute of Molecular Medicine (VIMM) in Padua, under the supervision of Prof. Nicola Elvassore. Part of the 3-year period of the Ph.D was spent acquiring ARVD-hiPS culture skills and metabolic maturation protocols at the Sanford-Burnham Medical Research Institute in La Jolla, California, under the supervision of Prof. H-S. Vincent Chen.

During my time as Ph.D student, I worked in a multidisciplinary environment, enjoying the challenges of biology/engineering cross-talk and expanding my skill set beyond the traditional biotechnological education. For this opportunity I would like to thank my supervisor Nicola Elvassore, whose patience I often challenged with pernickety biological arguments receiving enlightening and humbling comebacks.

Mandatory thanks are due to the people who supported me scientifically and personally in this work, which include all the present and past BioERA group members, with special mentions for Elena Serena, Susi Zatti, Federica Michielin, Giovanni G. Giobbe, Alessandro Zambon, Lia Prevedello, Stefano Giulitti and Alice Zoso.

I am also grateful for the financial support given me by Città della Speranza, Progetti di Eccellenza CaRiPaRo and the Italian Health Ministry.

All the material reported in this dissertation is original unless explicit references to studies carried out by other people are indicated.

During this 3 years of Ph.D studies the following publications have been produced:

- Susi Zatti, Sebastian Martewicz, Elena Serena, Narumi Uno, Giovanni Giobbe, Yasuhiro Kazuki, Mitsuo Oshimura, Nicola Elvassore. **Complete restoration of multiple dystrophin isoforms in genetically corrected Duchenne Muscular Dystrophy patient-derived cardiomyocytes** *Molecular Therapy – Methods and Clinical Development*, 1, 1, 2014. doi:10.1038/mtm.2013.1
- Sebastian Martewicz, Federica Michielin, Elena Serena, Alessandro Zambon, Marco Mongillo, Nicola **Elvassore Reversible alteration of calcium dynamics in cardiomyocytes during acute hypoxia transient in a microfluidic platform** *Integr Biol (Camb).* 2012 Feb;4(2):153-64

The following manuscripts are submitted or under submission:

- Sebastian Martewicz, Elena Serena, Susi Zatti, Gordon Keller, Nicola Elvassore. **Human cardiomyocytes derived from pluripotent stem cells require activation of mechanotransduction pathways by cell-substrate interaction for functional maturation** *Stem Cell Reports*, 2015, in submission
- Giovanni G. Giobbe, Federica Michielin, Sebastian Martewicz, Stefano Giulitti, Camilla Luni, Sirio Dupont, Annarosa Floreani, Nicola Elvassore **Integrated multi-stage tissue on a chip generation from human pluripotent stem cells** *Nature Methods*, 2015 in final revision

The following manuscripts are in preparation:

- Sebastian Martewicz, Marika Campesan, Giulia Gabrel, Marcella Canton, Fabio Di Lisa, Nicola Elvassore **Metabolic maturation is required in human cardiomyocytes derived from pluripotent stem cells for ischemia-reperfusion modeling in microfluidic chip**, in preparation

Parts of this thesis were presented at national and international conferences including:

- ISSCR's 12° Annual Meeting, June 18-21, 2014, Vancouver, Canada
- ISSCR's 11° Annual Meeting, June 12-15, 2013, Boston, MA, USA
- EMBO|EMBL Symposium, Cardiac Biology: From Development to Regenerative Medicine. June 7-10, 2013, Heidelberg, Germany
- Frontiers in Cardiac and Vascular Regeneration. May 30th – June 2nd, 2012, Trieste, Italy

Chapter 1

Human Pluripotent Stem Cells and Cardiac Disease Modeling

This chapter introduces the state of the art in the development of models for studying cardiac diseases. It also discusses the new perspectives introduced in the field with the derivation of human cardiac cells by differentiation of human pluripotent stem cells. An overview of the differentiation of human pluripotent stem cells into cardiomyocytes is presented, highlighting the current limitations of the hPS-derived cells for *in vitro* studies and disease modeling. Finally, the aim of this thesis is presented.

1.1 Study models for heart disease

The development of reliable and effective models for studying cardiac diseases is one of the most urgent needs in basic and translational research. The toll of pathological conditions associated with the heart muscle is extremely high from both human lives and economic expense perspectives. Cardiac ischemia alone is still at the top of the list among the death causes worldwide (Go *et al.,* 2014) and congenital cardiomyopathies affect a relevant portion of the population (Bruneau, 2008; Go *et al.,*2014) (Fig. 1.1A). The economic burden for the treatment of these conditions, both immediate and chronic, and the associated loss of productivity are counted by the billions in any currency taken into account (Go *et al.,* 2014) and they are at the top of the list when confronted with other diagnostic groups (NIH Fact Book, 2012; Go *et al.,*2014) (Fig. 1.1B). Moreover, the

expense for drug research has always been high and cardiac pre-clinical study models closely resembling the human physiology could help in reducing the costs of compound screenings and the losses due to failed trials or market withdrawals, being the drug-induced cardiotoxicity the leading cause for the latter (Gwathmey *et al.,* 2009) (Fig. 1.1C).

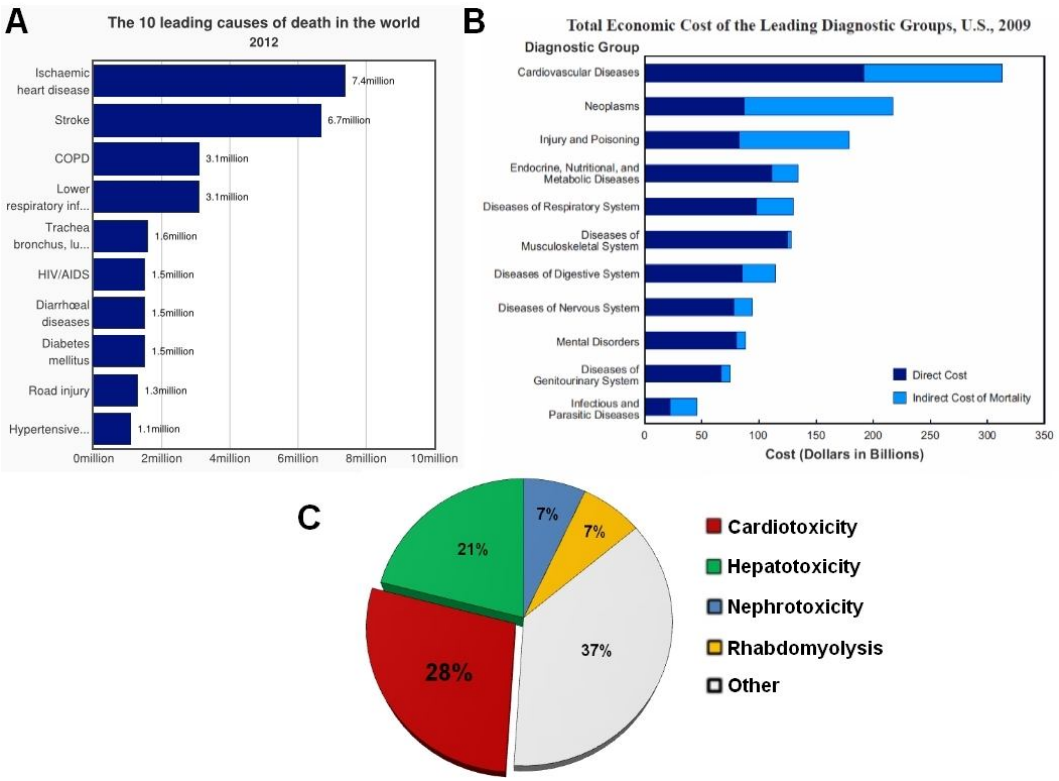

Fig. 1.1 Statistical data describing the impact of heart diseases on worldwide health and economy. (A) Worldwide mortality by diagnostic group (WHO, 2012). **(B)** Economic cost by diagnostic group (NIH Fact Book, 2012). **(C)** Causes of drug market withdrawal by organ-specific toxicity (adapted from Wilke *et al.,* 2007).

Animal models are the best tool for advancing the understanding of the mechanisms of human pathologies, but differences such as heart architecture, heart rate, protein expression and even resident stem cell populations can deeply impact the experimental outcome of therapeutic approaches (Zaragoza *et al.,* 2011). Small animals such as mice, rats, guinea pigs and rabbits are commonly employed because of the relatively low economic costs of housing and handling in respect to the high numbers of specimen. However, the intrinsic differences in anatomical structure and physiology, often produce in results untranslatable to other species (Terrar *et al.,* 2007) and are not cost effective, especially in pharmacological studies, in which they often fail to predict

cardiotoxicity (Mandenius *et al.,* 2011). In the past years bigger animals such as dogs, pigs and primates started being employed, in order to guarantee a closer resemblance to the human anatomical and physiological background (Netzer *et al.,* 2001; De Ponti *et al*., 2002; Zaragoza *et al.,* 2011). As the size (and resemblance to humans) of the animal model increases, the costs of specialized equipment, facilities and personnel grow accordingly to proportions in which their availability is limited to big companies or very well funded research groups (Zaragoza *et al.,* 2011). Nevertheless, these *in vivo* studies are still a mandatory and unavoidable step in the drug development pipeline, regardless many spectacular examples of misleading results sentencing the following phases on human patients to fail (Wilke *et al.,* 2007). As a specific example, studies on K_{ATP} channels involved in arrhythmogenic activity in the ischemic heart displayed extreme variability in drug function and sensitivity across rodents, rabbits and dogs, the latter two displaying more similarities to the human samples (Fedorov *et al.,* 2011).

Reliable *in vitro* models can cut down the number of approaches flowing into this expensive pre-clinical step, by providing the opportunity for cost-effective high-throughput screening campaigns (Carlson *et al.,* 2013). Current *in vitro* models, however, are either over-simplistic or affected by similar species-related downfalls as their *in vivo* counterparts. The simplest *in vitro* cell culture model is represented by heterologous or human cell lines over-expressing specific cardiac ion channels, most notably the potassium hERG channel (De Ponti *et al*., 2002). This is a perfect approach for studies on single-target drug studies, but only recorded signals of the complex multichannel phenotype of cardiac ion channels in their native environment can ensure reliable data on the compound effect and safety (Meyer *et al.,* 2004; Dick *et al.,* 2010). The most notable and widely reported example (De Ponti *et al*., 2002) of such difference is verapamil, which strongly blocks hERG K^+ channel (thus, failing the "cell line assay") but has not adverse effect at all in assays employing primary animal cardiomyocyte cultures, and it is considered a "safe" drug (Meyer *et al.,* 2004; Dick *et al.,* 2010). Although offering an already fully assembled "cardiomyocyte system", primary animal

cardiac cultures are still labor intensive, lack consistency and insufficient for large high-throughput approaches (Carlson *et al.,* 2013).

The only human *in vitro* model available today that surpasses the simplicity of cell cultures is represented by *ex vivo* experiments on isolated intact organs. Human explanted hearts could arguably be the "gold standard" for pre-clinical cardiac drug safety screenings, and represents to date a unique tool to explore direct and clinical effects of chemical compounds. The two main limitations to this approach comprise the extremely limited number of biological substrate available and the intrinsic shortcomings of an *ex vivo* procedure on a denervated and not physiologically normal, perfused organ which cannot be considered a healthy human heart, even from non-failing infarct-free donors (Fedorov *et al.,* 2011).

In this scenario, the constantly developing field of human pluripotent stem cell cultures will have a great impact in creating new approaches in compound screening and design of drug-safety assays. In particular for the cardiac research, since the first report of the derivation of cardiomyocytes from human embryonic stem cells in 2001 (Kehat *et al.,* 2001), great hopes are placed on this cells to fill the long-standing void in available preclinical models as surrogate for human myocardium (Turnbull *et al.,* 2014).

1.2 Human embryonic and induced pluripotent stem cells

Stem cells are defined by their ability to proliferate maintaining their original features in the daughter cells in a mechanism called self-renewal, which for most stem cells can go on indefinitely while the proper environmental conditions are preserved. The second defining characteristic of a stem cell is the ability to differentiate into other cell types when triggered by the right stimuli, and the number and type of these differentiation derivatives classifies stem cells in "potency" classes (Fig. 1.2).

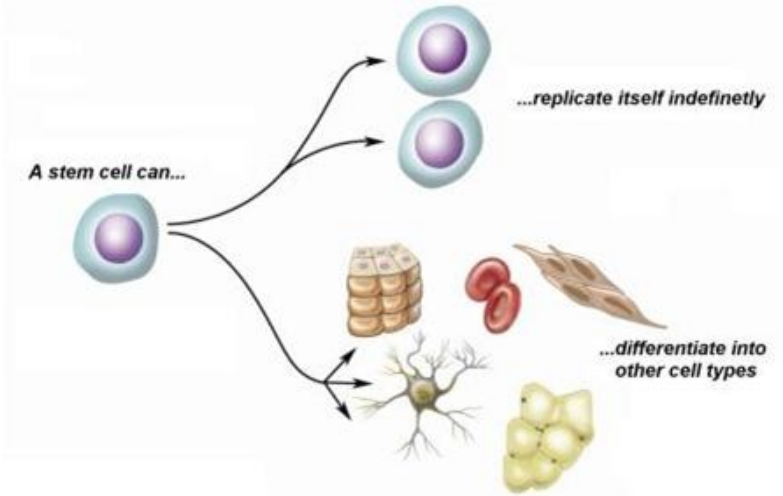

Fig. 1.2 Schematic representation of the defining features of stem cells (adapted from National Academies of Science Booklet, 2005)

Pluripotent stem cells (PSCs) can give rise to all the cells of an organism's body (exception made for the trophoblast) and are defined by the ability to generate all three embryonic germ layers. The pioneering works on mouse embryos in the early 1980s (Evans and Kaufman, 1981; Martin, 1981) paved the way to the derivation of the first pluripotent human embryonic stem cell (hES)-line in 1998 (Thomson *et al.,* 1998). hPSCs carry the promise of becoming an important source of models for a wide range of adult cell types (Pouton and Haynes, 2005), and since the first derivation huge improvements have been made in methods for their expansion and differentiation. From conditions entirely dependent on co-cultures with feeder cells and untargeted spontaneous differentiation now are available chemically-defined xeno-free culture protocols (ISCIC, 2010) producing large numbers of clinically relevant cells with constantly increasing subpopulation-specificity of post-mitotic cells (examples being neuronal populations (Compagnucci *et al.,* 2014), hepatic and pancreatic cells (Cheng *et al.,* 2013) and cardiac subtypes (David and Franz, 2012)).

A great breakthrough in the field was achieved in 2007, when human induced pluripotent stem cells (hiPS) were first reported (Takahashi *et al.,* 2007), one year after their first generation from murine somatic cells (Takahashi and Yamanaka, 2006). Sharing most hESC features (for hPSC characterization see Table 1.1) hiPS technology is groundbreaking for two main reasons: i) it overcomes some ethical issues of using fertilized human embryos and ii) it allows the generation of patient-specific cell lines, with the associated huge outcomes for autologous

therapeutic approaches and specific disease modeling (Passier *et al.,* 2008; Bellin *et al.,* 2012). Currently, the original reprogramming factors Oct4, Sox2, Klf4, c-Myc (Takahashi *et al.,* 2007), Lin28 and Nanog (Yu *et al.,* 2007) are employed in different combinations, delivered by xeno-free non-integrating vectors such as episomes (Okita *et al.,* 2008) and modified mRNA molecules (Warren *et al.,* 2010), that surpassed the original viral and genome integrating retro- and lenti-viral protocols in both efficiency and manipulation safety.

Table 1.1 List of assays and readouts describing the features describing hPSCs.

Feature	Description
Morphological assessment	Translucent colonies, densely packed with smooth and defined borders, round cell-shape with high nucleus/cytoplasm ratio, prominent nucleoli
Nuclear markers	OCT4, SOX2, NANOG, REX1
Surface markers	TRA1-60, TRA1-81, SSEA-3, SSEA-4
Enzymatic activity	Alkaline phosphatase, telomerase
Differentiation *in vitro*	Spontaneous (embryoid bodies) or directed differentiation with detection of protein markers from all three germ-layers
Differentiation *in vivo*	Teratoma formation with structures from all three germ-layers
Karyotype	Normal

The applications of hPSC, and in particular hiPSCs, are vastly dependent on our ability to drive and control their differentiation. Being the source material of virtually unlimited numbers of cells with the same characteristics, their derivatives can be employed in both cell-based therapeutic approaches (with an autologous transplantation strategy for hiPSCs) and for *in vitro* studies of drug screening and disease modeling (Fig. 1.3) (Bellin *et al.,* 2012).

Although very compelling, the application of hPSCs in clinic for most diseases is still years ahead (for a summary of ongoing hPSC trials, see Table 1.2) and the more immediate and straightforward field of application for these cells are *in vitro* studies. With restricted availability of tissues such as cardiac, hepatic or neuronal ones, patient-specific hiPSC-derivatives for those tissues are an

incredible source for studying pathological phenotypes in cell models of human origin (Benam *et al.,* 2015).

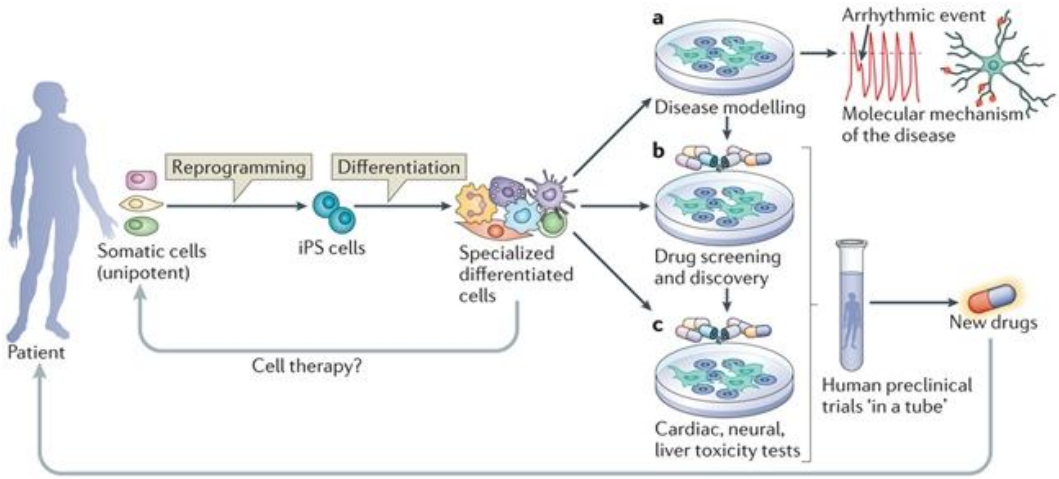

Fig. 1.3 Schematic representation of the hiPSC applications (adapted from Bellin *et al.,* 2012).

Moreover, the employment of these differentiated cells in pharmaceutical industry can provide an invaluable human platform in drug discovery and screening. In the right conditions, hPSC-derivatives could easily replace immortalized cell lines and animal primary cultures in preclinical studies and offer a "cheaper" alternative to *ex vivo* human tissue testing, being unrestrained by donor heart availability (Pouton and Haynes, 2005).

Table 1.2 Summary of clinical trials employing human pluripotent stem cell-derivatives

Disease treated	Accession # ClinicalTrials.gov	Cell type	Year	Notes	Reference
Spinal cord injury	---	hES	2010	Withdrawn in 2011	Ratcliffe *et al.,* 2013
Dry age-related macular degeneration	NCT01344993	hES	2011	First reports published 2014	Schwartz *et al.,* 2014
Stargardt's macular dystrophy	NCT01345006	hES	2011	First reports published 2014	Schwartz *et al.,* 2014
Type 1 Diabetes	NCT02239354	hES	2014	Began late 2014	Viacyte website, 2014
Wet age-related macular degeneration	Japanese Health Ministry, unknown	hiPS	2014	First hiPS trial, began late 2014	Cyranoski, 2014

For both clinical and *in vitro* applications of the human pluripotent stem cells, the main limiting step is our ability to tightly control their differentiation towards the desired cell type, this including both cell type specification and maturation degree. Of particular interest is the cardiac derivatives, as human heart samples are relatively rare and difficult to handle.

1.3 Human cardiomyocytes derived from hPSCs

Differentiation towards the cardiac lineage of pluripotent stem cells was first reported in 2001, when hESC cultured in suspension formed organoids called embryoid bodies (EBs) and displayed spontaneous contractions after 2 weeks in culture (Kehat *et al.,* 2001). Since then, the studies on murine embryonic development (Murry and Keller, 2008) propelled the optimization of *in vitro* differentiation conditions and resulting in three classical directed differentiation protocols:

- evidence of paracrine signaling of the endoderm germ-layer priming the mesodermal specification inspired the first cardiac differentiation protocol that improved the ~1% efficiency of the spontaneous differentiation to a ~12%-25% by co-culturing hPSC with the END-2 endodermal cell line (Mummery *et al.,* 2003; Graichen *et al.,* 2007);
- implementation of Activin/Nodal and BMP signaling in the *in vitro* differentiation process in monolayer cultures produced ~30% efficient protocols (Laflamme *et al.,* 2007);
- final optimization of the EB-based protocol to a >50% efficiency was achieved by integrating a chronologically defined cytokine stimulation regulating the Action/Nodal, BMP, Wnt, VEGF and FGF pathways (Yang *et al.,* 2008; Kattman *et al.,* 2011).

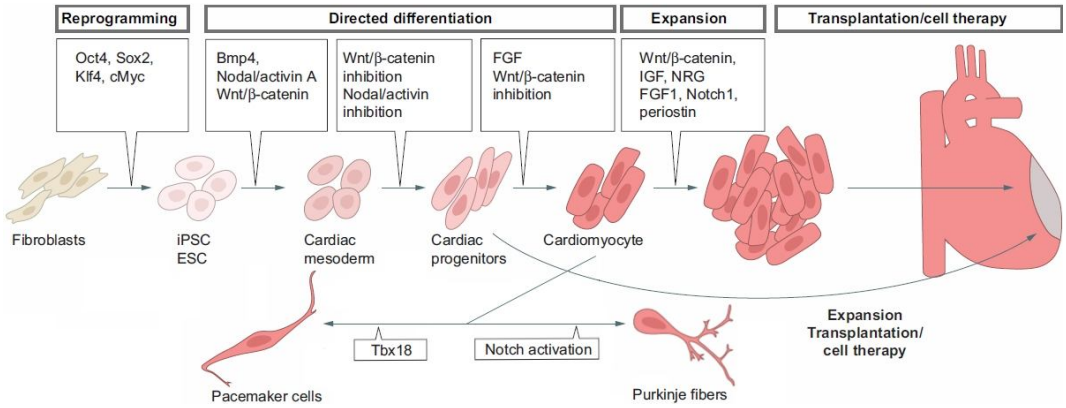

Fig. 1.4 Cardiac differentiation protocols recapitulate embryonic cardiac development by addition of growth factors and small molecules in a time- and dose-dependent manner (adapted from Später *et al.,* 2014).

Cardiomyocyte-enrichment steps following the cardiac differentiation protocols (Fig 1.4) are often required when the selection of pure cardiomyocyte cultures is necessary (>98% cardiac troponin T positive cells, $cTnT^{+}$). The most notable selection strategies, not involving genomic integration of selection markers such as $Puro^{r}$ or GFP^{+} under cardiac-specific promoters (Anderson *et al.,* 2007), include:

- surface-antigen sorting for SIRPα (Dubois *et al.,* 2011) and/or VCAM (Elliott *et al.,* 2011; Uosaki *et al.,* 2011);
- metabolic selection through glucose-to-lactate substitution in the culture medium (Tohyama *et al.,* 2013);
- sorting for cells with high mitochondrial content with fluorescent mitochondria-specific dyes (Hattori *et al.,* 2010).

More recently, new chemically defined and highly efficient cardiac differentiation protocol were published, based on the biphasic role of the Wnt signaling in murine embryonic cardiogenesis (Naito *et al.,* 2006; Ueno *et al.,* 2007). These protocols employ small-molecules to tune the Wnt signaling pathway, greatly reducing cell line- and passage number-dependent variability (Jiang *et al.,* 2012) and achieving differentiation efficiencies >90% (Lian *et al.,* 2012). A recent improvement to this protocol reduced drastically the number of components in the differentiation media employed, reporting the first

completely xeno-free and chemically defined differentiation protocol (Burridge *et al.,* 2014).

Finally, it is a matter of particular interest the opportunity to drive the cardiac differentiation selectively towards a restricted subtype of cardiomyocyte. Although some studies report subtype classification based on expression of molecular markers (such as MLC2a, MLC2v or HCN4), the main criterion of classification is the action potential phenotype, even if this method's reliability has been recently challenged (Du *et al.,* 2015). The differentiation protocols currently employed generate mainly atrial and ventricular myocytes, which proportions can be greatly altered by retinoic acid signaling tuning (Zhang *et al.,* 2011). Nodal and conduction system cells are present in various proportions (Blazeski *et al.,* 2012), with the first ones enriched upon NRG-1β/ErbB signaling pathway inhibition (Zhu *et al.,* 2010), while Notch signaling is involved in the generation of Purkinje-like cells (Rentschler *et al.,* 2012). Moreover, overexpression of specific proteins can promote subtype-specific phenotypes, as observed for sinoatrial-like cells by the force expression of Tbx18 and Tbx3 (Bakker *et al.,* 2012; Kapoor *et al.,* 2013). A better understanding of the *in vitro* sub-specification processes will provide explanation to experimental evidences such as nodal-like inhibition by culture substrate modification (Melkoumian *et al.,* 2010) or the ventricular-like phenotype enrichment as function of extended time in culture (Fu *et al.,* 2009; Lian *et al.,* 2012).

This exciting field of stem cell research evolves very rapidly integrating promptly findings from basic development science in the differentiation protocols employed. The derivatives of these protocols will provide in the near future a precious source for both clinical and *in vitro* applications, but before the full potential of the hPSC-CMs can be unlocked there are critical points that need to be faced.

1.4 Challenges and limitations of human pluripotent stem cell-derived cardiomyocytes

From a clinical perspective, the major concerns regarding human pluripotent stem cell-derived cardiomyocytes (hPSC-CMs) are summarized by three possible pathological outcomes of a cell therapy: teratoma formation, arrhythmogenesis and rejection (Prowse *et al.,* 2014). As the latter is a common concern in any transplantation/implantation medical procedure and it has a good chance of being surpassed by autologous transplantation of hCM derived from hiPS cells, the first two have to be addressed at the early stages of hCM production as rely on culture purity. Remaining undifferentiated $Oct4^+$ cells can generate teratomas or ectopic tissues resulting in dysfunction (Blin *et al.,* 2010), while hCM-subclass electrophysiological heterogeneity can generate pro-arrhythmic substrates in the reformed tissue (Chen *et al.,* 2009). Although purification might in the end become unnecessary with optimization of the cardiac differentiation and specification protocols, the enrichment approaches cited in **Paragraph 1.3** are difficult to scale-up to the cell numbers needed for human therapeutic applications (an estimated 10^9 hCM *per* treatment (Mummery *et al.,* 2012)) in a cost effective manner (Prowse *et al.,* 2014).

A relevant concern raised since the first derivation of hPSC-CMs in regard of their functional outputs is the early and immature phenotype displayed (Snir *et al.,* 2003). Although it could not be problematic for clinical purposes, as cardiomyocytes at earlier developmental stages display greater proliferative potential and are more malleable and adaptable (Reinecke *et al.,*1999), it is a highly desirable feature for *in vitro* studies. The best fitting comparison for hPSC-CMs are human fetal cardiomyocytes (Mummery *et al.,* 2003), with whom they share most of their phenotypic characteristics, thus defining them as similar to the early stages of cardiac development and "immature" in respect to adult cardiomyocytes. The most striking difference from the large rod-shaped adult cardiomyocytes (aCMs) is their multi-angular irregular morphology with mono-nuclear appearance typical of a proliferating and mitotically active cell (Cui *et al.,*

2007). Gene expression profiles are closely resembling those of fetal cardiac tissues more than the adult ones, nevertheless clearly indicating a full-on cardiac expression pattern (Cao *et al.,* 2008; Xu *et al.,* 2009). From the functional point of view, the gap between the hPSC-CM and the aCM phenotypes has been characterized with a plethora of different assays in terms of electrophysiology, calcium handling and force generation, with specific numerical values often very different from one another (Robertson *et al.,* 2013). All these differences (Table 1.3) are best condensed in the two main features cited above: morphology, which deeply reflects the internal ultrastructural organization of the cardiomyocyte, and gene expression patterns, determining the presence of the right components of the cardiac molecular machineries.

Table 1.3 Main reported differences between immature hPSC-CMs and adult hCM.

Cardiac feature	hPSC-CM	Adult hCM	Reference
Morphology	Multi-angular, occasionally oblong	Large, rod-shaped	Snir *et al.,* 2003
Number of nuclei	Mono-nuclear	Bi-nuclear, multi-nuclear	Kehat *et al.,* 2001
Proliferation	Some to low	None	McDevitt *et al.,* 2005
Chronotropic and inotropic response	Chronotropic	Both	Brito-Martins *et al.,* 2008
Contraction	Spontaneous	Only induced	Kehat *et al.,* 2001
Action potential features	Low diastolic potential (-30 mV to -75 mV) Slow depolarization rate (2 V/sec to 40 V/sec)	Diastolic potential (-85 mV) Depolarization rate (300 V/sec)	Kim *et al.,* 2010 Ma *et al.,* 2011
Ca^{2+} handling machinery	Absent to low: CSQ2, TRDN, Junctin, PLN Abnormal levels: others	All present at correct expression levels	Satin *et al.,* 2008 Itzhaki *et al.,* 2011
Force/frequency relationship	Negative	Positive	Dolnikov *et al.,* 2006
Metabolism	Glycolytic	Oxidative	Rana *et al.,* 2012

The three main functional features of a cardiac cells (action potential propagation, calcium-induced calcium release and contraction) require a finely orchestrated sequence of events, which in the aCMs is secured by tight structural organization and the correct genetic program. The functional performance of hPSC-CMs, missing either key molecular components or their right spatial distribution, results in unclear and conflicting experimental observations, and determines their immaturity.

With the differentiation protocols constantly improving the purity and the yields of human cardiomyocytes from hPS cells, the final challenge for the field is the maturation of the cardiomyocytes *in vitro.* Especially, understanding the triggering mechanisms of cardiac development is important in order to integrate the appropriate stimuli to cardiomyocyte cultures and promote their maturation, thus, providing the best *in vitro* model for human cardiac physiology available.

1.5 Aim of the thesis

This thesis aims at the *in vitro* maturation of human cardiomyocytes derived from pluripotent stem cells. We addressed the cardiac maturation from two perspectives: the structural and functional phenotype and the cardiomyocyte and its metabolic performance. The employment of microengineered surfaces for mechanical and topological control of the culture substrate provided insight in the molecular signaling involved in cardiac structural development and the associated improved functional performance. Moreover, the topological confinement of human cardiac cultures allowed to recreate *in vitro* multicellular complexes increasingly resembling the cellular organization *in vivo*. From the metabolic perspective, we show how development of novel technologies provides tool for hCM screening and testing during the optimization of culture methods aimed at modeling an adult-like metabolism *in vitro*.

Overall, the process of *in vitro* cardiac development is poorly understood and most of the maturation reported in literature (introduced in **Paragraph 2.1** and **Paragraph 3.1**) is based on experimental observations, without proposed mechanisms. Insight in the mechanisms driving cardiac maturation *in vitro* will provide a better understanding of the process and the development of enhanced culture methods aimed at the generation of adult-like hCMs.

In **Chapter 2** is presented the work on the influence of culture substrate on human cardiomyocytes, with particular focus on the structural maturation and functional performance improvement of the cardiac cell, providing insight in the physical cues necessary for the process and the important components of the cell signaling network.

In **Chapter 3** the focus is put on the metabolic maturation of the cardiomyocytes, with special regard to cell sensitivity to oxygen concentrations. We present a novel approach to control oxygen concentrations inside cell culture describing the design and validation of a new microfluidic device. This device serves as an assay for testing cardiomyocyte metabolic phenotype and performance in hypoxia/reperfusion conditions after the application of a metabolite-driven metabolic switch in human cardiomyocyte cell cultures.

Finally, in **Chapter 4** are presented two cardiac disease models set up by differentiation of patient-specific hiPS cells in cardiomyocytes. The cell models described in this chapter can be easily subjected to the maturation protocols defined in Chapters 2 and 3, thus providing the biological substrate for disease modeling *in vitro*.

1.6 References

Anderson D, Self T, Mellor IR, Goh G, Hill SJ, Denning C **(2007)** Transgenic enrichment of cardiomyocytes from human embryonic stem cells. *Mol Ther* 15, 2027–2036

Bakker ML, Boink GJJ, Boukens BJ, Verker AO, van den Boogaard M, den Haan AD, Hoogaars WMH, Buermans HP, de Bakker JMT, Seppen J, *et al.* **(2012)** T-box transcription factor TBX3 reprogrammes mature cardiac myocytes into pacemaker-like cells. *Cardiovasc. Res.* 94, 439-449

Bellin M, Marchetto MC, Gage FH, Mummery CL. **(2012)** Induced pluripotent stem cells: the new patient? *Nat Rev Mol Cell Biol.* Nov;13(11):713-26.

Benam KH, Dauth S, Hassell B, Herland A, Jain A, Jang KJ, Karalis K, Kim HJ, MacQueen L, Mahmoodian R, *et al.* **(2015)** Engineered in vitro disease models. *Annu Rev Pathol.* Jan 24;10:195-262

Blazeski A, R Zhu, Hunter DW, Weinberg SH, Boheler KR, Zambidis ET, L Tung. **(2012)** Electrophysiological and contractile function of cardiomyocytes derived from human embryonic stem cells. *Prog. Biophys. Mol. Biol.* 110:178–195

Blin G, Nury D, Stefanovic S, Neri T, Guillevic O, Brinon B, Bellamy V, Rücker-Martin C, Barbry P, Bel A, *et al.* **(2010)** A purified population of multipotent cardiovascular progenitors derived from primate pluripotent stem cells engrafts in postmyocardial infarcted nonhuman primates. *J Clin Invest* 120:1125-39

Brito-Martins M, Harding SE, Ali NN. **(2008)** beta(1)- and beta(2)-adrenoceptor responses in cardiomyocytes derived from human embryonic stem cells: Comparison with failing and nonfailing adult human heart. *Br J Pharmacol.* 153(4):751–759

Bruneau BG. **(2008)** The developmental genetics of congenital heart disease. *Nature*. Feb 21;451(7181):943-8

Burridge PW, Matsa E, Shukla P, Lin ZC, Churko JM, Ebert AD, Lan F, Diecke S, Huber B, Mordwinkin NM, *et al.* **(2014)** Chemically defined generation of human cardiomyocytes. *Nat Methods.* Aug;11(8):855-60

Cao F, Wagner RA, Wilson KD, Xie X, Fu JD, Drukker M, Lee A, Li RA, Gambhir SS,Weissman IL, et al. (2008) Transcriptional and functional profiling of human embryonic stem cell-derived cardiomyocytes. PLoS One 3:e3474

Carlson C, Koonce C, Aoyama N, Einhorn S, Fiene S, Thompson A, Swanson B, Anson B, Kattman S. **(2013)** Phenotypic screening with human iPS cell-derived cardiomyocytes: HTS-compatible assays for interrogating cardiac hypertrophy. *J Biomol Screen*. Dec;18(10):1203-11

Chen HS, Kim C, Mercola M. **(2009)** Electrophysiological challenges of cell-based myocardial repair. *Circulation* 120:2496-508

Cheng X, Tiyaboonchai A, Gadue P. **(2013)** Endodermal stem cell populations derived from pluripotent stem cells. *Curr Opin Cell Biol.* Apr;25(2):265-71

Compagnucci C, Nizzardo M, Corti S, Zanni G, Bertini E. **(2014)** In vitro neurogenesis: development and functional implications of iPSC technology. *Cell Mol Life Sci.* May;71(9):1623-39

Cui L, Johkura K, Takei S, Ogiwara N, Sasaki K. **(2007)** Structural differentiation, proliferation, and association of human embryonic stem cell-derived cardiomyocytes in vitro and in their extracardiac tissues. *J Struct Biol.* 158:307–317

Cyranoski D, **(2014)** Next-generation stem cells cleared for human trial. *Nature* Sep 10 doi:10.1038/nature.2014.15897

David R, Franz WM. **(2012)** From pluripotency to distinct cardiomyocyte subtypes. *Physiology (Bethesda).* Jun;27(3):119-29

De Ponti F, Poluzzi E, Cavalli A, Recanatini M, Montanaro N. **(2002)** Safety of non-antiarrhythmic drugs that prolong the QT interval or induce torsade de pointes: an overview. *Drug Saf.* 25(4):263-86.

Dick E, Rajamohan D, Ronksley J, Denning C. **(2010)** Evaluating the utility of cardiomyocytes from human pluripotent stem cells for drug screening. *Biochem Soc Trans.* Aug;38(4):1037-45

Dolnikov K, Shilkrut M, Zeevi-Levin N, Gerecht-Nir S, Amit M, Danon A, Itskovitz-Eldor J, Binah O. **(2006)** Functional properties of human embryonic stem cell-derived cardiomyocytes: intracellular Ca2+ handling and the role of sarcoplasmic reticulum in the contraction. *Stem Cells.* Feb;24(2):236-45

Du DT, Hellen N, Kane C, Terracciano CM. **(2015)** Action potential morphology of human induced pluripotent stem cell-derived cardiomyocytes does not predict cardiac chamber specificity and is dependent on cell density. *Biophys J.* Jan 6;108(1):1-4

Dubois NC, Craft AM, Sharma P, Elliott DA, Stanley EG, Elefanty AG, Gramolini A, Keller G. **(2011)** SIRPA is a specific cell-surface marker for isolating cardiomyocytes derived from human pluripotent stem cells. *Nat Biotechnol.* Oct 23;29(11):1011-8

Elliott DA, Braam SR, Koutsis K, Ng ES, Jenny R, Lagerqvist EL, Biben C, Hatzistavrou T, Hirst CE, Yu QC, *et al.,* **(2011)** NKX2-5(eGFP/w) hESCs for isolation of human cardiac progenitors and cardiomyocytes. *Nat Methods*. Oct 23;8(12):1037-40

Evans MJ, Kaufman MH. **(1981)** Establishment in culture of pluripotential cells from mouse embryos. *Nature.* Jul 9;292(5819):154-6.

Fedorov VV, Glukhov AV, Ambrosi CM, Kostecki G, Chang R, Janks D, Schuessler RB, Moazami N, Nichols CG, Efimov IR. **(2011)** Effects of KATP channel openers diazoxide and pinacidil in coronary-perfused atria and ventricles from failing and non-failing human hearts. *J Mol Cell Cardiol.* Aug;51(2):215-25.

Fu JD, Jiang P, Rushing S, Liu J, Chiamvimonvat N, Li RA. **(2010)** Na+/Ca2+ exchanger is a determinant of excitation-contraction coupling in human embryonic stem cell-derived ventricular cardiomyocytes. *Stem Cells Dev*. Jun;19(6):773-82

Go AS, Mozaffarian D, Roger VL, Benjamin EJ, Berry JD, Blaha MJ, Dai S, Ford ES, Fox CS, Franco S, *et al.,* **(2014)** Heart disease and stroke statistics--2014 update: a report from the American Heart Association. *Circulation*. Jan 21;129(3):399-410.

Graichen R1, Xu X, Braam SR, Balakrishnan T, Norfiza S, Sieh S, Soo SY, Tham SC, Mummery C, Colman A, Zweigerdt R, Davidson BP. **(2007)** Enhanced cardiomyogenesis of human embryonic stem cells by a small molecular inhibitor of p38 MAPK. *Differentiation*. Apr;76(4):357-70

Gwathmey JK, Tsaioun K, Hajjar RJ. **(2009)** Cardionomics: a new integrative approach for screening cardiotoxicity of drug candidates. *Expert Opin Drug Metab Toxicol*. Jun;5(6):647-60

Hattori F, Chen H, Yamashita H, Tohyama S, Satoh YS, Yuasa S, Li W, Yamakawa H, Tanaka T, Onitsuka T et al. (2010) Nongenetic method for purifying stem cell-derived cardiomyocytes. Nat Methods 7:61–66

ISCIC: International Stem Cell Initiative Consortium, *et al.* **(2010)** Comparison of defined culture systems for feeder cell free propagation of human embryonic stem cells. *In Vitro Cell Dev Biol Anim*. Apr;46(3-4):247-58

Itzhaki I, Rapoport S, Huber I, Mizrahi I, Zwi-Dantsis L, Arbel G, Schiller J, Gepstein L. **(2011)** Calcium handling in human induced pluripotent stem cell derived cardiomyocytes. *PLoS One.* Apr 1;6(4):e18037

Jiang J, Han P, Zhang Q, Zhao J, Ma Y. **(2012)** Cardiac differentiation of human pluripotent stem cells. *J Cell Mol Med.* Aug;16(8):1663-8

Kattman SJ, Witty AD, Gagliardi M, Dubois NC, Niapour M, Hotta A, Ellis J, Keller G. **(2011)** Stage-specific optimization of activin/nodal and BMP signaling promotes cardiac differentiation of mouse and human pluripotent stem cell lines. *Cell Stem Cell*. Feb 4;8(2):228-40

Kapoor N, Liang W, Marbán E, Cho HC **(2013)** Direct conversion of quiescent cardiomyocytes to pacemaker cells by expression of Tbx18. *Nat. Biotechnol.* 31, 54-62

Kim C, Majdi M, Xia P, Wei KA, Talantova M, Spiering S, Nelson B, Mercola M, Chen HS. **(2010)** Non-cardiomyocytes influence the electrophysiological maturation of human embryonic stem cell-derived cardiomyocytes during differentiation. *Stem Cells Dev*. Jun;19(6):783-95

Kehat I, Kenyagin-Karsenti D, Snir M, Segev H, Amit M, Gepstein A, Livne E, Binah O, Itskovitz-Eldor J, Gepstein L. **(2001)** Human embryonic stem cells can differentiate into myocytes with structural and functional properties of cardiomyocytes. *J Clin Invest.* Aug;108(3):407-14.

Laflamme MA, Chen KY, Naumova AV, Muskheli V, Fugate JA, Dupras SK, Reinecke H, Xu C, Hassanipour M. Police S, *et al.* **(2007)** Cardiomyocytes derived from human embryonic stem cells in pro-survival factors enhance function of infarcted rat hearts. *Nat Biotechnol*. 9, 1015-24

Lian X, Hsiao C, Wilson G, Zhu K, Hazeltine LB, Azarin SM, Raval KK, Zhang J, Kamp TJ, Palecek SP. **(2012)** Robust cardiomyocyte differentiation from human pluripotent stem cells via temporal modulation of canonical Wnt signaling. *Proc Natl Acad Sci U S A.* Jul 3;109(27):E1848-57

Ma J, Guo L, Fiene SJ, Anson BD, Thomson JA, Kamp TJ, Kolaja KL, Swanson BJ, January CT. **(2011)** High purity human-induced pluripotent stem cell-derived cardiomyocytes: electrophysiological properties of action potentials and ionic currents. *Am J Physiol Heart Circ Physiol*. Nov;301(5):H2006-17

Mandenius CF, Steel D, Noor F, Meyer T, Heinzle E, Asp J, Arain S, Kraushaar U, Bremer S, Class R, Sartipy P. **(2011)** Cardiotoxicity testing using pluripotent stem cell-derived human cardiomyocytes and state-of-the-art bioanalytics: a review. *J Appl Toxicol.* Apr;31(3):191-205

Martin GR. **(1981)** Isolation of a pluripotent cell line from early mouse embryos cultured in medium conditioned by teratocarcinoma stem cells. *Proc Natl Acad Sci U S A.* Dec;78(12):7634-8

McDevitt TC, Laflamme MA, Murry CE. **(2005)** Proliferation of cardiomyocytes derived from human embryonic stem cells is mediated via the IGF/PI 3-kinase/Akt signaling pathway. *J Mol Cell Cardiol.* 39(6):865–873

Melkoumian Z, Weber JL, Weber DM, Fadeev AG, Zhou Y, Dolley-Sonneville P, Yang J, Qiu L, Priest CA, Shogbon C, *et al.* **(2010)** Synthetic peptide-acrylate surfaces for long-term self-renewal and cardiomyocyte differentiation of human embryonic stem cells. *Nat. Biotechnol*. 28, 606-610

Meyer T, Leisgen C, Gonser B, Günther E. **(2004)** QT-screen: high-throughput cardiac safety pharmacology by extracellular electrophysiology on primary cardiac myocytes. *Assay Drug Dev Technol.* Oct;2(5):507-14

Mummery C, Ward-van Oostwaard D, Doevendans P, Spijker R, van den Brink S, Hassink R, van der Heyden M, Opthof T, Pera M, de la Riviere AB *et al.* **(2003)** Differentiation of human embryonic stem cells to cardiomyocytes: role of coculture with visceral endoderm-like cells. *Circulation.* Jun 3;107(21):2733-40.

Mummery CL, Zhang J, Ng ES, Elliott DA, Elefanty AG, Kamp TJ. **(2012)** Differentiation of human embryonic stem cells and induced pluripotent stem cells to cardiomyocytes: a methods overview. *Circ Res* 111:344-58

Murry CE, Keller G. **(2008)** Differentiation of embryonic stem cells to clinically relevant populations: lessons from embryonic development. *Cell.* Feb 22;132(4):661-80

Naito AT, Shiojima I, Akazawa H, Hidaka K, Morisaki T, Kikuchi A, Komuro I. **(2006)** Developmental stage-specific biphasic roles of Wnt/betacatenin signaling in cardiomyogenesis and hematopoiesis. *Proc. Natl. Acad. Sci. USA* 103, 19812-19817

National Academies of Science Booklet **(2005)** http://dels.nas.edu/resources/static-assets/materials-based-on-reports/booklets/Understanding_Stem_Cells.pdf

Netzer R, Ebneth A, Bischoff U, Pongs O. **(2001)** Screening lead compounds for QT interval prolongation. *Drug Discov Today*. Jan 1;6(2):78-84.

NIH Fact Book **(2012)** http://www.nhlbi.nih.gov/about/documents/factbook/2012

Okita K, Nakagawa M, Hyenjong H, Ichisaka T, Yamanaka S. **(2008)** Generation of mouse induced pluripotent stem cells without viral vectors. *Science.* Nov 7;322(5903):949-53

Passier R, van Laake LW, Mummery CL. **(2008)** Stem-cell-based therapy and lessons from the heart. *Nature*. May 15;453(7193):322-9

Pouton CW, Haynes JM. **(2005)** Pharmaceutical applications of embryonic stem cells. *Adv Drug Deliv Rev.* Dec 12;57(13):1918-34

Prowse AB, Timmins NE, Yau TM, Li RK, Weisel RD, Keller G, Zandstra PW. **(2014)** Transforming the promise of pluripotent stem cell-derived cardiomyocytes to a therapy: challenges and solutions for clinical trials. *Can J Cardiol*. Nov;30(11):1335-49

Rana P, Anson B, Engle S, Will Y **(2012)** Characterization of human-induced pluripotent stem cell-derived cardiomyocytes: bioenergetics and utilization in safety screening. *Toxicol Sci* 130:117–131

Ratcliffe E, Glen KE, Naing MW, Williams DJ. **(2013)** Current status and perspectives on stem cell-based therapies undergoing clinical trials for regenerative medicine: case studies. *Br Med Bull.* 108:73-94.

Reinecke H, Zhang M, Bartosek T and Murry CE **(1999)** Survival, integration, and differentiation of cardiomyocyte grafts: a study in normal and injured rat hearts. *Circulation* 100, 193-202

Rentschler S, Yen AH, Lu J, Petrenko NB, Lu MM, Manderfield LJ, Patel VV, Fishman GI, Epstein JA **(2012)** Myocardial Notch signaling reprograms cardiomyocytes to a conduction-like phenotype. *Circulation* 126, 1058-1066

Robertson C, Tran DD, George SC. **(2013)** Concise review: maturation phases of human pluripotent stem cell-derived cardiomyocytes. *Stem Cells*. 31, 829-37

Satin J, Itzhaki I, Rapoport S, Schroder EA, Izu L, Arbel G, Beyar R, Balke CW, Schiller J, Gepstein L. **(2008)** Calcium handling in human embryonic stem cell-derived cardiomyocytes. *Stem Cells.* Aug;26(8):1961-72

Schwartz SD, Regillo CD, Lam BL, Eliott D, Rosenfeld PJ, Gregori NZ, Hubschman JP, Davis JL, Heilwell G, Spirn M *et al.,* **(2014)** Human embryonic stem cell-derived retinal pigment epithelium in patients with age-related macular degeneration and Stargardt's macular dystrophy: follow-up of two open-label phase 1/2 studies. *Lancet.* Oct 15. pii: S0140-6736(14)61376-3.

Snir M, Kehat I, Gepstein A, Coleman R, Itskovitz-Eldor J, Livne E, Gepstein L. **(2003)** Assessment of the ultrastructural and proliferative properties of human embryonic stem cell-derived cardiomyocytes. *Am J Physiol Heart Circ Physiol.* 285:H2355–H2363

Später D, Hansson EM, Zangi L, Chien KR. **(2014)** How to make a cardiomyocyte. *Development.* Dec;141(23):4418-31

Takahashi K, Tanabe K, Ohnuki M, Narita M, Ichisaka T, Tomoda K, Yamanaka S. **(2007)** Induction of pluripotent stem cells from adult human fibroblasts by defined factors. *Cell.* Nov 30;131(5):861-72.

Takahashi K, Yamanaka S. **(2006)** Induction of pluripotent stem cells from mouse embryonic and adult fibroblast cultures by defined factors. *Cell.* Aug 25;126(4):663-76.

Terrar DA, Wilson CM, Graham SG, Bryant SM, Heath BM. **(2007)** Comparison of guinea-pig ventricular myocytes and dog Purkinje fibres for in vitro assessment of drug-induced delayed repolarization. *J Pharmacol Toxicol Methods.* Sep-Oct;56(2):171-85.

Thomson JA, Itskovitz-Eldor J, Shapiro SS, Waknitz MA, Swiergiel JJ, Marshall VS, Jones JM. **(1998)** Embryonic stem cell lines derived from human blastocysts. *Science*. Nov 6;282(5391):1145-7.

Tohyama S, Hattori F, Sano M, Hishiki T, Nagahata Y, Matsuura T, Hashimoto H, Suzuki T, Yamashita H, Satoh Y, *et al.,* **(2013)** Distinct metabolic flow enables large-scale purification of mouse and human pluripotent stem cell-derived cardiomyocytes. *Cell Stem Cell*. Jan 3;12(1):127-37

Turnbull IC, Karakikes I, Serrao GW, Backeris P, Lee JJ, Xie C, Senyei G, Gordon RE, Li RA, Akar FG, *et al.,* **(2014)** Advancing functional engineered cardiac tissues toward a preclinical model of human myocardium. *FASEB J.* Feb;28(2):644-54

Ueno S, Weidinger G, Osugi T, Kohn AD, Golob JL, Pabon L, Reinecke H, Moon RT, Murry CE **(2007)** Biphasic role for Wnt/betacatenin signaling in cardiac specification in zebrafish and embryonic stem cells. *Proc. Natl. Acad. Sci. USA* 104, 9685-9690

Uosaki H, Fukushima H, Takeuchi A, Matsuoka S, Nakatsuji N, Yamanaka S, Yamashita JK. **(2011)** Efficient and scalable purification of cardiomyocytes from human embryonic and induced pluripotent stem cells by VCAM1 surface expression. *PLoS One*. 6(8):e23657

Viacyte website, **(2014)** http://viacyte.com/press-releases/viacytes-vc-01-investigational-stem-cell-derived-islet-replacement-therapy-successfully-implanted-into-first-patient/

Warren L, Manos PD, Ahfeldt T, Loh YH, Li H, Lau F, Ebina W, Mandal PK, Smith ZD, Meissner A, *et al.* **(2010**) Highly efficient reprogramming to pluripotency and directed differentiation of human cells with synthetic modified mRNA. *Cell Stem Cell.* Nov 5;7(5):618-30

WHO **(2012)** http://www.who.int/mediacentre/factsheets/fs310/en/

Wilke RA, Lin DW, Roden DM, Watkins PB, Flockhart D, Zineh I, Giacomini KM, Krauss RM. **(2007)** Identifying genetic risk factors for serious adverse drug reactions: current progress and challenges. *Nat Rev Drug Discov.* Nov;6(11):904-16.

Xu XQ, Soo SY, Sun W, Zweigerdt R. **(2009)** Global expression profile of highly enriched cardiomyocytes derived from human embryonic stem cells. *Stem Cells.* 27:2163–2174.

Yang L, Soonpaa MH, Adler ED, Roepke TK, Kattman SJ, Kennedy M, Henckaerts E, Bonham K, Abbott GW, Linden RM, *et al.,* **(2008)** Human cardiovascular progenitor cells develop from a KDR+ embryonic-stem-cell-derived population. *Nature*. 7194, 524-8

Yu J, Vodyanik MA, Smuga-Otto K, Antosiewicz-Bourget J, Frane JL, Tian S, Nie J,Jonsdottir GA, Ruotti V, Stewart R, Slukvin II, Thomson JA. **(2007)** Induced pluripotent stem cell lines derived from human somatic cells. *Science.* Dec 21;318(5858):1917-20.

Zaragoza C, Gomez-Guerrero C, Martin-Ventura JL, Blanco-Colio L, Lavin B, Mallavia B, Tarin C, Mas S, Ortiz A, Egido J. **(2011)** Animal models of cardiovascular diseases. *J Biomed Biotechnol.* 2011:497841

Zhang Q, Jiang J, Han P, Yuan Q, Zhang J, Zhang X, Xu Y, Cao H, Meng Q, Chen L *et al.* **(2011)** Direct differentiation of atrial and ventricular myocytes from human embryonic stem cells by alternating retinoid signals. *Cell Res*. 21, 579-587

Zhu WZ, Xie Y, Moyes KW, Gold JD, Askari B, Laflamme MA. **(2010)** Neuregulin/ErbB signaling regulates cardiac subtype specification in differentiating human embryonic stem cells. *Circ Res.* Sep 17;107(6):776-86

Chapter 2

Structural and Functional Maturation of Human Cardiomyocytes Derived from Pluripotent Stem Cells

This chapter focuses on structural and functional maturation of the human pluripotent stem cell-derived cardiomyocytes. The state of the art of the approaches employed to increase *in vitro* maturation is presented, and the main differences between the resulting cardiac phenotype and the hPSC-CM features presented summarized in **Paragraph 1.4** are pointed out. It is then introduced the experimental approach we will follow address the improvement in structural organization and functional performance of the differentiated hCM, presented with the literature-derived motivations for such approach. Moreover, the technological bases for the experimental approach are laid out with the description of the biomaterial employment to modify cell physical environment. We then proceed with the presentation of the data on the improved structural and functional cardiac features in hCM cultured on compliant microengineered substrates and the molecular signaling mechanism behind the process.

Detailed cell cultures protocols, substrate fabrication are described in **Appendix A**, while molecular biology assays are presented in **Appendix C**. All experimental data presented in **Paragraph 2.4** are contained in manuscripts attached in **Annex 1**, with detailed material information.

2.1 *In vitro* maturation of human cardiomyocytes

The early and immature phenotype displayed by hPSC-CMs presented in **Paragraph 1.4** is a big concern for *in vitro* applications such as disease modeling and drug testing (Davis et al., 201). Although some degree of structural maturation and improved functional performance have been published (Robertson *et al.,* 2013), most reports are experimental observations and the mechanisms of the hCMs development towards the adult phenotype remain elusive.

The main determinant in most studies showing *in vitro* maturation is the extension of the time of culture (Lundy *et al.,* 2013; Kamakura *et al.,* 2013; Otsuji *et al.,* 2010; Sartiani *et al.,* 2007). The results of these studies can be summarized by dividing the hPSC-CMs in two major categories according to the length of the time in culture after differentiation: early-stage and late-stage, in which 60-90 days in culture is roughly the discriminating time frame (Fig. 2.1). Despite different differentiation approaches and culture maintenance techniques, there is a consensus of the cardiac features difference between the two classes:

i) sarcomeric organization improves over time, with progressive appearance of Z-, A-, H-, I- (Lundy *et al.,* 2013) and finally M-bands (Kamakura *et al.,* 2013) and time-dependent myofibril thickening in aligned bundles is observed;

ii) electrophysiological properties lean towards an adult-like phenotype in terms of action potential (AP) parameters: increasing maximal upstroke velocity, lower maximum diastolic potential, and amplitude (Lundy *et al.,* 2013); moreover, the performance of single ion channels and ion currents drug-response improves (Otsuji *et al.,* 2010; Sartiani *et al.,* 2007);

iii) calcium handling improves in terms of Ca^{2+} transient increased upstroke and decay velocities (Lundy *et al.,* 2013);

iv) time-dependent cardiac population subtype shift is observed, with increasing percentages of ventricular-like cardiomyocytes over time (Lian *et al.,* 2012; Kamakura *et al.,* 2013).

Further extension of time in culture (up to 1 years) did not promote relevant changes in cardiac phenotype, still far from adult-like.

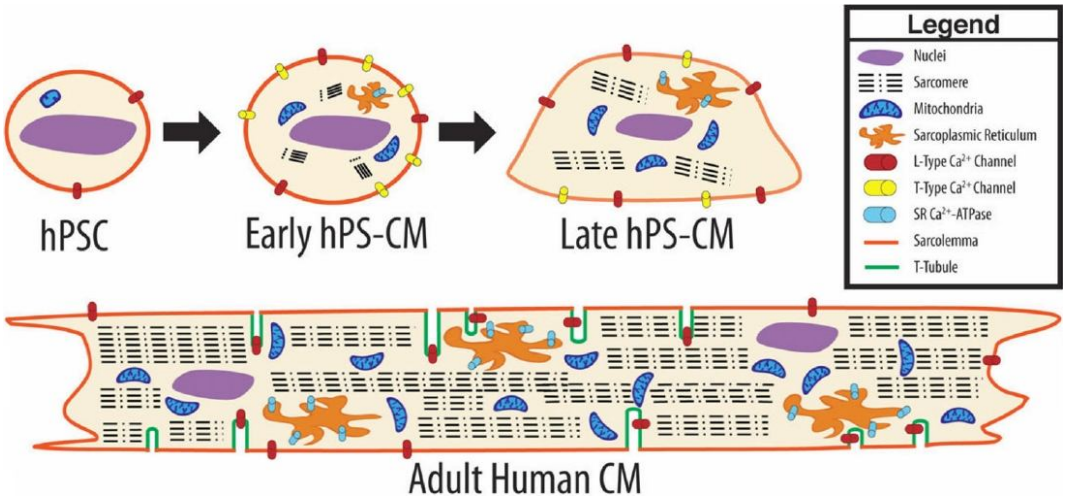

Fig. 2.1 Schematic representation of the *in vitro* maturation process of hPSC-CMs in comparison with adult myocytes. Cardiomyocyte fundamental structural features usually taken into account are represented (adapted from Robertson *et al.,* 2013)

In order to achieve more adult-like phenotypes for single cardiac functional features, such as calcium handling or action potential performances, approaches of ectopic delivery of missing molecular components has been proposed (Liu *et al*., 2009; Lieu *et al.,* 2013). To enhance Ca^{2+} handling ability of hESC-CMs it was sufficient to forcefully overexpress the usually absent calsequestrin (Liu *et al*., 2009), and similar results for were obtained for action potential profiles with Kir2.1 overexpression (Lieu *et al.,* 2013). Both the approaches, however, did not promote any other kind of maturation. Somehow similar results were reported with miRNA-based approaches (Fu *et al.,* 2011). In this case, overexpression of two miRNAs associated *in vivo* with cardiac developmental processes (miR-1 and miR-499) were shown to improve either ion handling performance (miR-1) or contraction machinery maturation (miR-499), but in this case as well neither promoted a coordinated cardiac maturation.

All the reports presented in this paragraph clearly show that the hPSC-CM *in vitro* cultures we study lack fundamental cues (or contain inhibiting cues) that regulate developmental progression towards more mature cardiac phenotypes. Moreover, it is clear how inserting (in a targeted or shotgun fashion) missing components of the immature functional cardiac machineries is unfeasible.

Thus, further understanding of the mechanisms that trigger cardiac development is necessary in order to make available an *in vitro* models representative of human adult cardiac physiology.

2.2 Motivations and experimental design

The work presented in this chapter aims at the investigation of the mechanical triggers of cardiomyocyte maturation *in vitro.* We here propose a molecular explanation of some of the experimental observations reported in literature of improved hPSC-CM cardiac phenotype, by linking the interaction between the cell and the culture substrate to structural and functional features. We show how the modification of cellular physical environment affects the cardiac maturation *in vitro*, thus providing proof of the benefits of integrating mechanical cues in the differentiation protocol to generate human cardiomyocytes with more mature phenotype. In our perspective, it is important to how the heart, from its early beginning, is a highly dynamic tissue, exposed to a combination of physical stimuli of different nature at all time-and size-scales (Cimetta *et al.,* 2013). It is the first organ generated during embryogenesis and forces such as shear, stretch, hydrostatic pressure ("mechanical loads") and electrical activity shape its development and function.

The importance of these purely physical stimuli, acting in concert with the soluble environment to which the cells are always exposed, is supported by experimental evidences of high degree hPSC-CM maturation after engraftment in a working myocardium (van Laake *et al.,* 2007; Chong *et al.,* 2014). These

observations prove that hPSC-CMs retain the potential to achieve adult-like phenotypes in the right environmental conditions (Dick *et al.,* 2010). Some reports provide proof that the integration of such electro-mechanical stimuli present *in vivo* drive functional hPSC-CM cardiac maturation (Hirt *et al.,* 2014; Chan *et al.,* 2013; Mihic *et al.,* 2014) . In most cases, though, these experiments are performed on engineered 3D cardiac tissues, culture condition already *per se* shown to provide remarkable structural and functional improvements in respect to 2D monolayer hPSC-CM cultures (Stevens *et al.,* 2009; Zhang *et al.,* 2013; Turnbull *et al.,* 2013). Thus, the uncoupling of the physical cues that drive the maturation is difficult, and the contribution of single mechanical triggers and the activation of molecular mechanisms is lost in the process. Reasoning on the 3D culture system and its differences from standard monolayer cultures, we decided to address the question whether the very proximal physical cell environment of the cardiomyocyte and its mechanical features take share in the cardiac maturation process. To investigate how the human cardiomyocytes interact with the adhesion substrate we cultured the hPSC-CMs on compliant hydrogels, tuning their mechanical properties in order to observe the cellular response in terms of structural and functional cardiac features. Further on, we investigated how the inhibition of cellular physical sensing ability affects its phenotype, thus providing a molecular signaling target which activation is necessary to drive *in* vitro cardiac maturation.

2.3 Biomaterials for tuning cell physical environment

Standard cell culture techniques have relied for decades on glass and plastic surfaces to maintain the cell populations employed as experimental models, but these adhesion substrates are far from anything the cell could ever experience *in vivo*, from both biochemical and physical perspectives (Wells, 2008). The elastic moduli of the human organs are in the range of a few dozen kilopascals (Pa = newton/m^2), with soft tissues such as brain and adipose centered below 1 kPa

and cartilage and bone surpassing 100 kPa (Discher *et al.,* 2009). The prominent importance of culture substrate stiffness in determining the cell phenotype came to light when evidence of stem cell directed differentiation by sole variation of substrate mechanical properties was reported (Engler *et al.,* 2006). In particular regard to the cardiac tissue, it has been shown in chick (Engler *et al.,* 2008) and murine cardiomyocytes (Jacot *et al.,* 2008) that culture on plastic or other stiff substrates is detrimental to cardiac functional features and substrates in the "physiological range" of elastic moduli for the human muscle (8 kPa – 25 kPa) can improve sarcomeric organization and calcium handling ability.

Providing cell cultures with defined biochemical and mechanical cues is not an easy task and requires the employment of engineered substrates and specific biomaterials (Ahearne, 2014). In the first attempts to study the effects of substrate on cell cultures natural polymer gels, such as collagen, fibrin and Matrigel, were employed (Wells, 2008). The major drawback of these approaches was the bioactivity of the biological gels, which determined the impossibility of uncoupling mechanical from biochemical cues of the cultures substrate (Nemir and West, 2010). Most commonly, synthetic polymeric hydrogels such as polyacrylamide- and PEG-based ones are best suited for this studies because of their biocompatibility, transparency, high water content and controllable physical features (Pelham and Wang, 1997; Ghosh *et al.,* 2007). For instance, polyacrylamide hydrogels are not biodegradable nor bioactive, suiting perfectly for *in vitro* studies on the influence of the substrate stiffness on cell behavior, as their elastic modulus can be very finely tuned by adjusting the acrylamide/bis-acrylamide ratio in the physiologically relevant range (Tse and Engler, 2010).

The mechanical features of the cellular environment are sensed by the cells through a process called mechanotransduction, which converts the physical forces, both dynamic (such as active stretching or fluid shear) and static (substrate elastic modulus), in biochemical signals inside the cell through kinase cascades (Jaalouk and Lammerding, 2009). In this pathways, cell-to-cell and cell-to-ECM adhesion membrane proteins play major a major role, in concert with

the structural components of the cytoskeleton on the cytoplasmic side of the system.

In the following paragraphs of this chapter are presented experimental observations and data regarding the influence of the cell-substrate interaction on *in vitro* cardiac maturation of human cardiomyocytes derived from pluripotent stem cells. We took advantage of the substrate modification techniques described in **Appendix A** to provide different physical stimuli to the cardiac cultures, and explored the involvement of a relevant mechanotransduction pathway in the determination of the observed phenotype.

2.4 Substrate-driven maturation of hPSC-CMs

To study the effects of culture substrate on cardiac *in vitro* culture, we selected two pluripotent stem cell lines (one hES and one hiPS, for details about cell line origin and culture media refer to **Appendix A and Annex 1**) and differentiated them towards the cardiac lineage with an EB-based protocol (Yang *et al.,* 2008). Both cell populations (undifferentiated and at the end-stage of the protocol) displayed stage-specific morphologies, with first contracting EBs observed after 10-12 days for hESC and after 7-9 days for the hiPSC, and were characterized for expression of pluripotent and cardiac markers, assessed by immunofluorescence (Fig. 2.2A&B). We decided to maintain the differentiated cardiomyocytes in EB aggregates cultured in suspension, in order to keep the cell in their native environment without addition of external mechanical stimuli. At desired time-points the EB were harvested and disaggregated to single-cell suspensions and replated for further analyses.

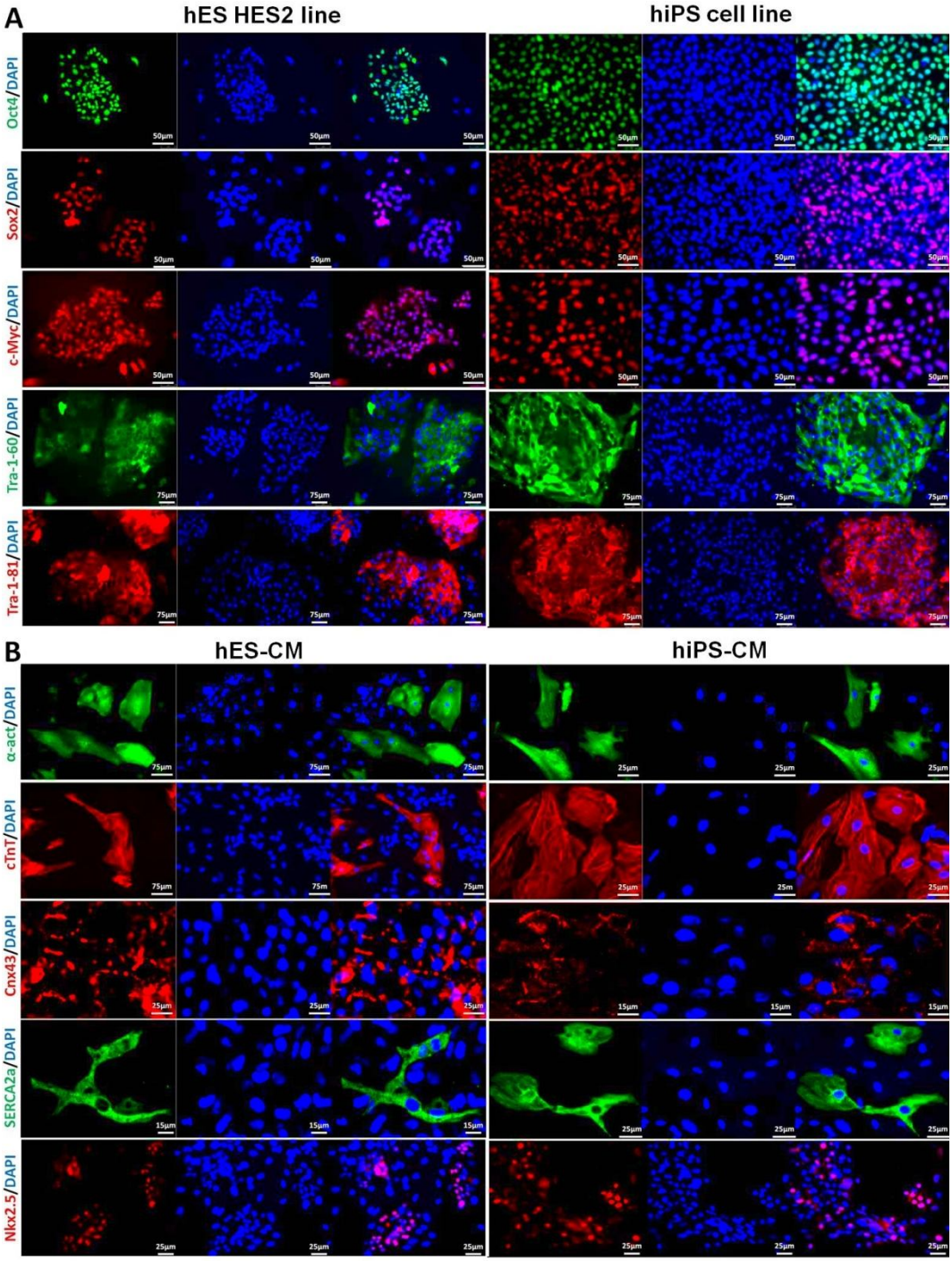

Fig. 2.2 Molecular markers in pluripotent and differentiated cells. (A) Expression of pluripotency markers in hES HES2 cell line and hiPS ADHF#1 cell line. **(B)** Expression of cardiac markers in human cardiomyocytes derived from the same two pluripotent stem cells lines.

2.4.1 Cell-substrate interaction promotes cardiac maturation

Dissociated single-cell cultures displayed both spontaneous and electrically elicited contractions and confocal line-scanning imaging with fluorescent probe fluo-4 confirmed they were accompanied by cardiac-like calcium transients (Fig. 2.1A)

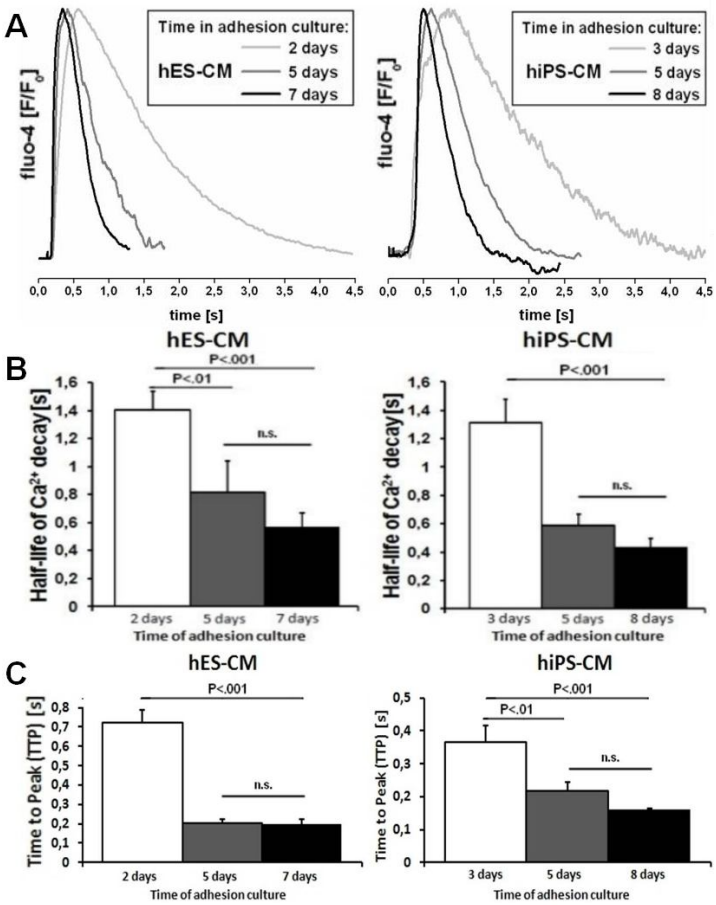

Fig. 2.3 Calcium dynamics in hPSC-CMs (A) Representative calcium traces of hES-CMs and hiPS-CMs and different times of adhesion culture. **(B)** Evaluation of calcium re-uptake rate by the half-life of calcium decay**. (C)** Time to peak estimates.

Intriguingly, calcium transients shortened upon extension of the monolayer culture time: Ca^{2+} transients lasting several seconds were recorded in the majority of cardiomyocytes early after single cell replating in adhesion, while almost disappearing already after few days, with calcium decay values stabilizing after 1 week (Fig. 2.3B). Ca^{2+} release rate increased in the same temporal span, as showed by the reduction of the time to peak (TTP) (Fig. 2.3C).

The increased calcium handling ability was associated with a marked improvement in organization of cardiac cell structural features. As opposed to cells clustered in embryoid bodies displaying round morphologies with high

nucleus-to-cytoplasm ratio and disorganized myofibrils (Fig. 2.4), cardiomyocytes cultured in monolayer showed increasing alignment and regular striation patterns of the cTnT staining (Fig. 2.4A). In terms of myofibril alignment, both cell lines displayed a marked increase in sarcomere organization after 1 week in monolayer culture, reaching nearly parallel sarcomeres (Fig. 2.4B). Western Blot analysis confirmed an increased expression of cardiac troponin T isoforms on cardiomyocytes cultured in adhesion (Fig. 2.4C).

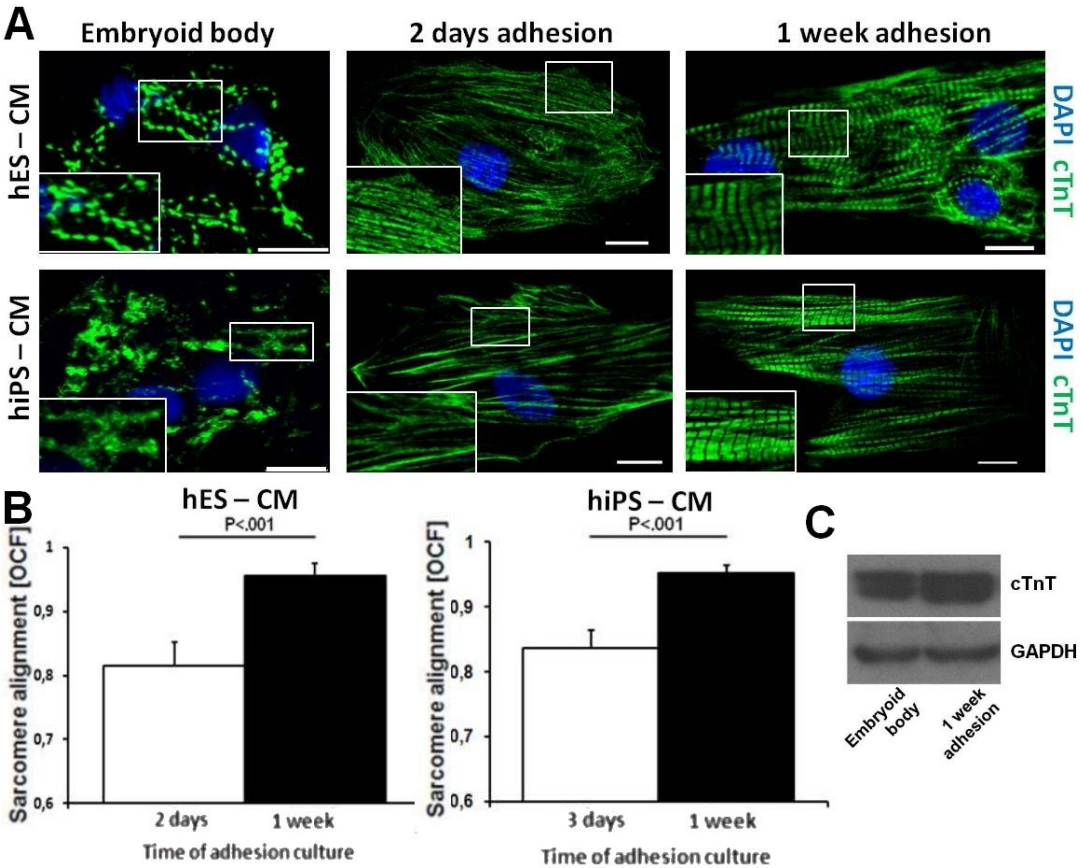

Fig. 2.2 Sarcomeric organization improves in replated hPSC-CMs. (A) Immunofluorescence against cTnT shows progressive generation of striated patterns of the myofibrils and **(B)** their increased alignment with the long axis of the polarized cells. (C) The expression of cTnT increases in monolayer culture, in terms of protein amount, tested by Western Blot.

Calcium cycling is orchestrated by several molecular components and the Ca^{2+} transient profile is the result of sum of their activities (Bers, 2002). The calcium re-uptake phase was most striking difference in the Ca^{2+} transient profiles we observed, thus we investigated the expression and distribution of the Sarco-Endoplasmic Reticulum Ca^{2+} ATPase 2 (SERCA2), the component of the calcium handling machinery mainly responsible for this phase in human cardiomyocytes.

Immunofluorescence staining showed a great increase in SERCA2a accumulation after 1 week in adhesion, with a striking reorganization of the SR, from a mostly perinuclear localization early after single-cell replating, towards a whole-cell spreading after 1 week (Fig. 2.5A). We evaluated the spreading area of the SERCA2a staining finding a significant increase in spreading area in both hES-CMs and in hiPS-CMs (Fig. 2.5B). We assessed by means of RT-PCR that SR calcium handling proteins triadin (TRDN), calsequestrin (CSQ2) and phospholamban (PLN), which are often found missing in hPSC-CMs and largely impact on the cell calcium handling ability (Fig. 2.5C).

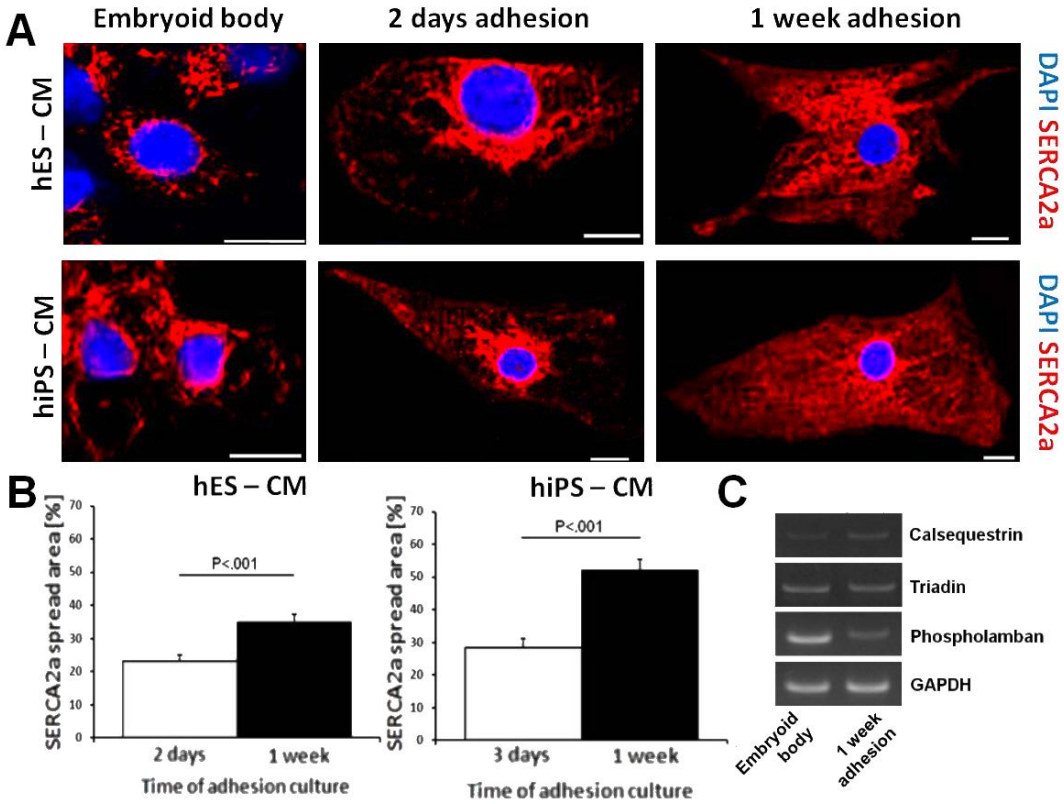

Fig. 2.3 Sarcoplasmic reticulum maturation. (A) Staining for calcium pump SERCA2a responsible for Ca^{2+} re-uptake shows SR spreading from a perinuclear localization towards a whole-cell volume distribution. **(B)** Quantification of the spread area of the staining in percentage to cell surface. **(C)** Expression of SR-associated Ca^{2+} handling proteins.

Consistently, as expected from a maturing sarcoplasmic reticulum, the cardiomyocyte performance in calcium handling improved after stimulation with 10 mM caffeine shown by representative traces at the two time points considered (Fig. 2.6A) and dynamics quantification (Fig. 2.6B); in particular

calcium release and re-uptake rates significantly increased and a two-fold increase in peak relative amplitude between 2 days and 1 week in adhesion was observed.

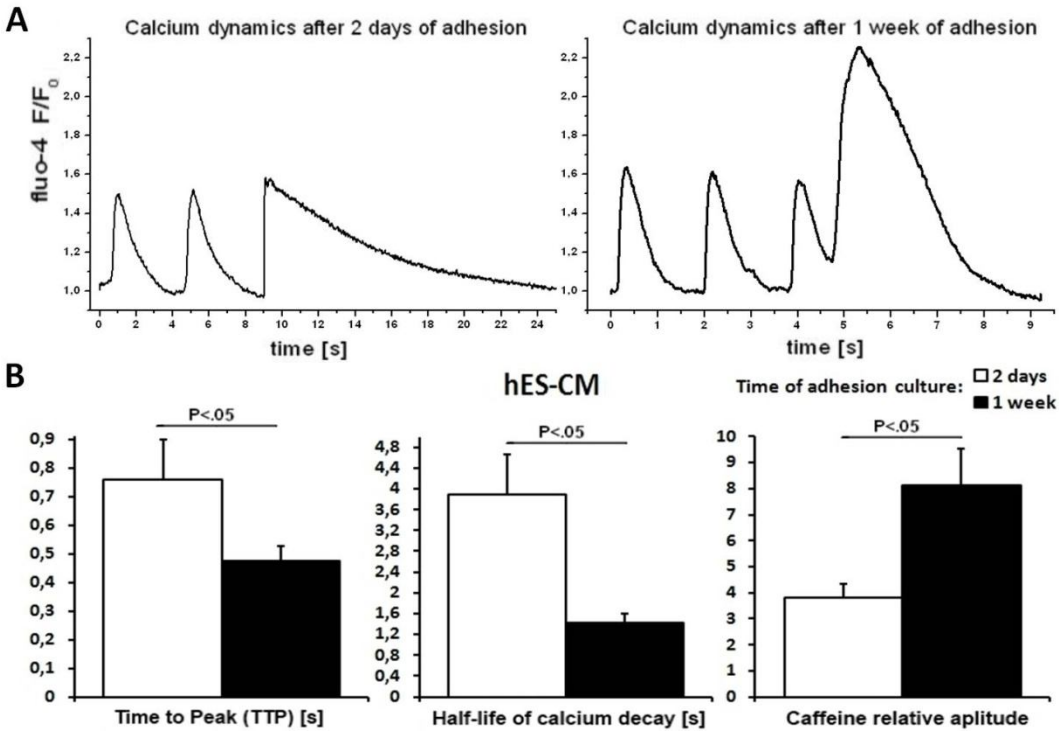

Fig. 2.4 Caffeine stimulation response in hESC-CMs. (A) Representative traces of Ca2+ transients during 10 mM caffeine stimulation at 2 days and 1 week on monolayer culture. **(B)** Quantification of caffeine-induced Ca2+ transient parameters.

At this point, we decided to assess whether the functional and structural maturation we observe is a result of the time in adhesion or EBs age by performing calcium handling analyses on different preparations (n=3) of both hES- and hiPS-derived EBs. Calcium cycling in cardiomyocytes results from the coordinated action of different molecular components and requiring a correct spatial distribution and sub-cellular compartments organization, thus condensing in one read-out several key cardiac features. EBs were maintained in suspension culture up to 3 months after differentiation protocol start and three time points were chosen for Ca^{2+} analyses: early after cardiac differentiation protocol end, 1 month and 2-3 months later. All experiments recapitulated the functional maturation of the calcium handling machinery in terms of Ca^{2+} reuptake rate (Fig. 2.7) for both hES-CMs and hiPS-CM, as function of time in adhesion. A very strong correlation (Two-Ways ANOVA, $p<.001$) was found between the calcium

transient shortening and the time in adhesion culture, but not EB age, thus highlighting the importance of the cues from the adhesion substrate over the age of EB for the improvement in functional performance.

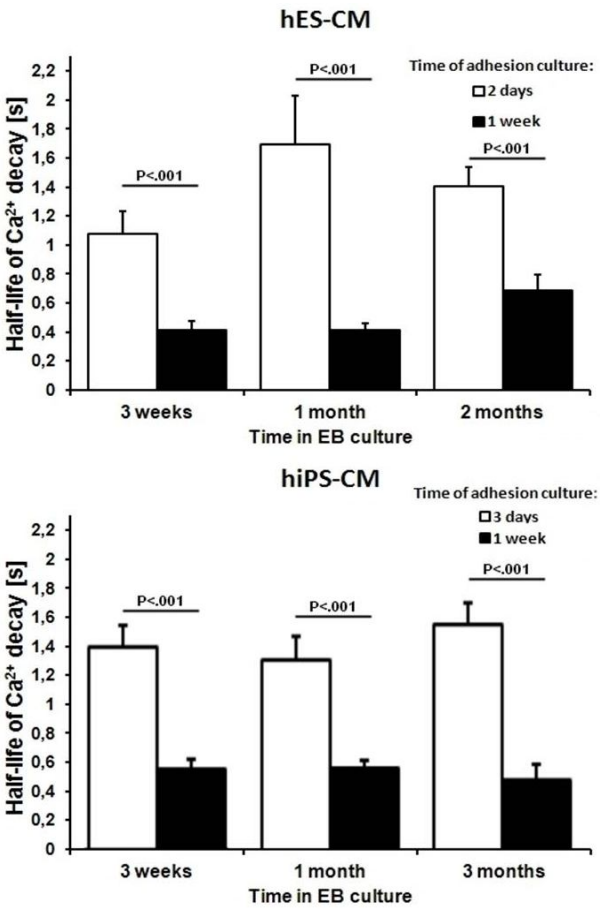

Fig. 2.5 Substrate interaction drives the Calcium handling maturation. Calcium handling ability in hPSC-CMs described as Ca^{2+} re-uptake rate. Ca^{2+} decay values drop after monolayer adhesion culture, regardless of EB age.

As previously cited in **Paragraph 2.1**, extension of the time of culture of differentiated hPSC-CMs produced cardiomyocytes displayed more mature features. In those studies, the maturation process spanned several months and the cells were maintained in beating clumps, thus the contribution of cell-substrate interactions could not be clearly investigated. In this paragraph, it is shown how in our cultures structural and functional cardiac maturation can be observed and quantified. Moreover, we prove that the condition prevalently contributing to this maturation is the time in adhesion to a substrate, regardless of the age of the embryoid body from which the hCMs are derived. We wanted to further investigate the interaction between cardiomyocyte and substrate modifying its mechanical properties.

2.4.2 Cardiac maturation depends on substrate stiffness

The elastic moduli of cardiac and skeletal muscle tissues are routinely estimated in a range between 8 kPa and 25 kPa and it has been proven that hydrogels in this range of stiffness provide the best adhesion substrate for muscle cells and

cardiomyocytes promoting their differentiation and maturation (Engler *et al.*, 2008; Serena *et al.*, 2010).

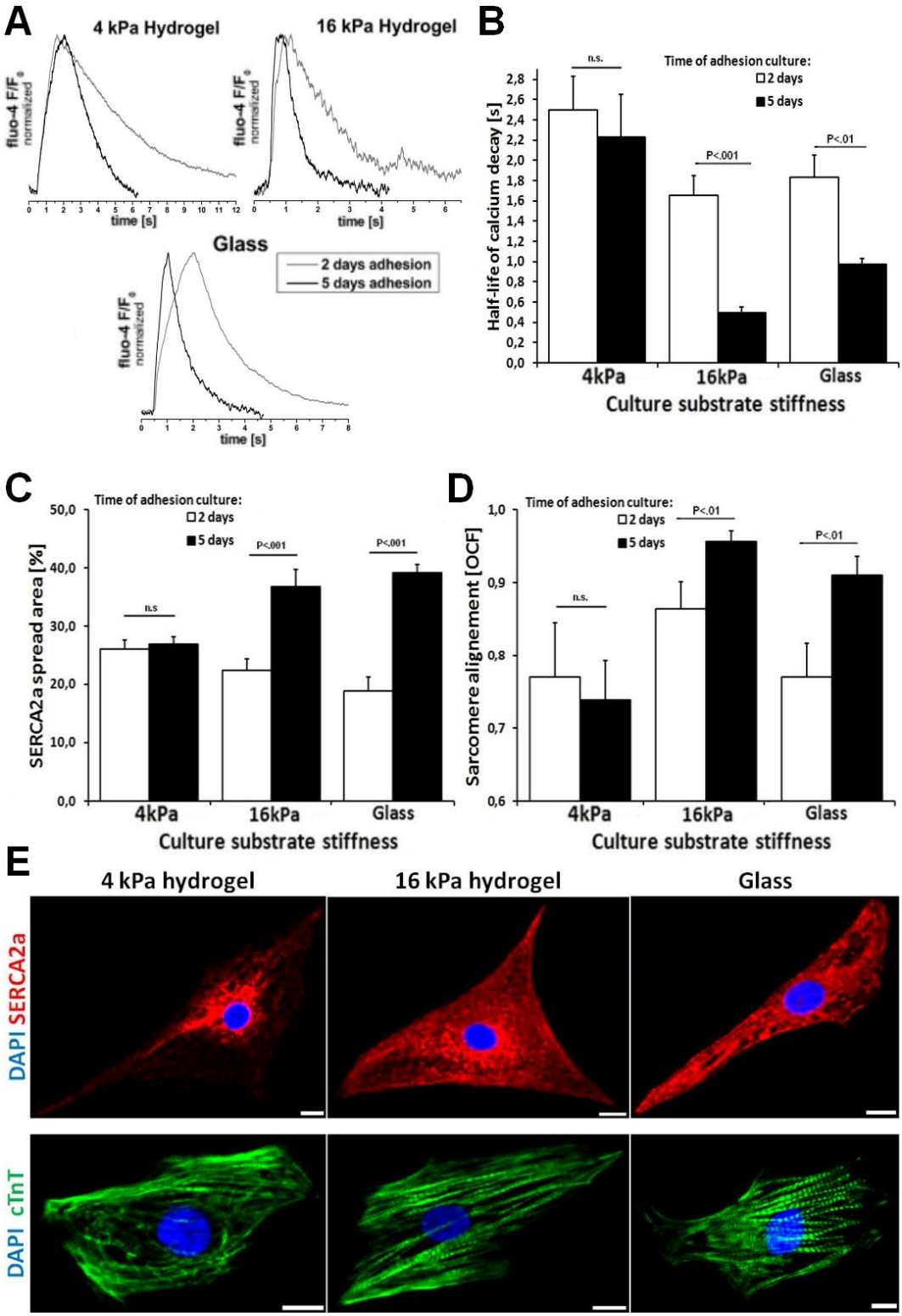

Fig. 2.6 Effect of substrate stiffness on cardiac maturation parameters. Calcium handling in **(A)** representative Ca^{2+} transient profiles and **(B)** quantification of Ca^{2+} transient decay rate. Quantification of SERCA2a spread area percentage **(C)** and sarcomere alignment **(D)** with representative images for all substrates after 5 days in adhesion culture.

To assess whether the hPSC-CM were affected in their adhesion culture-driven functional maturation by the stiffness of the culture substrate, we cultured hiPS-CM after EB disaggregation on polyacrylamide hydrogels of 4 kPa (soft substrate), 16 kPa (muscle-like substrate) and glass (stiff substrate). Human cardiomyocytes cultured on 16 kPa hydrogels and on glass recapitulated the previous results, with a positive correlation between time in adhesion culture and functional maturation, with calcium transients decreasing in duration (Fig. 2.8A), and increasing rate in Ca^{2+} re-uptake (Fig. 2.8B). In these substrate conditions, the structural features of the cardiac cells improved in time showing SR maturation and SERCA2a spreading (Fig. 2.8C&E) and proper sarcomere alignment (Fig. 2.8D&E). Instead, cardiomyocytes cultured on the 4 kPa hydrogel, did not show functional maturation in terms of calcium handling (Fig. 2.8A&B); consistently, the SERCA2a distribution maintained a perinuclear localization (Fig. 2.8C&E). The influence of the soft substrate on cardiomyocyte structural organization was evident as well in the lack of myofibril alignment and poor organization of sarcomeric structures (Fig. 2.8D&E).

2.4.3 Mechanotransduction is necessary for hPSC-CMs maturation

Cell sensing of the surrounding physical environment has its molecular basis in a limited number of signaling pathways (Jaalouk and Lammerding, 2009) transducing mechanical cues through pathways such as the RhoA-ROCK pathway (Wei *et al.,* 2001). The importance of this specific mechanotransduction pathway in cardiac development is demonstrated by severe alterations in heart morphogenesis of mouse and chick embryos (Zhao and Rivkees, 2003; Sakata *et al.,* 2007). Neonatal rat cardiomyocytes subjected to prolonged exposure to RhoA/ROCK inhibitors show a reduction in contraction force (Jacot *et al.,* 2008). Moreover, ROCK inhibition has been shown to effectively mimic the effect of soft substrates in terms of translocation of transcription factors and activating similar transcription profiles (Dupont *et al.,* 2011). This evidence identifies Rho-associated kinase as a suitable target of inhibition in order to convincingly

desensitize hPSC-CM from the mechanical environmental cues, thus providing insight in the molecular basis of their substrate-driven maturation.

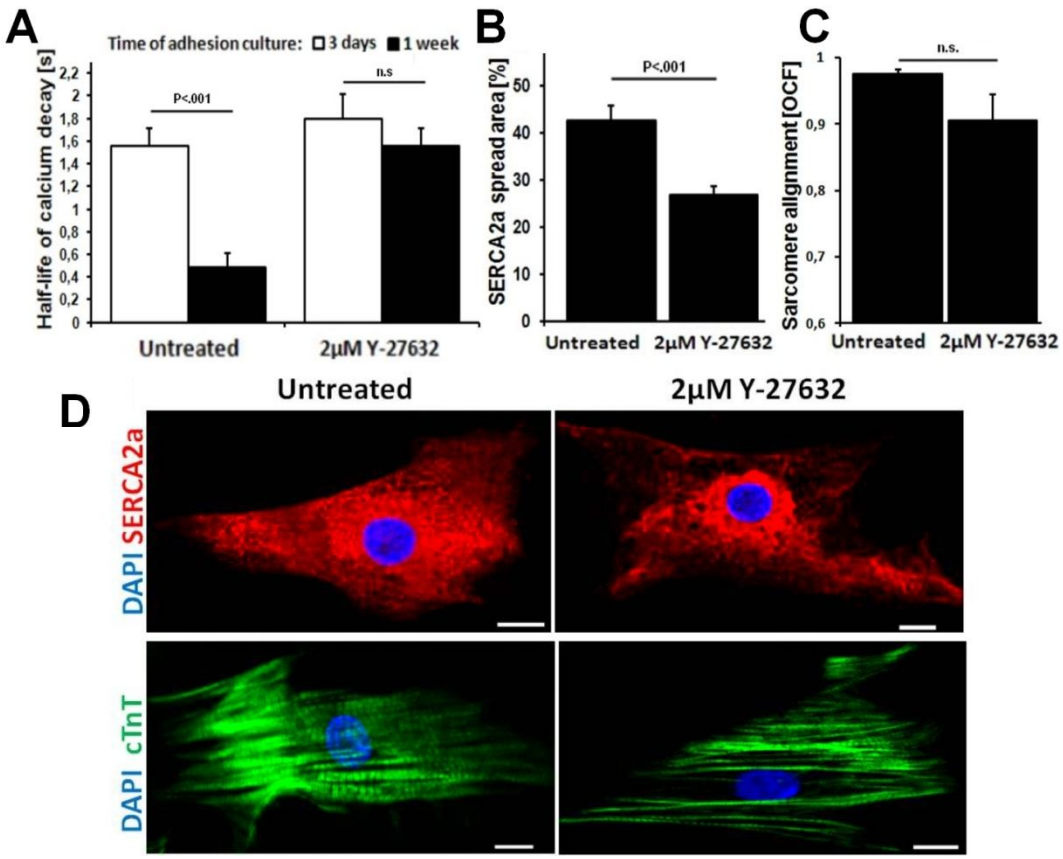

Fig. 2.7 RhoA/ROCK mechanotransduction pathway inhibition prevents cardiac maturation mimicking the phenotype displayed by cardiomyocytes culture on a soft substrate. **(A)** Calcium transient decay rate. **(B)** SERCA2a spread area and **(C)** myofibril alignment with representative images **(D)**.

We cultured hPSC-CM on a stiff substrate with or without 2 μM of ROCK inhibitor Y-27632 for 1 week and analyzed the cultures for calcium handling and structural features. As expected, the untreated cardiomyocytes recapitulated the results reported above (Ca^{2+} shortening and increased calcium reuptake rate) (Fig. 2.9A). This effect of adhesion culture was completely abrogated by the ROCK inhibition, with Ca^{2+} transients lasting several seconds even after 1 week and calcium reuptake rates fairly unchanged within this time in culture (Fig. 2.9A). In line with the previous results, in which calcium handling maturation was accompanied by pronounced SR maturation and SERCA2a enhanced expression and relocalization, SERCA2a staining revealed how the treated hPSC-CM maintains a perinuclear localization of the pump after 1 week without significant

spreading throughout the cell volume observed in the controls (Fig. 2.9B&D). Interestingly, human cardiomyocytes did not display significant alterations in myofibrils alignment, which organized in a parallel fashion with the long cell axis, although presenting less degree of sarcomere organization, resulting in thinner myofibrils compared to the controls (Fig. 2.9 C&D).

2.5 Conclusions

In this chapter, we addressed the issue of *in vitro* cardiac maturation of human cardiomyocytes derive from hPSCs. We presented the maturation approaches reported in literature, describing the resulting phenotype and highlighting the limitations of these experimental observations.

We provided evidence of phenotypes similar to those reported in our human cardiac cultures, but we show how time culture extension in clusters and cell aggregates is not the driving force behind the structurally and functionally matured phenotype. The cues derived from cell-to-substrate interaction upon single cell or monolayer culture are responsible for great structural reorganization that results in improved functional performance. This process can be observed son after cell replating and is independent on the age of the differentiated cells.

We then show how tuning the interaction between the cardiomyocyte and the adhesion substrate affects the maturation, proving that soft substrates do not provide enough passive mechanical stress to the cells and do not sustain structural reorganization and failing to improve functional performance. Biochemical disruption of mechanotransduction signaling "tricks" the cardiomyocyte into sensing a lower passive mechanical stress from the substrate, thus mimicking a soft-substrate culture and recapitulating the maturation-inhibited phenotype. With the specificity of the pharmacological target, we provide evidence of the involvement of the RhoA/ROCK pathway in the *in vitro*

cardiac maturation and state that the presence of cues positively regulating this signaling should be integrated in human cardiac culture to produce structurally and functionally more mature human cardiomyocytes for *in vitro* studies.

2.6 References

Ahearne M. **(2014)** Introduction to cell-hydrogel mechanosensing. *Interface Focus*. Apr 6;4(2):20130038

Bers DM. **(2002)** Cardiac excitation-contraction coupling. *Nature*. Jan 10;415(6868):198-205

Chan YC, Ting S, Lee YK, Ng KM, Zhang J, Chen Z, Siu CW, Oh SK, Tse HF. **(2013**) Electrical stimulation promotes maturation of cardiomyocytes derived from human embryonic stem cells. *J Cardiovasc Transl Res*. Dec;6(6):989-99

Chong JJ, Yang X, Don CW, Minami E, Liu YW, Weyers JJ, Mahoney WM, Van Biber B, Cook SM, Palpant NJ et al., **(2014)** Human embryonic-stem-cell-derived cardiomyocytes regenerate non-human primate hearts. *Nature*. Jun 12;510(7504):273-7

Cimetta E, Godier-Furnémont A, Vunjak-Novakovic G. **(2013)** Bioengineering heart tissue for in vitro testing. *Curr Opin Biotechnol*. Oct;24(5):926-32

Davis RP, van den Berg CW, Casini S, Braam SR, Mummery CL. **(2011)** Pluripotent stem cell models of cardiac disease and their implication for drug discovery and development. *Trends Mol Med.* 9, 475-84

Dick E, Rajamohan D, Ronksley J, Denning C. **(2010)** Evaluating the utility of cardiomyocytes from human pluripotent stem cells for drug screening. *Biochem Soc Trans*. Aug;38(4):1037-45

Discher DE, Mooney DJ, Zandstra PW. **(2009)** Growth factors, matrices, and forces combine and control stem cells. *Science*. Jun 26;324(5935):1673-7

Dupont S, Morsut L, Aragona M, Enzo E, Giulitti S, Cordenonsi M, Zanconato F, Le Digabel J, Forcato M, Bicciato S, et al., **(2011)** Role of YAP/TAZ in mechanotransduction. *Nature.* 474(7350):179-83

Engler AJ, Carag-Krieger C, Johnson CP, Raab M, Tang HY, Speicher DW, Sanger JW, Sanger JM, Discher DE. **(2008)** Embryonic cardiomyocytes beat best on a matrix with heart-like elasticity: scar-like rigidity inhibits beating. *J Cell Sci*. Nov 15;121(Pt 22):3794-802

Engler AJ, Sen S, Sweeney HL, Discher DE. **(2006)** Matrix elasticity directs stem cell lineage specification. *Cell.* Aug 25;126(4):677-89

Fu JD, Rushing SN, Lieu DK, Chan CW, Kong CW, Geng L, Wilson KD, Chiamvimonvat N, Boheler KR, Wu JC, *et al.* **(2011)** Distinct roles of microRNA-1 and -499 in ventricular specification and functional maturation of human embryonic stem cell-derived cardiomyocytes. *PLoS One.* 6(11):e27417

Ghosh K, Pan Z, Guan E, Ge S, Liu Y, Nakamura T,Ren XD, Rafailovich M, Clark RA (2007) Cell adaptation to a physiologically relevant ECM mimic with different viscoelastic properties. Biomaterials 28:671–679

Hirt MN, Boeddinghaus J, Mitchell A, Schaaf S, Börnchen C, Müller C, Schulz H, Hubner N, Stenzig J, Stoehr A, et al., **(2014)** Functional improvement and maturation of rat and human engineered heart tissue by chronic electrical stimulation. *J Mol Cell Cardiol*. May 19;74C:151-161

Jaalouk DE, Lammerding J. **(2009)** Mechanotransduction gone awry. *Nat Rev Mol Cell Biol.* Jan;10(1):63-73

Jacot JG, McCulloch AD, Omens JH. **(2008)** Substrate stiffness affects the functional maturation of neonatal rat ventricular myocytes. *Biophys J.* 7, 3479-87

Kamakura T, Makiyama T, Sasaki K, Yoshida Y, Wuriyanghai Y, Chen J, Hattori T, Ohno S, Kita T, Horie M et al. **(2013).** Ultrastructural maturation of human-induced pluripotent stem cell-derived cardiomyocytes in a long-term culture. *Circ J.* 77, 1307-14

Lian X, Hsiao C, Wilson G, Zhu K, Hazeltine LB, Azarin SM, Raval KK, Zhang J, Kamp TJ, Palecek SP. **(2012)** Robust cardiomyocyte differentiation from human pluripotent stem cells via temporal modulation of canonical Wnt signaling. *Proc Natl Acad Sci U S A.* Jul 3;109(27):E1848-57

Lieu DK, Fu JD, Chiamvimonvat N, Tung KC, McNerney GP, Huser T, Keller G, Kong CW, Li RA. **(2013)** Mechanism-based facilitated maturation of human pluripotent stem cell-derived cardiomyocytes. *Circ Arrhythm Electrophysiol*. 6, 191-201

Liu J, Lieu DK, Siu CW, Fu JD, Tse HF, Li RA. **(2009)** Facilitated maturation of Ca2+ handling properties of human embryonic stem cell-derived cardiomyocytes by calsequestrin expression. *Am J Physiol Cell Physiol.* 1, C152-9

Lundy SD, Zhu WZ, Regnier M, Laflamme MA **(2013)** Structural and functional maturation of cardiomyocytes derived from human pluripotent stem cells. *Stem Cells Dev*. Jul 15;22(14):1991-2002

Mihic A, Li J, Miyagi Y, Gagliardi M, Li SH, Zu J, Weisel RD, Keller G, Li RK. **(2014)** The effect of cyclic stretch on maturation and 3D tissue formation of human embryonic stem cell-derived cardiomyocytes. *Biomaterials.* Mar;35(9):2798-808

Nemir S1, West JL. (2010) synthetic materials in the study of cell response to substrate rigidity. Ann Biomed Eng. Jan;38(1):2-20

Otsuji TG, Minami I, Kurose Y, Yamauchi K, Tada M, Nakatsuji N. **(2010)** Progressive maturation in contracting cardiomyocytes derived from human embryonic stem cells: Qualitative effects on electrophysiological responses to drugs. *Stem Cell Res*. 4, 201-13

Pelham RJ, Wang Y (1997) Cell locomotion and focal adhesions are regulated by substrate flexibility. Proc. Natl Acad. Sci. USA 94:13661–13665

Robertson C, Tran DD, George SC. **(2013)** Concise review: maturation phases of human pluripotent stem cell-derived cardiomyocytes. *Stem Cells.* 31, 829-37

Sakata H, Sakabe M, Matsui H, Kawada N, Nakatani K, Ikeda K, Yamagishi T, Nakajima Y. **(2007)** Rho kinase inhibitor Y27632 affects initial heart myofibrillogenesis in cultured chick blastoderm. *Dev Dyn.* Feb;236(2):461-72

Sartiani L, Bettiol E, Stillitano F, Mugelli A, Cerbai E, Jaconi ME. **(2007)** Developmental changes in cardiomyocytes differentiated from human embryonic stem cells: a molecular and electrophysiological approach. *Stem Cells*. 5, 1136-44

Serena E, Zatti S, Reghelin E, Pasut A, Cimetta E, Elvassore N. **(2010)** Soft substrates drive optimal differentiation of human healthy and dystrophic myotubes. *Integr Biol (Camb)*. Apr;2(4):193-201

Stevens KR, Pabon L, Muskheli V, Murry CE **(2009)** Scaffold-free human cardiac tissue patch created from embryonic stem cells. *Tissue Eng.* A 15, 1211–1222

Tse JR, Engler AJ. **(2010)** Preparation of hydrogel substrates with tunable mechanical properties. *Curr Protoc Cell Biol.* Jun;Chapter 10:Unit 10.16

Turnbull IC, Karakikes I, Serrao GW, Backeris P, Lee JJ, Xie C, Senyei G, Gordon RE, Li RA, Akar FG, *et al.,* **(2014)** Advancing functional engineered cardiac tissues toward a preclinical model of human myocardium. *FASEB J.* Feb;28(2):644-54

van Laake LW, Passier R, Monshouwer-Kloots J, Verkleij AJ, Lips DJ, Freund C, den Ouden K, Ward-van Oostwaard D, Korving J, Tertoolen LG, et al., **(2007)** Human embryonic stem cell-derived cardiomyocytes survive and mature in the mouse heart and transiently improve function after myocardial infarction. *Stem Cell Res.* 1, 9-24

Wei L, Roberts W, Wang L, Yamada M, Zhang S, Zhao Z, Rivkees SA, Schwartz RJ, Imanaka-Yoshida K. **(2001)** Rho kinases play an obligatory role in vertebrate embryonic organogenesis. *Development*. Aug;128(15):2953-62

Wells RG **(2008)** The role of matrix stiffness in regulating cell behavior. *Hepatology*. Apr;47(4):1394-400

Yang L, Soonpaa MH, Adler ED, Roepke TK, Kattman SJ, Kennedy M, Henckaerts E, Bonham K, Abbott GW, Linden RM, *et al.,* **(2008)** Human cardiovascular progenitor cells develop from a KDR+ embryonic-stem-cell-derived population. *Nature*. 7194, 524-8

Zhao Z, Rivkees SA. **(2003)** Rho-associated kinases play an essential role in cardiac morphogenesis and cardiomyocyte proliferation. *Dev Dyn*. Jan;226(1):24-32.

Zhang D, Shadrin IY, Lam J, Xian HQ, Snodgrass HR, Bursac N. **(2013)** Tissue-engineered cardiac patch for advanced functional maturation of human ESC-derived cardiomyocytes. *Biomaterials* 34, 5813–5820

Chapter 3

Metabolic Maturation of Human Cardiomyocytes Derived from Pluripotent Stem Cells

This chapter introduces the metabolism as a characterizing feature of a cardiomyocyte, highlighting the importance of proper metabolic phenotype for *in vitro* applications of hPSC-CMs. First, the cardiac metabolism and the developmental changes are described and compared to the immature phenotype displayed by cardiomyocytes derived from hPSCs. Secondly, an assay for evaluating the metabolic hPSC-CMs maturation based on a hypoxia-resistance analysis is proposed; specifically, microfluidics-based technologies for oxygen control *in vitro* and human cell cultures developed. At last, a metabolite-driven metabolic maturation approach is proposed.

Detailed cell cultures protocols are described in **Appendix A**, while microfluidic device fabrication and validation procedure are reported in **Appendix B**. All experimental data presented in **Paragraph 3.3** are contained in manuscripts attached in **Annex 2** and **Annex 3**.

3.1 Cardiomyocyte metabolism

The heart is the most energetically demanding organ in the human body. In order to face the work load of continuous contraction activity with an average 70 beats *per* minute, it is estimated to burn at least 6 kilograms of ATP daily (Neubauer, 2007). The metabolic setup necessary to generate this amount of ATP characterizes a cardiomyocytes as much as the ability to use it through electrophysiological homeostasis, calcium cycling and contraction. Despite the high-energy demand, the adult heart does not have energy reserves and must continually produce energy, feature that accounts for its high susceptibility to nutrient-deprivation stresses during pathological events such as ischemia (Lopaschuk *et al.,* 2010).

The metabolism of adult cardiomyocyte relies for more than 90% on mitochondrial oxidation of energetic substrates and, although it can rapidly switch from one primary carbon source to another, the preferred substrate for oxidation are fatty acids (Fig 3.1A) (Lopaschuk and Jaswal, 2010). This preferential substrate usage reflects especially on the mitochondria content and structure: in adult cardiomyocytes mitochondria are tightly organized along the sarcomeric structures of the contractile machinery (Garcia-Perez *et al.,* 2008) and account for at least 30% of the cellular volume (Piquereau *et al.,* 2013); moreover, mitochondrial genes related to β-oxidation and respiratory chain are a hallmark of an adult phenotype from a transcriptomic and proteomic point of view (Fig. 3.1B) (Pohjoismäki *et al.,* 2013).

During the heart development, the embryonic and fetal cardiomyocytes display a strikingly different metabolic phenotype than the adult ones, relying mostly on glycolysis for their ATP production (Fig. 3.1C). The switch from a glycolytic towards an oxidative metabolism occurs very rapidly after birth, when in a matter of days blood levels of oxygen and fatty acids abruptly increase (Knopp *et al.,* 1986), while lactate and insulin average concentrations decrease more than tenfold (Medina, 1985; Girard *et al.,* 1992). The process is mirrored by transcriptome and proteome changes, with vast down-regulation of components

of the glycolytic pathway (such as GLUT-1 and HK-1) and up-regulation of those of the β-oxidation pathway (for example, ACADVL and CPT1b) (Pohjoismäki *et al.,* 2013).

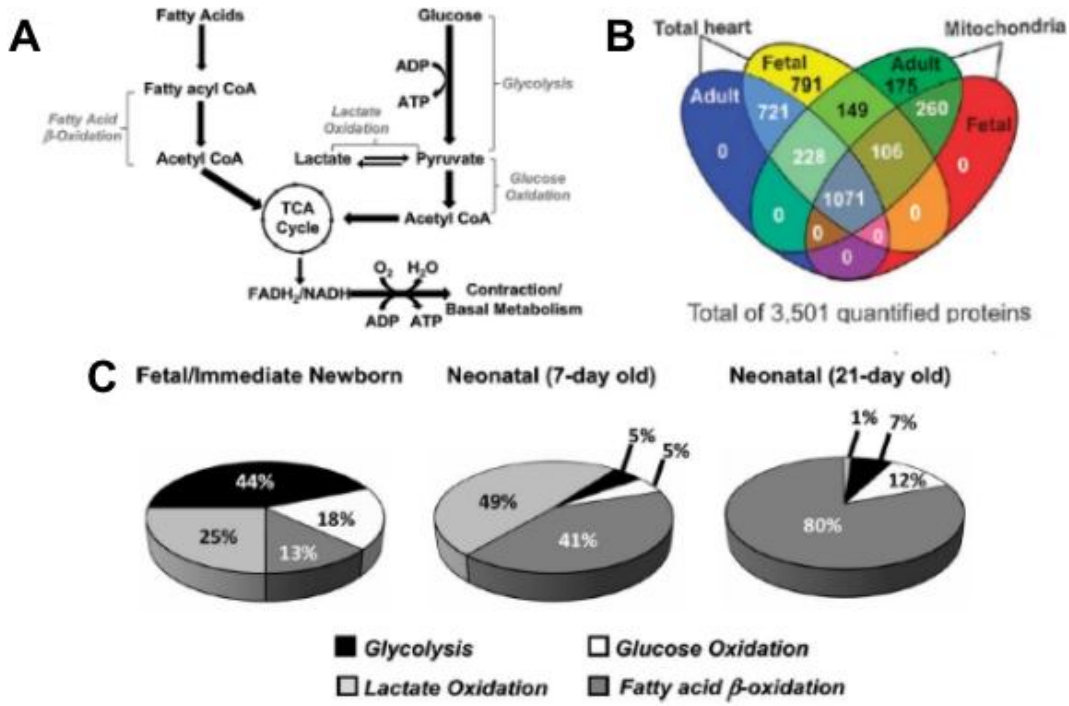

Fig. 3.1 Cardiac metabolism in development. (A) Pathways of energy substrate metabolism in ATP production of a cardiomyocyte. **(B)** Differentially expressed proteins in human adult and fetal heart samples. **(C)** Percent contributions of the different pathways to ATP production in isolated rabbit hearts (Lopaschuk and Jaswal, 2010; Pohjoismäki *et al.,* 2013).

The hiPS-derived cardiomyocytes are reported to closely resemble in culture fetal cardiomyocytes and their metabolic phenotype makes no exception (Robertson *et al.,* 2013). The bioenergetic profiling of hPSC-CM provided proof of primarily glucose-based (Rana *et al.,* 2012) or mixed (Hattori *et al.,* 2010) substrate usage, with the associated protein expression patterns heavily shifted toward fetal-like glycolytic programs (Chung *et al.,* 2007). The mitochondrial mass (Hattori *et al.,* 2010) and distribution (St. John *et al.,* 2005) reflects similarly the early phenotype, with a perinuclear distribution of small and poorly networked organelles. Nevertheless, even if at lower levels than human fetal cardiomyocytes (Cao *et al.,* 2008), expression of β-oxidation associated genes is present and the hPSC-CMs display some degree of adaptability in substrate usage, being able to metabolize lactate (Tohyama *et al.,* 2010) and switch to

galactose and fatty acids when completely deprived of glucose (Rana *et al.,* 2012).

3.2 Motivations and experimental design

The work presented in this chapter aims at the development of a fast and reliable screening assay to test the metabolic maturation of hPSC-derived cardiomyocytes. Moreover, we propose a feasible approach for promoting the switch of the hPSC-CMs bioenergetic profile *in vitro* towards a more mature phenotype with a metabolite-driven maturation.

In vitro maturation of hPSC-CMs is a key feature for this cell type to unlock its potential as a robust model for the human cardiac tissue (Cimetta *et al.,* 2013). As described in **Paragraph 2.1** much of the efforts to drive cardiac maturations has been put in structural and functional maturation, as features like electrophysiology are highly appealing for most drug screenings and have been the target of the first human cardiac *in vitro* disease models (**Paragraph 4.1**). Nevertheless, in order to provide a fully representative model of the human adult myocardium it is unavoidable to pursue metabolic maturation for both drug testing, with many drugs resulting in mitochondrial dysfunction (Rana *et al.,* 2011), and for disease modeling. In the latter case, metabolic diseases or pathologies with late onset require a fully mature cardiomyocyte in order to provide meaningful data *in vitro*. Recent reports of required metabolic maturation to recreate pathological phenotypes in hiPS-CM based models strongly support this concept. Chen and colleagues showed that hiPS-CMs derived from an ARVC/D patient, although displaying an aberrant molecular phenotype linked to the pathology, would not show aberrant adipogenesis typical of the disease unless metabolically activated (Kim *et al.,* 2013). In another example, Iacone and colleagues had to promote metabolic maturation and glycolytic-to-oxidative switch in order to model type 2 diabetic cardiomyopathy, a purely metabolic disease (Drawnel *et al.,* 2014).

The adult cardiomyocyte metabolism hugely relies on oxygen supply, as the vast majority of its energy comes from fatty acid mitochondrial oxidation (Harris and Das, 1991) in which O_2 acts as the final electron acceptor (Fig. 3.1A). The entire cardiac machinery depends on the impressive work volume of the mitochondrial network, and when oxygen levels rapidly drop in the cellular microenvironment, the energy shortage triggers stress-adaptive responses while by-products and respiration intermediates accumulate (Chouchani *et al.,* 2014). *In vivo*, such conditions are generated by ischemic events when blood supply is severed to parts of the myocardium and cardiomyocyte death is caused by extensive generation of reactive oxygen species (ROS) accompanying rapid re-oxidation of accumulated succinate following O_2 reintroduction in the electron transport chain (Chouchani *et al.,* 2014). By contrast, fetal cardiomyocytes develop in a low oxygen environment and rely on anaerobic glycolysis for their ATP production, resulting in a relatively hypoxia-resistant phenotype (Robertson *et al.,* 2013). Hence, we reasoned that a good indicator of cardiomyocytes metabolic maturation could be the survival rate to acute ischemia-like events, given that only cardiomyocytes with developed mitochondria and an oxidative metabolism would be affected in these conditions.

To recreate a spatiotemporally controlled hypoxic environment *in vitro*, we employed microengineering techniques and designed a microfluidic device. The use of microscale technologies allows extreme control over cell cultures and the miniaturization and *ad hoc* design of the device permits coupling the system with standard labware and analyses instruments.

In order to activate the metabolic maturation program, we decided to culture the hPSC-CMs in media containing different energetic substrates. Although hPSC-CMs prefer glucose even in presence of other carbon sources, it has been shown that they possess the ability to metabolize several other energetic substrates when cultured in glucose-free media (Rana *et al.,* 2012). This forced fuel-switch resulted in improvement of mitochondrial performance and promoted the expression of β-oxidation related genes at the expense of the glycolysis pathway. Moreover, a tight link between metabolism and cardiac gene expression

programs has been recently proposed, with hypothesis of metabolic signals being triggers for fetal/adult switch (Taegtmeyer *et al.,* 2010). Some evidence of such effect has been reported, when a metabolite-driven maturation of hiPS-derived cardiomyocytes resulted in maturation of structural and functional features along with metabolic switch, with sarcomeric alignment and elongation and improved electrophysiological properties (Drawnel *et al.,* 2014).

3.3 Microfluidic technologies for hypoxia generation

Constant exposure to ambient atmosphere during every handling step in a laboratory makes controlling gas concentrations in cell cultures very challenging, as the chemical gradients are hugely in favor of environmental conditions (i.e. 0.04% vs. 5% of CO_2, or 21% vs. <2% of O_2). In the same way as for routine CO_2 control, recreating a hypoxic environment has been conventionally pursued maintaining the cell cultures in airtight chambers or incubators with macroscopical control over the gas mixtures entering the setup (Fig. 3.2A). These systems are characterized by oxygen equilibration periods in the order of hours and require burdensome equipment for reagent equilibration, culture handling and real-time data acquisition (Allen *et al.,* 2001). The scale-down of the fluid volumes involved in the gas exchange processes is the most straightforward approach for reducing the physical parameters involved in the oxygen stripping process inside a cell culture (Fig. 3.2B) (Russ *et al.,* 2007). The evolution of microengineering techniques and the employment of appropriate biomaterials allow the fabrication of miniaturized culture systems providing new opportunities in controlling the cellular environment (Byrne *et al.,* 2014).

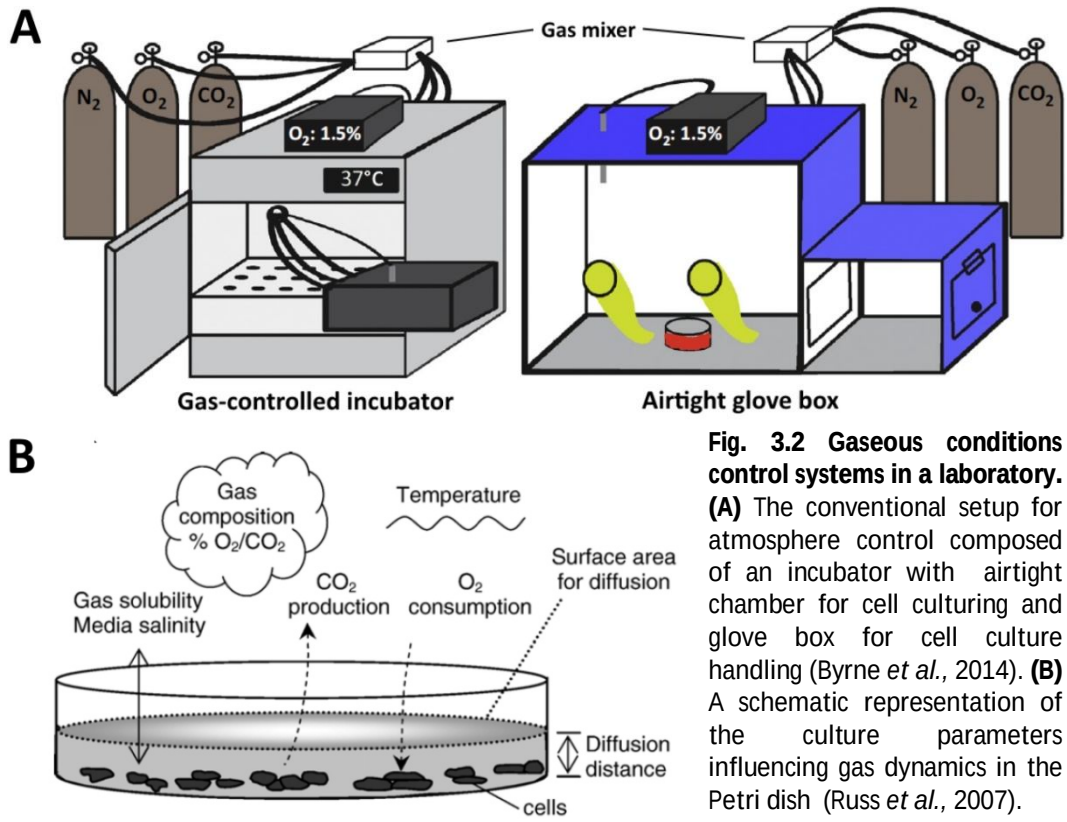

Fig. 3.2 Gaseous conditions control systems in a laboratory. (A) The conventional setup for atmosphere control composed of an incubator with airtight chamber for cell culturing and glove box for cell culture handling (Byrne *et al.,* 2014). **(B)** A schematic representation of the culture parameters influencing gas dynamics in the Petri dish (Russ *et al.,* 2007).

Microfluidic platforms are usually designed as small devices, reducing the operated liquid volumes to the order of microliters. Such dimensions enable precise control over the microenvironment of a cell culture lodged inside, allowing spatial and temporal regulation of specific chemical and gaseous conditions (Oppegard *et al.,* 2009). In particular, the huge increase in the surface-to-volume ratio and the diffusive-regime for mass transport in microfluidic channels benefit gas exchange speeding up enormously the process, thus providing a good opportunity to impose fast changes in oxygen concentrations of the culture media (Martewicz *et al.,* 2012). The two main microfluidic approaches for the design of oxygen controlling device are based on either feeding media pre-equilibration or direct control over the cell culture by laminar flow of oxygen-stripping fluids (Byrne *et al.,* 2014).

An example of the first approach is a device of our design: a bi-modular microfluidic platform composed by a gas-exchanger for medium pre-equilibration and a sealed perfusion microscope chamber for real-time confocal imaging (see **Annex 2** for detailed device description). The low volumes of the

glass channel inside the gas-exchanger (Fig 3.3A) allow rapid oxygen stripping of the flowing liquid and such preconditioned medium is delivered to the cell culture inside the perfusion chamber (Fig 3.3B). In this example of oxygen-controlling device, we showed that fast transients of hypoxia produce alterations of the calcium cycling in contracting cardiomyocytes (Martewicz *et al.,* 2012). However, this type of design does not suite long-term cultures due to the cumbersome handling of a bi-modular device and the need for constant medium flow, which has been proven detrimental to cell cultures by our group (Giulitti *et al.,* 2013).

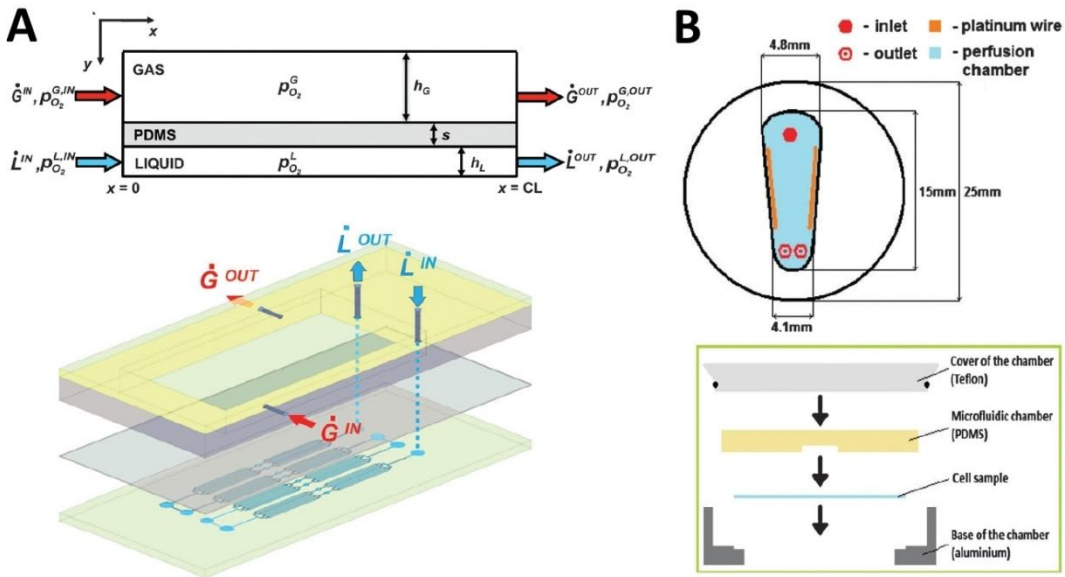

Fig. 3.3 Schematic representation of the bi-modular hypoxia microfluidic device. (A) The gas-exchanger unit is composed of a medium channel etched in glass with a gas chamber above and separated by a thin gas-permeable membrane. **(B)** The perfusion chamber is assembled over a microscope-slide with the cell culture. (Martewicz *et al.,* 2012)

The second microfluidic approach feasible for hypoxia generation is pairing a cell culture chamber with an oxygen-stripping chamber, filled with either oxygen scavenging chemical solutions (Chen *et al.,* 2011; Wang *et al.,* 2013) or gas mixtures (Polinkovsky *et al.,* 2009). In these approaches, oxygen gradients are generated by direct O_2 removal from the culture chamber and the remote control of the composition and flow-rate of the stripping fluids allows the control of the oxygen levels. Both approaches, though, require the maintenance of cell cultures inside the microfluidic device and require optimization of culture conditions, especially with delicate cell types such as hPSC and cardiomyocytes.

In order to develop a functional assay for cardiomyocytes metabolism, we first addressed the issue of long-term cultures of human pluripotent stem cells and human cardiomyocytes inside a microfluidic chip (Luni *et al.,* 2013). We employed a microfluidic platform composed of an array of cell culture channels capable of sustaining human cell cultures with remote control of the culture media (Fig 3.4A, for detailed device description see **Annex 3**). We determined the optimal culture conditions for expansion and maintenance of human pluripotent stem cells inside the microfluidic channels (Fig 3.4B), as well as the conditions for cardiac differentiation (Fig 3.4C). Human cardiomyocytes, either directly differentiated inside the chip or replated from a standard culture plate, maintained their functional features, such as spontaneous contraction and calcium cycling, and could be analyzed by live imaging with confocal microscopy (Fig 3.4D). The perfusion system allowed biochemical stimulation and cellular responses to stimulation with Ca^{2+} dynamics modifying drugs were recorded.

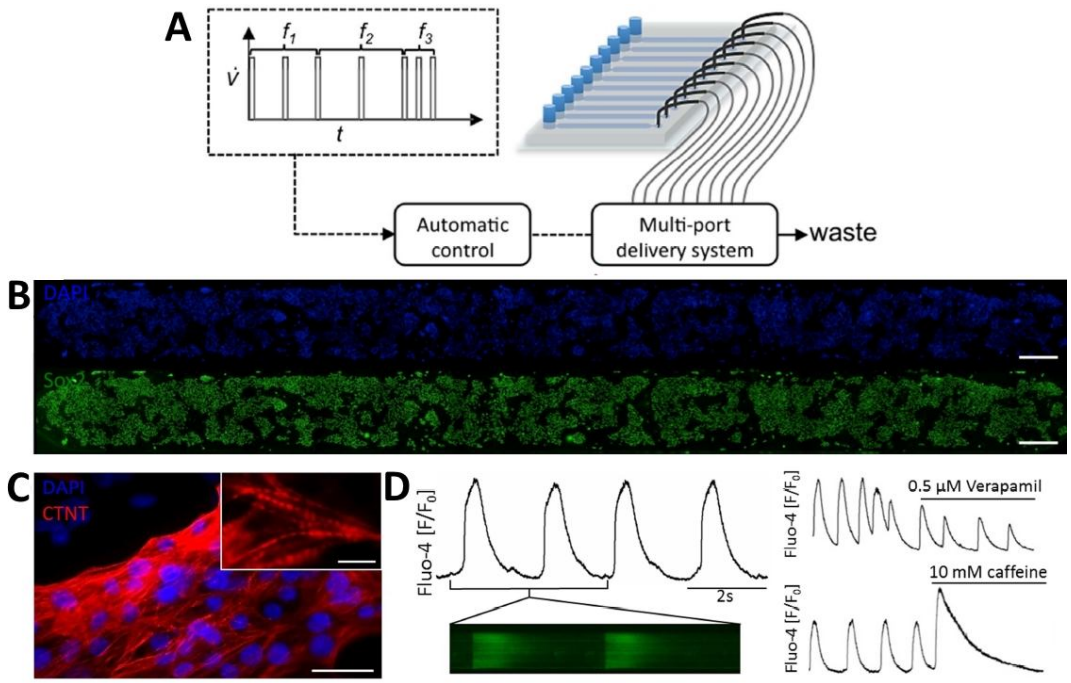

Fig. 3.4 hPSC and hPSC-CMs cultures inside microfluidic channels. (A) Schematic representation of the microfluidic device. **(B)** A culture of human embryonic stem cells inside the microfluidic channel assayed by immunofluorescence for the expression of SOX2 (green) and nuclei counter-stained with DAPI (blue) (scale bar = 100µm).. **(C)** hESC-derived cardiomyocytes inside the microfluidic channel stained for cardiac troponin T (red) (scale bar = 25 µm).displaying **(D)** cardiac-like calcium transients acquired by fluo-4 loading (green line scans) and responding to drug stimulation.

For the generation of stable and highly tunable oxygen conditions, necessary for the setup of the hypoxia-resistance assay, we integrated the technology of the gas-exchanger with the culture techniques optimized in the abovementioned microfluidic platform, achieving a device capable of tight control over the oxygen partial pressure inside a human cardiac culture viable for long-term culture in such experimental setup.

3.4 Hypoxia-resistance assay

In order to provide a tool for evaluating the metabolic differentiation by applying an a ischemic-like stress to a human cardiac culture a new microfluidic platform had to be designed. Hypoxia-resistance would be determined by the survival rate to a hypoxia/reperfusion sequence, quantified by live optical imaging of the cell culture labeled with Live&Dead fluorescent assay. Thus, optical accessibility, complete isolation from the ambient air during the stimulus and fast oxygen dynamics necessary for precise quantification of the stimulus length were required features for the device.

3.4.1 Microfluidic hypoxia device

We based the design of the cell culture chamber on the microfluidic platform employed in the optimization of pluripotent stem cell culture conditions (**Paragraph 3.3**), scaling down the dimensions for better and faster control of the pO_2 (Fig. 3.5A). To allow the O_2 exchange between the liquid and the gas phases, a multi-layer structure was produced, with a 50 μm thick PolyDiMethylSiloxane (PDMS) gas-permeable membrane as interface between a cell culture chamber and the a climatic chamber, where different gas mixtures can be pumped to control pO_2 (Fig. 3.5C). The overall dimensions for the chip were set in order to easily fit the system in a standard 6-well plate for cell cultures and suitable for most microscopy holders of 25 mm Ø (Fig. 3.5B).

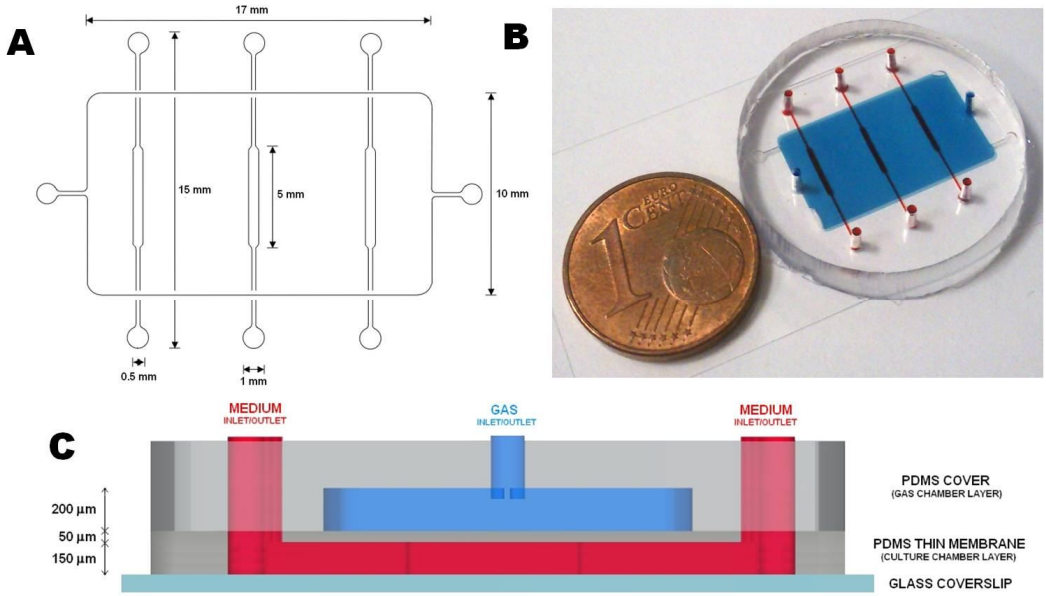

Fig. 3.5 Microfluidic chip for O_2-control in cardiac cultures. (A) Schematic design of the culture and climatic chambers with reported sizes of each component. **(B)** The assemble device with colored dyes as counter stain for the culture chambers (red) and the climatic chamber (blue). **(C)** Schematic cross-section of the device.

Coupling the device with an external gas mixing system allows to precisely control the pO_2 inside the climatic chamber. This was achieved by use of air, nitrogen and carbon dioxide mass flow meters controlled remotely and varying the proportion of N_2 and air, with constant 5% CO_2 for pH control. To test the oxygen equilibration period and the robustness of the system in maintaining the set oxygen levels, we performed experiments with the oxygen-sensitive dye tris(4,7-diphenyl-1,10-phenanthroline)-ruthenium(II) dichloride (Ru(ddp), already employed for the validation of the gas-exchanger (described in **Annex 2**). The dye Ru(ddp) emits green fluorescence when exited at 488 nm and its fluorescence is dynamically quenched by molecular O_2 in a quantitative manner, with linear correlation in the 0-21% pO_2 range (Fig. 3.6A). We, therefore, sequentially changed the composition of the gas entering the climatic chamber and verified fast and stable equilibration to the set pO2 inside the culture chamber (Fig. 3.6B).

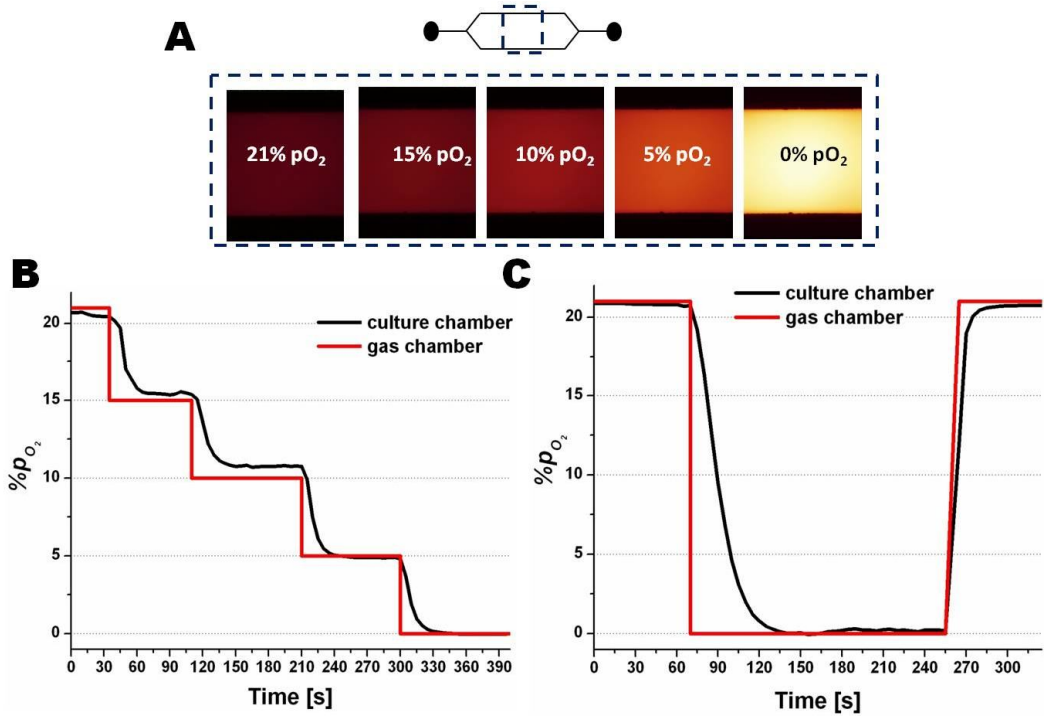

Fig. 3.6 Oxygen equilibration dynamics in the microfluidic device. (A) False-colors fluorescence photographs of the middle section of a culture chamber filled with Ru(ddp) oxygen-sensitive dye. Ru(ddp)fluorescence is proportional to molecular O_2 concentrations. **(B)** Quantification of Ru(ddp) fluorescence allows precise determination of the pO_2 inside the culture chamber. **(C)** The oxygen-stripping dynamics under sudden total oxygen deprivation are below 60 seconds.

The time scale of the oxygen dynamics at variations from 21% pO_2 to 0% pO_2 was assessed to be in the order of seconds, with plateau reached after 60 seconds of flow variation (Fig. 3.6C).

3.4.1 Assay validation with murine primary cultures

We then sought to integrate a cardiac cell culture with the microfluidic device and test the hypoxia-resistance assay. Primary cardiac cultures were obtained from newborn rats (p3) and used as *bona fide* cardiomyocyte model (Chlopcíková *et al.*, 2001). Optimization of the seeding and culturing conditions was necessary, as the 300 nl volume and limited height of the microfluidic channel pose significant differences relative to standard petri dish cultures. To achieve a homogeneous culture composed by 85%±2% of cardiomyocytes a high density plating of 8000 cells/µl was necessary, in order to provide immediate contact inhibition to proliferating fibroblast, and given the limited nutrient supply fresh medium was perfused every 12 hours (Fig. 3.7). Such cardiac cultures were

maintained up to 7 days without negative effects on normal cell morphology or spontaneous contraction.

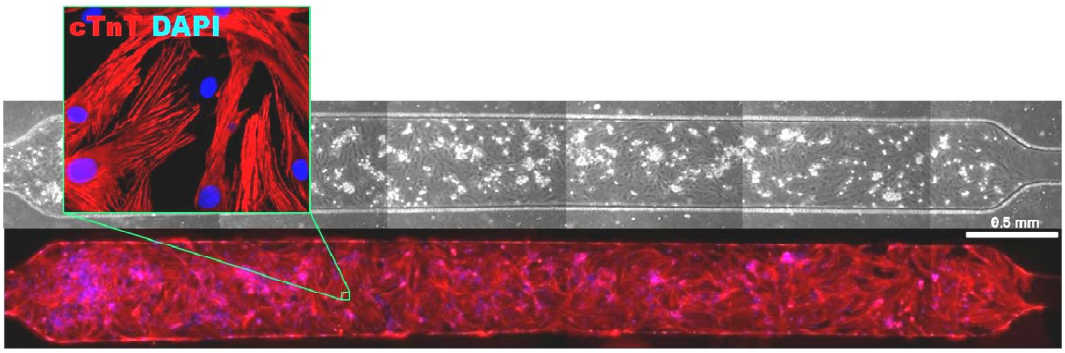

Fig. 3.7 Integration of cardiac culture with the hypoxia-device. Immunofluorescence staining for cardiac troponin T (cTnT, red) in rat neonatal cardiomyocytes cultured in the microfluidic chip for 4 days.

The neonatal rat cardiomyocytes were subjected to a 3 hours long hypoxia-stress followed by 3 hours of reperfusion with media equilibrated to ambient pO_2. Because neonatal cardiomyocytes still retain the ability to switch glycolysis when oxygen is not available, we employed a serum-free DMEM without glucose during the hypoxic period. The amount of cellular damage during hypoxia/reperfusion (H/R) events is deeply dependent on the duration of the hypoxic stimulus, thus we aimed at establishing threshold duration of the hypoxic phase at which the effect on cell survival would be prominent. In some published studies, we found that 150 minutes of hypoxia result in ~70% survival rate (Gorbe *et al.,* 2010), thus we designed our experimental protocol as described in Fig. 3.8A: 3 hours of hypoxia in DMEM without glucose, followed by 3 hours of reperfusion with cardiac culture medium. Exposing the cell to 1 and 2 hours of hypoxia (Fig. 3.8B&C) did not produced significant mortality, while a 3 hours exposure produced massive cell death, clearly visible in Fig. 3.8D. The quantification of di-ethidium bromide-stained nuclei resulted in a ~70% mortality rate, and this value was consistent through different analyzed samples (Fig. 3.8E).

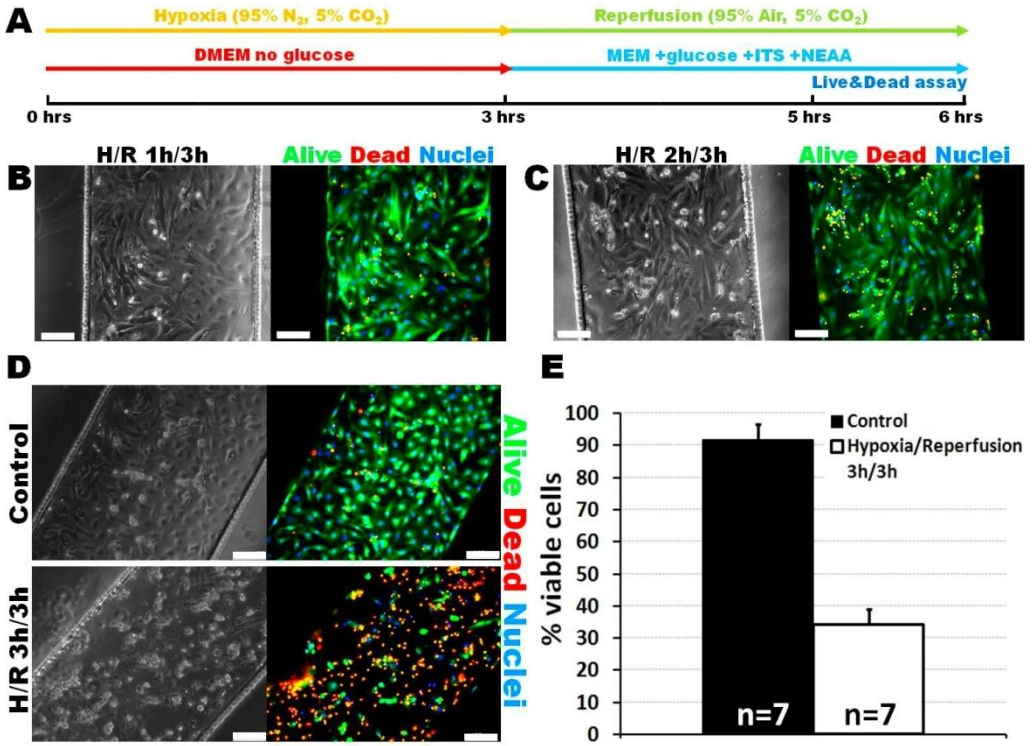

Fig. 3.8 Hypoxia-resistance validation with murine cardiomyocytes. (A) Experimental design for the hypoxia protocol. **(B)** One hour and **(C)** two hours of hypoxia followed by reperfusion do not affect sensibly the cardiomyocyte survival rate. **(D)** Representative images of Live&Dead staining inside the microfluidic channels for control samples (same media conditions, 3+3 hrs of 20% O2) and hypoxia-subjected samples. **(E)** Mortality quantification by count of di-ethidium Bromide stained nuclei. (scale bars = 100µm)

Microfluidic devices provide multiple advantages over standard culture methods, one of which is the precise spatial control over the cell environment. We analyzed the cardiac cultures along the microfluidic channel after the H/R stress in order to verify the absence of oxygen gradients that would make the mortality unreliable. As expected, the whole culture chamber displayed homogeneous mortality rates, but we were positively surprised by the presence of >90% viable cultures at the edges of the climatic chamber (Fig. 3.9). PDMS is a highly gas permeable polymer and allows oxygen diffusion at nearly the same rate as water (Martewicz *et al.,* 2012), thus the portions of the culture channels not underneath the climatic channel did not experience any hypoxic stress and were constantly maintained at the incubator atmosphere. The precision of the hypoxic environment localization is in the range of few tens of microns, and the presence of such "protected" areas provides a good internal control over the experimental conditions.

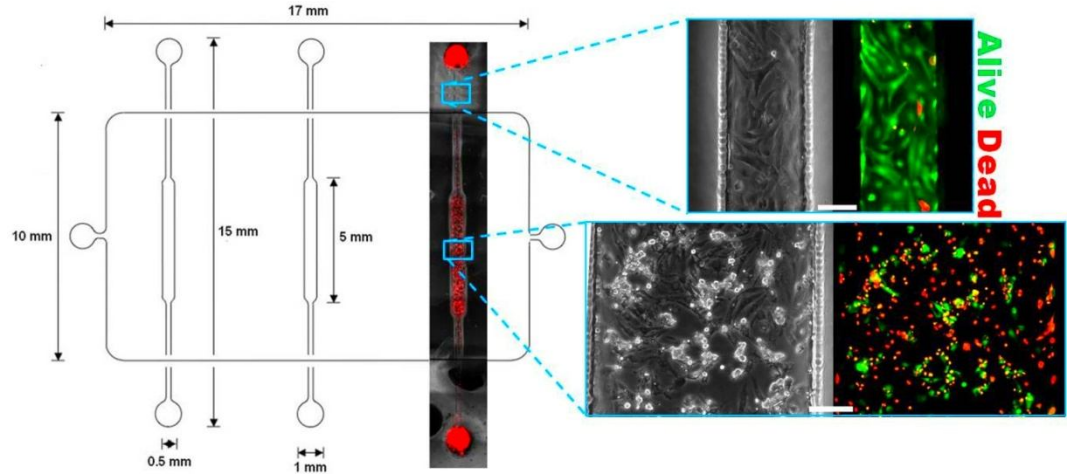

Fig. 3.9 Spatial control over the hypoxic environment. A schematic representation of the microfluidic device with a composite picture of a culture channel after cardiomyocytes were subjected to hypoxia/reperfusion (stained with ethidium bromide in red). The hypoxic stress affects only the cardiomyocytes inside the culture chamber area in contact with the climatic chamber, while protected areas remain viable (scale bar = 100µm).

3.5 Metabolite-driven hiPSC-CMs maturation

We then proceeded with analyzing the response to hypoxia of human cardiomyocytes differentiated from hPSC. We employed for these experiments the embryonic stem cell line HES2, already described in **Paragraph 2.4.1**, and the hiPS healthy cell line mRNA-Clone1. Data reported in this chapter refer to the latter line, unless otherwise stated, although both of the lines were used to the set up of the experimental conditions. In order to obtain large numbers of highly pure cardiomyocytes, we employed a monolayer differentiation approach (see **Appendix A**), that is more efficient in terms of cardiomyocyte yield and time of the cardiac differentiation process. The expression of pluripotency and cardiac markers for mRNA-Clone1 was routinely assessed (Fig. 3.10).

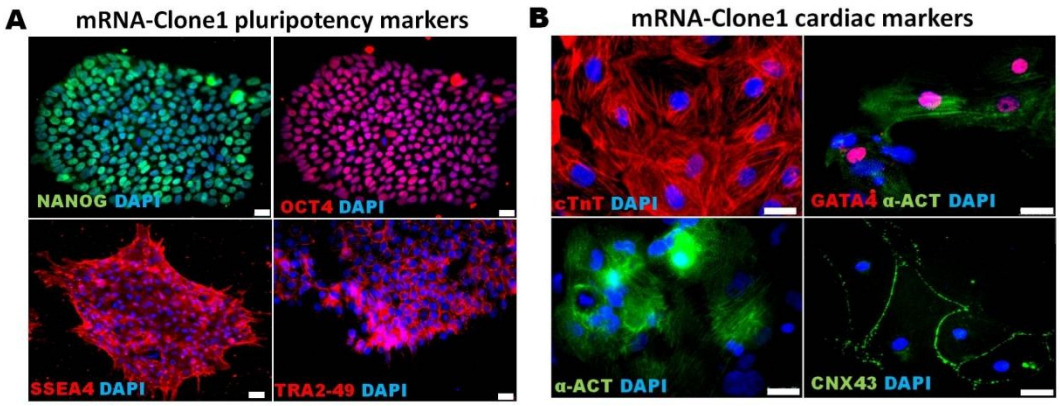

Fig. 3.10 Expression of pluripotency and cardiac markers in mRNA-Clone1. (A) Pluripotency-specific transcription factors and surface markers are expressed. **(B)** After differentiation mRNA-Clone1-derived cardiomyocytes spontaneously contract and express cardiac-specific proteins.

hiPS-CMs were replated in the microfluidic chip and maintained in culture for 4 days before further testing. Prior to hypoxia induction, the maintenance of wide spread spontaneous contractile activity was assessed.

As hiPS-CMs display fetal-like phenotype and they are known for high glycolytic capacity, it was not unexpected finding they were hypoxia-resistant, to the extent of the duration of the assay set up with the rat neonatal cardiomyocyte (Fig. 3.11A). In order to provide a more harsh stress to the cells, we attempted to couple hypoxia with complete nutrient deprivation, subjecting the culture to 3 hours of hypoxia in DPBS saline solution supplemented only with calcium and magnesium. Complete energy substrate deprivation did not produce any significant effect over the survival rate of the hCMs (Fig. 3.11B). Nutrient deprivation is a big issue for adult cardiomyocytes *in vivo* as they do not possess intracellular energy stores (Thijssen *et al.,* 2001), but hPSC-CMs are more immature and display increased plasticity in response to stressors. This made us investigate the possibility of glycogen accumulation in the hiPS-CMs, a feature to our knowledge never reported in literature in association to their metabolic phenotype.

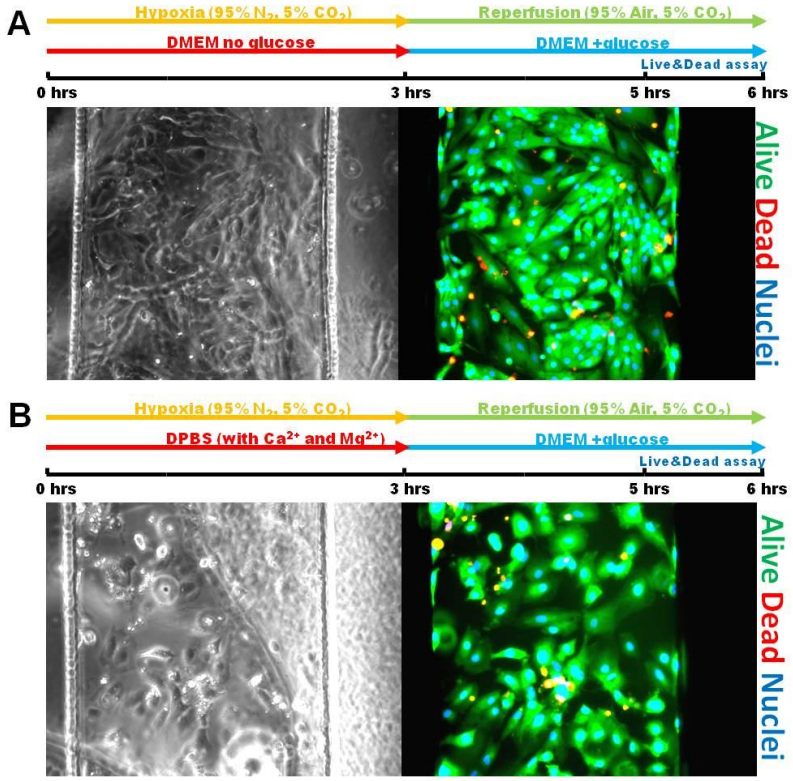

Fig. 3.11 Hypoxia-resistance assay on hiPS-CMs. (A) hCMs differentiate from hiPS cells (mRNA-Clone1) were replated inside the microfluidic chip and assayed for hypoxia-resistance. The human cardiac culture proves to be metabolically immature as the survival rate to the hypoxic stress id >90%. **(B)** Hypoxic stress delivered in pure saline solution (DPBS) proves high resistance of the cell type to hypoxia and nutrient deprivation.

We performed a periodic acid-Schiff (PAS) staining on the differentiated cardiac cultures, for both embryonic-derived and induced pluripotent-derived cardio myocytes, and observed strong accumulation of glycogen (Fig. 3.12). This feature provides a supplementary evidence of the early and immature phenotype of this cell type, but additionally provides a possible early readout for our metabolic maturation assay. Intracellular energy stores, especially feeding the anaerobic glycolytic metabolism, will compensate for any nutrient or oxygen deprivation stress we could provide to the cell culture, while being itself a hallmark of a fetal metabolic program.

The "basal medium" employed for the maintenance of hiPS-CMs is RPMI supplemented with B27, which was originally designed for culture of primary hippocampal neurons (Brewer and Cotman, 1989) and is very rich in proteins, hormones and especially energy carbon sources: D-glucose, D-galactose, L-carnitine and L-glutamine, and three different fatty acids (Burridge *et al.,* 2014).

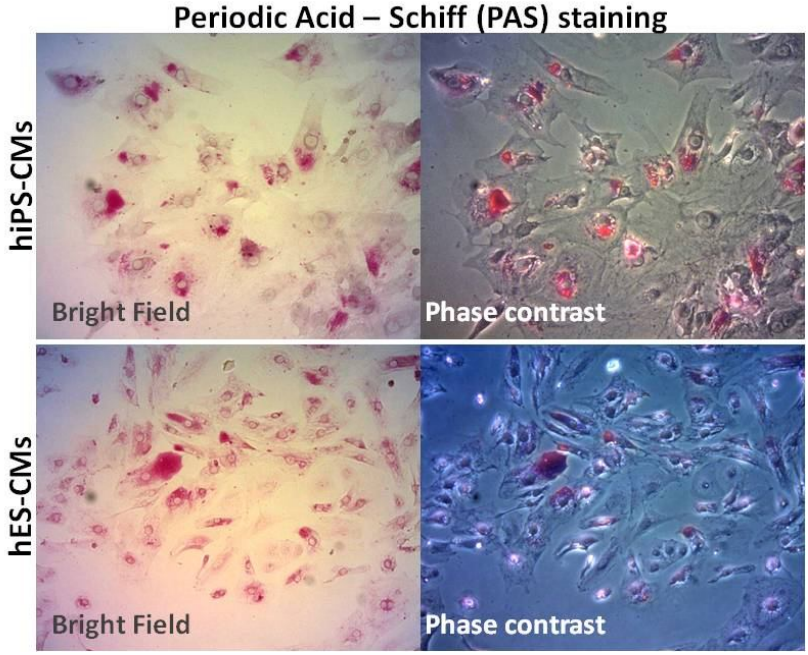

Fig. 3.12 Energy reserve stores in hPSC-CMs. The hCM derived from hPSC display big stores of glycogen in PAS staining. The glycogen stores account for the nutrient deprivation resistance and provide a readout for hPSC-CMs immaturity.

We decided to induce a metabolic switch in the human CMs by restraining the carbon source availability in the maintenance media in cardiac cultures 1 month old, in a similar fashion already reported by Rana and colleagues (Rana *et al.,* 2012).We designed two different induction media:

i) DMEM without D-glucose supplemented with 30 μM BSA-Linoleic acid and 0.1% insulin-transferrin-selenium solution (170 nM insulin);

ii) αMEM supplemented with 0.1% insulin-transferrin-selenium solution and 0.1% NonEssentialAmminoAcids.

In the first case, we avoided D-galactose to provide the cardiomyocytes with metabolite with solely mitochondrial catabolism (L-glutamine and fatty acids).

The second "essential cardiac medium" final formulation was derived by modifying murine neonatal cardiac culture media and contains as well 3 mitochondrial energy sources (L-gluamine, pyruvate and lipoic acid), but retains low 5.5 mM D-glucose concentration. We observed that the use of animal sera even at low concentrations (Martewicz *et al.,* 2012 and **Annex 2**) in primary cardiomyocyte maintenance media results in a high resistance to hypoxia,

accordingly to our assay (data not shown). Further literature research provided us with evidence of the use of serum-free maintenance media in many ischemia-reperfusion studies on cardiac *in vitro* cultures (Addlerley *et al.,* 1999; Akao *et al.,* 2001).

We treated the differentiated human cardiac cultures with the maturation media for 4 days and assayed them for glycogen accumulation. Control cells maintained in rich "basal medium" displayed a very strong PAS staining (Fig. 3.13), recapitulating the results previously obtained on dissociated single hCMs.

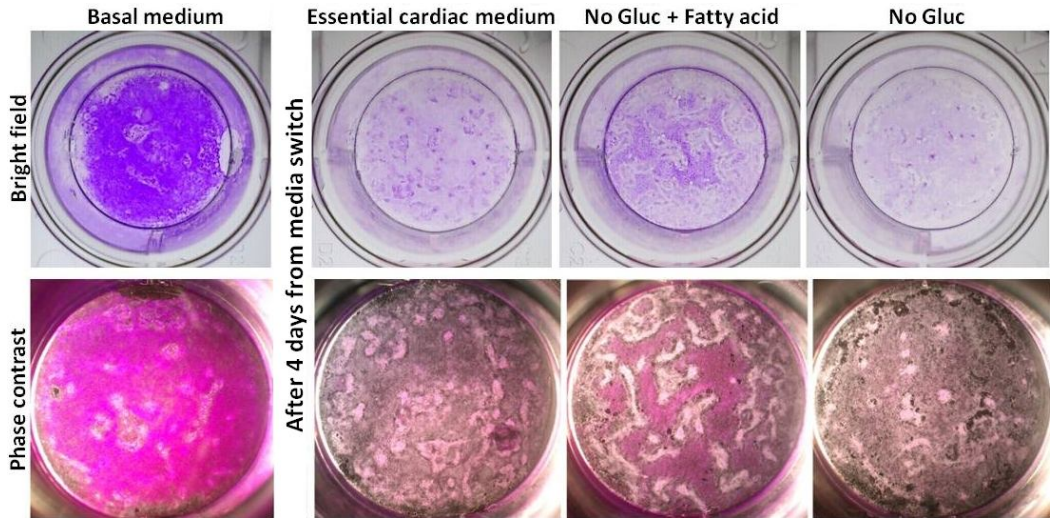

Fig. 3.13 Metabolite-driven metabolic switch. Human cardiomyocytes maintained in the basal differentiation medium maintain high stores of glycogen after differentiation. After switching from basal medium to media containing different carbon sources, hCMs deplete rapidly the glycogen stores

On the other hand, both maturation media drastically reduced the amount of glycogen present in the culture, with a better performance shown by the "essential cardiac medium". In cardiac cultures treated with media containing only linoleic acid, displayed a strong reduction in overall PAS staining, but cardiomyocytes still retained a significant glycogen stores (Fig. 3.13). In comparison cultures maintained as controls in only DMEM w/o D-glucose showed instead almost complete glycogen depletion. This result is in line with the effect of free fatty acids on glycogenesis and glycogenolysis, as the latter is inhibited in presence of high concentrations of fatty acids, while they are still preferred as energetic substrate by the cardiomyocytes. It is a worth noticing that cardiac cultures maintained in DMEM w/o D-glucose for 4 days still

displayed sustained and regular contractile activity, obviously burning out all the glycogen stores and perhaps the amino acids present in the DMEM. Unfortunately, extended culture with DMEM w/o D-glucose, either in presence of absence of fatty acids, could not support the human cardiac culture for longer than 7-10 days. Instead, cardiomyocytes cultured in the "essential cardiac medium" sustained contractile activity and long-term viability, up to 2 months.

We decided to proceed with exploratory experiment to assess the hypoxia-resistance of these cultures inside the microfluidic chip, noticing an increased susceptibility to replating, with fewer numbers of cardiomyocytes adhering to the glass slides. In order to avoid cell number variability inside the culture, the cardiomyocyte replating inside the chip was performed from the same cardiac cultures maintained in "basal medium" and switched to the maturation medium after 24hours of adhesion, for at least 4 days before further experimental procedure. The first attempts to assay these mature cultures for hypoxia-sensitivity resulted in high death rates of the human cardiomyocytes resulting in unreliable quantification for <10% of surviving cells (Fig. 3.14). This result could suggest a inferior resistance to hypoxic stress of the metabolically-induced cardiomyocytes, and an new optimization of the stimuli duration is required for robust data.

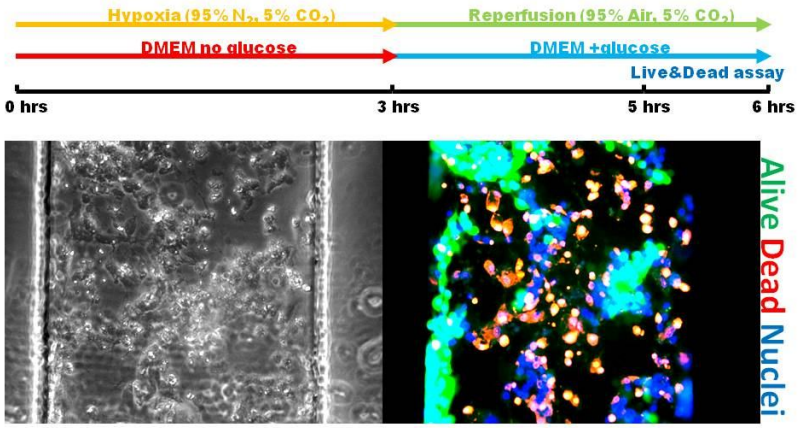

Fig. 3.14 Hypoxia-resistance assay on hCMs underwent metabolic switch. hPSC-CMs replated inside the microfluidic device and treated for 4 days with "essential cardiac medium" display high sensitivity to hypoxic stress, suggesting possible metabolic maturation.

Further investigations are ongoing on the transcriptomic and proteomic changes induced by short-term and long-term culture in the "essential cardiac medium", in order to characterize more in detail the metabolic and molecular phenotype acquired by these hypoxia-sensitive cardiomyocytes.

3.6 Conclusions

In this chapter we described the metabolic profile of an adult human cardiomyocytes, defining this phenotype as highly desirable in the *in vitro* human cardiac models based on hPSC-derived cardiomyocytes. For all the differentiation methods described in literature, almost no metabolic maturation is reported and all the cardiac differentiation derivatives display an early and immature mainly glycolytic metabolism. While most screening methods for maturation are based on evaluation of molecular markers expression, we designed here a functional approach, to rapidly screen maturation protocols and select those generating cardiomyocytes with hypoxia-sensitive phenotype for further characterization. In our perspective, hypoxia-sensitivity is the integration of several structural and proteomic changes in the developing cardiomyocyte, thus providing a holistic read-out on several maturation features at once.

We propose, as well, a simple method to drive the metabolic phenotype-switch in human cardiomyocyte derived from hPSCs, with variation in the composition of supplied metabolites, thus providing a "physiological" induction of the process without biochemical or genetic modification of the culture.

Moreover, the developed microfluidic platform has proven to be robust in delivering precisely tuned oxygen stimuli and capable of sustaining a cell culture for long-term experiments, thus can be used as a valuable tool for *in vitro* studies of ischemia/reperfusion models or long-term effects of different gaseous phase compositions in cell cultures.

3.7 References

Adderley SR, Fitzgerald DJ. **(1999)** Oxidative damage of cardiomyocytes is limited by extracellular regulated kinases 1/2-mediated induction of cyclooxygenase-2. *J Biol Chem*. Feb 19;274(8):5038-46.

Akao M, Ohler A, O'Rourke B, Marbán E. **(2001)** Mitochondrial ATP-sensitive potassium channels inhibit apoptosis induced by oxidative stress in cardiac cells. *Circ Res*. Jun 22;88(12):1267-75.

Allen CB, Schneider BK, White CW. **(2001)** Limitations to oxygen diffusion and equilibration in in vitro cell exposure systems in hyperoxia and hypoxia *Am J Physiol Lung Cell Mol Physiol.* Oct;281(4):L1021-7

Brewer GJ, Cotman CW. **(1989)** Survival and growth of hippocampal neurons in defined medium at low density: advantages of a sandwich culture technique or low oxygen. *Brain Res*. 494, 65–74

Burridge PW, Matsa E, Shukla P, Lin ZC, Churko JM, Ebert AD, Lan F, Diecke S, Huber B, Mordwinkin NM, *et al.* **(2014)** Chemically defined generation of human cardiomyocytes. *Nat Methods.* Aug;11(8):855-60

Byrne MB, Leslie MT, Gaskins HR, Kenis PJ. **(2014)** Methods to study the tumor microenvironment under controlled oxygen conditions. *Trends Biotechnol.* Nov;32(11):556-63

Cao F, Wagner RA, Wilson KD, Xie X, Fu JD, Drukker M, Lee A, Li RA, Gambhir SS,Weissman IL, *et al.* **(2008)** Transcriptional and functional profiling of human embryonic stem cell-derived cardiomyocytes. *PLoS One* 3:e3474

Chen YA, King AD, Shih HC, Peng CC, Wu CY, Liao WH, Tung YC. **(2011)** Generation of oxygen gradients in microfluidic devices for cell culture using spatially confined chemical reactions. *Lab Chip* 11, 3626–3633

Chlopcíková S, Psotová J, Miketová P. **(2001)** Neonatal rat cardiomyocytes--a model for the study of morphological, biochemical and electrophysiological characteristics of the heart. *Biomed Pap Med Fac Univ Palacky Olomouc Czech Repub*. Dec;145(2):49-55

Chouchani ET, Pell VR, Gaude E, Aksentijević D, Sundier SY, Robb EL, Logan A, Nadtochiy SM, Ord EN, Smith AC, *et al.* **(2014)** Ischaemic accumulation of succinate controls reperfusion injury through mitochondrial ROS. *Nature.* Nov 20;515(7527):431-5

Chung S, Dzeja PP, Faustino RS, Perez-Terzic C, Behfar A, Terzic A. **(2007)** Mitochondrial oxidative metabolism is required for the cardiac differentiation of stem cells. *Nat Clin Pract Cardiovasc Med.* Feb;4 Suppl 1:S60-7

Cimetta E, Godier-Furnémont A, Vunjak-Novakovic G. **(2013)** Bioengineering heart tissue for in vitro testing. *Curr Opin Biotechnol*. Oct;24(5):926-32

Drawnel FM, Boccardo S, Prummer M, Delobel F, Graff A, Weber M, Gérard R, Badi L, Kam-Thong T, Bu L, *et al.* **(2014)** Disease modeling and phenotypic drug screening for diabetic cardiomyopathy using human induced pluripotent stem cells. *Cell Rep*. Nov 6;9(3):810-21

Garcia-Perez C, Hajnoczky G, Csordas G **(2008)** Physical coupling supports the local Ca2+ transfer between sarcoplasmic reticulum subdomains and the mitochondria in heart muscle. *J Biol Chem* 283:32771–32780.

Girard J1, Ferré P, Pégorier JP, Duée PH. **(1992)** Adaptations of glucose and fatty acid metabolism during perinatal period and suckling-weaning transition. *Physiol Rev*. Apr;72(2):507-62

Giulitti S, Magrofuoco E, Prevedello L, Elvassore N. **(2013)** Optimal periodic perfusion strategy for robust long-term microfluidic cell culture. *Lab Chip.* Nov 21;13(22):4430-41

Gorbe A, Giricz Z, Szunyog A, Csont T, Burley DS, Baxter GF, Ferdinandy P. **(2010)** Role of cGMP-PKG signaling in the protection of neonatal rat cardiac myocytes subjected to simulated ischemia/reoxygenation. *Basic Res Cardiol.* Sep;105(5):643-50

Harris DA, Das AM **(1991)** Control of mitochondrial ATP synthesis in the heart. *Biochem J* 280:561–573.

Hattori F, Chen H, Yamashita H, Tohyama S, Satoh YS, Yuasa S, Li W, Yamakawa H, Tanaka T, Onitsuka T *et al.* **(2010)** Nongenetic method for purifying stem cell-derived cardiomyocytes. *Nat Methods* 7:61–66

Kim C, Wong J, Wen J, Wang S, Wang C, Spiering S, Kan NG, Forcales S, Puri PL, Leone TC *et al.* **(2013)** Studying arrhythmogenic right ventricular dysplasia with patient-specific iPSCs. *Nature.* Feb 7;494(7435):105-10

Knopp RH, Warth MR, Charles D, Childs M, Li JR, Mabuchi H, Van Allen MI. **(1986)** Lipoprotein metabolism in pregnancy, fat transport to the fetus, and the effects of diabetes. *Biol Neonate.* 50:297–317

Lopaschuk G, Jaswal J. **(2010)** Energy metabolic phenotype of the cardiomyocyte during development,differentiation and postnatal maturation. *J Cardiovasc Pharmacol.* 56(2):130–140

Lopaschuk GD, Ussher JR, Folmes CD, Jaswal JS, Stanley WC. **(2010)** Myocardial fatty acid metabolism in health and disease. *Physiol Rev*. Jan;90(1):207-58

Luni C, Michielin F, Barzon L, Calabrò V, Elvassore N. **(2013)** Stochastic model-assisted development of efficient low-dose viral transduction in microfluidics. *Biophys J.* Feb 19;104(4):934-42

Martewicz S, Michielin F, Serena E, Zambon A, Mongillo M, Elvassore N. **(2012)** Reversible alteration of calcium dynamics in cardiomyocytes during acute hypoxia transient in a microfluidic platform. *Integr Biol (Camb).* Feb;4(2):153-64.

Medina JM. **(1985)** The role of lactate as an energy substrate for the brain during the early neonatal period. *Biol Neonate.* 48:237–244

Neubauer S. **(2007)** The failing heart--an engine out of fuel. *N Engl J Med*. Mar 15;356(11):1140-51

Oppegard SC, Nam KH, Carr JR, Skaalure SC, Eddington DT. **(2009)** Modulating temporal and spatial oxygenation over adherent cellular cultures. *PLoS One*. Sep 3;4(9):e6891

Pohjoismäki JL, Krüger M, Al-Furoukh N, Lagerstedt A, Karhunen PJ, Braun T. **(2013)** Postnatal cardiomyocyte growth and mitochondrial reorganization cause multiple changes in the proteome of human cardiomyocytes. *Mol Biosyst.* Jun;9(6):1210-9

Polinkovsky M, Gutierrez E, Levchenko A, Groisman A. **(2009)** Fine temporal control of the medium gas content and acidity and on-chip generation of series of oxygen concentrations for cell cultures. *Lab Chip.* Apr 21;9(8):1073-84

Piquereau J, Caffin F, Novotova M, Lemaire C, Veksler V, Garnier A, Ventura-Clapier R, Joubert F **(2013)** Mitochondrial dynamics in the adult cardiomyocytes: which roles fora highly specialized cell? *Front Physiol* 4:102.

Rana P, Anson B, Engle S, Will Y **(2012)** Characterization of human-induced pluripotent stem cell-derived cardiomyocytes: bioenergetics and utilization in safety screening. *Toxicol Sci* 130:117–131

Rana P, Nadanaciva S, Will Y. **(2011)** Mitochondrial membrane potential measurement of H9c2 cells grown in high-glucose and galactose-containing media does not provide additional predictivity towards mitochondrial assessment. *Toxicol In Vitro*. Mar;25(2):580-7

Robertson C, Tran DD, George SC. **(2013)** Concise review: maturation phases of human pluripotent stem cell-derived cardiomyocytes. *Stem Cells.* 31, 829-37

Russ AL, Haberstroh KM, Rundell AE. **(2007)** Experimental strategies to improve in vitro models of renal ischemia. *Exp Mol Pathol.* Oct;83(2):143-59

St John JC, Ramalho-Santos J, Gray HL, Petrosko P, Rawe VY, Navara CS, Simerly CR, Schatten GP **(2010)** The expression of mitochondrial DNA transcription factors during early cardiomyocyte in vitro differentiation from human embryonic stem cells. *Cloning Stem Cells* 7:141–153ù

Taegtmeyer H, Sen S, Vela D **(2010)** Return to the Fetal Gene Program: A Suggested Metabolic Link to Gene Expression in the Heart. *Ann. N. Y. Acad. Sci.* 1188, 191–198

Thijssen VL, Ausma J, Borgers M**. (2001)** Structural remodelling during chronic atrial fibrillation: act of programmed cell survival. *Cardiovasc Res*. Oct;52(1):14-24

Tohyama S, Hattori F, Sano M, Hishiki T, Nagahata Y, Matsuura T, Hashimoto H, Suzuki T, Yamashita H, Satoh Y*, et al.,* **(2013)** Distinct metabolic flow enables large-scale purification of mouse and human pluripotent stem cell-derived cardiomyocytes. *Cell Stem Cell*. Jan 3;12(1):127-37

Wang, L, Liu W, Wang Y, Wang JC, Tu Q, Liu R, Wang J. **(2013)** Construction of oxygen and chemical concentration gradients in a single microfluidic device for studying tumor cell–drug interactions in a dynamic hypoxia microenvironment. *Lab Chip* 13,695–705

.

Chapter 4

hiPS Technology for *In Vitro* Modeling of Human Cardiac Diseases

This chapter introduces the concept of *in vitro* modeling of human cardiac diseases with the hiPSC-technology. In particular, two human genetic diseases of interest are presented in detail: Duchenne Muscular Dystrophy and Arrhythmogenic Right Ventricular Cardiomyopathy/Dysplasia. Their cardiac fallout is described, as well as the currently employed study models for these diseases and the limitations associated each individual approach. The use of induced pluripotent stem cells derived from patients affected by DMD and ARVC/D allows derivation of cardiomyocytes carrying the patient-associated mutations. For each disease, evidence of aberrant phenotype displayed *in vitro* is presented. Finally their future perspectives for *in vitro* studies are discussed.

4.1 Motivations and experimental design

The work presented in this chapter aims at the derivation of cell models for two human genetic diseases with prominent impact on cardiac function. In order to set up an *in vitro* model, the employed cell type must display the necessary features to represent the target of the study, and for the human heart there has been a shortage for such biological material for a long time.

hiPS cells can be derived from somatic cells of any given individual, thus carrying their specific genetic background and individual polymorphism or mutations. Since the beginning of the hiPSC era, this opportunity carried the great potential for both patient-specific self-therapies and patient-specific "disease-in-a-dish" (Savla *et al.,* 2014). *In vitro* modeling of heart diseases is particularly difficult due to the scarce availability of human tissues, as cardiac biopsies from patients are a very invasive procedure and we lack viable methods of maintaining human adult cardiomyocytes in culture (Sallam *et al.,* 2014). Since 2010, when the first cellular model of the human LQT1 syndrome was published on the New England Journal of Medicine (Moretti *et al.,* 2010) a plethora of other human cardiac diseases has been tackled, of which a comprehensive summary is reported in Table 4.1. The hiPSC generation and differentiation protocols are constantly evolving making the derivation of patient-specific cardiomyocytes relatively easy, and many of the proposed models have successfully proven that it is possible to recreate the *in vivo* pathological phenotype *in vitro* to some degree (Karakikes *et al.,* 2014).

Table 4.1 Summary of published hiPS-based models for cardiac diseases.

Hereditary cardiac diseases		
Arrhythmogenic Right Ventricular Cardiomyopathy/Dysplasia		
	Mutation	**Reference**
	Heterozygous PKP2 (A324fs335X)	Caspi *et al.* 2013
	Homozygous PKP2 c.2484C>T Heterozygous PKP2 c.2013DelC	Kim *et al.,* 2013
	Heterozygous PKP2 (L614P)	Ma *et al.,* 2013
Brugada Syndrome		
	Mutation	**Reference**
	Homozygous PKP2 c.2484C>T	Cerrone *et al.,* 2014
Catecholaminergic Polymorphic Ventricular Tachycardia		
	Mutation	**Reference**
	Heterozygous RYR2 (F2483I)	Zhang *et al.,* 2013
	Heterozygous RYR2 (F2483I)	Di Pasquale *et al.,* 2013
	Homozygous CSQ2 (D307H)	Novak *et al.,* 2012

	Heterozygous RYR2 (P2328S)	Kajula *et al.,* 2012
	Heterozygous RYR2 (M4109R)	Itzhaki *et al.,* 2012
	Heterozygous RYR2 (S406L)	Jung *et al.,* 2012
	Heterozygous RYR2 (F2483I)	Fatima *et al.,* 2011
Dilated CardioMyopathy		
	Mutation	**Reference**
	Heterozygous DES (A285V)	Tse *et al.,* 2013
	Heterozygous LMNA (R225X)	Siu *et al.,* 2012
	Heterozygous TNNT2 (R173W)	Sun *et al.,* 2012 Liang *et al.,* 2013
	Heterozygous LMNA (S17fs40X)	Ho *et al.,* 2011
Hypertrophic CardioMyopathy		
	Mutation	**Reference**
	Heterozygous MYH7 (R442G)	Han *et al.,* 2014
	Heterozygous MYH7 (R663H)	Lan *et al.,* 2013 Liang *et al.,* 2013
Friedreich's Ataxia		
	Mutation	**Reference**
	Heterozygous FXN mutation (GAA expanded repeats intron1)	Hick *et al*., 2013
LEOPARD syndrome		
	Mutation	**Reference**
	Heterozygous PTPN11 (T468M)	Carvajal-Vergara *et al.,* 2010
Long QT syndrome		
	Mutation	**Reference**
	Heterozygous KCNH2 (A561T)	Matsa *et al.,* 2013
	Heterozygous SCN5A (V1763M)	Ma *et al*., 2013
	Heterozygous KCNH2 (N996I)	Bellin *et al*., 2013
	Heterozygous KCNQ1 (G269S)	Liang *et al.,* 2013
	Heterozygous SCN5A (F1473C) & KCNH2 (K897T)	Terrenoire *et al*., 2012
	Heterozygous KCNQ1 (P631fs/33)	Egashira *et al.,* 2012
	Heterozygous KCNH2 (R176W)	Lahti *et al*., 2012
	Heterozygous KCNH2 (A614V)	Itzhaki *et al*., 2011
	Heterozygous KCNH2 (A561T)	Matsa *et al*., 2011
	Heterozygous CACNA1C (G406R)	Yazawa *et al*., 2011
	Heterozygous KCNQ1 (R190Q)	Moretti *et al*., 2010

Pompe Syndrome		
	Mutation	**Reference**
	Homozygous GAA (ex18Del) Heterozygous GAA (c.1441DelT & W746X)	Raval *et al.*, 2014
	Heterozygous GAA (ex18Del & c.525DelT) Heterozygous GAA (ex18Del & ex2Del)	Higuchi *et al.*, 2014
	Homozygous GAA (D645E) Heterozygous GAA (c.1935C>A & c.2040+1G>T)	Huang *et al.*, 2011
Fabry Disease		
	Mutation	**Reference**
	Hemizygous GLA (W162X) Hemizygous GLA (R220X)	Itier *et al.*, 2014
Barth Syndrome		
	Mutation	**Reference**
	Hemizygous TAZ c.517delG Hemizygous TAZ c.328T>C	Wang *et al.*, 2014
Hypoplastic Left Heart Syndrome		
	Mutation	**Reference**
	not published	Jiang *et al.*, 2014
Duchenne Muscular Dystrophy		
	Mutation	**Reference**
	Hemizygous DMD ex50Del	Guan *et al.*, 2014
	Hemizygous DMD ex4-43Del	Zatti *et al.*, 2014
	Hemizygous DMD ex48-50Del Hemizygous DMD ex47-50Del Hemizygous DMD c.3217G>T Hemizygous DMD ex45-52Del Hemizygous DMD c.10171C>T Hemizygous DMD c.4918-4919DelTG Hemizygous DMD c.7437G>A	Dick *et al.*, 2013
Other acquired cardiac diseases		
Type 2 Diabetic Cardiomyopathy		
	high glucose, h-endothelin, cortisol	Drawnel *et al.*, 2014
Viral Myocarditis		
	coxackievirus infection	Sharma *et al.*, 2014

Further development of new models for novel pathologies means creating not only a biological substrate for studies on a specific disease and patient-specific therapeutic design, but will provide as well a growing panel of functional aberrations giving more and more insight in the molecular mechanisms regulating cardiac and cardiomyocyte function.

4.2 Duchenne Muscular Dystrophy

Muscular dystrophies are a heterogeneous group of disorders characterized by progressive wasting and weakness of muscle tissues, with cardiac myopathies and dysfunctions often contributing to the severity of the clinical phenotype (Verhaert *et al.,* 2011). In particular, Duchenne Muscular Dystrophy (DMD) is a severe X-linked disease affecting 1/3500 newborn males, in which genetic mutations in the dystrophin gene account for the pathological phenotype associated with loss-of-function of the muscle-specific dystrophin isoform Dp427m. Dystrophin is the largest gene in the human genome, spanning over 2.4 Mbp and containing 79 exons with at least 7 different internal promoters driving the transcription of 5 classes of different molecular-weight isoforms, each with several splice variants (Muntoni *et al.,* 2003) (Fig. 4.1). Given these characteristics, the tissue-specific transcriptional regulation of these isoforms is uber-complex and even decades its genetic characterization the research on the molecular pathological mechanisms is still a hot topic (Hoffman *et al.,* 1987).

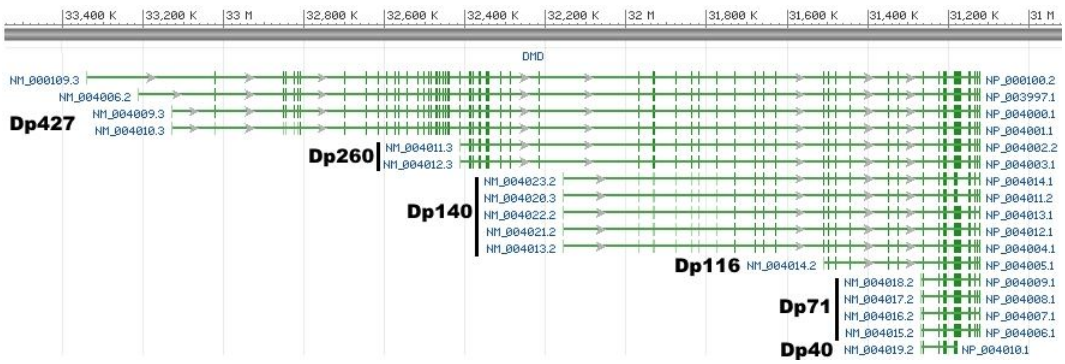

Fig. 4.1 Representation of the organization of the DMD gene and all the different isoforms indicate. Most of the dystrophin isoforms have splice-variants, thus increasing the overall number of differentially expressed mRNA species (adapted from NCBI Gene database, DMD gene card).

In muscle cells the mainly expressed isoform is the large 427 kDa molecule (Dp427) localizing at the sarcolemma and functioning as connector between the actin contraction machinery and the multimeric glycoprotein complex anchoring the cell to the extra-cellular matrix (Rafael *et al.,* 1996). The dystrophin function is closely related to the physical forces acting on the myocyte membrane during contraction against the surrounding tissue, stabilizing it and protecting from shear damage (Pasternek *et al.,* 1995). In dystrophin-deficient myocytes the sarcolemma is fragile causing membrane ruptures (Menke and Jockusch, 1995), and in concurrence of an increased sensitivity to stretch-activated Ca^{2+} channels (Franco-Obregon and Lansman, 1994), in produces abnormal ion fluxes leading to protease activation (Fong *et al.,* 1990), reactive oxygen species production (Prosser *et al.,* 2012) and activation of cell-death programs (Jung *et al.,* 2008). All these effects of dystrophin absence produce widespread muscle damage and degeneration, causing the clinical phenotype of muscle weakness and wasting leading to the patient's death in early teens by respiratory failure (Wells and Wells, 2002).

4.2.1 DMD cardiac phenotype

Even if Duchenne Muscular Dystrophy is mainly associated with skeletal muscle dysfunction, the cardiac muscle is deeply affected becoming in some cases the predominant manifestation of the genetic disorder (Verhaert *et al.,* 2011). With the improvement of the efficacy of palliative treatment and advances in respiratory care, the lifespan of the DMD patients has increased and the effects of dystrophin absence on the cardiac muscle is becoming a prominent issue, with nearly all patients surviving to the third decade of life developing severe cardiomyopathies (McNally, 2007) and approximately 20% of the deaths ascribed to arrhythmias and conduction system abnormalities (Spurney, 2011). Moreover, the lyonization process, in which one of the two female X chromosomes is randomly inactivated, can lead to pathological mosaicism in the heart causing female carriers to develop dystrophinopathic cardiomyopathy (Nolan *et al.,* 2003). Besides the still unclear effects of the dystrophin at cellular level, the

DMD phenotype at heart level is characterized by sub-epicardial fibrosis of the inferolateral wall (Frankel and Rosser, 1976) that has been postulated to result from the mechanical stress imposed on a metabolically and structurally abnormal myocardium (Verhaert *et al.,* 2011).

Clinical data suggest that pharmacological treatment similar to standard heart failure therapy prevent or delay the onset of cardiomyopathic remodeling in DMD patients, thus proving how cardioprotection can further improve patients lifespan and quality of life (Ishikawa *et al.,* 1999; Duboc *et al.,* 2005).

4.2.2 DMD study models

Currently the most common study model for DMD is the *mdx* mouse (Collins and Morgan, 2003). It is historically the longest and best characterized animal model, despite being far from representative of human physiopathology and many attempts to model therapeutic approaches on this animal failed in the translation to human patients (Miller *et al.,* 1997). A part from the classical physiological species-related differences, the absence of dystrophin in the *mdx* mice results in a mild pathological phenotype, with low muscle functional impairment and fairly normal phenotype throughout most of the animal's lifespan (Muller *et al.,* 2001).

A much better DMD model is the Golden retriever muscular dystrophic (GRMD) dog, which physiology and dimensions are more closely resembling the human one, resulting in the pathological phenotype and the outcomes of therapeutic approaches to be highly similar between the two species (Howell *et al.,* 1997). This model shares the same drawbacks of all the other large animal models: expensiveness of maintenance, difficulty of genetic manipulation and the moral barrier of working with highly sentient and emotive animals (Collins and Morgan, 2003).

In vitro modeling of DMD relies mostly on the employment of myogenic cell lines such as C2C12 immortalized murine cell line or primary culture of satellite cultures of satellite cells and myoblasts from both animal and human sources

(Huard *et al.,* 2003). The skeletal muscle *in vitro* modeling is one of the few human tissues allowing the possibility of genuine human cultures on-a-dish, with several cell banks around the world preserving myoblasts and satellite cells from affected patients. For the opposite reason, currently there are no *in vitro* human cardiac models for DMD as human cardiac primary material is hardly available and there are no progenitor sources for cardiomyocyte derivation.

4.2.3 iPS-derived human DMD cardiomyocytes

To obtain dystrophic hCMs, we differentiated toward the cardiac lineage an hiPS clone derived from a DMD patient with deletion of exons 4–43 of the muscle isoform Dp427m (DMD hiPS cells). First, DMD-hiPSC were cultured and expanded in their undifferentiated state for up to 10 passages. During expansion, hiPS cell colonies maintained the classical morphology of pluripotent stem cells cultures in colonies and expressed pluripotency markers such as Oct4, Sox2, c-Myc, Tra-1-60, and Tra-1-81, as evaluated routinely by immunofluorescence. The expanded colonies were then used for embryoid bodies (EBs) generation and differentiated towards the cardiac lineage with a protocol adapted from the "Keller protocol" (Kattman *et. al.,* 2011) and outlined in Fig. 4.2A. This 16-day differentiation procedure resulted in contracting EBs around day 12 of differentiation. Data presented in **Paragraph 2.4** show that proper cardiac differentiation requires cell-substrate interaction to promote functional and structural maturation of hiPS cell–derived CMs. For this reason, contracting EBs were cultured in suspension up to day 20 and then treated with collagenase and replated on 16 kPa hydrogels for additional 4 days.

After adhesion the DMD-CMs were screened for expression of proteins of the functional cardiac machineries: α-actinin and cardiac troponin T for the contraction machinery, connexin-43 for the electrical conduction system and SERCA2a for the calcium handling machinery (Fig. 4.2B). Spontaneous contractions and electrically elicited one were observed and confocal imaging showed paired calcium transients with the contractions (Fig 4.2C&D). For further experiments two different control cell type were employed: hiPSC derived from a

healthy patient (ADHF#1 cell line) and a line of DMD-hiPSC corrected with a Human Artificial Chromosome (HAC) carrying the whole genomic sequence of the dystrophin gene (DysHAC-hiPSC).

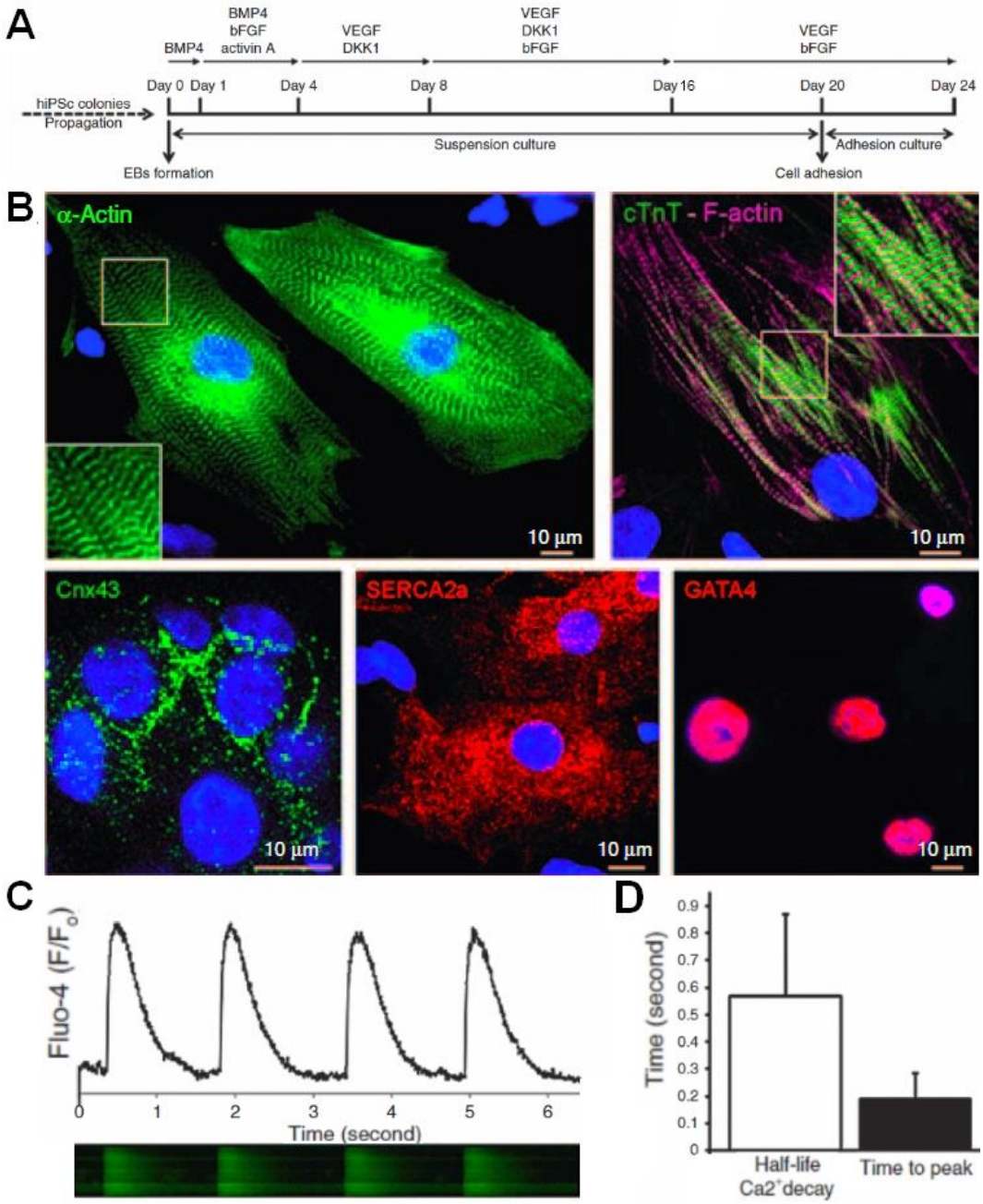

Fig. 4.2 Cardiac differentiation of DMD hiPSC. (A) The differentiation protocol adapted from Kattman *et al.*, 2011. **(B)** Immunofluorescence against cardiac markers. **(C)** The cardiomyocytes display cardiac-like calcium transients visualized by fluo-4 dye loading under a line-scanning confocal microscope and **(D)** the transient kinetic parameters show fast Ca^{2+} release and re-uptake rates.

An HAC is an artificially created exogenous minichromosome having the ability to replicate and segregate autonomously in target human cells and to be stably

maintained at episomal level, without integration into the host genome. In addition, HACs have the capacity to carry large genomic loci with all their regulatory elements (Kazuki *et al.,* 2011). An HAC vector carrying, for the first time, the whole dystrophin genomic locus including the associated regulatory elements (DysHAC) was developed by prof. Mitsuo Oshimura's group (Hoshiya *et al*., 2009*;* Kazuki *et al.,* 2010) demonstrating the complete correction of hiPS cells derived from a DMD patient. The use of HAC technology might have a great impact in therapeutic approaches of gene therapy and delivery of healthy copies of the mutated DMD gene in dystrophic patients. Furthermore, the DysHAC-corrected DMD cells can be a unique tool for *in vitro* studies as they represent the rescue phenotype with the same genetic background of the diseased cells use to model DMD.

We differentiated the DysHAC-hiPSC according to the same differentiation protocol summarized in Fig4.2A, following at each step the expression of EGFP, used as a molecular marker for the HAC vector. The green fluorescence was assessed by standard epifluorescence microscopy and proved the retention of the HAC construct throughout all the differentiation process (Fig. 4.3).

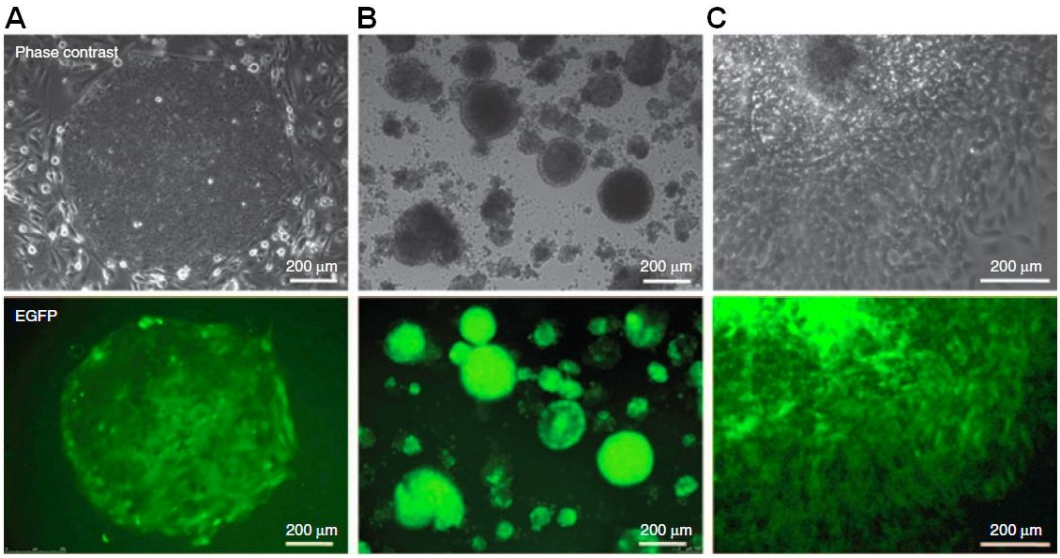

Fig. 4.3 HAC maintenance during differentiation. Epifluorescence imaging for EGFP expression shows the retention of the HAC construct through differentiation from pluripotent state **(A)** to the EB intermadiate phase **(B)** and in fully differentiated beating cardiomyocytes **(C).**

4.2.4 Dystrophin expression recovery with HAC technology

DysHAC is the first vector carrying the whole dystrophin genomic locus, including all the associated regulatory elements. This potentially allows proper activation of the complex mechanism regulating dystrophin expression of tissue-specific isoforms and exon-skipping and exon-scrambling events, which are finely regulated in both development- and tissue-specific manner.

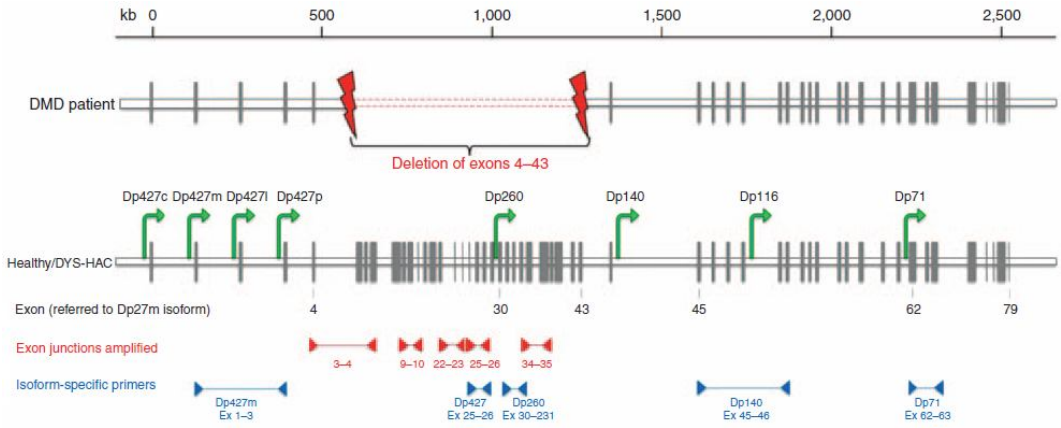

Fig. 4.4 Schematic representation of the human dystrophin gene. (Top) The deletion of the patient spans from exon 4 to exon 43. (Bottom) The positions relative to dystrophin exons of the primers employed for transcriptomic analyses are reported. The green arrows indicate different promoters driving tissue-specific isoforms of dystrophin transcripts.

We proceeded to assess the expression of the dystrophin transcripts, first of all investigating the sequences deleted in the patient's genome (Fig. 4.4). Exon junction-spanning primers were designed to target the deleted gene sequences and RT-PCR confirmed the absence of such transcripts in DMD-CMs (Fig. 4.5). As controls healthy hiPSC-CMs and heart- and skeletal muscle-tissues were used. The analyses showed as well the recovery of transcripts relative to the deleted exons in the DysHAC-CMs, highlighting the activation of transcription from the ectopic vector (Fig 4.5).

Further investigation was performed on the transcription of specific isoforms of dystrophin. We assessed the presence of transcripts of the full length muscle-specific Dp427m isoform, the cardiac- and brain-specific Dp260 isoform, the brain-specific Dp140 isoform and the ubiquitously expressed short dystrophin Dp71.

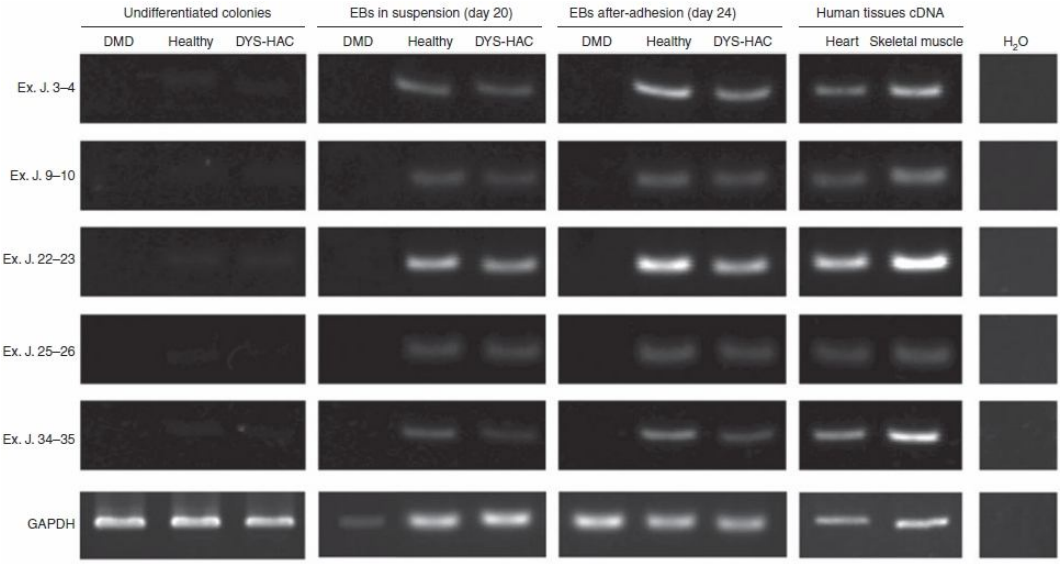

Fig. 4.5 Transcription of mRNA sequences from inside the deleted exons in the DMD-patient. Exon-junctions refer to the primer sets depicted in red in Fig. 4.4.

All of the primer pairs were designed to fall in the unique 3' UTR regions of all the isoforms in order to assess the effective initiation of transcription and we used cDNA samples from heart, skeletal muscle, brain, kidney and liver tissues as controls. For this reason, we observed even in DMD-CMs the presence of a transcript corresponding the Dp427m-specific amplicon (Fig. 4.5A). The promoter region of the full-length dystrophin transcript is fully functional, thus the transcription begins normally before it stops after the deletion. This is true as well for the Dp140 and Dp71 isoforms, both controlled by promoters outside of the deletion, thus functioning properly. The presence of Dp140 transcripts, a brain-specific isoform, is not surprising as the differentiation protocol employed does not yield pure cardiac populations and contaminants from the ectoderm layer, while low in percentage, are common. On the other hand, the Dp260 promoter is in intron 29, right in the middle of the big deletion of the DMD-patient, and the amplicon is absent in DMD-CMs, but is present in healthy cardiomyocytes and is recovered in DysHAc-CMs.

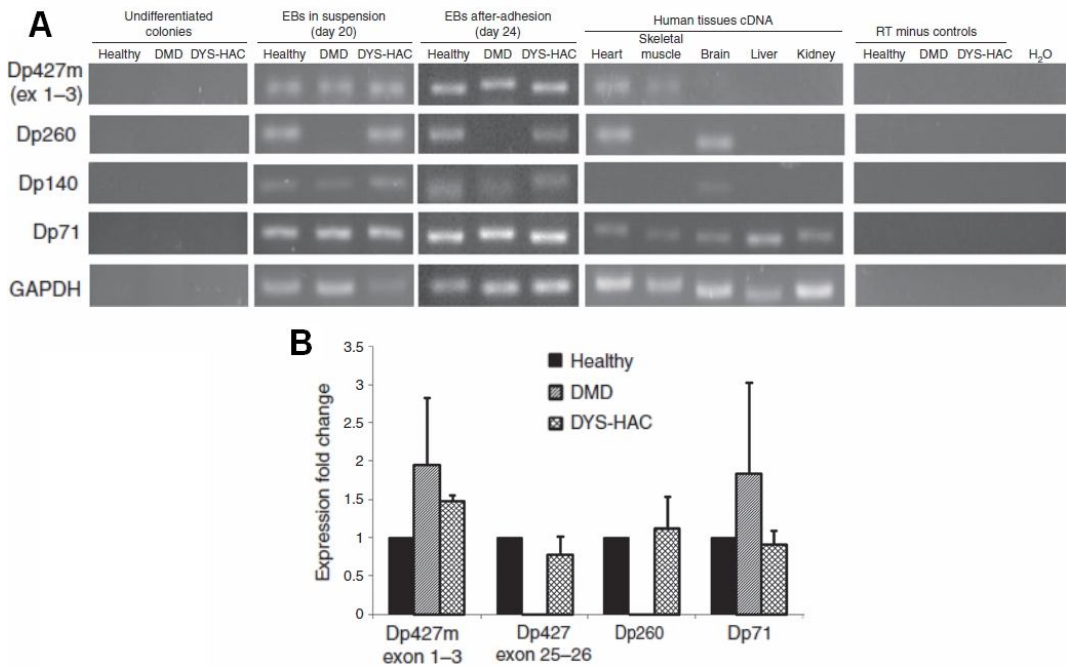

Fig. 4.6 Expression of tissue-specific dystrophin isoforms. (A) RT-PCR results for isoform-specific amplicons. (B) Real Time PVCR results for transcript levels.

We then concluded that the HAC construct indeed managed to recover the expression of the missing transcripts in DysHAC-CMs, and we addressed the question whether it was able to regulate their levels as well. We performed Real Time PCR analyses on the samples aiming at the full-length isoform Dp427m, the missing Dp260 and the Dp71 as control. We decided to detect the presence of the Dp427m isoform with two sets of primers, one in the region preceding the deletion (exons 1 to 3) and one inside the deletion (exons 25 to 26). We assessed that indeed not only the cDNA sequences from inside the deletion were detectable again, but their levels of expression were comparable to those detected in healthy cardiomyocytes (Fig. 4.6B). Interestingly, the expression levels of the dystrophin isoforms present in DMD-CMs seemed abnormal, but never reached statistical significance (n=3).

In healthy cardiomyocytes, dystrophin is a key structural protein creating a bridge across the sarcolemma, which provides a flexible connection between the ECM and the contractile machinery. For this important role, dystrophin should be correctly folded and localized under the plasma membrane of skeletal and cardiac muscle cells. For this reason, we verified the proper restoration of

dystrophin expression at protein level and its sub-cellular localization by immunofluorescence and confocal microscopy. Analyses were performed 4 days after EB adhesion on substrate. EBs derived from healthy hiPSCs displayed a clear dystrophin expression at membrane localization, drawing the boundaries of cTnT-positive CMs (Fig. 4.7). Similar dystrophin staining was observed in DysHAC-hiPSC-derived EBs. On the other hand, as expected, in DMD-EBs, no dystrophin staining was observed.

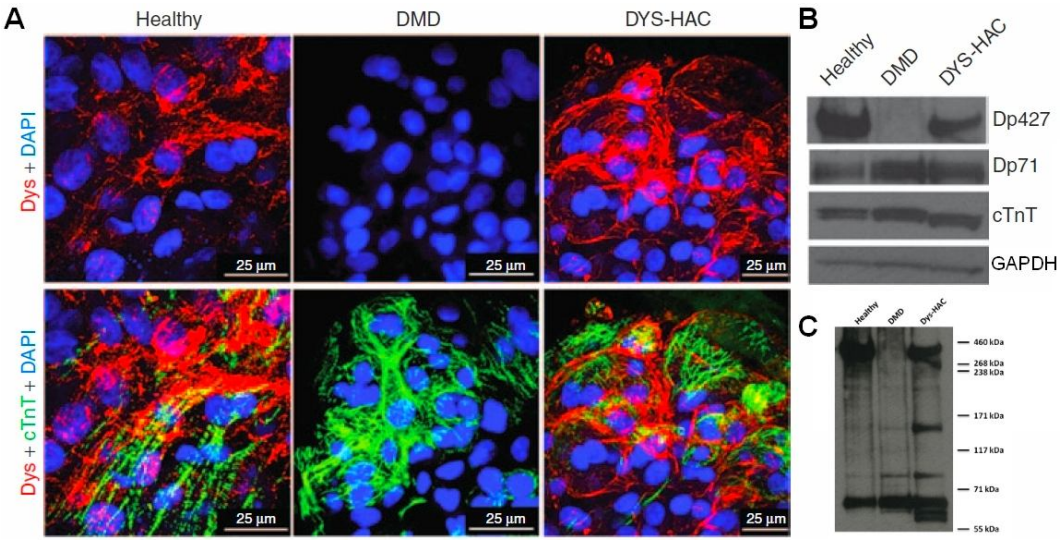

Fig. 4.7 Dystrophin protein expression. Dystrophin is present at the correct sub-sarcolemmal localization in HAC-carrying cardiomyocytes. **(A)** Immunofluorescence analyses for dystrophin and cardiac troponin T in differentiated EBs. **(B)** and **(C)** Western Blot analyses for C-term region of the dystrophin protein detecting all dystrophin isoforms.

These results were confirmed by Western Blot analyses, in which full-length high molecular weight dystrophin was not observed in DMD-CMs, whereas its expression was perfectly restored in DMD-CMs corrected with the DysHAC (Fig. 4.7B). Although much less abundant, other dystrophin isoforms were also detectable in DysHAC-CMs when the employing an antibody recognizing a C-term epitope common to all dystrophin isoforms (Fig. 4.7C).

4.2.5 Conclusions and perspectives

In this paragraph is presented the set up of the first human model of cardiac cells affected by mutations in the dystrophin gene. We show that the differentiation into cardiomyocytes of DMD-hiPS cells is possible and the molecular pathological phenotype is conserved. In this work, we employ as

controls both healthy cells and DMD-corrected ones, providing a unique and valuable biological material to study the pathology *in vitro.* Moreover, we prove on a cardiac model, that the HAC technology is able of restoring the dystrophin mRNA transcript and proteins. In particular, the expression at correct levels of dystrophin isoforms absent in the diseased samples shows that the HAC vector can drive the expression of absent transcripts with proper physiological regulation of all the regulatory elements present in the genomic sequence.

In ultimate analysis, we provide an excellent tool for *in vitro* studies of the DMD pathological mechanisms, with the best positive control available.

4.3 Arrhythmogenic Right Ventricular Cardiomyopathy/ Dysplasia

The Arrhythmogenic Right Ventricular Cardiomyopathy/Dysplasia (ARVC/D) is a hereditary cardiomyopathy, usually characterized by an autosomal-dominant pattern. The pathology presents itself with fibro-fatty infiltrations in the myocardium leading to life-threatening arrhythmias and sudden death. Because of the largely unknown pathogenesis, the proper designation for the disease has been a matter of debate evolving from "dysplasia" at its first comprehensive description in 1978 (Frank *et al.,* 1978), to "cardiomyopathy" in 1995 (Angelini *et al.,* 1996; Richardson *et al.,* 1996) and subsequently it has been assigned the "Arrhythmogenic Ventricular Cardiomyopathy (AVC)" designation in 2011 by HRS and EHRA organizations, following the growing evidence of left ventricle involvement in many affected individuals (Ackerman *et al.,* 2011).

The genetic mutations behind ARVC/D pathological phenotype impair the function of proteins involved in the formation of intercalated disc structures. The incidence rates are generally reported as 1:2000, but regionally the numbers of individuals carrying mutations can dramatically increase (up to 1:200 in Italian Veneto region) making it a fairly frequent genetic condition (Basso *et al.,* 2009). Characterized by a unique among primary cardiomyopathies early concealed

phase without gross structural abnormalities, ARVC/D is often diagnosed only *post mortem* with autoptic analyses and may be asymptomatic until the first ventricular tachycardic and fibrillatory events, which are the leading cause of sudden deaths in young adults under 35 years of age (Saguner *et al.,* 2014). In affected patients with characterized pathogenic genotypes, mutations in three desmosomal proteins alone account for almost 80% of the cases: plakophillin-2 (PKP2), desmoplakin (DSP) and desmoglein-2 (DSG2) (Herren *et al.,* 2009). This evidence, together with the frequent association with cutaneous phenotypes, focused the research on ARVC/D pathogenesis on the cell-to-cell junctions (Delmar and McKenna, 2010), associating the disease to desmosome or desmosome-associated proteins (Table 4.2).

Table 4.2 OMIM classification of Arrhythmogenic Ventricular Cardiomyopathies.
TGF - Transforming Growth Factor; RyR - Ryanodine Receptor; TTN - titin; TMEM43 - transmembrane protein 43; DSP - desmoplakin; DSC - desmocollin; JUP - junction plakoglobin

AVC subtype	Chromosomal locus	Inheritance	Protein
ARVC/D 1	14q23-q24	Autosomal dominant	TGFβ3
ARVC/D 2	1q42-q43	Autosomal dominant	RyR2
ARVC/D 3	14q12-q22	Autosomal dominant	-
ARVC/D 4	2q32	Autosomal dominant	TTN
ARVC/D 5	3p23	Autosomal dominant	TMEM43
ARVC/D 6	14p12-p14	Autosomal dominant	-
ARVC/D 7	10q22	Autosomal dominant	-
ARVC/D 8	6p24	Autosomal dominant	DSP
ARVC/D 9	12p11	Autosomal dominant	PKP2
ARVC/D 10	18q12	Autosomal dominant	DSG2
ARVC/D 11	18q12.1	Autosomal dominant	DSC2
ARVC/D 12	17q21	Autosomal dominant	JUP
Naxos disease	17q21	Autosomal recessive	JUP

The precise origin of the fibro-fatty infiltrations characterizing the disease is still unclear, while the "defective desmosome" hypothesis is widely supported for being the key factor in the generation of arrhythmic events, often present in absence of overt structural abnormalities (Bauce *et al.,* 2011). The desmosome (Fig. 4.8) is the mechanical junction between two cardiomyocytes, but its function has been extended in recent years to a structure tightly coordinated with other membrane complexes such as gap junctions and ion channel clusters (Gomes *et al.,* 2012). Evidence of connexon disruption with altered expression levels of connexin-43 in absence of functional desmosomes strongly supports this hypothesis (Oxford *et al.,* 2007). Moreover, ion channels such as voltage-gated sodium channels ($Na_V1.5$) have been reported to display aberrant localization and function in presence of mutations to desmosomal components (Sato *et al.,* 2009). Overall, this reports provide a molecular basis of the aberrations of the intercalated disc structures that represent the interface between one cardiomyocyte and the other, forming the "functional syncytium" of the myocardial tissue.

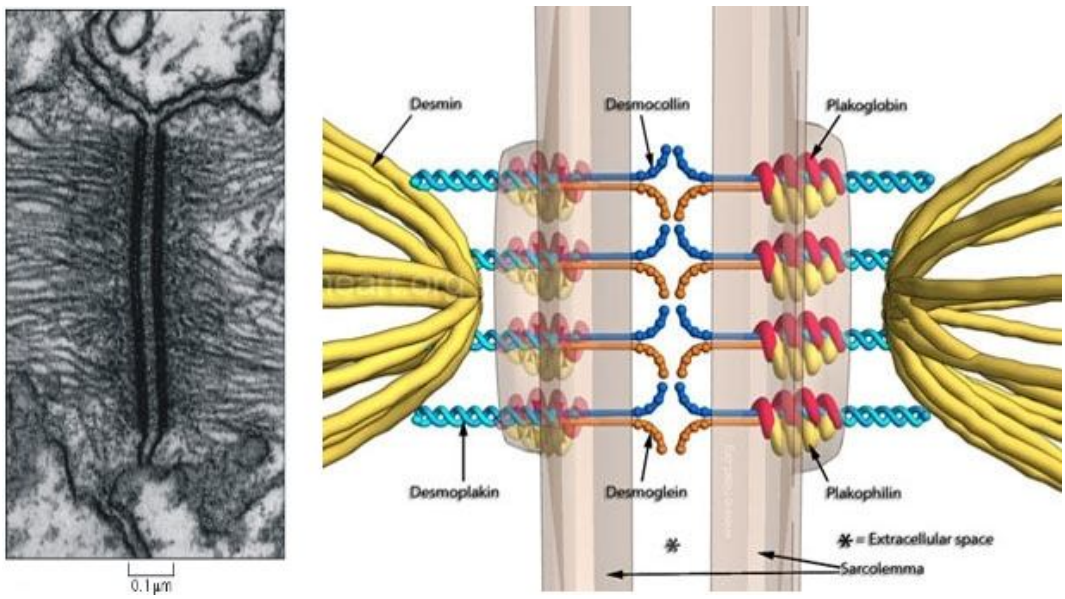

Fig. 4.8 The desmosome organization. An electron microscopy micrograph of a desmosome (left) and a schematic representation of its molecular components (right)

The aberrations are exacerbated in later stages of the disease when the fibrotic and adipose tissues replace the muscle tissue. For this event, there are contrasting hypotheses: i) cardiomyocyte or cardiac progenitor trans-

differentiation in adipocytes; ii) inflammatory response to damaged myocardium (Angelini *et al.,* 1996); and iii) fibroblast and pre-adipocyte invasion from the epicardium following cardiomyocyte apoptosis and the associated electromechanical instability (*Mallat et al.,* 1996; *Basso et al.,* 2006). While *in vitro* observations often disprove the first hypothesis, the latter two could be different responses to myocardial damage in which infiltration of lymphocytes and fibroblasts are a common feature (Bauce *et al.,* 2005). It is worth noting, however, that epicardium-derived human primary culture from PKP2-mutated patients display abnormally enhanced migratory and proliferative features (Matthes *et al.,* 2011), consistent with the directional epi-to-endocardium infiltration often observed in clinic.

4.3.1 ARVC/D study models

Characterization of the molecular mechanisms underlying ARVC/D pathogenesis in human patients is highly limited by constrains inherent to human research, especially due to the strictly cardiac- and cardiomyocyte-related nature of the disease. As for DMD (**Paragraph 4.2.2**), the canine model is currently the most reliable and representative one, with the purebred boxer dogs displaying strikingly similar clinical phenotypes in spontaneous mutations (Basso *et al.,* 2004). The major drawback of this specific model is the unidentified genetic background for the pathology, at the same time well reflecting the human condition, in which at least 50% of cases have no characterized genetic abnormalities (Corrado *et al.,* 2000; Basso *et al.,* 2004).

The murine models for the disease rely on knock-out/knock-in animals and recapitulate some of the molecular features of the disease, but mostly fail to provide the pathological phenotype for ARVC/D heart muscle, with often no evidence of effect on cardiac rhythm, sudden death and only minor electrophysiological aberrations (Delmar and McKenna, 2010). The complete knock-out of the desmosomal genes DSP, PKP2 results in high embryonic lethality (Grossman *et al.,* 2004; Gallicano *et al.,* 1998), in the same way as overexpression of some human DSP mutants (Yang *et al.,* 2006). Other models

relying on over-expression systems, in which the mutant allele acts above the basal expression of wild-type proteins, must consider the evidence of studies in which the observed phenotype was deeply expression level-dependant (Pilichou *et al.,* 2009).

In vitro models rely mostly on animal primary cultures in which RNA silencing or standard overexpression techniques are employed to hamper with the cardiac molecular machineries. A human cell line of squamous carcinoma SCC9 has been used as well, as a model to study desmosome assembly in a human genetical background (Yang *et al.,* 2006). Although bound by the standard limitations of cellular models, the experiments carried out *in vitro* share remarkably consistent results with *in vivo* models providing confidence in their applicability (Delmar and McKenna, 2010).

4.3.2 iPS-derived human ARVC/D cardiomyocytes

To model the ARVC/D pathology *in vitro*, we first derived cardiomyocytes from hiPS derived from a patient affected by a homozygous mutation in exon 12 of the PKP2 gene, causing a cryptic splicing site generating a mutated frame-shift C-terminus of the protein (Awad *et al.,* 2006). The ARVD-hiPS and a control healthy line, αMHC-Puro^{r} (αSkin119) were kindly provided by prof. H-S. Vincent Chen, from the Sanford-Burnham Medical Research Institute in La Jolla, California. Both hiPS cell lines were characterized at the SBMR Institute and maintained a characteristic pluripotent morphology during all passages of culture. The monolayer cardiac differentiation protocol was successfully applied to both cell lines.

We analyzed the derived cardiomyocytes for abnormal molecular phenotypes usually associated with ARVC/D-affected patients. The first target of enquiry was the protein mutated in the patient, the desmosomal PKP2. The mutation carried by the patient is a C-terminal frame-shift, without any early termination codon, thus a protein product is still predicted to be produced. We analyzed the ARVC/D-CMs with two antibodies raised against the N-terminal and C-terminal portions of the PKP2 protein, expecting the first one to recognize a proteic target

as the mutation affects the latter portion of the native protein. The specificity of the two antibodies was confirmed by staining in the healthy-hiPS controls, both correctly localizing at the junctional membrane portions between two cardiomyocytes (Fig. 4.9).

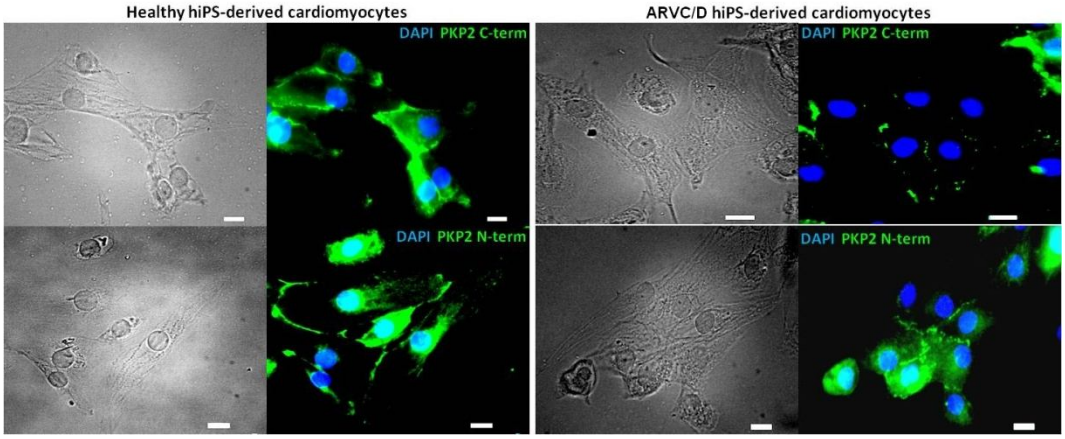

Fig. 4.9 Molecular characterization of the PKP2-mutated cardiomyocytes. Expression and localization of the PKP2 protein in healthy (left) and ARVC/D-affected (right) hiPS-CMs. The two used antibodies recognize the same protein, but in different portions of the polypeptide sequence. (scale bar = 10 μm)

As anticipated, the C-terminus antibody did not recognize any target in the mutated cardiomyocytes. Surprisingly, the N-terminus targeted antibody did positively stain the junctional membrane, providing evidence that a protein product of the mutated gene is stable and correctly targeted to the cardiomyocyte membrane (Fig. 4.9). Indeed, the N-terminal portion of PKP2 is reported to interact with the membrane, anchoring the protein to the sarcolemma domain of the desmosome, while the C-terminus is supposed to interact with molecular partners such as desmoplakin and connexin-43 (Joshi-Mukherjee *et al.,* 2008). Working on this hypothesis, we sought for aberrant localizations of important functional cardiac proteins, which could interact with PKP2 C-terminus.

A recent report found tight association between the sodium current channel (in particular its subunit $Na_V1.5$ encoded by the *SCN5A* gene) and PKP2 (Cerrone *et al.,* 2014). Mutations in *SCN5A* are associated with cardiac conduction diseases such as Brugada syndrome and LQT3, and the abnormal localization of the $Na_V1.5$ subunit in PKP2-mutated cardiac cells could generate an arrhythmogenic

substrate. Double immunostaining for PKP2 and $Na_V1.5$ showed the close association between the two proteins in healthy cardiomyocytes, with vast co-localization (Fig. 4.10) at the junctional membrane of both proteins. In ARVC/D-cardiomyocytes, the co-localization was disrupted, despite the membrane localization of the mutated PKP2 protein (Fig. 4.9).

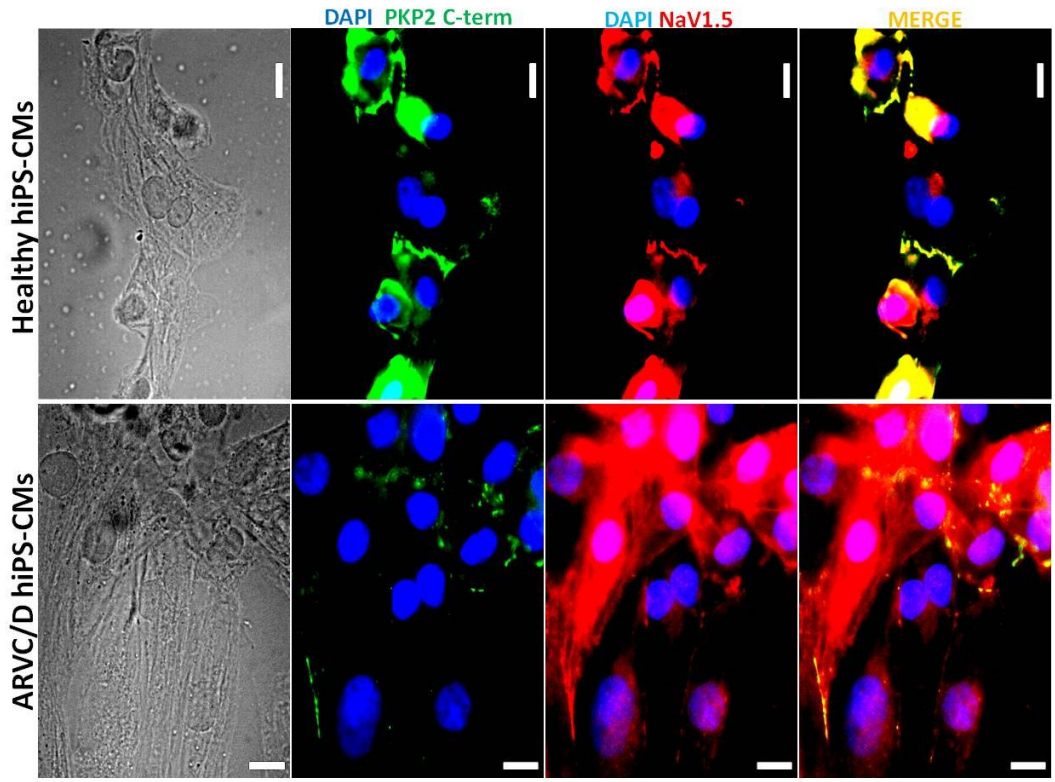

Fig. 4.10 Co-localization of plakophillin-2 and sodium voltage gated channel, subunit alpha. Top panel shows the co-localization at the junctional membrane of PKP2 and $Na_V1.5$, with nearly no staining of the latter in the cytosolic domains. In the bottom panel, the staining shows membrane-exclusion of the NaV1.5 subunit in cells with mutated PKP2 C-terminus. (scale bar = 10 μm)

ARVC/D cardiomyocytes display a wide-spread cytosolic staining for $Na_V1.5$, indicative of the failed membrane anchoring oh the sodium channel.

Another desmosome-associated protein often displaying abnormal localization and function in ARVC/D samples is plakoglobin (PKG) (Munkholm *et al.*, 2015). This protein, sometimes known as γ-catenin, is normally anchored to membrane at cell-to-cell junctions, but in abnormal conditions it is reported to translocate to the nucleus and alter the β-catenin transcriptional activity (Garcia-Gras *et al.*, 2006), and this has been shown to occur in presence of mutated PKP2 C-terminus (Kim *et al.*, 2013). Staining for PKG in hiPS-derived cardiomyocytes

resulted in normal and exclusive membrane localization in healthy human cardiomyocytes, while its anchoring to the membrane domain was altered in PKP2-mutated ones (Fig. 4.11).

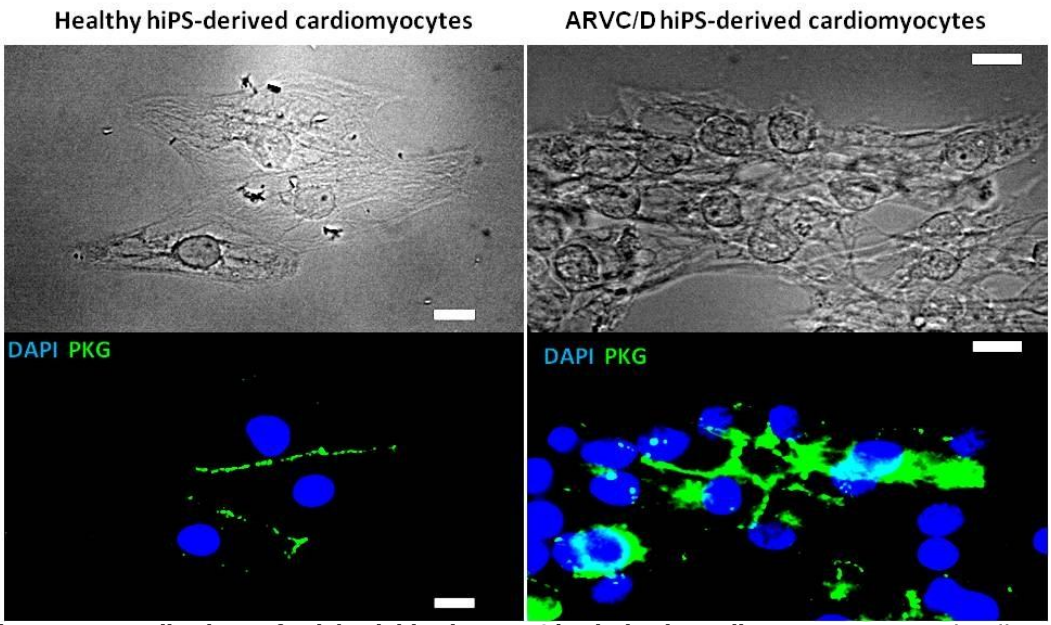

Fig. 4.11 Localization of plakoglobin in ARVC/D-derived cardiomyocytes. PKG localizes exclusively at the membrane in healthy cardiomyocytes, while displays altered localization in PKP2-mutated hCMs. (scale bar = 10 μm)

Taken together, these evidences provide a good picture of the aberrant molecular phenotype of the diseased cardiomyocytes *in vitro*, and although mutated, the ARVC/D cardiomyocytes still retain contractile function and do form cell-to-cell junctions. More interestingly, the targeting and localization of the mutant PKP2 is still intact and can form junctional structures between two cell, but its ability to coordinated partner proteins through the C-terminal portion is clearly impaired and provides an excellent model to address the function of that specific domain of PKP2 in the assemble of the intercalated disc structures. Nevertheless, standard monolayer cultures do not provide the same geometrical cues for cell-to-cell junction and structural organization as they display high isotropy in the arrangement of the culture. This reflects poorly on the ultrastructural organization of the cardiac features, especially as the cardiomyocytes maintain sustained contractions, thus generating mechanical forces in all directions and not in an organized fashion as in the native myocardium (Chan *et al.,* 2013).

4.3.3 Intercalated disc reconstruction *in vitro*

The heart muscle *in vivo* is organized in concentric layers of cardiomyocytes that form, unlike skeletal muscle, a "functional syncytium", connecting their contractile apparatus to the adjacent cardiomyocytes and maintaining a tight ion continuity within communicating cells, but retain a separate and defined single-cell identity. This follows an aligned pattern in which adjacent cells form a continuous array of synchronously contracting cells.

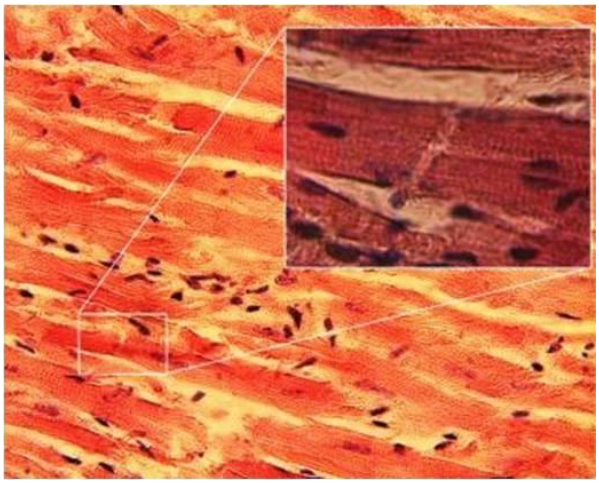

Fig. 4.12 *In vivo* cardiac muscle organization. The myocardium is organized as a functional syncytium of polarized cardiomyocytes connected through intercalated disc structures with one another (inset) (Dr. S. Girod, Anton Becker, Wikipedia)

The structure that functions as interface between one cardiomyocyte and the next is the intercalated disc (Fig. 4.12). These cardiac-specific structures enable mechanical and electrical coupling and account for the synchronous work of the aligned cardiac cells (Wang *et al.,* 2012). The intercalated disc is composed mainly by the types of junctions: gap junctions, adherens junctions and desmosomes, each accounting for one type un functional communication between two cells, such as ion handling of mechanical force transmission (Perriard *et al.,* 2003). The cardiac cell organization in this system is highly polarized and results in the elongation of the cell in an anisotropic manner, providing and receiving electric and mechanical stimuli in directional manner.

In order to recreate such polarized organization inside the *in vitro* cultures, we employed techniques of cell patterning based on the generation of adhesion-exclusion areas on the culture substrates. The correct chemical modification of a glass surface, with covalent bonding of cell-repellant polymers with a precise geometry, allows the cells to attach only on the unmodified areas. The

topological definition of the surface modification was achieved by photoactivation of the polymer (linear acrylamide) synthesis, and photomasks with the desired geometries were used to cover from the activating light the cell-adherent areas. We designed photomasks with linear patterns of varying width, and analyzed the cell culture organization in every condition (Fig. 4.13).

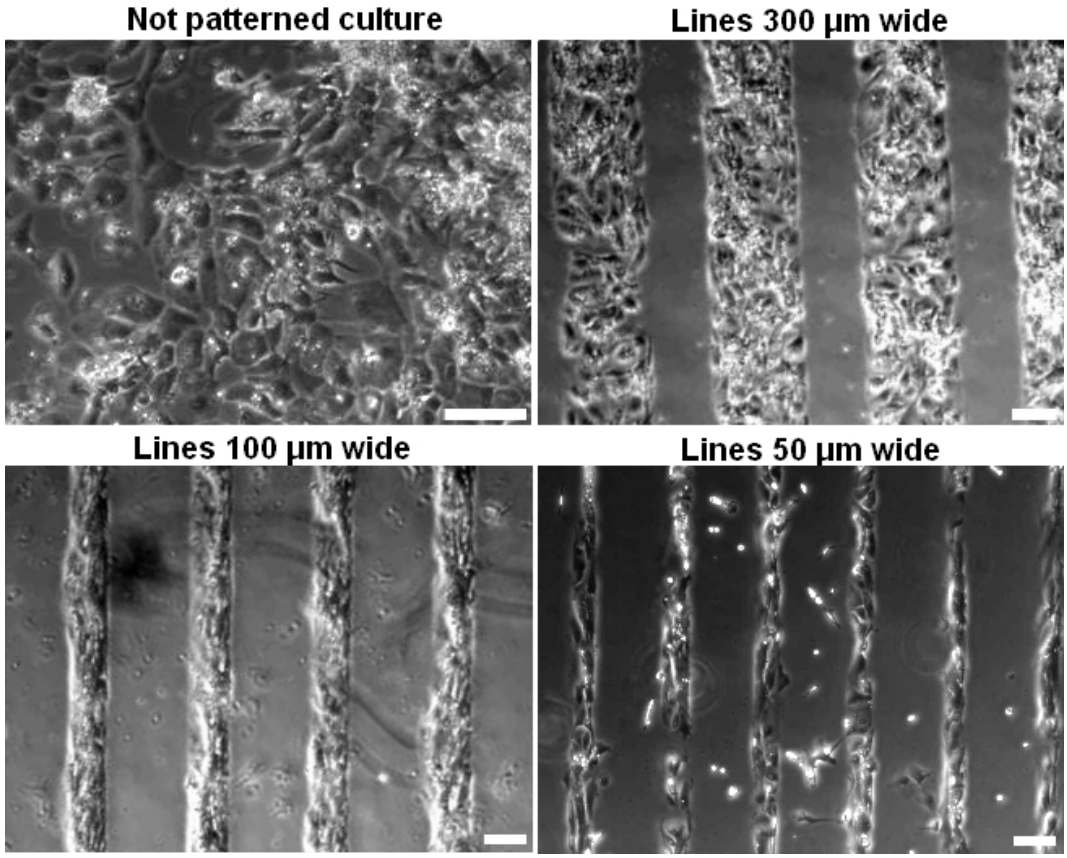

Fig. 4.13 Patterned human cardiac cultures. Geometrical patterning of cell cultures can be achieved by selective adhesion of the cell to the culture substrate. Microfabrication techniques allow precise control over the cell adhesion surface. Here are shown patterned cultures of human contracting cardiomyocytes in line-patterned of varying width. (scale bar = 100 µm)

On wide patterns, such as 300 µm, h cardiomyocytes still retained an isotropic organization at the single cell level, although it is clear how precisely this technique can induce cell adhesion to the culture substrate. Decreasing the width of the lines, we scaled down to a 50 µm wide pattern and a low density seeding condition, in which we could observe aligned cardiomyocytes with a single cell-to-cell interaction (Fig. 4.13). Cardiomyocytes culture on these microengineered substrates displayed sustained spontaneous contractile activity, but the direction of contraction was anisotropic and all the cells contracted along

the cell long-axis, parallel to the patterned lines (Fig. 4.14). Moreover, the visible sarcomeric structures displayed a perpendicular to the lines organization, with an alignment homogeneity rarely seen in standard monolayer cultures.

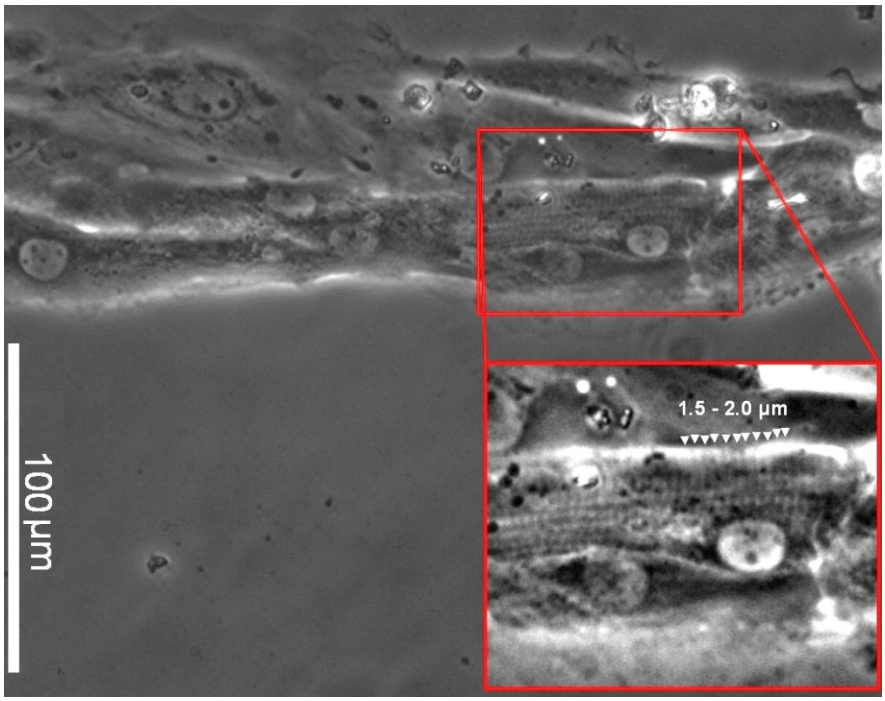

Fig. 4.14 Anisotropic contraction in patterned human cardiomyocytes. hCMs cultured on the linear patterns displayed contractions directed along the axis of the pattern. The sarcomeric organization of the contracting cells was clearly aligned along the same direction, in an organized fashion rarely observed in isotropic standard monolayers.

We assayed the patterned cultures with immunofluorescence against proteins of the intercalated disc structure, in particular the components of the desmosomal mechanical junctions. As expected, standard monolayers show un-polarized cells and cell-to-cell connections without defined orientation (Fig. 4.15A).

Plakophillin-2 staining was always absent or concentrated in a perinuclear region in single cells, not connected with other cardiomyocytes , as they localizes preferentially on the in junctional membrane domains (Fig. 4.15B). Aligned cardiomyocytes, on the other hand, formed linear structures with strong and polarized staining in the junctional portions of the sarcolemma, indicating big specificity in localization (Fig. 4.15C). Other desmosome-associated proteins screened, such as plakoglobin, displayed as well polarized staining with targeting

on the cell-to-cell junctions (Fig. 4.15D). Interestingly, in many cases PKG staining in a striated organization was observed, with a pace of 1.5-2 μm very similar to the sarcomere pace in these cultures (Fig 4.14), thus providing evidence of ultrastructural maturation of the geometrically confined cardiomyocytes.

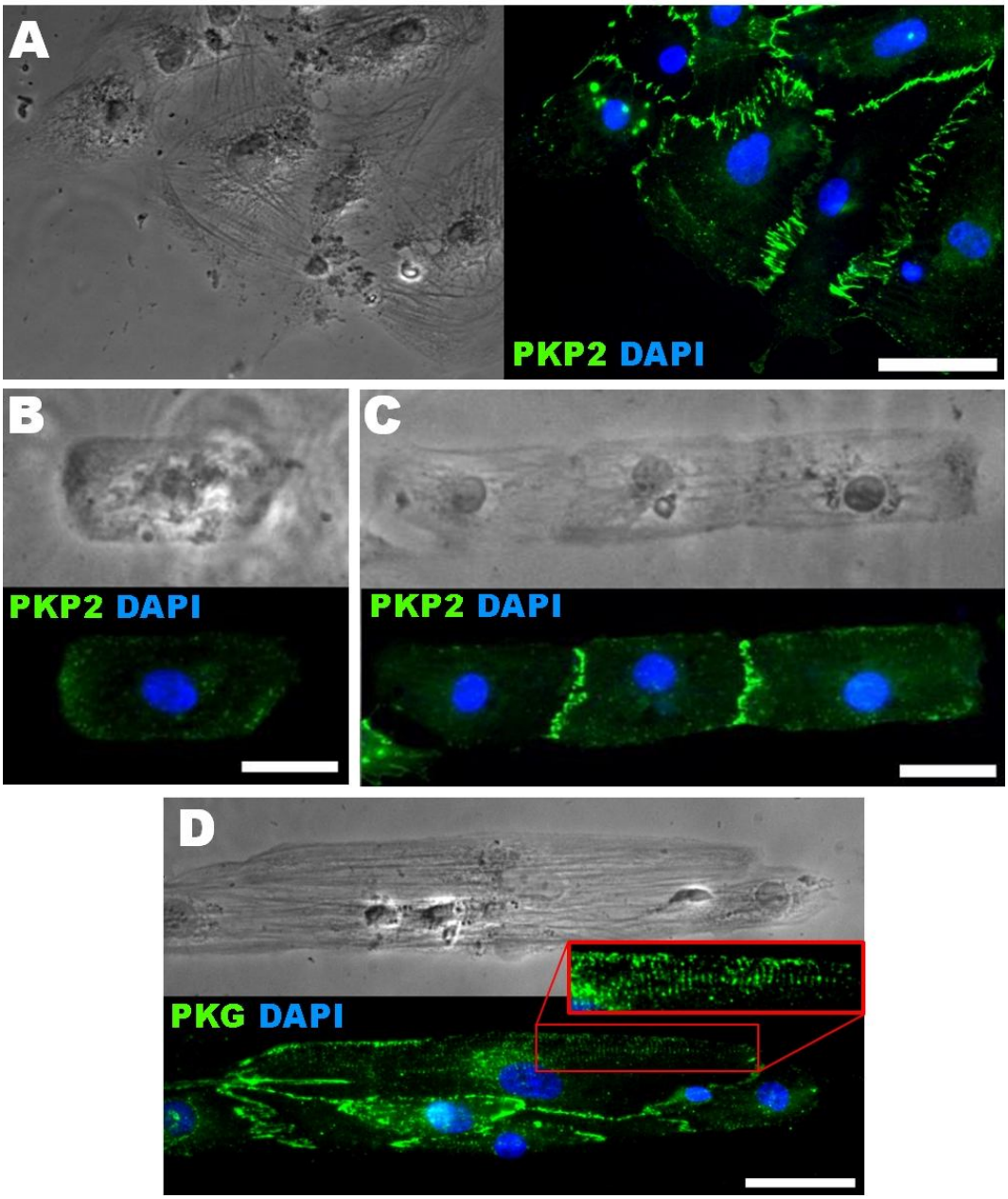

Fig. 4.15 Cardiomyocyte polarization in patterned culture substrates. (A) Immunofluorescence for desmosomal protein PKP2 in standard not patterned human cardiac cultures show not polarized cell-to-cell junctions. **(B)** Cell-to-cell interaction is required in order to form desmosomes. **(C)** Aligned cardiomyocyte on linear pattern form cell-to-cell junctions in a polarized fashion. **(D)** Plakoglobin localizes at the cardiac membrane in a patterned culture and striations corresponding to co-localization with the contractile machinery can be observed along the direction of the linear pattern (inset). (scale bar = 50 μm)

4.3.4 Conclusions and perspectives

In this paragraph, we presented the derivation of cardiomyocytes carrying a mutation of an ARVC/D patient. This cardiomyocytes display abnormal molecular features, often seen in the heart muscle *in vivo* in such pathological conditions and are suitable for modeling the disease *in vitro*. Moreover, the specific type of mutation (a C-terminal frame-shift in the *PKP2* gene, producing a stable polypeptide) provides an excellent human cardiac cell substrate to study the interaction of palkophillin-2 with its molecular partners at the intercalated disc structure.

The modeling of a disease affecting the structural organization of a functional cell domain is not easy, as it requires the recreating *in vitro* of such structure. The intercalated disc has been sometimes regarded as an "organelle" as multiple highly organized macro-complexes contribute to its structural complexity and define its very specific function (Delmar and McKenna, 2010). Regeneration *in vitro* of such structure requires improvement of the standard culture, integrating microengineered substrates to provide topological confinement and drive a polarized organization of the cardiomyocyte network. We provided here proof of the viability of such approach, obtaining human cardiac cultures with aligned contracting cells that display a highly polarized phenotype and show a correct directional localization of the desmosomal proteins.

We envision that the integration of the cellular model set up from the patient-specific hiPS cells with our engineered substrates could provide a good starting point for modeling both the desmosome-associated disease and the desmosome organization itself.

4.4 Conclusions

In this chapter, we showed how human induced pluripotent stem cells can be used for derivation of a cell type not commonly available for *in vitro* studies, as is the cardiomyocyte. The hiPS technology and the availability of cell samples from patients affected by genetic diseases can provide big insights in both physiology and pathophysiology of the cardiac cells.

In our particular case, we derived *bona fide* cardiomyocytes from patients affected by severe forms of Duchenne Muscular Dystrophy and Arrhythmogenic Right Ventricular Cardiomyopathy/Dysplasia, and showed how they recapitulate *in vitro* at least the molecular pathological phenotype of the patient.

For DMD, we set up the first human cardiac *in vitro* model for the disease, finally published in close timing with two other reports of hiPS-based DMD models (see Table 4.1). The advantage of our experimental set up is the availability of a unique and valuable control represented by the patients genetic correction with an episomic human artificial chromosome carrying the whole dystrophin genomic sequence, thus providing the cell with a fully physiological control over the levels, timing and isoform-specific expression of dystrophin.

For ARVC/D we derived cardiomyocyte from a patient carrying a homozygous mutation with very appealing characteristics both for the ARVC/D disease modeling and for molecular and structural studies. We provide as well an engineered method of culturing the cardiomyocytes that provides an unmatched possibility in regenerating *in vitro* a cardiac-specific structural and functional features rarely reported in literature.

For the cardiac derivatives of both hiPS cell lines is possible to apply the maturation protocols described in **Chapter 2** and **Chapter 3** to drive their maturation towards more adult-like phenotypes and generating a good *in vitro* model to study pathogenesis and pathological cardiac phenotypes of DMD and ARVC/D.

4.5 References

Ackerman MJ, Priori SG, Willems S, Berul C, Brugada R, Calkins H, Camm AJ, Ellinor PT, Gollob M, Hamilton R. **(2011)** HRS/EHRA expert consensus statement on the state of genetic testing for the channelopathies and cardiomyopathies: this document was developed as a partnership between the Heart Rhythm Society (HRS) and the European Heart Rhythm Association (EHRA). *Europace.* 13:1077-1109

Angelini A, Basso C, Nava A, Thiene G. **(1996)** Endomyocardial biopsy in arrhythmogenic right ventricular cardiomyopathy. *Am Heart J.* 132:203-206

Awad MM, Dalal D, Tichnell C, James C, Tucker A, Abraham T, Spevak PJ, Calkins H, Judge DP **(2006)** Recessive arrhythmogenic right ventricular dysplasia due to novel cryptic splice mutation in PKP2. *Hum Mutat.* Nov;27(11):1157.

Basso C, Corrado D, Marcus FI, Nava A, Thiene G. **(2009)** Arrhythmogenic right ventricular cardiomyopathy. *Lancet.* 373:1289-1300

Basso C, Czarnowska E, Della Barbera M, Bauce B, Beffagna G, Wlodarska EK, Pilichou K, Ramondo A, Lorenzon A, Wozniek O, *et al.* **(2006)** Ultrastructural evidence of intercalated disc remodelling in arrhythmogenic right ventricular cardiomyopathy: an electron microscopy investigation on endomyocardial biopsies. *Eur Heart J* 2006; 27:1847-1854

Basso C, Fox PR, Meurs KM, Towbin JA, Spier AW, Calabrese F, Maron BJ, Thiene G. **(2004)** Arrhythmogenic right ventricular cardiomyopathy causing sudden cardiac death in boxer dogs: a new animal model of human disease. *Circulation.* 109:1180 –1185

Bauce B, Basso C, Rampazzo A, Beffagna G, Daliento L, Frigo G, Malacrida S, Settimo L, Danieli G, Thiene G, *et al.* **(2005)** Clinical profile of four families with arrhythmogenic right ventricular cardiomyopathy caused by dominant desmoplakin mutations. *Eur Heart J* 26: 1666-1675

Bellin M, Casini S, Davis RP, D'Aniello C, Haas J, Ward-van Oostwaard D, Tertoolen LG, Jung CB, Elliott DA, Welling A, *et al.* **(2013)** Isogenic human pluripotent stem cell pairs reveal the role of a KCNH2 mutation in long-QT syndrome. *EMBO J* 32:3161–75

Carvajal-Vergara X, Sevilla A, D'Souza SL, Ang YS, Schaniel C, Lee DF, Yang L, Kaplan AD, Adler ED, Rozov R, *et al.* **(2010)** Patient-specific induced pluripotent stem-cell derived models of LEOPARD syndrome. *Nature* 465:808–12

Caspi O, Huber I, Gepstein A, Arbel G, Maizels L, Boulos M, Gepstein L. **(2013)** Modeling of arrhythmogenic right ventricular cardiomyopathy with human induced pluripotent stem cells. *Circ Cardiovasc Genet* 6:557–68

Chan YC, Ting S, Lee YK, Ng KM, Zhang J, Chen Z, Siu CW, Oh SK, Tse HF. **(2013**) Electrical stimulation promotes maturation of cardiomyocytes derived from human embryonic stem cells. *J Cardiovasc Transl Res*. Dec;6(6):989-99

Cerrone M, Lin X, Zhang M, Agullo-Pascual E, Pfenniger A, Chkourko Gusky H, Novelli V, Kim C, Tirasawadichai T, Judge DP, *et al.* **(2014)** Missense mutations in plakophilin-2 cause sodium current deficit and associate with a Brugada syndrome phenotype. *Circulation*. Mar 11;129(10):1092-103

Collins CA, Morgan JE. **(2003)** Duchenne's muscular dystrophy: animal models used to investigate pathogenesis and develop therapeutic strategies. *Int J Exp Pathol.* Aug;84(4):165-72

Corrado D, Basso C, Thiene G. **(2000)** Arrhythmogenic right ventricular cardiomyopathy: Diagnosis, prognosis, and treatment. *Heart* 83:588–595

Delmar M, McKenna WJ. **(2010)** The cardiac desmosome and arrhythmogenic cardiomyopathies: from gene to disease. *Circ Res*. 107:700-714

Di Pasquale E, Lodola F, Miragoli M, Denegri M, Avelino-Cruz JE, Buonocore M, Nakahama H, Portararo P, Bloise R, Napolitano C, *et al.* **(2013)** CaMKII inhibition rectifies arrhythmic phenotype in a patient-specific model of catecholaminergic polymorphic ventricular tachycardia. *Cell Death Dis* 4:e843

Drawnel FM, Boccardo S, Prummer M, Delobel F, Graff A, Weber M, Gérard R, Badi L, Kam-Thong T, Bu L, *et al.* **(2014)** Disease modeling and phenotypic drug screening for diabetic cardiomyopathy using human induced pluripotent stem cells. *Cell Rep*. Nov 6;9(3):810-21

Duboc D, Meune C, Lerebours G, Devaux JY, Vaksmann G, Bécane HM. **(2005)** Effect of perindopril on the onset and progression of left ventricular dysfunction in Duchenne muscular dystrophy. *J Am Coll Cardiol.* Mar 15;45(6):855-7

Egashira T, Yuasa S, Suzuki T, Aizawa Y, Yamakawa H, Matsuhashi T, Ohno Y, Tohyama S, Okata S, Seki T, *et al.* **(2012)** Disease characterization using LQTS-specific induced pluripotent stem cells. *Cardiovasc Res* 95 419–29

Fatima A, Xu G, Shao K, Papadopoulos S, Lehmann M, Arnáiz-Cot JJ, Rosa AO, Nguemo F, Matzkies M, Dittmann S, *et al.* **(2011)** In vitro modeling of ryanodine receptor 2 dysfunction using human induced pluripotent stem cells. *Cell Physiol Biochem* 28:579–92

Fong PY, Turner PR, Denetclaw WF, Steinhardt RA. **(1990)** Increased activity of calcium leak channels in myotubes of Duchenne human and MDX mouse origin. *Science.* 250:673– 676

Franco-Obregon A Jr, Lansman JB. **(1994)** Mechanosensitive ion channels in skeletal muscle from normal and dystrophic mice. *J Physiol.* 481:299–309

Frank R, Fontaine G, Vedel J, Mialet G, Sol C, Guiraudon G, Grosgogeat Y. **(1978)** Electrocardiology of 4 cases of right ventricular dysplasia inducing arrhythmia. *Arch Mal Coeur Vaiss*. 71:963-972

Frankel KA, Rosser RJ. **(1976)** The pathology of the heart in progressive muscular dystrophy: epimyocardial fibrosis. *Hum Pathol.* 7:375–386

Gallicano GI, Kouklis P, Bauer C, Yin M, Vasioukhin V, Degenstein L, Fuchs E. **(1998)** Desmoplakin is required early in development for assembly of desmosomes and cytoskeletal linkage. *J Cell Biol.* 143:2009–2022

Garcia-Gras E, Lombardi R, Giocondo MJ, Willerson JT, Schneider MD, Khoury DS, Marian AJ. **(2006)** Suppression of canonical Wnt/beta-catenin signaling by nuclear plakoglobin recapitulates phenotype of arrhythmogenic right ventricular cardiomyopathy *J Clin Invest.* Jul;116(7):2012-21

Gomes J, Finlay M, Ahmed AK, Ciaccio EJ, Asimaki A, Saffitz JE, Quarta G, Nobles M, Syrris P, Chaubey S, *et al.* **(2012)** Electrophysiological abnormalities precede overt structural changes in arrhythmogenic right ventricular cardiomyopathy due to mutations in desmoplakin-A combined murine and human study. *Eur Heart J* 33: 1942-1953

Grossmann KS, Grund C, Huelsken J, Behrend M, Erdmann B, Franke WW, Birchmeier W. **(2004)** Requirement of plakophilin 2 for heart morphogenesis and cardiac junction formation. *J Cell Biol.* 167:149 –160

Guan X, Mack DL, Moreno CM, Strande JL, Mathieu J, Shi Y, Markert CD, Wang Z, Liu G, Lawlor MW,*et al.* **(2014)** Dystrophin-deficient cardiomyocytes derived from human urine: new biologic reagents for drug discovery. *Stem Cell Res*.Mar;12(2):467-80

Han L, Li Y, Tchao J, Kaplan AD, Lin B, Li Y, Mich-Basso J, Lis A, Hassan N,London B, *et al.* **(2014)** Study familial hypertrophic cardiomyopathy using patient-specific induced pluripotent stem cells. *Cardiovasc Res.* Nov 1;104(2):258-69

Herren T, Gerber PA, Duru F. **(2009)** Arrhythmogenic right ventricular cardiomyopathy/dysplasia: a not so rare "disease of the desmosome" with multiple clinical presentations. *Clin Res Cardiol.* 98:141-158

Hick A, Wattenhofer-Donzé M, Chintawar S, Tropel P, Simard JP, Vaucamps N, Gall D, Lambot L, André C, Reutenauer *et al.,* **(2013)** Neurons and cardiomyocytes derived from induced

pluripotent stem cells as a model for mitochondrial defects in Friedreich's ataxia. *Dis Model Mech.* May;6(3):608-21

Higuchi T, Kawagoe S, Otsu M, Shimada Y, Kobayashi H, Hirayama R, Eto K, Ida H, Ohashi T, Nakauchi H, Eto Y**. (2014)** The generation of induced pluripotent stem cells (iPSCs) from patients with infantile and late-onset types of Pompe disease and the effects of treatment with acid-α-glucosidase in Pompe's iPSCs. *Mol Genet Metab*. May;112(1):44-8

Ho JC, Zhou T, Lai WH, Huang Y, Chan YC, Li X, Wong NL, Li Y, Au KW, Guo D, *et al.* **(2011)** Generation of induced pluripotent stem cell lines from 3 distinct laminopathies bearing heterogeneous mutations in lamin A/C. *Aging (Albany NY)* 3:380–90

Hoffman EP, Brown RH, Kunkel LM. **(1987)** Dystrophin: the protein product of the Duchenne muscular dystrophy locus. *Cell* 51, 919–928

Hoshiya, H, Kazuki, Y, Abe, S, Takiguchi, M, Kajitani, N, Watanabe, Y *et al.* **(2009)**. A highly stable and nonintegrated human artificial chromosome (HAC) containing the 2.4 Mb entire human dystrophin gene. *Mol Ther* 17: 309–317.

Howell JM, Fletcher S, Kakulas BA, O'Hara M, Lochmuller H, Karpati G. **(1997)** Use of the dog model for Duchenne muscular dystrophy in gene therapy trials. *Neuromuscul Disord.* Jul;7(5):325-8

Huang HP, Chen PH, Hwu WL, Chuang CY, Chien YH, Stone L, Chien CL, Li LT, Chiang SC, Chen HF. **(2011)** Human Pompe disease-induced pluripotent stem cells for pathogenesis modeling, drug testing and disease marker identification. *Hum Mol Genet.* Dec 15;20(24):4851-64

Huard J, Cao B, Qu-Petersen Z. **(2003)** Muscle-derived stem cells: potential for muscle regeneration. *Birth Defects Res C Embryo Today*. Aug;69(3):230-7

Ishikawa Y, Bach JR, Minami R**. (1999)** Cardioprotection for Duchenne's muscular dystrophy. *Am Heart J.* May;137(5):895-902

Itier JM, Ret G, Viale S, Sweet L, Bangari D, Caron A, Le-Gall F, Bénichou B, Leonard J, Deleuze JF *et al.* **(2014)** Effective clearance of GL-3 in a human iPSC-derived cardiomyocyte model of Fabry disease. *J Inherit Metab Dis*. Nov;37(6):1013-22

Itzhaki I, Maizels L, Huber I, Gepstein A, Arbel G, Caspi O, Miller L, Belhassen B, Nof E, Glikson M, *et al*. **(2012)** Modeling of catecholaminergic polymorphic ventricular tachycardia with patient-specific human-induced pluripotent stem cells. *J Am Coll Cardiol* 60:990–1000

Itzhaki I, Maizels L, Huber I, Zwi-Dantsis L, Caspi O, Winterstern A, Feldman O, Gepstein A, Arbel G, Hammerman H, *et al.* **(2011)** Modelling the long QT syndrome with induced pluripotent stem cells. *Nature* 471:225–9

Jiang Y, Habibollah S, Tilgner K, Collin J, Barta T, Al-Aama JY, Tesarov L, Hussain R, Trafford AW, Kirkwood G, *et al.* **(2014)** An induced pluripotent stem cell model of hypoplastic left heart syndrome (HLHS) reveals multiple expression and functional differences in HLHS-derived cardiac myocytes. *Stem Cells Transl Med*. Apr;3(4):416-23

Joshi-Mukherjee R, Coombs W, Musa H, Oxford E, Taffet S, Delmar M. **(2008)** Characterization of the molecular phenotype of two arrhythmogenic right ventricular cardiomyopathy (ARVC)-related plakophilin-2 (PKP2) mutations. *Heart Rhythm*. Dec;5(12):1715-23

Jung C, Martins AS, Niggli E, Shirokova N. **(2008)** Dystrophic cardiomyopathy: amplification of cellular damage by Ca2+ signalling and reactive oxygen species-generating pathways. *Cardiovasc Res.* 77:766 –773

Jung CB, Moretti A, Mederos y Schnitzler M, Iop L, Storch U, Bellin M, Dorn T, Ruppenthal S, Pfeiffer S, Goedel A, *et al.* **(2012)** Dantrolene rescues arrhythmogenic RYR2 defect in a patient-specific stem cell model of catecholaminergic polymorphic ventricular tachycardia. *EMBO Mol Med* 4:180–91

Karakikes I, Termglinchan V, Wu JC. **(2014)** Human-induced pluripotent stem cell models of inherited cardiomyopathies. *Curr Opin Cardiol*. May;29(3):214-9

Kattman SJ, Witty AD, Gagliardi M, Dubois NC, Niapour M, Hotta A, Ellis J, Keller G. **(2011)** Stage-specific optimization of activin/nodal and BMP signaling promotes cardiac differentiation of mouse and human pluripotent stem cell lines. *Cell Stem Cell*. Feb 4;8(2):228-40

Kazuki, Y, Hiratsuka, M, Takiguchi, M, Osaki, M, Kajitani, N, Hoshiya, H *et al.* **(2010)** Complete genetic correction of ips cells from Duchenne muscular dystrophy. *Mol Ther* 18: 386–393.

Kazuki Y, Hoshiya H, Takiguchi M, Abe S, Iida Y, Osaki M, Katoh M, Hiratsuka M, Shirayoshi Y, Hiramatsu K, *et al.* **(2011)** Refined human artificial chromosome vectors for gene therapy and animal transgenesis. *Gene Ther* 18: 384–393

Kim C, Wong J, Wen J, Wang S, Wang C, Spiering S, Kan NG, Forcales S, Puri PL, Leone TC *et al.* **(2013)** Studying arrhythmogenic right ventricular dysplasia with patient-specific iPSCs. *Nature.* Feb 7;494(7435):105-10

Kujala K, Paavola J, Lahti A, Larsson K, Pekkanen-Mattila M, Viitasalo M, Lahtinen AM, Toivonen L, Kontula K, Swan H, *et al.* **(2012)** Cell model of catecholaminergic polymorphic ventricular tachycardia reveals early and delayed afterdepolarizations. *PLoS One* 7:e44660

Lahti AL, Kujala VJ, Chapman H, Koivisto AP, Pekkanen-Mattila M, Kerkelä E, Hyttinen J, Kontula K, Swan H, Conklin BR, *et al.* **(2012)** Model for long QT syndrome type 2 using human iPS cells demonstrates arrhythmogenic characteristics in cell culture. *Dis Model Mech* 5:220–30

Lan F, Lee AS, Liang P, Sanchez-Freire V, Nguyen PK, Wang L, Han L, Yen M, Wang Y, Sun N, *et al.* **(2013)** Abnormal calcium handling properties underlie familial hypertrophic cardiomyopathy pathology in patient-specific induced pluripotent stem cells. *Cell Stem Cell* 12:101–13

Liang P, Lan F, Lee AS, Gong T, Sanchez-Freire V, Wang Y, Diecke S, Sallam K, Knowles JW, Wang PJ, *et al.,* **(2013)** Drug screening using a library of human induced pluripotent stem cell-derived cardiomyocytes reveals disease-specific patterns of cardiotoxicity. *Circulation.* Apr 23;127(16):1677-91

Ma D, Wei H, Lu J, Ho S, Zhang G, Sun X, Oh Y, Tan SH, Ng ML, Shim W, *et al.* **(2013)** Generation of patientspecific induced pluripotent stem cell-derived cardiomyocytes as a cellular model of arrhythmogenic right ventricular cardiomyopathy. *Eur Heart J* 34:1122–33

Ma D, Wei H, Zhao Y, Lu J, Li G, Sahib NB, Tan TH, Wong KY, Shim W, Wong P, Cook SA, *et al.* **(2013)** Modeling type 3 long QT syndrome with cardiomyocytes derived from patient-specific induced pluripotent stem cells. *Int J Cardiol* 168:5277–86

Mallat Z, Tedgui A, Fontaliran F, Frank R, Durigon M, Fontaine G. **(1996)** Evidence of apoptosis in arrhythmogenic right ventricular dysplasia. *N Engl J Med* 335: 1190-1196

Matthes SA, Taffet S, Delmar M. **(2011)** Plakophilin-2 and the migration, differentiation and transformation of cells derived from the epicardium of neonatal rat hearts. *Cell Commun Adhes* 18: 73-84

Matsa E, Dixon JE, Medway C, Georgiou O, Patel MJ, Morgan K, Kemp PJ, Staniforth A, Mellor I, Denning C. **(2014)** Allelespecific RNA interference rescues the long-QT syndrome phenotype in human-induced pluripotency stem cell cardiomyocytes. *Eur Heart J* 35:1078–87

Matsa E, Rajamohan D, Dick E, Young L, Mellor I, Staniforth A, Denning C. **(2011)** Drug evaluation in cardiomyocytes derived fromhuman induced pluripotent stem cells carrying a long QT syndrome type 2 mutation. *Eur Heart J* 32:952–62

McNally EM. **(2007)** New approaches in the therapy of cardiomyopathy in muscular dystrophy. *Annu Rev Med*. 58:75– 88

Menke A, Jockusch H. **(1995)** Extent of shock-induced membrane leakage in human and mouse myotubes depends on dystrophin. *J Cell Sci.* 108:727–733

Miller RG, Sharma KR, Pavlath GK, Gussoni E, Mynhier M, Lanctot AM, Greco CM, Steinman L, Blau HM. **(1997)** Myoblast implantation in Duchenne muscular dystrophy: the San Francisco study. *Muscle Nerve*. Apr;20(4):469-78.

Moretti A, Bellin M, Welling A, Jung CB, Lam JT, Bott-Flügel L, Dorn T, Goedel A, Höhnke C, Hofmann F, *et al.* **(2010)** Patient-specific induced pluripotent stem-cell models for long-QT syndrome. *N Engl J Med* 363:1397–409

Muller J, Vayssiere N, Royuela M, Leger ME, Muller A, Bacou F, Pons F, Hugon G, Mornet D. **(2001)** Comparative evolution of muscular dystrophy in diaphragm, gastrocnemius and masseter muscles from old male mdx mice. *J Muscle Res Cell Motil.* 22(2):133-9

Munkholm J, Andersen CB, Ottesen GL. **(2015)** Plakoglobin: A diagnostic marker of arrhythmogenic right ventricular cardiomyopathy in forensic pathology? *Forensic Sci Med Pathol.* Jan 1

Muntoni F, Torelli S, Ferlini A. **(2003)** Dystrophin and mutations: one gene, several proteins, multiple phenotypes. *Lancet Neurol*. Dec;2(12):731-40

Nolan MA, Jones OD, Pedersen RL, Johnston HM. **(2003)** Cardiac assessment in childhood carriers of Duchenne and Becker muscular dystrophies. *Neuromuscul Disord.* 13:129 –132

Novak A, Barad L, Zeevi-Levin N, Shick R, Shtrichman R, Lorber A, Itskovitz-Eldor J, Binah O. **(2012)** Cardiomyocytes generated from CPVTD307H patients are arrhythmogenic in response to b-adrenergic stimulation. *J Cell Mol Med* 16:468–82

Oxford EM, Musa H, Maass K, Coombs W, Taffet SM, Delmar M. **(2007)** Connexin43 remodeling caused by inhibition of plakophilin-2 expression in cardiac cells. *Circ Res.* 101:703–711

Pasternak C, Wong S, Elson EL. **(1995)** Mechanical function of dystrophin in muscle cells. *J Cell Biol*. 128:355–361

Perriard JC, Hirschy A, Ehler E. **(2003)** Dilated cardiomyopathy: a disease of the intercalated disc? *Trends Cardiovasc Med*. 13:30–38

Pilichou K, Remme CA, Basso C, Campian ME, Rizzo S, Barnett P, Scicluna BP, Bauce B, van den Hoff MJ, de Bakker JM, *et al.* **(2009)** Myocyte necrosis underlies progressive myocardial dystrophy in mouse dsg2-related arrhythmogenic right ventricular cardiomyopathy. *J Exp Med.* 206:1787–1802

Prosser BL, Khairallah RJ, Ziman AP, Ward CW, Lederer WJ. **(2013)** X-ROS signaling in the heart and skeletal muscle: stretch-dependent local ROS regulates [Ca2+]i. *J Mol Cell Cardiol.* May;58:172-81

Raval KK, Tao R, White BE, De Lange WJ, Koonce CH, Yu J, Kishnani PS, Thomson JA, Mosher DF, Ralphe JC et al. **(2014)** Pompe disease results in a Golgi-based glycosylation deficit in human induced pluripotent stem cell-derived cardiomyocytes. *J Biol Chem.* Dec 8

Richardson P, McKenna W, Bristow M, Maisch B, Mautner B, O'Connell J, Olsen E, Thiene G, Goodwin J, Gyarfas I. **(1996)** Report of the 1995 World Health Organization/International Society and Federation of Cardiology Task Force on the Definition and Classification of cardiomyopathies. *Circulation*. 93:841-842

Saguner AM, Brunckhorst C, Duru F. **(2014)** Arrhythmogenic ventricular cardiomyopathy: A paradigm shift from right to biventricular disease. *World J Cardiol.* Apr 26;6(4):154-74

Sallam K, Kodo K, Wu JC. **(2014)** Modeling inherited cardiac disorders. *Circ J.* 78(4):784-94

Savla JJ, Nelson BC, Perry CN, Adler ED. **(2014)** Induced pluripotent stem cells for the study of cardiovascular disease. *J Am Coll Cardiol.* Aug 5;64(5):512-9

Sato PY, Musa H, Coombs W, Guerrero-Serna G, Patino GA, Taffet SM, Isom LL, Delmar M. **(2009)** Loss of plakophilin-2 expression leads to decreased sodium current and slower conduction velocity in cultured cardiac myocytes. *Circ Res.* 105:523–526

Sharma A, Marceau C, Hamaguchi R, Burridge PW, Rajarajan K, Churko JM, Wu H, Sallam KI, Matsa E, Sturzu AC *et al.* **(2014)** Human induced pluripotent stem cell-derived cardiomyocytes as an in vitro model for coxsackievirus B3-induced myocarditis and antiviral drug screening platform. *Circ Res.* Aug 29;115(6):556-66

Siu CW, Lee YK, Ho JC, Lai WH, Chan YC, Ng KM, Wong LY, Au KW, Lau YM, Zhang J, *et al.* **(2012)** Modeling of lamin A/C mutation premature cardiac aging using patient-specific induced pluripotent stem cells. *Aging (Albany NY)* 4:803–22

Spurney, CF **(2011)** Cardiomyopathy of Duchenne muscular dystrophy: current understanding and future directions. *Muscle Nerve* 44: 8–19

Sun N, Yazawa M, Liu J, Han L, Sanchez-Freire V, Abilez OJ, Navarrete EG, Hu S, Wang L, Lee A, *et al.* **(2012)** Patient-specific induced pluripotent stem cells as a model for familial dilated cardiomyopathy. *Sci Transl Med* 4:130ra47

Terrenoire C, Wang K, Tung KW, Chung WK, Pass RH, Lu JT, Jean JC, Omari A, Sampson KJ, Kotton DN, *et al.* **(2013)** Induced pluripotent stem cells used to reveal drug actions in a long QT syndrome family with complex genetics. *J Gen Physiol* 141:61–72

Tse HF, Ho JC, Choi SW, Lee YK, Butler AW, Ng KM, Siu CW, Simpson MA, Lai WH, Chan YC, *et al.* **(2013)** Patient-specific induced-pluripotent stem cells-derived cardiomyocytes recapitulate the pathogenic phenotypes of dilated cardiomyopathy due to a novel DES mutation identified by whole exome sequencing. *Hum Mol Genet*. Apr 1;22(7):1395-403

Verhaert D, Richards K, Rafael-Fortney JA, Raman SV. **(2011)** Cardiac involvement in patients with muscular dystrophies: magnetic resonance imaging phenotype and genotypic considerations. *Circ Cardiovasc Imaging. Jan*;4(1):67-76

Wang G, McCain ML, Yang L, He A, Pasqualini FS, Agarwal A, Yuan H, Jiang D,Zhang D, Zangi L, *et al.* **(2014)** Modeling the mitochondrial cardiomyopathy of Barth syndrome with induced pluripotent stem cell and heart-on-chip technologies. *Nat Med.* Jun;20(6):616-23

Wang Q, Lin JL, Wu KH, Wang DZ, Reiter RS, Sinn HW, Lin CI, Lin CJ. **(2012)** Xin proteins and intercalated disc maturation, signaling and diseases. *Front Biosci (Landmark Ed*). Jun 1;17:2566-93

Yang Z, Bowles NE, Scherer SE, Taylor MD, Kearney DL, Ge S, Nadvoretskiy VV, DeFreitas G, Carabello B, Brandon LI, *et al.* **(2006)** Desmosomal dysfunction due to mutations in desmoplakin causes arrhythmogenic right ventricular dysplasia/cardiomyopathy. *Circ Res.* 99:646–655.

Yazawa M, Hsueh B, Jia X, Pasca AM, Bernstein JA, Hallmayer J, Dolmetsch RE. **(2011)** Using induced pluripotent stem cells to investigate cardiac phenotypes in Timothy syndrome. *Nature* 471:230–4

Zatti S, Martewicz S, Serena E, Uno N, Giobbe GG, Kazuki Y, Oshimura M, Elvassore N. **(2014)** Complete restoration of multiple dystrophin isoforms in genetically corrected Duchenne muscular dystrophy patient–derived cardiomyocytes. *Mol Ther - Meth & Clin Dev* 1

Zhang XH, Haviland S, Wei H, Sarić T, Fatima A, Hescheler J, Cleemann L, Morad M. **(2013)** Ca2þ signaling in human induced pluripotent stem cell-derived cardiomyocytes (iPS-CM) from normal and catecholaminergic polymorphic ventricular tachycardia (CPVT)-afflicted subjects. *Cell Calcium* 54:57–70

Chapter 5

Conclusions and Future Perspectives

In this thesis we showed how the phenotype displayed *in vitro* by human cardiomyocytes derived by differentiation of pluripotent stem cells can be modified and driven towards later developmental stages than the fetal one. Promoting the maturation of hPSC-CMs is a desirable process for the generation of a robust and representative model of human cardiac physiology and physiopathology. The applications of such cellular models span across all the field of *in vitro* studies, from disease modeling to compound screening and drug testing, down to basic understanding of the cardiomyocyte biology.

For most reported applications, the main reference nowadays are animal models and *in vivo* studies (De Ponti *et al.,* 2002). These approaches, despite being valuable sources of knowledge and still an unavoidable step in understanding cardiac physiology and pathophysiology on the background of a whole complex organism, are characterized by big economic and scientific shortcomings (Zaragoza *et al.,* 2011). From an economic point of view, the maintenance and experimentation on animals, especially those more representative of human anatomy and physiology, are a great burden and could be reduced by preceding "cheaper" models. Currently, this bottleneck is represented by animal cardiac primary cultures, that offer the advantage of a fully developed and *bona fide* cardiac cell (Chlopcíková *et al.,* 2001), but are very limited considering the lack of consistency between preparations, the required

labor intensity and the insufficient cost-effective amount for proper high-throughput screenings (Carlson *et al.,* 2013).

In this scenario, the availability of a virtually infinite source of human cardiac cells provides a groundbreaking alternative to the animal models and will revolutionize the field of cardiac tissue modeling (Acimovic *et al.,* 2014). The species-identity with human patients and the cardiac nature of hPSC-CMs will provide better insight in human cardiac function in physiological, pathological and pharmacologically-altered conditions, and will become a cost effective safety screening tool for therapeutic approaches (Dick *et al.,* 2010). In order to do so, though, hPSC-CMs must gain the status of *bona fide* cardiomyocytes and understanding the mechanisms of *in vitro* cardiac development and maturation is of paramount importance to consciously generate robust human cardiomyocytes, along with developing technologies for assaying their functional performance.

In this thesis we showed, how the normally employed extension-of-time-in-culture approach for hPSC-CMs maturation, which is ill-advised for routine manufacture (Prowse *et al.,* 2014), can be circumvented by enhancing cell-substrate interaction and activating proper mechano-signaling. We prove that human cardiomyocytes cultured in adhesion improve their ultrastructural organization and functional performance and that the physical properties of the culture substrate constitute the driving force in such process. The molecular mechanotransduction plays a pivotal role in this structural and functional maturation, as its inhibition abrogates the substrate positive effect.

From the metabolic perspective, we approached the issue of the fetal-like metabolism displayed by hPSC-CMs designing a functional assay that allows fast screening for the effects of maturation protocols. We proposed as the experimental read-out the resistance of the cardiomyocytes to prolonged hypoxic stimuli, and evaluated their survival rate upon ischemic-like stresses. The severity of an ischemic-stress experienced by the cardiomyocyte deeply depends on the preferred energetic substrate, genetic expression patterns and

mitochondrial performance (Chouchani *et al.,* 2014), thus hypoxia-sensitivity synthesizes in one cellular response a plethora of upstream features characterizing a mature metabolic profile. We prove as well that a metabolite-driven maturation protocol of our design, analogous to those present in the literature, is a viable and easy approach to promote a more adult-like cardiac phenotype *in vitro*.

Finally, taking advantage of the induced pluripotent stem cell-technology, we set up the basis for human *in vitro* cardiac models for two genetic diseases, generating cultures of patient-specific cardiomyocytes. We show how the generated cardiomyocytes from patients affected by Duchenne's muscular dystrophy (DMD) and arrhythmogenic right ventricular cardiomyopathy/ dysplasia (ARVC/D) recapitulate the aberrant molecular phenotype of the disease *in vitro*, thus providing a good source material for further studies of the pathologies in the human genetic and physiological background offered by hPSC-CMs.

Modeling a disease *in vitro* requires in first instance the availability of a biological source material faithfully reproducing the *in vivo* counterpart. With the advent of the induced pluripotent stem cell-technology, the playground for disease modeling has been broadened from few spontaneously occurring animal conditions (for example the *mdx* mouse or the boxer cardiomyopathy (Fong *et al.,* 1990; Basso *et al.,* 2004)) or laboriously generated transgenic animals to the whole panel of human genetic backgrounds. Since, 2007 countless genetic pathologic conditions have been addressed with hiPSC generation and *in vitro* models have been set up through differentiation of those pluripotent stem cells towards the specific lineage of interest. In this thesis, we provide proof of such approach with derivation of the first *in vitro* cardiac model of DMD-affected hiPSC and we generated cardiomyocytes from an already established ARVC/D-affected hiPS line (Kim *et al.,* 2013). With the constantly developing reprogramming and differentiation technologies, the panel of available cell lines with different genetic backgrounds will keep increasing rapidly in the next years.

The issue of the maturation degree and target-cell resemblance has been widely discussed in this thesis and the strive for better and more adult-like hPSC-derivatives will result in improved culture methods and understanding of basic developmental processes in human cells.

5.1 References

Acimovic I, Vilotic A, Pesl M, Lacampagne A, Dvorak P, Rotrekl V, Meli AC. **(2014)** Human pluripotent stem cell-derived cardiomyocytes as research and therapeutic tools. Biomed Res Int. 2014:512831

Basso C, Fox PR, Meurs KM, Towbin JA, Spier AW, Calabrese F, Maron BJ, Thiene G. **(2004)** Arrhythmogenic right ventricular cardiomyopathy causing sudden cardiac death in boxer dogs: a new animal model of human disease. *Circulation.* 109:1180 –1185

Carlson C, Koonce C, Aoyama N, Einhorn S, Fiene S, Thompson A, Swanson B, Anson B, Kattman S. **(2013)** Phenotypic screening with human iPS cell-derived cardiomyocytes: HTS-compatible assays for interrogating cardiac hypertrophy. *J Biomol Screen*. Dec;18(10):1203-11

Chlopcíková S, Psotová J, Miketová P. **(2001)** Neonatal rat cardiomyocytes--a model for the study of morphological, biochemical and electrophysiological characteristics of the heart. *Biomed Pap Med Fac Univ Palacky Olomouc Czech Repub*. Dec;145(2):49-55

Chouchani ET, Pell VR, Gaude E, Aksentijević D, Sundier SY, Robb EL, Logan A, Nadtochiy SM, OrdEN, Smith AC, *et al.* **(2014)** Ischaemic accumulation of succinate controls reperfusion injury through mitochondrial ROS. *Nature.* Nov 20;515(7527):431-5

De Ponti F, Poluzzi E, Cavalli A, Recanatini M, Montanaro N. **(2002)** Safety of non-antiarrhythmic drugs that prolong the QT interval or induce torsade de pointes: an overview. *Drug Saf.* 25(4):263-86.

Dick E, Rajamohan D, Ronksley J, Denning C. **(2010)** Evaluating the utility of cardiomyocytes from human pluripotent stem cells for drug screening. *Biochem Soc Trans.* Aug;38(4):1037-45

Du DT, Hellen N, Kane C, Terracciano CM. **(2015)** Action potential morphology of human induced pluripotent stem cell-derived cardiomyocytes does not predict cardiac chamber specificity and is dependent on cell density. *Biophys J.* Jan 6;108(1):1-4

Fong PY, Turner PR, Denetclaw WF, Steinhardt RA. **(1990)** Increased activity of calcium leak channels in myotubes of Duchenne human and MDX mouse origin. *Science.* 250:673– 676

Kim C, Wong J, Wen J, Wang S, Wang C, Spiering S, Kan NG, Forcales S, Puri PL, Leone TC *et al.* **(2013)** Studying arrhythmogenic right ventricular dysplasia with patient-specific iPSCs. *Nature.* Feb 7;494(7435):105-10

Miller EW, Lin JY, Frady EP, Steinbach PA, Kristan WB Jr, Tsien RY. **(2012)** Optically monitoring voltage in neurons by photo-induced electron transfer through molecular wires. *Proc Natl Acad Sci U S A.* Feb 7;109(6):2114-9

Prowse AB, Timmins NE, Yau TM, Li RK, Weisel RD, Keller G, Zandstra PW. **(2014)** Transforming the promise of pluripotent stem cell-derived cardiomyocytes to a therapy: challenges and solutions for clinical trials. *Can J Cardiol*. Nov;30(11):1335-49

Zaragoza C, Gomez-Guerrero C, Martin-Ventura JL, Blanco-Colio L, Lavin B, Mallavia B, Tarin C, Mas S, Ortiz A, Egido J. **(2011)** Animal models of cardiovascular diseases. *J Biomed Biotechnol.* 2011:497841

Appendix A

Cell Culture and Substrate Engineering

This appendix section reports the origin and culture methods of the cell cultures employed in this thesis. Not standard culture substrates, such as hydrogels and patterned surfaces, are presented in detail and the fabrication process is described.

A.1 Pluripotent stem cell cultures

For detailed compositions of the cited media and solutions please refer to the "Annex" section, at the "Materials and Methods" section of the attached papers. The designation and origin of the human pluripotent stem cells lines employed for the work described in this thesis are listed in the Table A.1.

The lines HES2, ADHF#1, DMD-hiPS and DysHAC-hiPS were maintained and expanded in mitomycin-C inactivated MEF-feeder conditions and passaged enzimatically before reaching full confluence by 60 seconds incubation at 37°C with either trypsin 0.25%-EDTA solution (HES2, see **Annex 1**) or CTK solution (ADHF#1, DMD-hiPS and DysHAC-hiPS, see **Annex 4**). The cultures were checked daily under a stereomicroscope and spontaneously differentiated areas were removed by mechanical picking. The media were changed daily with fresh ones.

The lines H9, mRNA-Clone1, αSkin119 and JK#11 were maintained and expanded in feeder-free conditions and passaged by mechanical dissociation (see **Annex 4**).

Table A.1 List of human pluripotent stem cell lines employed in this work.

Line	Type	Origin	Vector	Mutation	Reference
HES2	hES	WiCell cell bank	--	healthy	
H9	hES	WiCell cell bank	--	healthy	
ADHF#1	hiPS	Oshimura's Lab	Lentiviral infection	healthy	Kazuki et al., 2010
DMD-hiPS	hiPS	Oshimura's Lab	Lentiviral infection	DMD gene, exon 4-43 deletion	Kazuki et al., 2010
DysHAC-hiPS	hiPS	Oshimura's Lab	Lentiviral infection and HAC insertion	DMD gene, exon 4-43 deletion	Kazuki et al., 2010
mRNA-Clone1	hiPS	Elvassore's Lab	mmRNA transfecti on	healthy	
αSkin119	hiPS	Chen's Lab	Lentiviral infection	healthy, αMHC-Puro^r	Kim et al., 2013
JK#11	hiPS	Chen's Lab	Lentiviral infection	PKP2 gene, c.2484C.T	Kim et al., 2013

A.2 Cardiac differentiation of hPSC

The cardiomyocytes described in this thesis were derived from pluripotent stem cells applying two different cardiac differentiation protocols based on the work of prof. Gordon Keller and colleagues ("Keller protocol") (Kattman *et al.*, 2010) and prof. Sean Palecek and colleagues ("Palecek protocol") (Lian *et al.*, 2012).

All human cardiomyocytes described in **Paragraph 2.4** and **Paragraph 4.1** were derived with the "Keller protocol" (Fig. A.1), based on differentiation in embryoid bodies (EBs) maintained in suspension.

For EB formation, the cells were passaged at high density on culture plates coated with 5 mg/ml Growth Factors Reduced Matrigel for 48 hours in hPSC culture medium. They were then detached and transferred to ultra-low adhesive

plates and maintained for 24 hours in StemPRO-34 medium, 2 mM L-glutamine, 150 µg/ml transferrin, 50 µg/ml ascorbic acid, 0.4 mM monothioglycerol, 50 units and 50 mg/ml penicillin and streptomycin, and supplemented with 10 ng/ml rhBMP4. From day 1 today 4, EBs were cultured in basal medium with 10 ng/ml rhBMP4, 5 ng/ml hbFGF, and 6 ng/ml hActivin A. From day 4 to day 8, the EB culture medium consisted of basal medium and 10 ng/ml $hVEDF_{165}$ and 150 ng/ml hDKK-1. Finally, from day 8 to day 14, the EB culture medium consisted of basal medium supplemented with 10 ng/ml $hVEDF_{165}$, 150 ng/ml hDKK-1 and 5 ng/ml hbFGF. Cultures were maintained in a 5% CO_2, 5% O_2, and 90% N_2 environment for the first 16 days and then transferred to a 5% CO2 air environment and maintained in basal medium supplemented with 10 ng/ml $hVEDF_{165}$ and 5 ng/ml hbFGF before further experimental procedures.

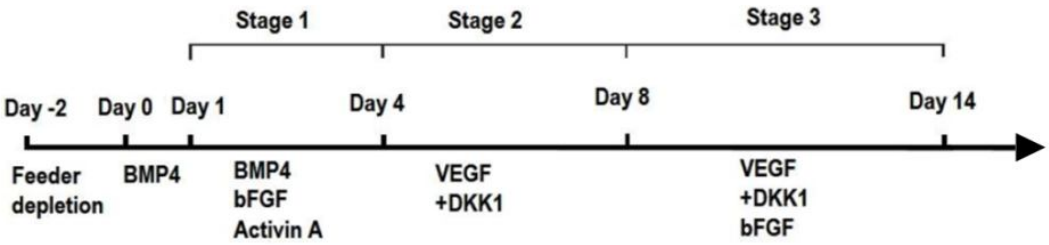

Fig. A.1 Schematic time course representation of the "Keller" cardiac differentiation protocol (adapted from Yang *et al.,* 2008)

All cardiomyocytes described in **Paragraph 3.4**, **Paragraph 3.5**, **Paragraph 4.2** were derived with the "Palecek protocol" (Fig. A.2), based on a chemically-defined and small molecule-based monolayer differentiation.

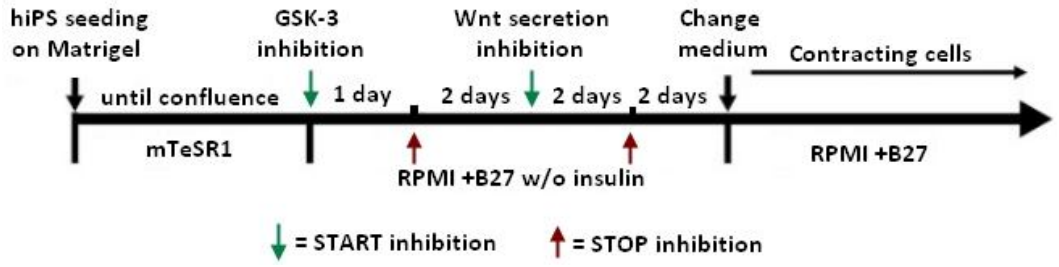

Fig. A.2 Schematic time course representation of the "Palecek" cardiac differentiation protocol (adapted from Lian *et al.,* 2012)

Before differentiation, the hPSCs were passaged in fresh culture plates coated with 50 µg/ml Growth Factors Reduced Matrigel and maintained in mTeSR1 medium until confluence was reached. At that point, the medium was switched

to RPMI + 1x B27 supplement without insulin (basal medium) with CHIR99021 inhibitor for 24 hours (concentrations of the inhibitor were optimized for each cell line and are reported in Table A.2). After 48 hours in basal medium, Wnt secretion was suppressed for 48 hours by medium change to basal medium with 10 μM IWP-4. From day 7 the cultures were maintained in RPMI + 1x B27 complete medium before further experimental procedures.

Table A.2 Concentrations of CHIR99021 for optimal GSK3-β inhibition in the first 24 hours of cardiac differentiation.

hPS cell line	Optimal [CHIR99021]
HES2	12 μM
H9	6 μM
mRNA-Clone1	8 μM
αSkin119	10 μM
JK#11	12 μM

A.3 Human cardiac media

For the maintenance of human cardiomyocytes differentiated from hPSCs, were used the media cited in **Paragraph A.2**. These two media are supplemented with proprietary synthetic nutrients in the form of StemPro-34 SFM Nutrient Supplement (Lifetechnologies cat#10641-025) and B27 Nutrient Supplement (Lifetechnologies cat#17504-044), which complete formulation is not disclosed.

For the experiments on metabolite-driven metabolic maturation the following two media were prepared and the energetic sources are listed in **Table A.3**, while the complete media formulations are available on-line on the manufacturers website.

Table A.3 Carbon sources in metabolic induction media from Paragraph 3.5.

Essential cardiac medium		Basic fatty acid medium	
D-Glucose	**5.5 mM**	L-Glutamine 4mM	**4 mM**
Sodium Pyruvate	**1 mM**	BSA-Linoleic Acid	**30 μM**
L-Glutamine	**2mM**		
Lipoic Acid	**1 μM**		

Essential cardiac medium: αMEM (Lifetechnologies cat#22561-021) + 0.1% NonEssentialAminoAcids (Lifetechnologies cat#11140-035) + 0.1% Insulin-Trasferrin-Selenite (Lifetechnologies cat#41400-045)

Basic fatty acid medium: DMEM w/o D-Glucose (Lifetechnologies cat#11966-025) + 1% BSA-Linoleic Acid (Sigma cat#L9530) + 0.1% Insulin-Trasferrin-Selenite (Lifetechnologies cat#41400-045)

When "No Glucose" control is cited, the basic DMEM w/o D-Glucose was used without any other addition.

A.4 Murine cardiac primary cultures

Neonatal rat cardiomyocytes were obtained from Sprague-Dawley pups 1–3 days old. The cell isolation process was carried out keeping the tissue samples constantly on ice after the heart extraction and during the blood removal and mincing processes. The tissue samples were then incubated over-night at 4°C in a 1 mg/ml trypsin-HBSS solution with gentle rocking (75 rpm). After trypsin wash out, the samples were digested at 37°C with 1mg/ml collagenase A in HBSS for 2 minutes rounds, collecting every single digestion suspension until complete tissue digestion. The suspension culture is then plated in MEM medium supplemented with 10% FBS for 1 hour to deplete the cell suspension of most of the present fibroblasts, recovered and ready for further experimental procedures. The cardiac cultures were maintained in MEM medium supplemented with 0.1% non-essential amminoacids, 0.1% insulin-transferrin-selenium and 1% penicillin-streptomycin. The animals were housed and operated at the Animal Colonies of either the Venetian Institute of Molecular Institute or the Biology Department. All experiments with animals were approved by Padua University's Institutional Animal Care Committee (CEASA).

A.5 Hydrogel fabrication

In order to fabricate compliant culture substrate with different stiffness features, the polyacrylamide hydrogel technique was employed. When in presence of an initiator (such as ammonium persulphate (APS) or IRGACURE 2959) a free radical-driven polymerization occurs, and the ratio between the monomer and the cross-linker in the solution defines the elastic modulus of the final hydrogel. In Table A.4 are summarized the concentrations of both reagents in the milliQ water-dissolved prepolymer (Tse and Engler, 2006).

Table A.3 The percentages of monomer (acrylamide) and cross-linker (bis-acrylamide) in the solutions for hydrogel of different stiffness.

Elastic modulus	Acrylamide	bis-Acrylamide
4 kPa	5%	0.15%
16 kPa	10%	0.15%
40 kPa	8%	0.48%
160 kPa	12%	0.6%

The physical support for the gels were glass slides with surfaces previously chemically modified in order to covalently bond with the gel. The glass slide were plasma treated for 2 minutes immediately followed by a 4 minutes incubation with a solution of 94% ethanol, 5% acetic acid and 1% 3-(Trimethoxysilyl)propyl methacrylate (Fig. A.3). The glass slides were then washed once in ethanol and three times in ddH_2O and air dried before hydrogel polymerization.

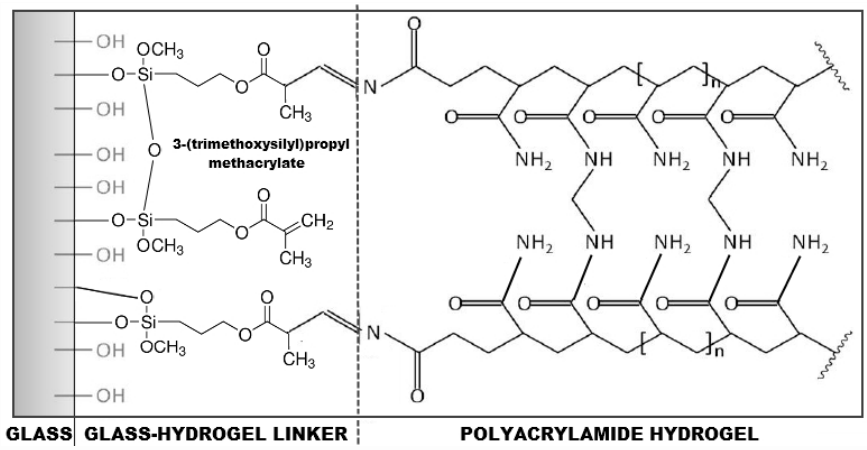

Fig. A.3 Schematic representation of the hydrogel chemistry covalently bound to the glass surface.

Hydrogels were polymerized for 20 minutes against a flat glass surface pretreated with hexamethyldisilazane (HMDS), through chemical initiation with 1% APS and 0.1% N,N,N',N'-Tetramethylethylenediamine (TEMED), in a solution volume calculated to yield an hydrogel height of 100 μm.

Polyacrilamide hydrogels are naturally cell repellent. In order to perform cell cultures, after air drying and UV sterilization, the hydrogels were coated for 1 hour at 37°C with a solution containing 100 μg/ml laminin and 50 μg/ml fibronectin and then air dried again before cell seeding. This coating protocol allows cultures up to 5 days without cell detachment from the substrate (see **Annex 1**).

A.6 Production of patterned surfaces

Patterned cultures of desired geometry were obtained by defining cell-adhesive and cell-repellant areas on the culture substrate.

For glass surfaces, patterns were achieved by selective photo-polymerization of linear acrylamide (8% acrylamide solution in milliQ water in presence of 0.1M HEPES) on glass slides pretreated as described in **Paragraph A.5**. Photo-polymerization was carried out by exposure to 365 nm UV light (delivered by optic fiber onto the sample) for a total energy amount of 900 mJ (Fig. A.4). The photo-initiator used was IRGACURE 2959, dissolved in methanol at a concentration of 350 mg/ml and diluted in the prepolymer 1:10. The desired

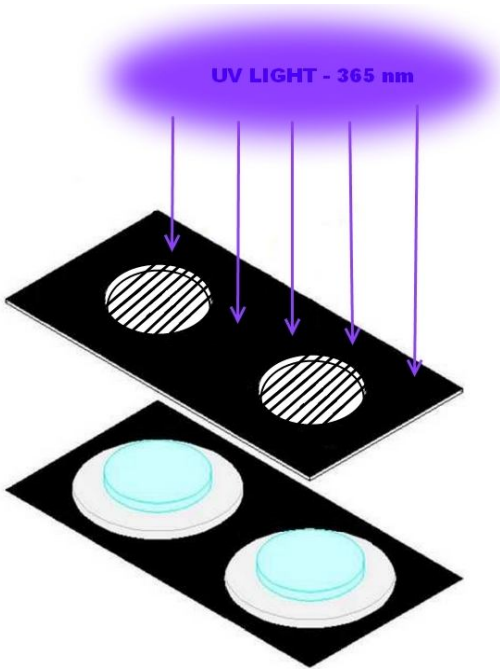

Fig. A.4 Schematic representation of the photo-mask used to generate linear patterns. The UV light irradiates the prepolymer solution (blue) generating a cell-repellant polymer and leaving bare the glass surface shielded by the printed pattern (black).

geometries (i.e. linear patterns 50-300 μm wide) were printed on polyacetate transparent sheets with commercially available printers and the photo-mask was placed at close distance to the sample in order to prevent polymerization in the desired areas. Linear acrylamide polymers are cell-repellant even after protein coating (either laminin/fibronectin coating or 50 μg/ml Growth Factors Reduced Matrigel).

A.7 References

Kattman SJ, Witty AD, Gagliardi M, Dubois NC, Niapour M, Hotta A, Ellis J, Keller G. **(2011)** Stage-specific optimization of activin/nodal and BMP signaling promotes cardiac differentiation of mouse and human pluripotent stem cell lines. *Cell Stem Cell*. Feb 4;8(2):228-40

Kazuki, Y, Hiratsuka, M, Takiguchi, M, Osaki, M, Kajitani, N, Hoshiya, H *et al.* **(2010)** Complete genetic correction of ips cells from Duchenne muscular dystrophy. *Mol Ther* 18: 386–393.

Kim C, Wong J, Wen J, Wang S, Wang C, Spiering S, Kan NG, Forcales S, Puri PL, Leone TC *et al.* **(2013)** Studying arrhythmogenic right ventricular dysplasia with patient-specific iPSCs. *Nature.* Feb 7;494(7435):105-10

Liang P, Lan F, Lee AS, Gong T, Sanchez-Freire V, Wang Y, Diecke S, Sallam K, Knowles JW, Wang PJ, *et al.,* **(2013)** Drug screening using a library of human induced pluripotent stem cell-derived cardiomyocytes reveals disease-specific patterns of cardiotoxicity. *Circulation.* Apr 23;127(16):1677-91

Tse JR, Engler AJ. **(2010)** Preparation of hydrogel substrates with tunable mechanical properties. *Curr Protoc Cell Biol.* Jun;Chapter 10:Unit 10.16

Yang L, Soonpaa MH, Adler ED, Roepke TK, Kattman SJ, Kennedy M, Henckaerts E, Bonham K, Abbott GW, Linden RM, *et al.,* **(2008)** Human cardiovascular progenitor cells develop from a KDR+ embryonic-stem-cell-derived population. *Nature*. 7194, 524-8

Appendix B

Microfabrication techniques

This appendix reports the microfabrication techniques employed for the construction of the microfluidic devices. Moreover, the quantification of oxygen concentration is described in detail. All the material details and procedure are reported as well in **Annex 2** and **Annex 3**.

B.1 Litography

The microfluidic device was fabricated by photo-lithographic technique, followed by softlithografy replica molding (Gómez-Sjöberg *et al.,* 2007). The hypoxia microfluidic chip was designed as a multilayer platform, so 2 different silica-photoresist casts had to be made: one for the three-channel culture chamber layer and one for the climatic chamber. The procedure is described in detail below, but briefly: a hardened photoresist cast was made on 4" silica wafers, with the desired geometry and height, and was reused every time to produce PolyDiMethylSiloxane (PDMS) soft replicas (Fig. B.1). PDMS is a silicon biomaterial, made of a monomer and a cross-linker in liquid state that react upon heating forming a transparent, non-toxic, highly gas-permeable solid polymer. Thus, a solution of liquid monomer/cross-linker can be poured on the silica cast, baked and easily detached maintaining the impressed form of the cast.

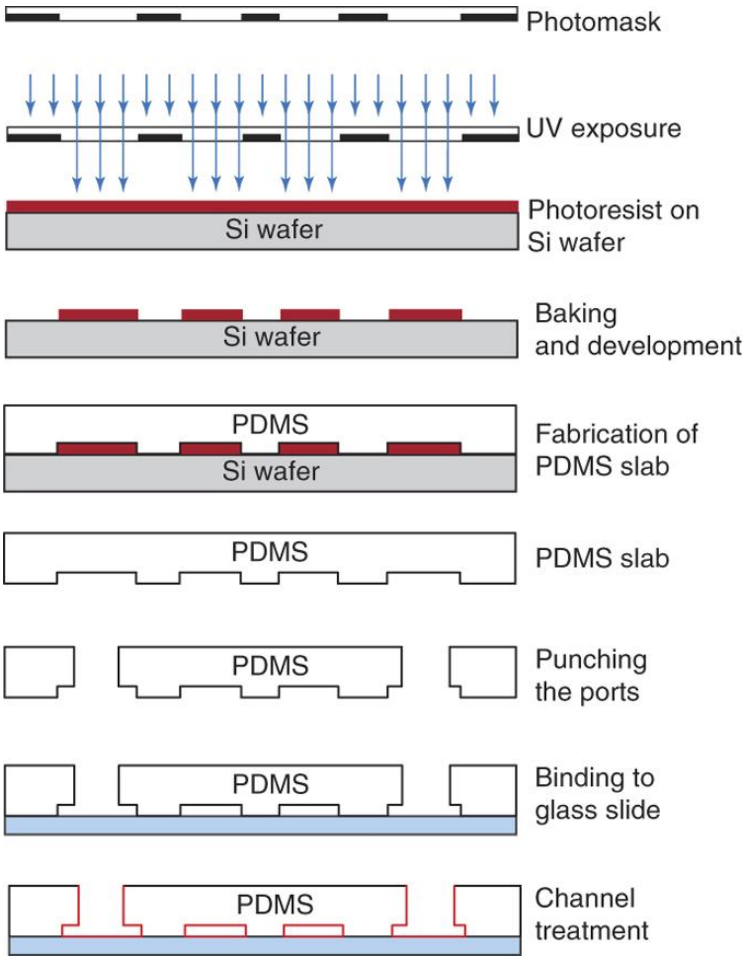

Fig. B.1 Schematic representation of the photo-lithography and replica molding techniques. (adapted from Mazutis *et al.*, 2013)

For the silica cast production 4" silica wafers are cleaned rinsing consecutively with Acetone, Methanol and distilled water and baked at 110 °C for 10 minutes to completely dry the surface. The wafer is then treated with hexamethyldisilazane (HDMS) vapor for 10 min at room temperature and spin-coated with a thin layer of SU-8 2100 negative photoresist. The height set for the layer was 150 µm for the culture chambers and 200 µm for the climatic chamber. After two steps of soft-bake of 5 minutes at 65°C and 30 minutes at 90°C, the photoresist is exposed to 260-350 mJ/cm^2 UV irradiation (365 nm) through a high resolution transparency mask containing the design of the channels. The mask is printed at high resolution from an AutoCAD design file. The photoresist reticulation is then completed with a post exposure bake for 5 minutes at 65°C and 15 minutes and 95°C and developed with SU-8 developer for 2-5 minutes, rinsing with isopropanol.

The silica wafer can be then used as the cast for soft-replica molding with PDMS. Prior to pouring an uncured PDMS solution of 10:1 monomer:cross-linker, the wafer is treated with HDMS vapor for 20 minutes to allow easy detachment of the baked PDMS. The PDMS liquid prepolymer is mixed and de-gassed by vacuum and baked for 2 hours at 70°C in order to achieve full PDMS reticulation. For the culture chamber layer, a thin membrane of PDMS was needed in order to achieve the best performance in oxygen exchange, thus the PDMS pre-polymer was spin-coated at 300 rpm for 90 second. This procedure results in a 200 μm layer of PDMS on top of the 150 μm thick photoresist cast.

Once baked, the two PDMS layers are covalently bound by 2 minutes plasma treatment and brief 100°C baking, and the same procedure was performed to bond the PDMS layers to the glass slide, after and punching inlet/outlet holes with a 21G stainless steel needle. The chip was then washed with isopropanol and sterilized by 90% ethanol flow and superficial UV irradiation.

For cell adhesion, the cultures channels were coated with porcine gelatin 0.1% (neonatal rat cardiomyocytes) or 50 μg/ml Growth Factors Reduced Matrigel (human cardiomyocytes) for 2 hours at 37°C.

B.2 Oxygen measures

Oxygen measure inside the microfluidic chip described in **Paragraph 3.4** were performed by use of an oxygen sensitive dye tris(4,7-diphenyl-1,10-phenanthroline)-ruthenium(II)-dichloride. The fluorescence of this ruthenium complex is dynamically quenched by molecular oxygen, thus in presence of atmospheric pO_2 it is weakly fluorescent when exited at 488 nm. The fluorescence intensity increases upon oxygen stripping, in a linear manner in the 0-20% pO_2 range, thus allowing precise quantification of pO_2 inside the chamber in real time by fluorescence imaging.

A 100 µM solution of Ru(ddp) in a 30% ethanol in PBS 1X solution was and fluorescence was detected by an inverted fluorescence microscope LeicaDMI6000B equipped with a mercury short-arc reflector lamp, excited at BP 450-490 nm and acquired at LP 590. The degree of quenching can be correlated to the oxygen partial pressure of the sample by Stern-Volmer equation:

$$\frac{I_0}{I} = 1 + kp_{O_2}$$

where I_0 is the fluorescence intensity at zero partial pressure of oxygen, I is the fluorescence intensity at a particular p_{O_2} and k is the Stern-Volmer constant which depends on the chemical composition of the sensor and on the temperature. The calibration of the system was performed by flowing gas mixture of known composition in the climatic chamber at a 100 ml/min flow rate and acquiring the fluorescence after 10 minutes of equilibration. There was no liquid flow inside the culture chamber during equilibration nor acquisition. The gas mixtures were generated by three EL-FLOW Mass FlowMeters/Controllers (Bronkhorst High-Tech) setting a volumetric ratio between N_2, air and CO_2.

B.6 References

Gómez-Sjöberg R., Leyrat A.A., Quake S.R. **(2007)** Versatile, fully automated, microfluidic cell culture system. *Anal. Chem.* 79:8557–8563

Mazutis L, Gilbert J, Ung WL, Weitz DA, Griffiths AD, Heyman JA. **(2013)** Single-cell analysis and sorting using droplet-based microfluidics. *Nat Protoc.* May;8(5):870-91

Appendix C

Cell Culture Analyses Protocols

This appendix section reports the protocols for the molecular biology, immuno-detection and histochemical assays performed on cell cultures. Detailed materials and procedure are also included in **Annex 1**, **Annex 2, Annex 3 and Annex 4.**

C.1 Immunofluorescence

All the immunofluorescence were performed according to standard five step protocol comprising fixation, permeabilization, blocking and two steps of antibody incubation (primary protein-specific antibody and secondary fluorescent-labeled antibody). The details of each step for each antibody used are summarized in **Table C.1**.

The secondary antibodies employed were all from Life Technologies. Species-specific antibodies were visualized by either Alexa Fluor-488 or Alexa Fluor-594 fluorophores. Pictures were taken by epifluorescence Leica DMI6000B microscope equipped with a mercury short-arc reflector lamp or Leica SP5 confocal microscope equipped with Ar laser.

Supplementary information for the anybodies listed can be retrieved in the Annex Section.

Table C.1 Summary of all the primary antibodies employed in this thesis, with all the parameters of the assay listed.

Antibody	Manufacturer	Fixation	Permeabilization	Blocking	Dilution	Incubation
cTnT	Thermo Scientific #MS295P	4% PFA, 10 min, RT	15 min, 0.25% Triton-X	10% FBS	1:250	60 min, 37°C
dystrophin	Abcam #AB15277	4% PFA, 10 min, RT	15 min, 0.25% Triton-X	10% FBS	1:250	60 min, 37°C
α-actinin	Sigma-Aldrich #A7811	4% PFA, 10 min, RT	15 min, 0.25% Triton-X	10% FBS	1:250	60 min, 37°C
SERCA2a	Santa Cruz #SC8094	4% PFA, 10 min, RT	10 min, 0.25% Triton-X	10% FBS	1:200	60 min, 37°C
GATA4	Santa Cruz #SC1237	1% PFA, 8 min, RT	constant, 0.1% Triton-X	10% FBS	1:100	12 hrs, 4°C
Nkx2.5	Santa Cruz #SC8697	1% PFA, 8 min, RT	constant, 0.1% Triton-X	10% FBS	1:100	12 hrs, 4°C
Cnx-43	Millipore #MAB3067	Acetone, 20 min, -20°C	10 min, 0.25% Triton-X	10% FBS	1:200	12 hrs, 4°C
Oct4	Santa Cruz #SC5279	4% PFA, 10 min, RT	constant, 0.1% Triton-X	10% FBS	1:500	12 hrs, 4°C
Nanog	ReproCell #RCAB0004P-F	4% PFA, 10 min, RT	constant, 0.1% Triton-X	10% FBS	1:100	12 hrs, 4°C
Klf4	Santa Cruz #SC20691	4% PFA, 10 min, RT	constant, 0.1% Triton-X	10% FBS	1:250	12 hrs, 4°C
c-Myc	Santa Cruz #SC764	4% PFA, 10 min, RT	constant, 0.1% Triton-X	10% FBS	1:250	12 hrs, 4°C
Sox2	Santa Cruz #SC17320	4% PFA, 10 min, RT	constant, 0.1% Triton-X	10% FBS	1:200	12 hrs, 4°C
TRA1-81	Millipore #MAB4381	4% PFA, 10 min, RT	none	10% FBS	1:200	60 min, 37°C
TRA1-60	Cell Signaling #4746	4% PFA, 10 min, RT	none	10% FBS	1:200	60 min, 37°C
TRA2-49	Millipore #MAB4349	4% PFA, 10 min, RT	none	10% FBS	1:200	60 min, 37°C
SSEA-4	Santa Cruz #SC21704	4% PFA, 10 min, RT	none	10% FBS	1:200	60 min, 37°C
PKP2 N-term	Santa Cruz #SC136039	2% PFA, 8 min, RT	5 min, 0.2% Triton-X	1% BSA	1:100	60 min, 37°C
PKP2 C-term	Progen #651101	2% PFA, 8 min, RT	5 min, 0.2% Triton-X	1% BSA	1:100	60 min, 37°C
PKG	Thermo Scientific #13-8500	Acetone, 20 min, -20°C	5 min, 0.2% Triton-X	1% BSA	1:100	12 hrs, 4°C
$Na_V1.5$	Alomone Labs #ASC005	2% PFA, 8 min, RT	5 min, 0.2% Triton-X	1% BSA	1:100	60 min, 37°C

C.2 Western blot

For western blot analyses the antibodies listed in Table C.1 were used with slightly different antibody dilutions: dystrophin (1:500, 12 hrs at 4°C), cTnT (1:500 1 hour at RT). The reference protein was GAPDH (1:2,000; 60 minutes at room temperature; Abcam; #ab8245). The set up of the electropheresi was as follows: a NuPAGE 3–8% Tris-acetate polyacrylamide gel was resolved and transferred for 6 hours at 4°C on a polyvinylidene difluoride membrane with a BioRad cassette. Detection was performed with Novex ECL Kit after incubating for 45 minutes with rabbit anti-mouse secondary horseradish peroxidase–conjugated antibody. For more detailed protocols, see **Annex 4**.

C.3 Polymerase chain reaction

Molecular biology analyses for mRNA transcript expression was carried out by standard RT-PCR or real-time PCR. RNA was isolated by means of Trizol extraction coupled with RNeasy Mini Kit by Qiagen. Briefly, the cells were lysated with Trizol and the first step of purification was carried out with chloroform addition and 12000x *g* centrifugation. The aqueous supernatant containing RNA was then recovered, diluted 1:1 with ethanol 70% and loaded in the RNeasy spin column and the purification was carried out according to manufacturer's instructions. After RNA quantification, retrotrascription was performed by High-Capacity cDNA Reverse Transcription Kit according to manufacturer's instructions. For standard PCR on cDNA samples, Platinum Taq Polymerase kit was used, while for real-time PCR the Sybr Green detection approach was followed. In Table C.2 are reported the primer sequences for all the amplified genes. For more detailed protocols, see **Annex 1** and **Annex 4**.

Table C.2 Summary of the PCR primer sequences employed for this thesis.

	Forward primer	Reverse primer
Dp427m	TCGCTGCCTTGATATACACTTTTCA	GGTTCTCAATATGCTGCTTCCCA
Dp260	AGGAAGCTGCGAAATCTGTCTTAC	GGCAGACTGGATGCTCTGTTCA
Dp140	ACCGAAAGAGGTTTTTGCACACC	ACTGGCATCTGTTTTTGAGGATTGC
Dp71	CATGAGGGAACAGCTCAAAGGC	CAGTCTTCGGAGTTTCATGGCA
Dys ex 5-6	CCTGACAGGGCAAAAACTGCCAA	TGTGTGGCTGACTGCTGGCAA
Dys ex 11-12	CGGAGCCCATTTCCTTCACAGCATT	CCGGCCCTGATGGGCTGTCA
Dys ex 24-25	GACTCGGGGAATTGCAGGCTT	GGGCAGGCCATTCCTCCTTCA
Dys ex 27-28	GGCCTGCCCTTGGGGATTCA	TCTGGCATAGACCTGTTGGCACA
Dys ex 37-38	TGCCTGGGGAAAGGCTACTCA	GCAGTGGTCACCGCGGTTTG
NKX2.5	GCGATTATGCAGCGTGCAATGAGT	AACATAAATACGGGTGGGTGCGTG
cTnT	TTCACCAAAGATCTGCTCCTCGCT	TTATTACTGGTGTGGAGTGGGTGTGG
MLC2v	ACATCATCACCCACGGAGAAGAGA	ATTGGAACATGGCCTCTGGATGGA
GAPDH RT-PCR	CCCCTTCATTGACCTCAACTACA	TTGCTGATGATCTTGAGGCTGT
GAPDH real-time PCR	GAAGGTGAAGGTCGGAGTCAAC	CAGAGTTAAAAGCAGCCCTGGT
TRDN	CGTGATGCTATGGAGGAAACC	GATGCTACCTCCAAACCCCT
CSQ2	AAATCACAGCACCCACTACCA	GCAAATCAACCTCCCATCCCA
PLN	CCCCAGCTAAACACCCGTAA	TCCTGTCTGCATGGGATGAC

C.4 Calcium imaging

Calcium imaging was performed by mean of confocal line scanning of cardiomyocytes loaded with Ca2+ binding dye, fluo-4. Fluo-4 has been loaded as an acetyl-methyl ester in order to increase its liposolubility and facilitating the crossing of cell membrane, in presence of Pluronic F-127 as mild detergent. In all the incubation media sulphinpyrazone was included as anionic transporter inhibitor to reduce dye active extrusion from the cell. As cell membrane counter-stain di-8-ANEPPS was used, in order to distinguish separate cells. Line scanning mode of the Leica SP5 laser confocal microscope was use, for faster acquisition. For more detailed protocols, see **Annex 1** and **Annex 2**.

When cell were imaged simultaneously for calcium dynamics and membrane potential, Fura Red dye was employed instead. Fura Red 10 µM solution in DMEM with 2 µM Pluronic F-127 and 20 µM sulfinpyrazone was incubated for 60 minutes at 37°C, followed by 20 minute of incubation at 37°C without the dye prior to acquisition. During the 20 minutes resting period, the voltage sensitive dye could be added the medium at a 0,2 µM concentration.

C.5 Live and Dead assay

Live & Dead assay was carried according to manufacturer's instructions (Life Technologies). Briefly, cells were incubated for 60 minutes with DMEM containing 4 µM di-ethidium bromide, 2 µM calcein-AM and nuclei were counter stained with 1 µg/ml HOECHST 33342. Fluorescent pictures of the culture were taken immediately with epifluorescence Leica DMI6000B microscope equipped with a mercury short-arc reflector lamp.

C.6 PAS staining assay

PAS staining was performed according to manufacturer's instructions (Sigma-Aldrich). Briefly, cell were washed twice with 1x DPBS and fixed for 10 minutes with 4% PFA. Washed twice again with double distilled water (ddH_2O) and incubated for 5 minutes with periodic acid. Washed 5 times with ddH_2O and incubated for 15 minutes with Schiff's base. Before imaging in bright field and contrast microscopy the cells were washed again 5 times in ddH_2O for at least 10 minutes.

Annex 1

Human cardiomyocytes derived from pluripotent stem cells require activation of mechanotransduction pathways by cell-substrate interaction for functional maturation

Sebastian Martewicz [1,2], Elena Serena [1,2], Susi Zatti [1,2], Gordon Keller [3], and Nicola Elvassore [1,2,]

[1] Dipartimento di Ingegneria Industriale, University of Padova, via Marzolo 9, 35131 Padova, Italy.

[2] Venetian Institute of Molecular Medicine, via Orus 2, 35129 Padova, Italy

[3] McEwen Centre for Regenerative Medicine, University Health Network, 101 College Street, Toronto, Ontario M5G 1L7, Canada

Manuscript for resubmission
Stem Cell Reports
2015

Abstract

Application of human pluripotent stem cell-derived cardiomyocytes in *in vitro* studies is limited by their early and immature phenotype. *In vivo*, the cardiac muscle develops in a dynamic environment, in which continuous active and passive mechanical signals drive cardiomyocyte organization and maturation. Integrating soluble signals in differentiation media with physical cues is necessary to activate proper genetic programs is required to avoid cardiomyocyte *in vitro* maturation arrest at an immature stage.

Here, we report how proper cardiac differentiation requires cell-substrate interactions to promote maturation of hPSC-CM. In both hES-CMs and hiPS-CMs, calcium release and reuptake rates increased after adhesion culture regardless of EB age and both sarcoplasmic reticulum and contractile machinery structural organization improved significantly. This maturation depends heavily on the culture substrate stiffness as these physical cues activate mechanotransduction pathways needed for cardiac development. In particular, inhibition of RhoA/ROCK pathway prevented further maturation highlighting its importance in cardiomyocyte *in vitro* maturation.

Human cardiomyocytes derived through *in vitro* differentiation of pluripotent stem cells (hPSC-CM) represent a promising opportunity in regenerative medicine, pharmacological research and, in general, for *in vitro* cardiological studies. Although the ability of hPSC-CMs to engraft and improve cardiac function in compromised animal hearts (Chong et al., 2014; Shiba et al., 2012; Laflamme et al., 2007; Caspi et al., 2007) proves their viability in future therapeutical approaches in treating cardiac dysfunctions, a more straightforward application is in drug testing (Braam et al., 2010) and in the early pharmacological development pipeline (Kraushaar et al., 2012). However, the early and immature phenotype displayed by hPSC-CMs is the biggest concern for these applications (Davis et al., 2011), focusing research on understanding the molecular mechanisms underlying cardiac maturation and developing methods to improve their maturation *in vitro*.

The cardiac differentiation protocols mimic processes of embryonic development driving the pluripotent cells towards early mesoderm specification and cardiac progenitors by chronologically defined delivery of cytokines, growth factors and small molecules up to the generation of early stage cardiomyocytes (Lian et al., 2012; Kattman et al., 2011; Laflamme et al., 2007; Mummery et al., 2003). The maturation arrest at this immature phenotype is represented by expression of embryonic isoforms of cardiac markers, poor calcium handling ability and immature electrical activity.

Empirical observations showed that extended time in culture (which span several months) can result in limited enhancement of cardiac maturation (Lundy et al., 2013; Kamakura et al., 2013; Sartiani et al., 2007; Otsuji et al., 2010). Moreover, adult-like phenotypes can be achieved for single cardiac functional features such as calcium handling or action potential by ectopic overexpression of proteic components of mature cardiomyocytes (Lieu et al., 2013; Liu et al., 2009).

Evidence of maturation of hPSC-CMs after myocardial engraftment (van Laake et al., 2007) highlights the importance of considering of a proper electrical/mechanical environment in designing the best conditions for cardiac maturation (Dick et al., 2010). In this perspective, the integration of electrical stimulation (Hirt et al., 2014; Chan et al., 2013) and mechanical strains (Mihic et al., 2014) in cardiac differentiation protocols proved successful in improving structural features and functional performance of hPSC-CMs *in vitro*.

Although integrating the signals from the soluble environment with mechanical cues better mimics the development of the highly dynamic cardiac tissue (Jacot et al., 2010), the mechanisms underlying this phenomena remain poorly understood.

Here, we report that hPSC-CMs at single cell level require cell-substrate interaction to promote structural organization and improve functional performance. We show in human cardiomyocytes that this process relies upon the activation by the cell-substrate interaction of a specific mechanotransduction pathway, which inhibition by either change in substrate stiffness or biochemical inhibition negates the structural cardiomyocyte reorganization and prevents the improvement in functional performance.

Results

hPSC-CM functional and structural features are enhanced by adhesion culture. We cultured and differentiated two pluripotent stem cell lines: a hES line (HES2) and a hiPS line. Both cell lines displayed undifferentiated morphology and were tested for common pluripotency markers (Fig. S1A) before undergoing embryoid bodies (EBs) formation and cardiac differentiation protocol. First contracting EBs were observed after 10-12 days for the HES2 line and after 7-9 days for the hiPS cells. Single cell cardiomyocytes obtained by disaggregation of EBs and cultured in monolayer expressed most of the cardiac specific markers, such as cardiac troponin T (cTnT), α-actinin (α-act), SERCA2a, Nkx2.5 and Cnx43 (Fig. S1B). Spontaneous and electrically stimulated contractions were accompanied by cardiac-like calcium transients (Fig. 1A). Intriguingly, calcium transients shortened upon extension of the monolayer culture time. Calcium transients lasting several seconds were recorded in the majority of cardiomyocytes early after single cell replating in adhesion culture.

Long calcium transients were almost completely replaced by shorter transients after 1 week for both hES- and hiPS-derived cardiomyocytes populations, as showed by representative calcium traces (Fig. 1A) and calcium decay rate (n=21 and n=34, respectively) (Fig. S2A and Fig. 1B). An improvement in calcium release rate was observed as well, as showed by the reduction of the time-to-peak (TTP) parameter (Fig. S2B and Fig. S3A).

The observed calcium handling enhancement was associated with a marked improvement in organization of cardiac cell structural features. As opposed to cells clustered in embryoid bodies displaying round morphologies with high nucleus-to-cytoplasm ratio and disorganized myofibrils (Fig. 1C), cardiomyocytes cultured in monolayer showed increasing alignment and regular striation patterns of the cTnT staining (Fig. 1C). In terms of myofibril alignment (Fig. S2C), both cell lines displayed a marked increase in sarcomere organization after 1 week in monolayer culture, reaching nearly parallel sarcomeres (Fig. 1D, hES n=37, hiPS n=44). Western Blot analysis confirmed an increased expression of cardiac troponin T isoforms on cardiomyocytes cultured in adhesion (Fig. S3B).

We asked if there was a correlation between the observed calcium transient shortening and the expression of the major component of calcium handling machinery responsible for Ca^{2+} re-uptake, SERCA2a. Immunofluorescence staining showed a great increase in SERCA2a accumulation after 1 week in adhesion, with a striking reorganization of the SR, from a mainly perinuclear localization early after single cell replating, towards a whole-cell spreading after 1 week (Fig 1E). We evaluated the spreading area of the SERCA2a staining (Fig. S2D) finding a significant increase in spreading area in hES-CMs (n=24) and in hiPS-CMs (n=31) (Fig. 1F). We assessed the expression of other SR calcium handling proteins (Triadin, Calsequestrin and Phospholamban) by means of RT-PCR (Fig. S3C) and we found that cardiac calsequestrin was upregulated after 1 week of adhesion culture. Interestingly, the expression of cardiac calsequestrin was rarely reported in hPSC-CM literature (Robertson et al., 2013) and its transgenic over-expression have been proved to boost cardiomyocytes

maturation in terms of calcium handling (Liu et al., 2009). Consistently, as expected from a maturing sarcoplasmic reticulum, the cardiomyocyte performance in calcium handling improved after stimulation with 10 mM caffeine shown by representative traces at the two time points considered (Fig. S3D) and dynamics quantification (Fig S3E); in particular calcium release and re-uptake rates significantly increased and a two-fold increase in peak relative amplitude between 2 days and 1 week in adhesion was observed. To assess whether the functional and structural maturation is a result of the time in adhesion or EBs age, we performed experiments with different preparations (n=3) of both hES- and hiPS-derived EBs cultures. EBs were maintained in suspension culture up to 3 months after differentiation protocol start. At different time points (early after cardiac differentiation protocol end, 1 month and 2-3 months later) single cell cultures of hPSC-CM in monolayer were set up and whole-cell calcium imaging was performed. All experiments recapitulated the functional maturation of the calcium handling machinery in terms of Ca^{2+} reuptake rate (Fig. 1G&H) for both hES-CMs (n=56) and hiPS-CM (n=74) as function of time in adhesion, from 2 days after EB disaggregation to 1 week of culture. A very strong correlation (Two-Ways ANOVA, $p<.001$) was found between the calcium transient shortening and the time in adhesion culture, but not EB age, thus highlighting the importance of mechanical cues from the adhesion substrate over the age of EB for the improvement in functional performance at later stages in human pluripotent stem cells cardiac differentiation.

Substrate stiffness affects cardiomyocyte maturation. To assess whether the hPSC-CM were affected in their adhesion culture-driven functional maturation by the stiffness of the culture substrate, we cultured hPSC-CM after EB disaggregation on polyacrilammide hydrogels of 4 kPa (soft substrate), 16 kPa (muscle-like substrate) and glass (stiff substrate). Human cardiomyocytes cultured on 16kPa hydrogels (n=21) and on glass (n=17) recapitulated the previous results, with a positive correlation between time in adhesion culture and functional maturation, with calcium transients decreasing in duration (Fig. S4A), and increasing rate in Ca^{2+} re-uptake (Fig 2A). In these substrate conditions, the structural features of the cardiac cells improved in time showing SR maturation and SERCA2a spreading (Fig. 2B) and proper sarcomere alignment (n=37 and 44, respectively) (Fig. 2C). Instead, cardiomyocytes cultured on the 4 kPa hydrogel (n=23), did not show functional maturation in terms of calcium handling (Fig 2A and Fig. S4A); consistently, the SERCA2a distribution maintained a perinuclear localization (n=35) (Fig 2D and Fig. S4B). The influence of the soft substrate on cardiomyocyte structural organization was evident as well in the lack of myofibril alignment and poor organization of sarcomeric structures (Fig S4C&D).

We then asked if influence of the substrate's stiffness on the hCMs was merely on the structural organization of cellular features or was driving transcriptional changes as well. We set up cultures in hydrogels of increasing elastic moduli (from 4 kPa to 160 kPa) and performed real-time PCR analyses on mRNA levels of cardiac transcripts. Experiments carried on mixed population of cardiomyocytes

and non-cardiac contaminants in the EBs resulted in high variability between the samples (data not shown) and urged for a more sensitive approach. In order to generate robust data on the sole cardiac population, we employed for this experiments an α-MHC-Puro^r hiPSC line enabling us to effectively select for the cardiomyocytes in differentiated EBs for further testing. The cardiomyocytes obtained from this new hiPS line recapitulated the structural/functional maturation observed previously (Supplementary Data).

RhoA/ROCK pathway is involved in cardiomyocyte maturation. In order to assess the involvement of known mechano-sensing signaling pathways in cardiomyocyte maturation, we cultured hPSC-CM on a stiff substrate with or without 2 μM of ROCK inhibitor Y-27632 for 1 week and analyzed the cultures for calcium handling and structural features (n=21). As expected, the untreated cardiomyocytes recapitulated the results reported above (Ca^{2+} shortening and increased calcium reuptake rate) (Fig. 3A). This effect of adhesion culture was completely abrogated by the ROCK inhibition, with Ca^{2+} transients lasting several seconds even after 1 week and calcium reuptake rates fairly unchanged within this time in culture (Fig. 3A). In line with the previous results, in which calcium handling maturation was accompanied by pronounced SR maturation and SERCA2a enhanced expression and relocalization, we expected to observe the great inhibition in SERCA2a expression and spreading after Y-27632 treatment. As a matter of fact, SERCA2a staining revealed how the treated hPSC-CM maintains a perinuclear localization of the pump after 1 week (Fig. 3B) without significant spreading throughout the cell volume observed in the controls (n=18) (Fig. 3C). Interestingly, human cardiomyocytes did not display significant alterations in myofibrils alignment, which organized in a parallel fashion with the long cell axis, although presenting less degree of sarcomere organization, resulting in thinner myofibril compared to the controls (n=16) (Fig. 2B&D).

Discussion

In this work we demonstrate in human cardiomyocytes that cell-substrate interaction is required to activate mechanosensing pathway RhoA/ROCK in order to promote their maturation after differentiation from embryonic and induced pluripotent stem cells. Our data show that monolayer culture, with the associated morphological changes and enhanced mechano-associated signaling from the stiff culture substrate, allows structural and functional maturation of hPSC-CM. Progressive maturation of human cardiomyocytes has been reported by other groups upon extension of culture time and replating procedures of embryoid bodies, both in regard to electrophysiological properties (Sartiani et al., 2007; Otsuji et al., 2010) and to the ultrastructural organization of the contractile apparatus (Kamakura et al., 2013). In these works, the maturation process spanned several months and the cells were maintained in beating clumps, thus the contribution of cell-substrate interactions and mechanotransduction associated processes could not be clearly investigated. Here, we show how monolayer culture promotes functional and structural maturation in a substrate-driven fashion within days, disregarding of the EB age up to three months (Fig. 1G&H).

Cardiomyocyte shape has been recently proven to be one of the regulators of functionally fundamental myocyte features, such as assembly and organization of sarcomeric structure and proper calcium handling ability (Yin et al., 2004; Kuo et al., 2012). Shape-dependent modulation of cardiac ion channel properties, including Ca^{2+} channels, has been reported as well (Walsh and Parks, 2002). In EB structures as well as in replated beating clumps, cells are clustered maintaining round-shaped morphology and disorganized myofibrils, while the cell-substrate interaction and the morphological changes in adhesion promote cardiac maturation and structural organization (Fig. 1C). This maturation is described by means of improved calcium handling (Fig. 1A&B and Fig. S3A) and of myofibrils alignment to the long axis of the cell, as for skeletal and cardiac muscle (Young and Engler, 2011) (Fig. 1D). Round cell morphology is characterized by high nucleus-to-cytoplasm ratio, thus preventing ultrastructural organization of cell compartments like the sarcoplasmic reticulum and further development of proper calcium handling. In adult human cardiomyocytes, the majority of Ca^{2+} after contraction is recovered by the SERCA2a pumps back into the SR (Bers, 2002), whereas it has been often reported how for hPSC-CMs the diastolic calcium is extruded through Na^{+}/Ca^{2+} exchanger (Fu et al., 2010). Upon extension of adhesion culture, we observed marked maturation of the calcium transient profile with an increased calcium re-uptake rate, temporally correlating to SERCA2a increased protein expression and re-localization (Fig. 1E&F).

In the latter years, the influence of substrate mechanical cues on cell behavior has come to light as an important player in development and differentiation (Discher et al., 2009). Employment of compliant substrates, like polyacrilammide hydrogels, with defined elastic moduli, showed how the cell physical environment is an important determinant of stem cell state and commitment, capable even for itself of directing differentiation towards one cell type or another, according to the physiological stiffness of the cell type of destination (Engler et al., 2006). For cardiac and muscle cells the optimum elastic modulus was routinely estimated in a range between 10 and 16 kPa (Engler et al., 2004).

In our study, we demonstrate how culturing hPSC-CMs on soft substrates not providing the necessary mechanical cues to cardiac maturation resulted in the abrogation of any type of functional or structural maturation (Fig 2A&B&C). Hydrogels with cardiac-like elastic modulus and stiff substrates, instead, allowed maturation in terms of calcium transient shortening, sarcomeric and SR organization. These findings highlight the importance in cardiac functional maturation of cues deriving from the mechanical environment and, particularly, the signaling activated by substrate stiffness.

Cell sensing of the surrounding physical environment has its molecular basis in a limited number of signaling pathways (Jaalouk and Lammerding, 2009) which translate mechanical signals into kinases cascades, thus transducing mechanical cues through pathways such as the RhoA-ROCK pathway (Wei et al., 2001). The importance of this specific mechanotransduction pathway in cardiac development is demonstrated by severe alterations in heart morphogenesis of mouse and chick embryos (Zhao and Rivkees, 2003; Sakata et al., 2007). Neonatal rat cardiomyocytes subjected to prolonged exposure to RhoA/ROCK inhibiting

molecules show a reduction in contraction force (Jacot et al., 2008). Moreover, mechanotransduction pathways are sensitive to cell shape, as proven by our recent discovery of mechanotransduction pathways crosstalk through the ROCK kinase (Dupont et al., 2011). This evidence identifies Rho-associated kinase as a suitable target of inhibition in order to convincingly desensitize hPSC-CM from the mechanical environmental cues, thus providing insight in the molecular basis of their substrate-driven maturation.

Culturing human cardiomyocytes in presence of 2 μM Y-27632 ROCK inhibitor maintained normal cell morphology, but prevented cardiac maturation in terms of calcium handling, with no improvement in calcium dynamics features (Fig. 3A), and SERCA2a relocalization, which maintained a perinuclear localization even after 1 week of culture (Fig. 3B&C). For this latter finding, our data are in accordance with reports of RhoA/ROCK pathway involvement in the transcriptional regulation of SERCA2a gene, identifying its promoter as downstream target of yet unknown effectors (Vlasblom et al., 2010).

Cardiac differentiation protocols from pluripotent stem cells are, to date, the best promise for a human cardiac *in vitro* model feasible for drug screening and disease modeling. The immature phenotype of the derived cardiomyocytes is still a matter of concern for these applications and understanding the processes behind *in vitro* maturation is of great interest. Here, we showed how cell interaction with the adhesion substrate promotes cardiac maturation, identifying a mechanotransduction pathway involved in this process, allowing generation of cardiomyocytes more feasible for *in vitro* modeling of human mature cardiac cells within few days after EB disaggregation.

Methods

Pluripotent stem cell culture and differentiation. The hES cell line HES2 was obtained from WiCell and cultured according to suppliers guidelines. The hiPS line was kindly provided by prof. Mitsuo Oshimura laboratory and maintained in culture according to the protocol described by Kazuki and colleagues (Kazuki et al., 2010). Human cardiomyocytes were derived according to an EB based protocol described previously by Yang and colleagues (Yang et al., 2008). Briefly, pluripotent colonies of both cell lines were cultured for 24-48 hours Growth Factors Reduced Matrigel coated dishes (BD) and then detached and transferred to ultra-low adhesive dishes (Corning) for the EB formation in basal medium (StemPRO-34 (Invitrogen), 2 mM L-glutamine (Invitrogen), 150 μg/ml hTrasferrin (Roche), 50 μg/ml ascorbic acid (Sigma), 0.4 mM monothioglycerol (Sigma), 50 U/ml penicillin (Invitrogen), 50 μg/ml streptomycin (Invitrogen) supplemented with 10ng/ml hBMP4 (R&D). From day 1 to day 4 EB were cultured in basal medium with 10 ng/ml hBMP4, 5 ng/ml hbFGF (R&D) and 6 ng/ml hActivin A (R&D). At day 4 to day 8, the medium consisted of basal medium and 10 ng/ml hVEGF (R&D) and 150 ng/ml hDKK (R&D). Finally, from day 8 to day 14, the culture medium consisted of basal medium and 10 ng/ml hVEGF and 5 ng/mL hbFGF. Cultures were maintained in a 5% CO_2, 5% O_2, 90% N_2 environment for the first 14 days and then transferred into a 5% CO_2 air

environment. The obtained EB were maintained in the last medium described until further experimental procedures. The α-MHC-Puro^r hiPS line used for Real-Time PCR experiments was kindly provided by prof. H-S Vincent Chen and maintained in culture on Growth Factors Reduced Matrigel (BD) coated dishes in E8 medium (StemCell Technologies). The cardiac differentiation protocol was carried out as described above, the cytokines used were purchased from Peprotech.

Hydrogel preparation. Polyacrilammide hydrogels were prepared as previously described by Tse and Engler (Tse and Engler, 2010). In order to tune the hydrogel stiffness different ratios of acrilammide/bisacrilammide in milliQ water were prepared as follows: hydrogels of 4 kPa 5%/0.15%, 16 kPa hydrogels 10%/0.15%, 40 kPa hydrogels 8%/0.48% and 160kPa hydrogels 12%/0.6%. The polymerization was induced by addition of 10% ammonium persulfate and 0.1% TEMED. All reagents were from Sigma.

Cardiomyocyte adhesion culture. Fully differentiated EBs were disaggregated to single cells in order to perform experiments on monolayer adherent cultures. HES2-derived EBs were treated with 2 mg/ml Collagenase Type I (Invitrogen) for 45 minutes at 37°C and with Trypsin-EDTA 0,25% (Invitrogen) for 5 minutes at 37°C. Trypsin was quenched with 1:1 FBS/IMDM (Invitrogen). Resuspension of the loosened EBs ensured the obtainment of a single cell suspension. hiPS-derived EBs were treated with digestion solution consisting in 2 mg/ml Collagenase Type I, 0,5 mg/ml Collagenase Type IV (Invitrogen) and 3 U/ml DNase I (Invitrogen) for 25 minutes at 37°C under gentle agitation, with subsequent digestion with Trypsin-EDTA 0,25% for 4 minutes quenched with 1:1 FBS/IMDM. Single cell suspensions were then plated on glass slides incubated for 1 hour with 20 μg/ml laminin (BD) at a 100-200 cells/mm^2 density. For the different stiffness experiments, the hydrogels were incubated for 30 minutes with 100 μg/ml laminin and 50 μg/ml human fibronectin (Sigma), as well as the control glass slides. Cell cultures were kept at 37°C, 5% CO_2, in the last EB medium. For experiments with ROCK inhibitor, 2 μM of Y-27632 (Sigma) was added to the culture medium since day 0 of adhesion culture.

Calcium measurements. Confocal calcium measurements were performed as reported previously (Martewicz et al., 2012). Briefly, cardiomyocytes were loaded in serum-free 25mM HEPES D-MEM (Invitrogen) supplemented with 2,5 μM fluorescent calcium dye Fluo-4 AM (Invitrogen) for 20 minutes at 37°C in the presence of 2 μM Pluronic F-127 (Invitrogen) and 20 μM sulfinpyrazone (Sigma), then incubated for additional 10 minutes at 37°C without Fluo-4 AM to allow complete de-esterification of the dye, and added with 0.2 μM di-8-ANEPPS (Invitrogen). Cell dynamics were acquired in recording solution: NaCl 125 mM, KCl 5 mM, Na_3PO_4 1 mM, $MgSO_4$ 1 mM, Hepes 20 mM, $CaCl_2$ 2 mM, glucose 5.5 mM, to pH 7.4 with NaOH. Line scans were acquired with a Leica TCS SP5 confocal microscope equipped with a 63x, 1.4 NA oil immersion objective, with 488 nm Ar laser line as an excitation source, 400 Hz acquisition frequency. To reduce dye photo-bleaching and photo-toxic effects on the analyzed cells, the laser power was set at minimum possible. In experiments with caffeine (Sigma), a 20 μl puff of 10 mM caffeine (in recording solution) was administered in the

proximity of the acquired field. All experiments were performed at room temperature within 20-30 minutes from the end of loading procedures.

Immunofluorescence analysis. A standard immunofluorescence protocol was used. Primary antibodies for pluripotency markers were Oct3/4 (Santa Cruz), Sox2 (Millipore), c-Myc (Santa Cruz), TRA1-81 (Millipore) and TRA1-60 (Millipore). Primary antibodies against cardiac markers were troponin T (NeoMarkers), α-actinin (Sigma), connexin 43 (Chemicon), Nkx2.5 (Santa Cruz), SERCA2a (Santa Cruz). Secondary antibodies used were: Alexa-488 goat anti-mouse (Invitrogen), Cy3 donkey anti-goat (Jackson ImmunoLab). Nuclei were counterstained with DAPI (Sigma) and samples were mounted with Elvanol and viewed under Leica TCS SP5 confocal microscope. Immunofluorescence on EB samples were performed on 20 μm cryosections of OCT (Kaltech) enclosed EBs mounted on poly-L-lysine coated glass microscope slides.

Real-Time PCR analysis. Analysis of mRNA expression was assessed on EBs and monoloyer α-MHC-Puro^r cultures pretreated with 1,5μg/ml of puromycin (Sigma) for 24 hours. Expression levels were analyzed by Power SYBR Green Master mix kit (Invitrogen). Data are presented as expression fold change relative to the 16 kPa sample, normalized for GAPDH expression. Pfaffl method for relative fold expression change was applied.

Data analysis. For evaluation of the calcium re-uptake rate after contraction, the half-life of the calcium decay was used. A first order exponential decay curve was fitted to the acquired calcium transient, as shown in Fig. S2A, and the value of τ was extrapolated. For the calcium release phase, the time to peak value was calculated considering time from base-line to minimum of the second derivative of the calcium transient, as depicted in Fig S2b. All numerical data were manipulated with Origin 8.1 software. Calculation of the orientation correlation function (OCF) was performed as previously described by Young and Engler[20] and as depicted in supplementary figure (Fig. S2C). Briefly, a long cellular axis was identified and was calculated the incident angle to the axis of at least 10 major cTnT fibers. OCF was calculates as $OCF = 0.5(\cos(2\theta)+1)$ where θ is the mean incident angle of the cardiomyocytes: an OCF equal to 1 mean a perfectly parallel aligned myofibril, while an OCF of 0,5 represents an unaligned diagonal myofibril. Quantification of SERCA2a spread area were performed as depicted in supplementary figure (Fig. S2D). Briefly, immunofluorescence images of single cardiomyocytes were thresholded with the IJ_IsoData algorithm and the percentage of red areas over cell area (nuclei excluded) was calculated. Cell edges were identified with selection tool. All image analysis were performed with ImageJ software.

Statistical analysis. Data are presented as means ± standard error of means (SEM). Data pairs were compared by non-directional Student's t-test, while group data by one-way ANOVA followed by Bonferroni's mean comparison. The EB vs. Adhesion culture was evaluated with two-way ANOVA. All data manipulation and computation was performed with Origin 8.1 software.

Acknowledgements

This research was supported by Progetti di Eccellenza CaRiPaRo, Fondazione Città della Speranza and Progetti di Eccellenza Giovani Ricercatori of Ministero della Salute.

Contributions

S.M. performed most of the experimental work; E.S., S.Z. and S.M. performed pluripotent stem cell cultures, cardiac differentiation and molecular characterization; G.K. provided hES-CMs and discussed research activity; S.M., E.S. and N.E. designed the research; S.M. and N.E. wrote the manuscript.

References

Bers DM.(2002) Cardiac excitation-contraction coupling. Nature. 6868, 198-205.

Braam SR, Tertoolen L, van de Stolpe A, Meyer T, Passier R, Mummery CL.(2010) Prediction of drug-induced cardiotoxicity using human embryonic stem cell-derived cardiomyocytes. Stem Cell Res. 2, 107-16.

Caspi O, Huber I, Kehat I, Habib M, Arbel G, Gepstein A, Yankelson L, Aronson D, Beyar R, Gepstein L. (2007) Transplantation of human embryonic stem cell-derived cardiomyocytes improves myocardial performance in infarcted rat hearts. J Am Coll Cardiol. 19, 1884-93.

Chan YC, Ting S, Lee YK, Ng KM, Zhang J, Chen Z, Siu CW, Oh SK, Tse HF. (2013) Electrical stimulation promotes maturation of cardiomyocytes derived from human embryonic stem cells. J Cardiovasc Transl Res. Dec;6(6):989-99.

Chong JJ, Yang X, Don CW, Minami E, Liu YW, Weyers JJ, Mahoney WM, Van Biber B, Cook SM, Palpant NJ et al., (2014) Human embryonic-stem-cell-derived cardiomyocytes regenerate non-human primate hearts. Nature. Jun 12;510(7504):273-7.

Davis RP, van den Berg CW, Casini S, Braam SR, Mummery CL.(2011) Pluripotent stem cell models of cardiac disease and their implication for drug discovery and development. Trends Mol Med. 9, 475-84.

Dick E., Rajamohan D., Ronksley J., Denning C., (2010) Evaluating the utility of cardiomyocytes from human pluripotent stem cells for drug screening. Biochem Soc Trans. 4, 1037-45.

Discher DE, Mooney DJ, Zandstra PW. (2009) Growth factors, matrices, and forces combine and control stem cells. Science. Jun 26;324(5935):1673-7.

Dupont S, Morsut L, Aragona M, Enzo E, Giulitti S, Cordenonsi M, Zanconato F, Le Digabel J, Forcato M, Bicciato S, et al., (2011) Role of YAP/TAZ in mechanotransduction. Nature. 474(7350):179-83

Engler AJ, Sen S, Sweeney HL, Discher DE. (2006) Matrix elasticity directs stem cell lineage specification. Cell. Aug 25;126(4):677-89.

Engler AJ, Griffin MA, Sen S, Bönnemann CG, Sweeney HL, Discher DE. (2004) Myotubes differentiate optimally on substrates with tissue-like stiffness: pathological implications for soft or stiff microenvironments. J Cell Biol. Sep 13;166(6):877-87.

Fu JD, Jiang P, Rushing S, Liu J, Chiamvimonvat N, Li RA. (2010) Na+/Ca2+ exchanger is a determinant of excitation-contraction coupling in human embryonic stem cell-derived ventricular cardiomyocytes. Stem Cells Dev. Jun;19(6):773-82.

Hirt MN, Boeddinghaus J, Mitchell A, Schaaf S, Börnchen C, Müller C, Schulz H, Hubner N, Stenzig J, Stoehr A, et al., (2014) Functional improvement and maturation of rat and human engineered heart tissue by chronic electrical stimulation. J Mol Cell Cardiol. May 19;74C:151-161.

Jaalouk DE, Lammerding J. (2009) Mechanotransduction gone awry. Nat Rev Mol Cell Biol. Jan;10(1):63-73.

Jacot JG, McCulloch AD, Omens JH. (2008) Substrate stiffness affects the functional maturation of neonatal rat ventricular myocytes. Biophys J. 7, 3479-87

Jacot JG, Martin JC, Hunt DL. (2010) Mechanobiology of cardiomyocyte development. J Biomech. 1, 93-8.

Kamakura T, Makiyama T, Sasaki K, Yoshida Y, Wuriyanghai Y, Chen J, Hattori T, Ohno S, Kita T, Horie M et al. (2013). Ultrastructural maturation of human-induced pluripotent stem cell-derived cardiomyocytes in a long-term culture. Circ J. 77, 1307-14.

Kattman SJ, Witty AD, Gagliardi M, Dubois NC, Niapour M, Hotta A, Ellis J, Keller G.(2011) Stage-specific optimization of activin/nodal and BMP signaling promotes cardiac differentiation of mouse and human pluripotent stem cell lines. Cell Stem Cell. Feb 4;8(2):228-40.

Kazuki Y, Hiratsuka M, Takiguchi M, Osaki M, Kajitani N, Hoshiya H, Hiramatsu K, Yoshino T, Kazuki K, Ishihara C et al. (2010). Complete genetic correction of ips cells from Duchenne muscular dystrophy. Mol Ther. 18, 386-93.

Kraushaar U, Meyer T, Hess D, Gepstein L, Mummery CL, Braam SR, Guenther E.(2012) Cardiac safety pharmacology: from human ether-a-gogo related gene channel block towards induced pluripotent stem cell based disease models. Expert Opin Drug Saf. Mar;11(2):285-98.

Kuo PL, Lee H, Bray MA, Geisse NA, Huang YT, Adams WJ, Sheehy SP, Parker KK. (2012), Myocyte shape regulates lateral registry of sarcomeres and contractility. Am J Pathol. 181, 2030-7

Laflamme MA., Chen KY., Naumova AV., Muskheli V., Fugate JA., Dupras SK., Reinecke H., Xu C., Hassanipour M., Police S., et al. (2007) Cardiomyocytes derived from human embryonic stem cells in pro-survival factors enhance function of infarcted rat hearts. Nat Biotechnol. 9, 1015-24.

Lian X, Hsiao C, Wilson G, Zhu K, Hazeltine LB, Azarin SM, Raval KK, Zhang J, Kamp TJ, Palecek SP. (2012) Robust cardiomyocyte differentiation from human pluripotent stem cells via temporal modulation of canonical Wnt signaling. Proc Natl Acad Sci U S A. Jul 3;109(27):E1848-57.

Lieu DK, Fu JD, Chiamvimonvat N, Tung KC, McNerney GP, Huser T, Keller G, Kong CW, Li RA. (2013) Mechanism-based facilitated maturation of human pluripotent stem cell-derived cardiomyocytes. Circ Arrhythm Electrophysiol. 6, 191-201

Liu J, Lieu DK, Siu CW, Fu JD, Tse HF, Li RA. (2009) Facilitated maturation of Ca2+ handling properties of human embryonic stem cell-derived cardiomyocytes by calsequestrin expression. Am J Physiol Cell Physiol. 1, C152-9.

Lundy SD, Zhu WZ, Regnier M, Laflamme MA (2013) Structural and functional maturation of cardiomyocytes derived from human pluripotent stem cells. Stem Cells Dev. Jul 15;22(14):1991-2002

Martewicz S, Michielin F, Serena E, Zambon A, Mongillo M, Elvassore N. (2012), Reversible alteration of calcium dynamics in cardiomyocytes during acute hypoxia transient in a microfluidic platform. Integr Biol (Camb). 4, 153-64.

Mihic A, Li J, Miyagi Y, Gagliardi M, Li SH, Zu J, Weisel RD, Keller G, Li RK. (2014) The effect of cyclic stretch on maturation and 3D tissue formation of human embryonic stem cell-derived cardiomyocytes. Biomaterials. Mar;35(9):2798-808.

Mummery C, Ward-van Oostwaard D, Doevendans P, Spijker R, van den Brink S, Hassink R, van der Heyden M, Opthof T, Pera M, de la Riviere AB *et al.* (2003) Differentiation of human embryonic stem cells to cardiomyocytes: role

of coculture with visceral endoderm-like cells. *Circulation.* Jun 3;107(21):2733-40.

Otsuji TG, Minami I, Kurose Y, Yamauchi K, Tada M, Nakatsuji N. (2010),Progressive maturation in contracting cardiomyocytes derived from human embryonic stem cells: Qualitative effects on electrophysiological responses to drugs. Stem Cell Res. 4, 201-13.

Robertson C, Tran DD, George SC. (2013) Concise review: maturation phases of human pluripotent stem cell-derived cardiomyocytes. Stem Cells. 31, 829-37

Sakata H, Sakabe M, Matsui H, Kawada N, Nakatani K, Ikeda K, Yamagishi T, Nakajima Y.(2007) Rho kinase inhibitor Y27632 affects initial heart myofibrillogenesis in cultured chick blastoderm. Dev Dyn. Feb;236(2):461-72

Sanger JW, Kang S, Siebrands CC, Freeman N, Du A, Wang J, Stout AL, Sanger JM. (2005) How to build a myofibril. J Muscle Res Cell Motil. 26(6-8):343-54.

Sartiani L, Bettiol E, Stillitano F, Mugelli A, Cerbai E, Jaconi ME. (2007) Developmental changes in cardiomyocytes differentiated from human embryonic stem cells: a molecular and electrophysiological approach. Stem Cells. 5, 1136-44.

Shiba Y, Fernandes S, Zhu WZ, Filice D, Muskheli V, Kim J, Palpant NJ, Gantz J, Moyes KW, Reinecke H et al. (2012) Human ES-cell-derived cardiomyocytes electrically couple and suppress arrhythmias in injured hearts. Nature. 489, 322-5.

van Laake LW, Passier R, Monshouwer-Kloots J, Verkleij AJ, Lips DJ, Freund C, den Ouden K, Ward-van Oostwaard D, Korving J, Tertoolen LG, et al., (2007) Human embryonic stem cell-derived cardiomyocytes survive and mature in the mouse heart and transiently improve function after myocardial infarction. Stem Cell Res. 1, 9-24.

Walsh KB, Parks GE (2002) Changes in cardiac myocyte morphology alter the properties of voltage-gated ion channels. Cardiovasc Res. 55, 64-75.

Vlasblom R, Muller A, Beckers CM, van Nieuw Amerongen GP, Zuidwijk MJ, van Hardeveld C, Paulus WJ, Simonides WS. (2009) RhoA-ROCK signaling is involved in contraction-mediated inhibition of SERCA2a expression in cardiomyocytes. Pflugers Arch. 4, 785-93.

Wei L, Roberts W, Wang L, Yamada M, Zhang S, Zhao Z, Rivkees SA, Schwartz RJ, Imanaka-Yoshida K. (2001) Rho kinases play an obligatory role in vertebrate embryonic organogenesis. Development. Aug;128(15):2953-62.

Yang L, Soonpaa MH, Adler ED, Roepke TK, Kattman SJ, Kennedy M, Henckaerts E, Bonham K, Abbott GW, Linden RM, et al., (2008) Human cardiovascular progenitor cells develop from a KDR+ embryonic-stem-cell-derived population. Nature. 7194, 524-8.

Yin L., Bien H., Entcheva E. (2004) Scaffold topography alters intracellular calcium dynamics in cultured cardiomyocyte networks. Am J Physiol Heart Circ Physiol. 287, H1276-85

Yoshida T. (2008) MCAT elements and the TEF-1 family of transcription factors in muscle development and disease. Arterioscler Thromb Vasc Biol. Jan;28(1):8-17.

Young JL, Engler AJ. (2011) Hydrogels with time-dependent material properties enhance cardiomyocyte differentiation in vitro. Biomaterials. 4, 1002-9

Zhao Z, Rivkees SA. (2003) Rho-associated kinases play an essential role in cardiac morphogenesis and cardiomyocyte proliferation. Dev Dyn. Jan;226(1):24-32

Main figures

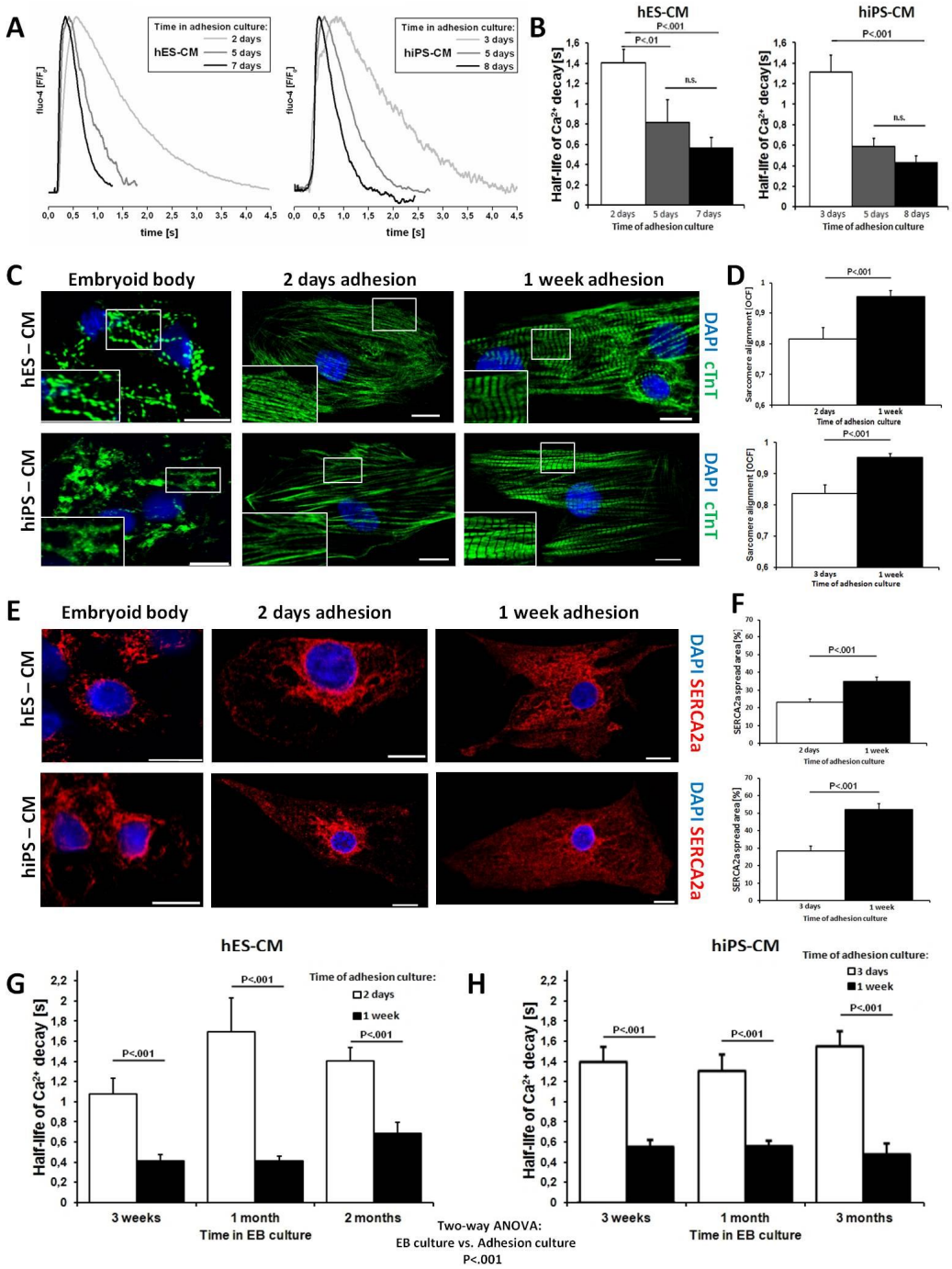

Fig. 1 hPSC-CM maturation in monolayer culture. (A) Representative calcium traces of hES-CMs and hiPS-CMs and different times of adhesion culture. **(B)** Evaluation of calcium re-uptake rate by the half-life of calcium decay. **(C)** Cardiac troponin T staining of hES-CMs and hiPS-CMs at different time points. Bar= 10 µm. **(D)** Sarcomeric alignment in terms of orientation correlation factor (OCF). **(E)** SERCA2a staining of hES-CMs and hiPS-CMs at different time points. Bar= 10 µm. **(F)** Evaluation of cell surface coverage of the SERCA2a staining. **(G)** Evaluation of the calcium re-uptake rate as function of time in EB culture and adhesion culture for hES-CMs. **(H)** Evaluation of the calcium re-uptake rate as function of time in EB culture and adhesion culture for hiPS-CMs.

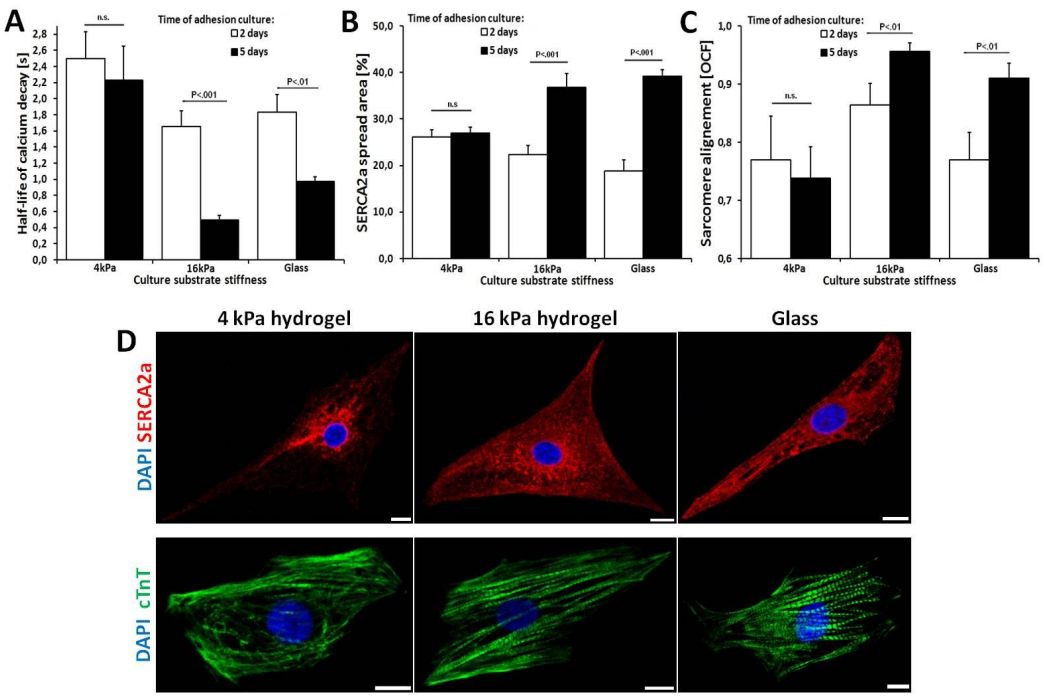

Fig. 2 Culture substrate stiffness influences cardiomyocyte maturation. **(A)** Calcium transient shortening in terms of half-life of calcium decay in hCMs on different substrates. **(B)** SERCA2a spreading in hCMs cultured on different substrates. **(C)** Sarcomeric alignment in hCMs cultured on different substrates. **(D)** Immunostaining for SERCA2a (upper panel) and cardiac troponin T (lower panel) on different substrates after 5 days in adhesion culture. Bar=10 µm.

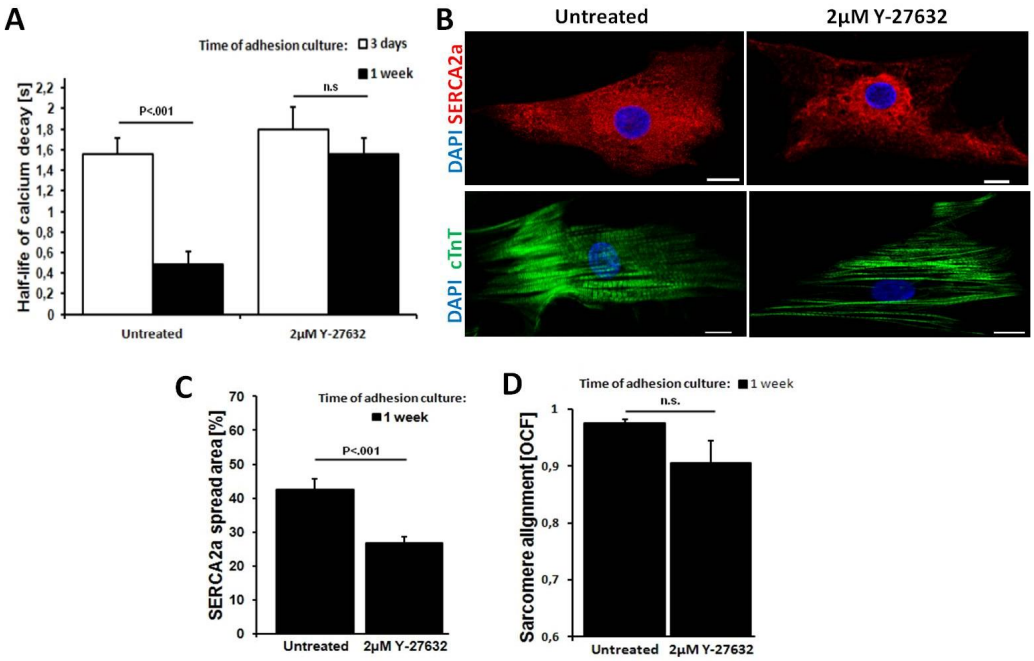

Fig. 3 Mechanotransduction through ROCK kinase is necessary for cardiac *in vitro* maturation. **(A)** Evaluation of the effect of ROCK inhibitor on the calcium re-uptake rate. **(B)** Immunostaining for SERCA2a (upper panel) and cardiac troponin T (lower panel) in hCMs treated with ROCK

inhibitor for 1 week in adhesion culture. Bar=10 μm **(C)** Evaluation of cell surface coverage of the SERCA2a staining. **(D)** Evaluation of sarcomeric alignment after 1 week of culture in presence of ROCK inhibitor Y-27632.

Supplementary experimental procedures.

RNA isolation and RT-PCR. RNA was isolated from differentiated EBs or monolayer cultures with TRIzol Reagent (Invitrogen) followed by purification with RNeasy Mini Kit (Qiagen). 1 μg of extracted RNA was retrotranscribed with High Capacity cDNA Reverse Transcription Kit (Invitrogen) and used as template for standard 30-cycle PCR analysis with Platinum Taq DNA polymerase (Invitrogen). Primer sequences (Sigma) were: GAPDH Frw 5'- CCCCTTCATTGACCTCAACTACA Rev 5'- TTGCTGATGATCTTGAGGCTGT; Triadin Frw 5'- CGTGATGCTATGGAGGAAACC Rev 5'- GATGCTACCTCCAAACCCCT; Calsequestrin Frw 5'- AAATCACAGCACCCACTACCA Rev 5'- GCAAATCAACCTCCCATCCCA; Phospholamban Frw 5'- CCCCAGCTAAACACCCGTAA Rev 5'- TCCTGTCTGCATGGGATGAC.

Real-Time PCR. Analysis of mRNA expression was assessed by Power SYBR Green Master mix kit (Invitrogen). Data are presented as expression fold change relative to the 16 kPa sample, normalized for GAPDH expression. Pfaffl method for relative fold expression change was applied.

Western Blot analysis. Protein samples were recovered from the organic phase of the TRIzol Reagent extraction. SDS-PAGE was performed on 4-12% Bis-Tris gels (Invitrogen) in MES buffer (Invitrogen). Primary antibodies were: cardiac troponin T (NeoMarkers, clone 13-11)[1] and GAPDH (Abcam). For chemo-luminescent detection were used anti-mouse HRP conjugated secondary antibody (BioRad) and ECL Kit (Invitrogen).

Supplementary references

Anderson PA, Greig A, Mark TM, Malouf NN, Oakeley AE, Ungerleider RM, Allen PD, Kay BK. **(1995)** Molecular basis of human cardiac troponin T isoforms expressed in the developing, adult, and failing heart. *Circ Res*. Apr;76(4):681-6

Supplementary figures

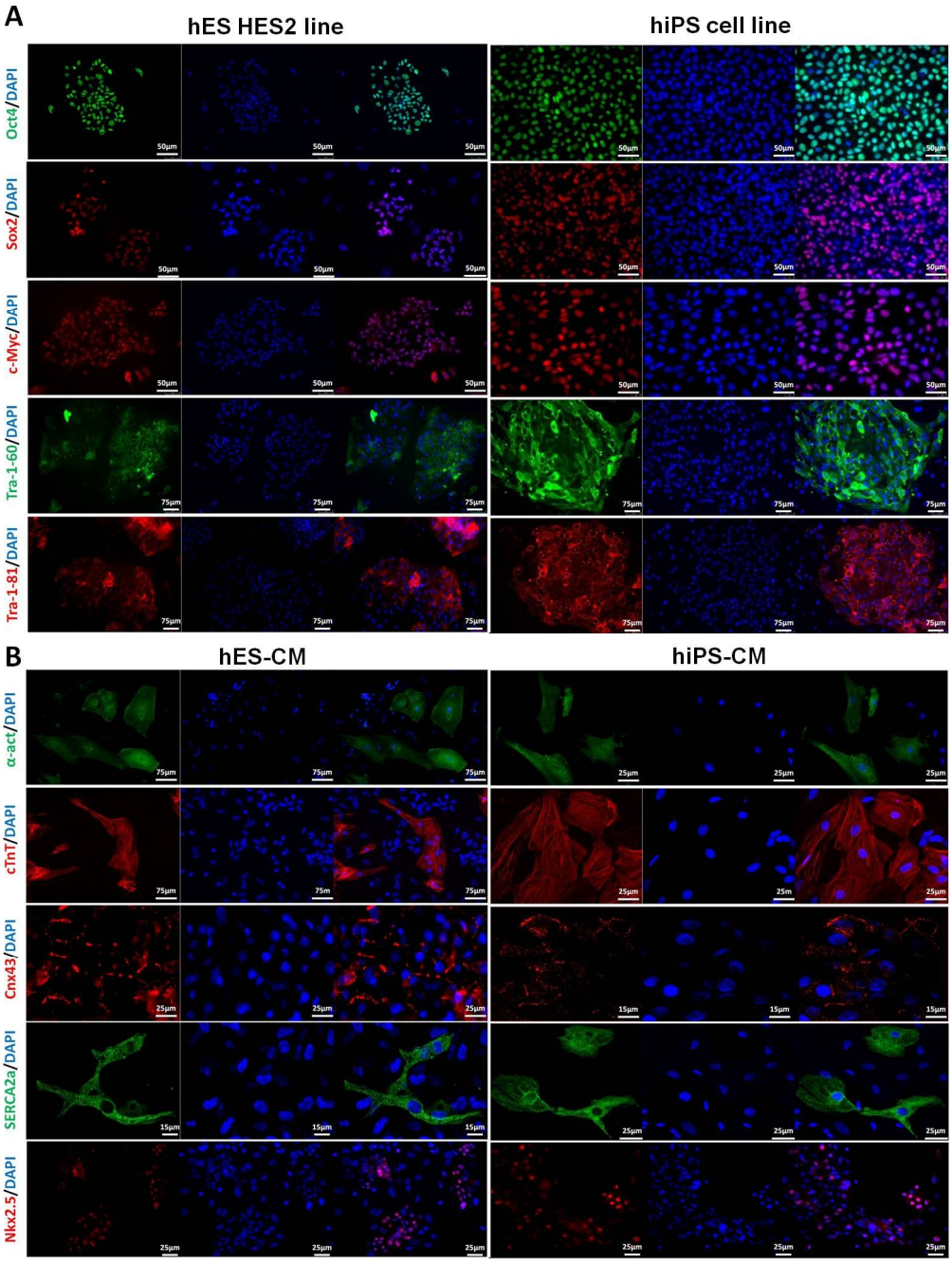

Fig. S1 Molecular markers of pluripotent and differentiated cells. (A) Expression of pluripotency markers in hES HES2 cell line and hiPS cell line. **(B)** Expression of cardiac markers in human cardiomyocytes derived from pluripotent stem cells.

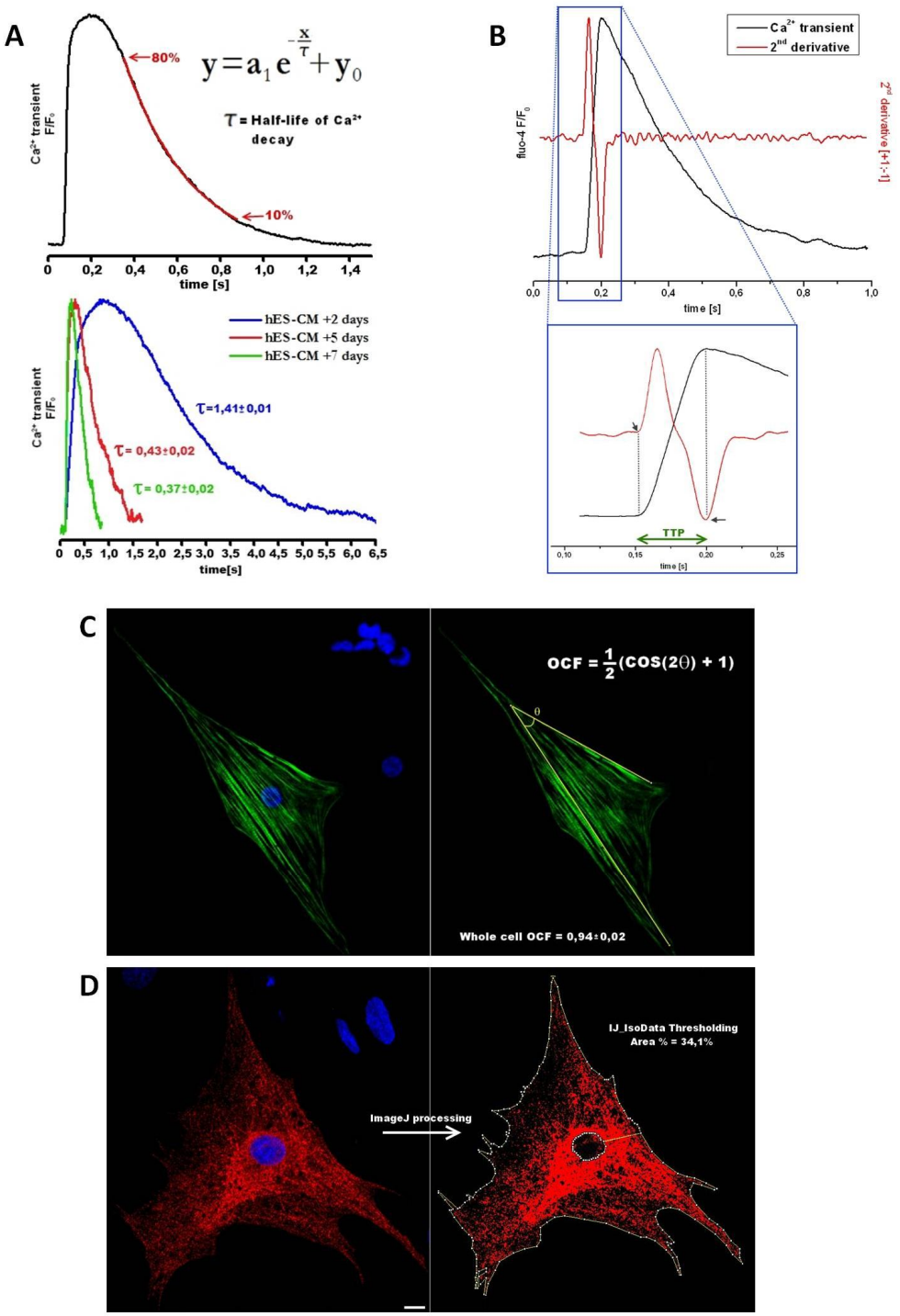

Fig. S2 Data analysis. (A) First order exponential decay fitting on experimental calcium transient (upper picture) and examples of tau value related to calcium traces (lower picture). **(B)** Evaluation of time to peak through analysis of the second derivative of the calcium transient. **(C)** Evaluation of the sarcomere alignment through calculation of the orientation correlation function (OCF). **(D)** Evaluation of the cell surface covered by SERCA2a immunostaining.

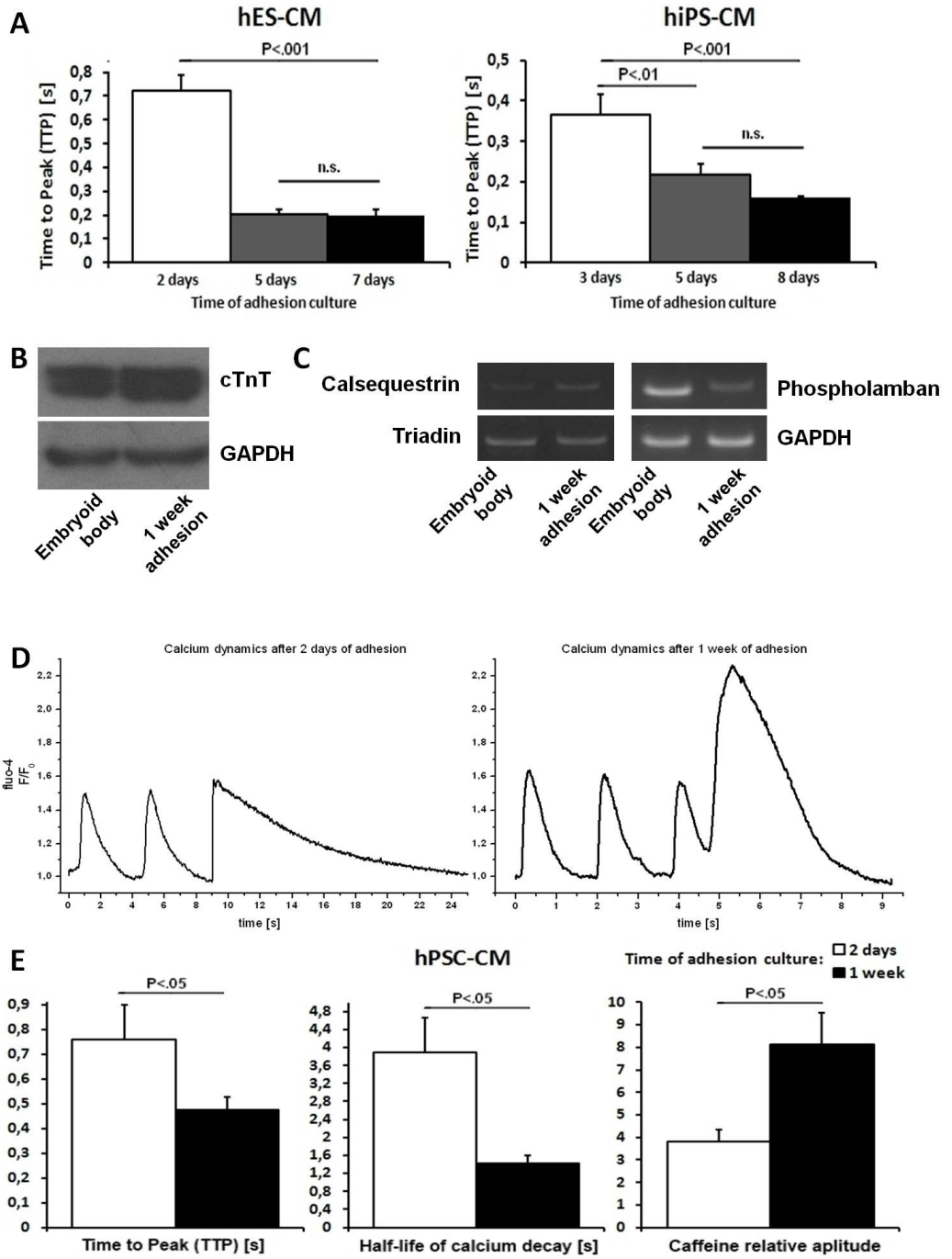

Fig. S3 Human cardiomyocyte maturation as function of adhesion culture time. (A) Time to peak decrease in maturing human cardiomyocytes derived from hES and hiPS cells. **(B)** Western Blot for cTnT and GAPDH in EB and adherent differentiated cells**. (C)** RT-PCR for components of the SR calcium handling machinery. **(D)** Response to 10 mM caffeine stimulation in hCMs at different time point of adhesion culture. **(E)** Quantitative parameters of the caffeine response in hCMs.

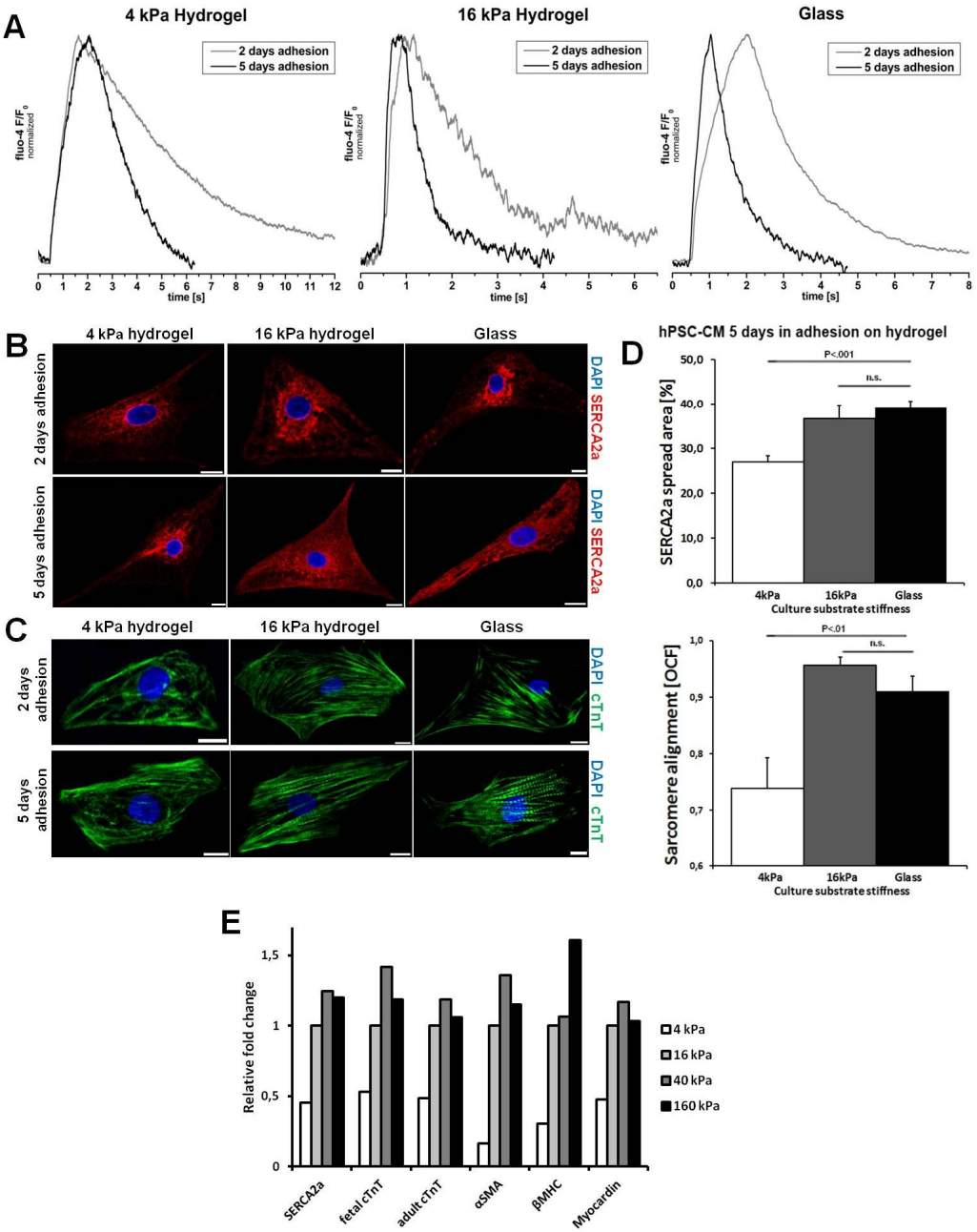

Fig. S4 Human cardiomyocytes culture on substrate of different stiffness. (A) Representative calcium traces on substrates of increasing stiffness. **(B)** Immunostaining for SERCA2a in hCMs on cultured different substrates. **(C)** Immunostaining for cardiac troponin T in hCMs on cultured different substrates. **(D)** Evaluation of SERCA2a spread area and sarcomere alignment in hCMs after 5 days of adhesion culture on different substrate stiffness. **(E)** Real-Time PCR results for cardiac genes in hCMs cultured on hydrogels of different stiffness.

Annex 2

Reversible alteration of calcium dynamics in cardiomyocytes during acute hypoxia transient in microfluidic platform

Sebastian Martewicz [1,2*], Federica Michielin [1,2*], Elena Serena [1,2], Alessandro Zambon [1], Marco Mongillo [2,3], and Nicola Elvassore [1,2,]

[1] Dipartimento di Ingegneria Industriale, University of Padova, via Marzolo 9, 35131 Padova, Italy.

[2] Venetian Institute of Molecular Medicine, via Orus 2, 35129 Padova, Italy

[3] Dipartimento di Scienze Biomediche, University of Padova, via Colombo 3, 35131 Padova, Italy.

* These authors equally contributed

Integrative Biology
Volume 4, pages 153-64 (2012);
DOI: 10.1039/c1ib00087j.

Abstract

Heart diseases is the leading cause of mortality in western countries. Apart from congenital and anatomical alterations, ischemia is the most common agent causing myocardial damage. During ischemia, a sudden decrease in oxygen concentration alters cardiomyocyte function and compromises cell survival. The calcium handling machinery, which regulates the main functional features of a cardiomyocyte, is heavily compromised during acute hypoxic events. Alterations in calcium dynamics have been linked to both short- and long-term consequences of ischemia, ranging from arrhythmias to heart failure.

In this perspective, we aimed at investigating the calcium dynamics in functional cardiomyocytes during the early phase of a hypoxic event. For this purpose, we developed a microfluidic system specifically designed for controlling fast oxygen-concentration dynamics through a gas micro-exchanger allowing in line analysis of intracellular calcium concentration by confocal microscopy. Experimental results show that exposure of Fluo-4 loaded neonatal rat cardiomyocytes to hypoxic conditions induced changes in intracellular Ca^{2+} transients. Such behavior was reversible and was detected for hypoxic levels below 5% of oxygen partial pressure. The observed changes in Ca^{2+} dynamics were mimicked using specific L-type Ca^{2+} channel antagonists, suggesting that alterations in calcium channel function occur at low oxygen levels. Reversible alteration in ion channel function, that takes place in response to changes in cellular oxygen, might represent an adaptive mechanism of cardiopreservation during ischemia.

Insight, innovation, integration

Recreating in vitro a low oxygen environment is fundamental for a better understanding of the cellular consequences of hypoxia and to screen novel therapeutic strategies targeting common ischemic diseases, e.g. coronary heart disease. Here, we present a microfluidic platform specifically developed to expose cultured cardiomyocytes to acute hypoxic stimuli, allowing robust and high quality live confocal imaging.

Thanks to this novel technology, we were able to observe rapid and reversible changes in the electrically-induced cardiomyocyte calcium transients following the acute decrease of oxygen partial pressure in the cell environment. Similar changes in calcium dynamics were observed upon pharmacological inhibition of L-type Ca^{2+} channels, suggesting a possible target of hypoxia in cardiac cells.

Introduction

Cardiovascular diseases are the leading cause of mortality and morbidity in the Western countries. Heart diseases due to coronary dysfunction alone were responsible for nearly 22% of all deaths in Europe in 2008.[1] Cardiac ischemia occurs when blood supply to part of the organ is suddenly reduced or completely interrupted for a discrete amount of time. Ischemic tissues undergo rapid changes in cellular environment such as reduced nutrient supply, accumulation of metabolic wastes, drop in oxygen concentration and increase in carbon dioxide concentration. In a highly energy demanding tissue, like the myocardium, hypoxic conditions that are generated when oxygen demand exceeds oxygen supply are reached in very short time.[2]

The time scale of the changes in oxygen concentration has a great importance for cell physiology, viability and adaptation to stress conditions. In particular, the cellular response to hypoxia depends on its onset kinetics and duration: (i) rapid acute hypoxia (seconds or minutes) leads to alterations of the preexisting protein pool through post-translational modifications and protein interactions; (ii) sustained chronic hypoxia (hours or days) results in whole proteome changes through activation of different gene expression patterns.[3]

In order to recreate *in vitro* ischemia pathological models, accurate gas concentration dynamics are one of the most difficult parameters to control; for instance, in hypoxia studies, gas leakage through liquid-air interface or gas permeable materials is extremely difficult to detect and may lead to low experimental reproducibility. Studies on chronic hypoxia (lasting hours or days) can be easily performed by culturing the cells in airtight chambers in which the oxygen concentration control is exerted by tuning the gaseous partial pressure inside the chamber. In this steady state experiments, the cell response at desired time points is commonly independent from the oxygen dynamics at the initial experiment set up.[4] On the other hand, observing cellular responses to fast hypoxic transients, simulating the early phase of acute ischemic events, is essential in understanding how cell biology and physiology are affected by sudden changes in oxygen concentrations. However, investigating the immediate

effects of a rapid drop in oxygen partial pressure requires tight control on the cellular environment, a condition hard to achieve with standard culture methods. As such, current technological limitations have hindered cellular experiments on hypoxia.

In this perspective, we aimed to develop a novel tool for *in vitro* investigation of the acute cellular response of cultured cardiomyocytes to fast changes in the environmental conditions, including components of the culture medium, drugs and oxygen concentration. In this work, we used such approach to investigate the effect of acute hypoxic events on Ca^{2+} homeostasis, through in line confocal image acquisition.

Cardiomyocyte function relays upon proper ion handling during contraction cycles, involving both ion channels regulating membrane potential and intracellular calcium release. Hypoxia has been proven to modify the activity of most of the molecular components concerned in these features, resulting in unbalanced ion fluxes and generation of arrhythmias.[5] Rat ventricular cardiomyocytes in low p_{O2} conditions displayed an increase of the late Na^+ current ($I_{Na\text{-}L}$) while the fast Na^+ (I_{Na}) current appeared reduced.[6,7] Effects on potassium channels were also described in guinea-pig cardiomyocytes as a decrease in the slow component of the delayed rectifier K^+ channel (I_{Ks}) current, without affection of the rapid component (I_{Kr}).[8] Ca^{2+} handling, essential in both action potential generation and contraction triggering, seems to be influenced by hypoxia as well. In particular, the activity of the L-type Ca^{2+} channel is altered with a decrease of basal current ($I_{Ca\text{-}L}$) and unchanged current–voltage (*I-V*) relationship.[9,10] Sensitivity of the channel to β-adrenergic stimulation appears to be increased resulting in a pro-arrhythmic substrate during ischemic events.[11] The precise mechanism through which hypoxia modifies the function of the L-type Ca^{2+} channel is still unclear. Both direct modifications in the C-terminal region of the channel[12,13] and indirect modulation of its function through mechanisms involving mitochondrial ROS formation[14] or protein kinases A and C[15] have been proposed.

All these studies clearly show that rapid changes in oxygen concentration affect ion handling in cardiac myocytes, but so far no hypoxia-induced effects on calcium handling during excitation-contraction coupling were reported, although many components of this machinery appear to be altered in ischemia-mimetic conditions.[16,17]

In this work, we aimed at analyzing calcium dynamics in Fluo-4-loaded functional rat cardiomyocytes in response to brief and sudden transients of hypoxia. In particular, we focused on the early response to hypoxia induction and re-oxygenation, by monitoring electrically stimulated Ca^{2+} changes.

For this reason, we designed and developed a device enabling confocal microscopy analysis while finely tuning the oxygen concentration in the culture medium and maintaining proximal cell environment isolated from atmospheric conditions. In addition, the device allows exposure of the cells to fast transient changes in the environment without perturbing the data acquisition process. Particular care has been placed to avoid, manipulation of the liquid phase that

could generate pressure waves in the cell culture chamber and cause loss of focal plane leading to artifactual changes in fluorescence signals.

As mentioned above, conventional humidified chambers or incubators with a controlled p_{O2} in the gas phase show equilibration time of the order of hours,[19] due to the great volumes involved and the low oxygen diffusion coefficient in the culture medium (2.1×10^{-5} cm^2 s^{-1}).[18] Such characteristic time can only be slightly decreased using particular expedients like gas-permeable membrane-based dishes[20] or by forcing gas exchange through bubbling of gas mixtures in chemostats or flasks.

In this perspective, technology developed at the microscale level can be an effective practical solution for obtaining a system able to accurately control oxygen partial pressure for two main reasons:

(i) at microscale liquid flow regime is typically laminar, allowing to accurately control the delivery of nutrients, soluble species and gas in the culture medium;[21-23]

(ii) the time scale of diffusive mass transport phenomena are related to the characteristic length of the system and scaling down the system highly accelerates the gas exchange dynamics.

For this reason, many microfluidic bioreactors were developed to provide solely moderate to long-term control of the cellular environment, including dissolved gas concentrations.[24-27] Some miniaturized devices include gas-microexchangers that generate spatial gradients of oxygen partial pressure by on-chip gas mixing and allow to study the influence of the oxygen concentration on the cell growth.[28-30]

However, only few microfluidic devices for rapid generation of hypoxic conditions in cell culture were designed, due to the difficulty in obtaining fast oxygen concentration transients from a saturated level to a very low partial pressure, without perturbing the cell culture environment and the data acquisition system. For instance, Oppergard *et al.* have developed a microfabricated insert that nests into a standard multiwell plate and serves as a passive microfluidic gas network with a permeable membrane aimed to modulate oxygen delivery to adherent cell with an equilibration time on the order of few minutes,[31] however no in-line analysis can be made with such device. Other groups have developed an *ad hoc* system to rapidly set the oxygen partial pressure in the cell culture and study particular cellular responses under hypoxic conditions.[32,33]

The complexity of the devices previously described induces to find out a structurally simpler microfluidic platform able to perform and control fast oxygen concentration dynamics and that could be coupled with any other miniaturized bioreactor or culture chamber. Unlike other works, we are aimed to engineer a new oxygen micro-exchanger to carry out on line analysis on the cell culture, for example using confocal microscopy, during an oxygen shift in the culture medium, and acquire particular cellular responses without any perturbation of the detection system.

Experimental methods

Experimental set up

Our investigation on calcium transient requires a fine tuning of oxygen partial pressure inside a microfluidic cell culture chamber by a multilayer microfluidic gas-exchanger. The device has to ensure a fast and accurate oxygen concentration control inside the culture chamber in order to provide a precise and repeatable hypoxic stimulus to the cell culture. Hypoxic stimuli on a cardiomyocyte population are generated by setting only the oxygen partial pressure in the gas phase without perturbing flowing medium. Cellular calcium dynamics were analyzed directly on line by a fluorescence confocal microscope. An external system for control and data acquisition allowed to precisely set gas phase partial pressures and flow rates, while an uniform medium flow rate was maintained during all the experiments (Fig.1).

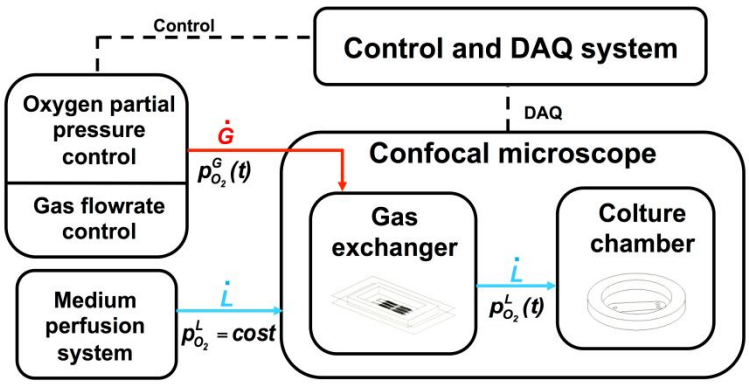

Figure 1. **Schematic view of experimental set up**. Fast and accurate control of oxygen partial pressure inside a microfluidic cell culture chamber is performed by a multilayer microfluidic gas-exchanger. Hypoxic stimuli on a cardiomyocytes population are generated by setting gas oxygen partial pressure and cells' calcium dynamics are analyzed in line by a confocal microscopy. An external system for control and data acquisition ensures fine tuning of gas phase partial pressure and flow rate, whereas a stable medium flow rate is maintained during experiments.

Microfluidic gas exchanger fabrication

Fig. 2A shows a schematic view of the multilayer microfluidic gas exchanger. The oxygen exchange process between the gas and liquid compartments takes place through a thin, non-porous, permeable membrane. Microfluidic gas exchanger consists in a three-layer structure: a fluidic layer containing cell culture medium, a gas chamber for gas flow with defined oxygen partial pressure and an oxygen permeable membrane. The fluidic layer is formed by a network of microfluidic channels in an oxygen non-permeable glass substrate to achieve complete gas sealing. The micrometric thickness of the gas permeable membrane ensures low oxygen diffusion resistance. The gas domain is a milliliter rectangular chamber that allows high gas flow rate and, consequently, almost uniform oxygen partial pressure within the gas chamber.

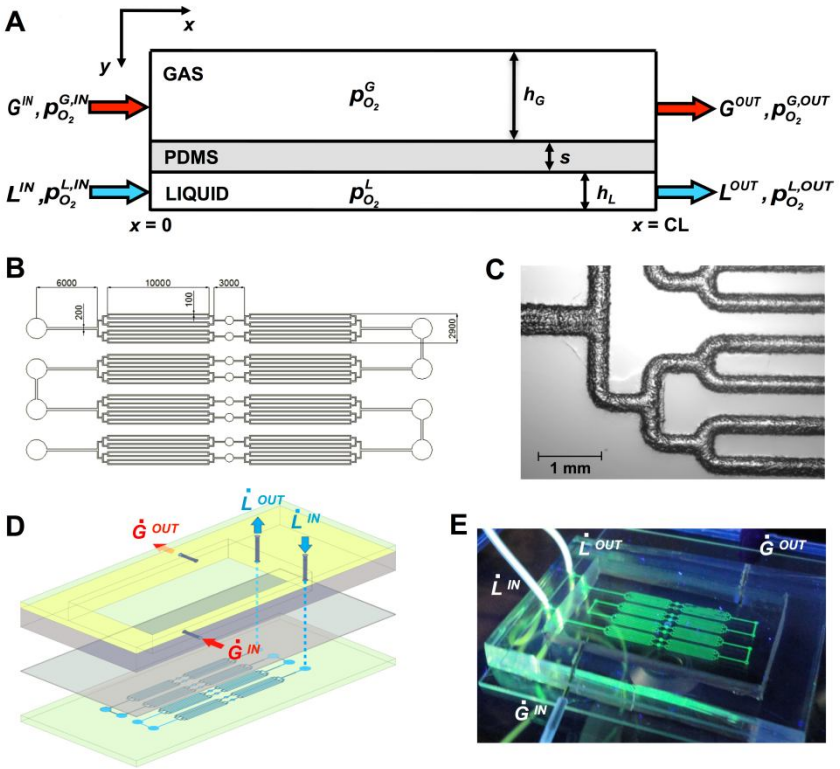

Figure 2. **Microfluidic gas exchanger**. (A) Schematic representation of the three-layered microfluidic system; inlet/outlet flow rates and oxygen partial pressure are shown for both gas, G, and liquid, L, phase. (B) Top view of the fluidic layer channel network (all dimensional values are in µm). (C) Image of glass-etched microfluidic channels network obtained by wet-etching technique and observed under inverted optical microscope. (D) Schematic view of the three different layer of the gas exchanger. Red and blue arrows show gas and liquid phase inlet and outlet inside the platform. (E) Image of the gas-exchanger with inlet/outlet connections for liquid and gas phase perfusion. The microfluidic channels are perfused with 1 mM fluorescein solution.

In the fluidic layer, the flow channels network is characterized by a series of gas exchanger unit and each unit is formed by 8 parallel microchannels 100 µm wide (Fig. 2B). This modular design allows to add series of units, up to obtain the total length required for a given exchange efficiency. The imprinting of microchannels in the glass slide was achieved by wet-etching technique. A borosilicate glass slide 50 × 75 mm was cleaned using MICRO90 Cleaning Solution (Sigma-Aldrich, USA), placed in an oven for 1 h at 403 K, cooled at 303 K and silanized with hexamethyldisilazane, HDMS, (Sigma-Aldrich, USA) for 3 minutes at 403 K. The glass slide was spin-coated with 5 g of SPR220-7.0 positive photoresist (Rohm&Haas, Dow, USA), to obtain an homogeneous film with a thickness of 15 µm and subsequently photolithografically patterned using standard procedures.[34] The glass slide was immersed in an aqueous 40% fluoridric acid solution (HF, Sigma-Aldrich, USA) at 298 K and only exposed areas were etched. After patterning, the slide was washed with distilled water, deep into an aqueous 98% sulfuric acid solution (H_2SO_4, Sigma-Aldrich, USA) to remove etching-reaction byproducts and rinsed with distilled water. The protective photoresist layer was removed with 1-methyl-2-pyrrolidone (Sigma-Aldrich, USA) and the patterned glass slide was cleaned in piranha solution (H_2SO_4:H_2O_2, 3:1). Fig. 2C

shows an image of the etched microchannels on glass under an inverted microscope (Leica, Germany).

Channels section shape and depth were analyzed with a profilometer (Alpha Step IQ surface profiler, KLA Tencor, USA). Rounded cross-section shape was observed, while channels depth resulted etching-time dependent; depths of 40, 70 and 100 μm were obtained with an immersion time in HF solution of 2.5, 5 and 7.5 min, respectively.

A thin polydimethylsiloxane, PDMS, permeable membrane with defined and homogenous thickness was obtained by spinning the unpolimerized solution on a silicon wafer. A premixed 10:1 ratio of PDMS prepolymer and curing agent (Sylgard 184 kit, Dow Corning, USA) was spin-coated on a previously silanized 5 in Si wafer at 1400 rpm for 1 min to obtain a thickness of 40 ± 5 μm and cured on a hotplate at 353 K for 1 h.

The gas layer consists in a 5 cm^3 PDMS chamber in which gas phase flows at defined flow rate and p_{O2}. Residence time is only of few seconds to maintain an uniform oxygen partial pressure during steady-state experiments.

PDMS layers were punched with a 22G stainless steel needle (Small Parts Inc, USA) to obtain gas and liquid inlet/outlet holes. A 50 × 75 mm glass cover slide, gas chamber, PDMS membrane and fluidic layer were assembled and sealed by plasma bonding (Plasma Cleaner, Harrick Plasma, USA). All fluidic connections to the microfluidic device were made using PTFE microtubing (Cole Parmer, USA). Fig. 2D shows a schematic view of the assembled layers. The red arrows indicate gas inlet/outlet, whereas blue lines show the liquid track inside the platform.

Different liquid flow rates through the fluidic microchannels were obtained by a syringe pump (Harvard Pump, Harvard Apparatus, USA). A constant gas flow rate and oxygen composition were maintained in the gas chamber using air and nitrogen mass flow meters (Bronkhorst, The Netherlands), controlled through software FlowDDE32.

Oxygen measurement

A 100 μM solution of tris(4,7-diphenyl-1,10-phenanthroline)-ruthenium(II)-dichloride, Ru(ddp), (Sigma-Aldrich, USA) in a 30% ethanol in PBS 1X (Invitrogen, USA) solution was used to measure oxygen partial pressure inside the microfluidic channels. Fluorescence of Ru(ddp) was detected by an inverted fluorescence microscope LeicaDMI6000B equipped with a mercury short-arc reflector lamp (Leica, Germany) excited at BP 450-490 nm and acquired at LP 590 (Fig. 2E).

Oxygen partial pressure was also continuously monitored with a fiber optic oxygen sensor (OceanOptics, USA) at the microchannel outlet. Fluorescence intensity is linearly correlated to the oxygen partial pressure in the sample. Both sensors are based on fluorescence quenching that increases with the oxygen partial pressure. The degree of quenching can be correlated to the oxygen partial pressure of the sample by Stern-Volmer equation:

$$\frac{I_0}{I} = 1 + kp_{O_2} \qquad (1)$$

where I_0 is the fluorescence intensity at zero partial pressure of oxygen, I is the fluorescence intensity at a particular p_{O_2} and k is the Stern-Volmer constant which depends on the chemical composition of the sensor and on the temperature. Calibration of the sensor at 298 K was achieved using five liquid standards, obtained by bubbling a gas mixture with a partial pressure of 0%, 5%, 10%, 15% and 21%. Complete oxygen removal was achieved with 8 hours of humidified argon bubbling (Rivoira, Italy). Stern-Volmer constant value was obtained by correlating experimental data.

Microfluidic cell culture chamber

Microfluidic cell culture chamber was made by standard soft-litography technique.[34] Briefly, design shown in Fig. 3A was produced by CAD program and patterned in a silicon substrate using negative photoresist SU8-2100 (Microchem, Germany). After silanization with HDMS under vacuum for 1 h, 10:1 ratio of PDMS prepolymer and curing agent was casted and cured for 2 h at 343 K in an oven. Through a 27 mm punch, PDMS mold was extracted. In order to ensure an electrical stimulation to the cell culture, a platinum wire was inserted in the PDMS mold and wired to an electrical stimulator. The glass slide hosting the cell culture was located in a standard microscopy aluminum holder (20 mm diameter hole), covered by the PDMS mold and pressure sealed by a teflon cover (Fig. 3B).

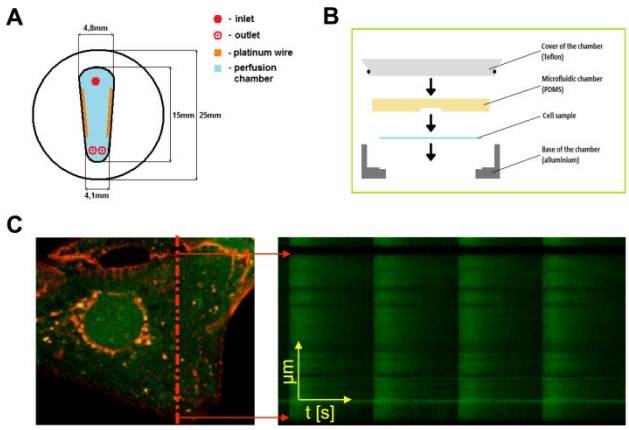

Figure 3. **Cell culture chamber and calcium dynamic acquisition.** (A) Microfluidic cell culture chamber top view. The chamber is characterized by 1 inlet and 2 outlets and by 2 platinum wires placed in the lateral walls to electrically stimulate cells. (B) Assembly of the microfluidic chamber within microscope holder to perform on line detection. (C) Confocal image and calcium dynamic of a cardiomyocyte under electrical stimulation. Line scan (yellow line) is placed between nucleus and sarcolemma of the cell and calcium transient are continuously detected as a function of time.

The perfusion culture chamber was connected to the microfluidic exchanger through silica tubings in order to avoid external oxygen infiltrations. All the experiments were performed with a 100 µl min^{-1} flow rate using syringe pumps (Harvard Pump, Harvard Apparatus, USA) allowing fast exchange of medium without any apparent change in cellular calcium dynamics.

Cardiomyocytes isolation and culture

Neonatal rat cardiomyocytes were obtained from Sprague-Dawley pups 1-3 days old. The cells were plated on 20 µg/ml laminin-coated (BD Bioscience, USA) glass coverslips in Day1 medium: 25 mM Hepes Dulbecco's Modified Eagle's Medium (Gibco, USA), 17% Medium M199 (Gibco, USA) 10% Horse Serum (Gibco, USA), 5% Newborn Calf Serum (Gibco, USA), 2 mM L-Glutammine (Gibco, USA), Penicillin-Streptomycin (EuroClone, Italy). After 24 hours, the Day1 medium was replaced with Day2 medium: Day1 medium with 5% Horse Serum and 0.5% Newborn Calf Serum. Experiments were performed 4 days after plating. The animals were housed and operated at the Animal Colony of the Venetian Institute of Molecular Institute. All experiments with animals were approved by Padova University's Institutional Animal Care Committee (Comitato Etico di Ateneo per la Sperimentazione Animale).

Calcium dynamic acquisition and analysis

Confocal Calcium measurements were performed as reported in Fig. 3C. Cardiomyocytes were loaded in serum-free D-MEM (Gibco, USA) supplemented with 3 µM fluorescent calcium dye fluo-4 AM (Invitrogen, USA) for 20 minutes at 310 K in presence of 2 µM Pluronic F-127 (Invitrogen, USA) and 20 µM sulfinpyrazone (Sigma-Aldrich, USA), then incubated for additional 10 minutes at 310 K in Fluo-4-free D-MEM to allow complete de-esterification of the dye, and added with 0.2 µM di-8-ANEPPS (Invitrogen, USA). After loading, the coverslips were transferred to the microfluidic chamber and perfused with recording solution: NaCl 125 mM, KCl 5 mM, Na_3PO_4 1 mM, $MgSO_4$ 1 mM, Hepes 20 mM, $CaCl_2$ 2 mM, Glucose 5.5 mM, to pH 7.4 with NaOH. Line scan was acquired with Leica TCS SP5 confocal microscope equipped with a 63×, 1.4 NA oil immersion objective, with 488 nm Ar laser line as excitation source, 700 Hz acquisition frequency. To reduce dye photo-bleaching and photo-toxic effects on the analyzed cells, the laser power was set at minimum possible. During all the experiments, the culture was constantly filed-stimulated with electrical pulses at 0.7 Hz, 20 V cm^{-1}, to overcome spontaneous beating activity allowing acquisition at the same beating rate in all cells. Nifedipine and Verapamil (Sigma-Aldrich, USA) were dissolved in DMSO (Sigma-Aldrich, USA) or deionized H_2O, respectively, at a 10 mM starting concentration and diluted to the desired concentration in recording solution immediately prior to the experiments. All data analysis were performed with ImageJ and Origin7 software.

Data are presented as means of percentage decrease normalized on the reference conditions ± standard error of mean (SEM). The effects of different oxygen concentrations on calcium transients were compared by a one way ANOVA followed by Bonferroni's mean comparison. We considered $P < 0.01$ to be statistically significant.

Mathematical modeling

The oxygen concentration profile, and consequently the oxygen partial pressure, within the liquid phase domain of the microfluidic gas exchanger was described by simplified analytical model and by computational solution of the

species mass balance. The simplified model was validated with computational analysis and used for a proper gas exchanger design.

Mass transfer was assumed to be governed by convective transport in the gas phase, diffusive resistance in the permeable membrane and convective-diffuse regime in the liquid phase. The concentration in the gas phase was assumed constant along spatial coordinates because, according to the high gas flow rate, the permanence time in the gas chamber is much smaller than the characteristic time of the membrane oxygen exchange process.

On the other hand, the oxygen concentration in the liquid phase changes from the inlet (x = 0) to the outlet (x = CL) of the microfluidic gas exchanger. For this reason, in order to describe oxygen concentration profile along y-coordinate (height of the microfluidic channel), both hydrodynamic and mass transport models should be solved simultaneously. Due to the low Reynolds numbers (1÷10) an analytical solution of fully developed hydrodynamic profile between flat planes was assumed.[35] Considering that Péclet number (convection/diffusion ratio) is much greater than 1 for all experimental conditions tested in this work, we assumed that diffusive flux is relevant only in the y-direction, whereas convective flux occurs in the x-direction. Moreover, we define h_L as the equivalent channel height, which is obtained as the area of the cross-section divided by the width of the channel.

Under these assumptions and considering all mass transfer resistances localized at the interfaces, the steady-state mass balance equation in the liquid domain takes the following form:

$$\begin{cases} \dfrac{u}{H}\dfrac{\partial p_{O_2}^{L}(x)}{\partial x} + N_{O_2,y}\left(x, y = h_L\right) = 0 \\ p_{O_2}^{L}(x=0) = p_{O_2}^{L,IN} \end{cases} \tag{2}$$

where $p_{O_2}^{L}$ is the oxygen partial pressure of the liquid phase, u is the axial velocity, H is the Henry's constant of oxygen solubility in water at experimental temperature condition, $N_{O_2,y}\left(x, y = h_L\right)$ is the total oxygen flux at liquid-membrane interface along x-coordinate and $p_{O_2}^{L,IN}$ is the boundary condition at channel inlet. The total oxygen flux at liquid-membrane interface, $N_{O_2,y}\left(x, y = h_L\right)$, can be expressed as the product of the overall mass transfer resistance and the total driving force:

$$N_{O_2,y}\left(x, y = h_L\right) = < K_G > \left(p_{O_2}^{L}(x) - p_{O_2}^{G}\right)a \tag{3}$$

$p_{O_2}^{G}$ is the constant oxygen partial pressure in gas phase, a is specific surface, which corresponds to the inverse of the equivalent channel height h_L, whereas $< K_G >$ is the averaged overall mass transfer coefficient. The analytical expression of $< K_G >$ is derived by equating oxygen fluxes for the three different domains and its general form can be expressed as follows:

$$\frac{1}{< K_G >} = \frac{1}{k_G} + \frac{s}{p} + \frac{H}{k_L}. \quad (4)$$

k_G and k_L are the mass transfer coefficients in the gas and liquid phase respectively, p the oxygen permeability in PDMS and s the membrane thickness.

Integration of equation (2) from the inlet to the outlet of the channel leads to the following relation:

$$\frac{p_{O_2}^{L,OUT} - p_{O_2}^{G}}{p_{O_2}^{L,IN} - p_{O_2}^{G}} = \exp\left(-\frac{< K_G > HL}{h_L u}\right) \quad (5)$$

Equation (5) relates the oxygen partial pressure in the microchannel to the length and geometry of the channel, operative conditions and mass transfer properties. This relation is used to calculate the minimal channel length necessary to ensure a defined oxygen concentration at the outlet of the system.

The solution of equation (5) requires a proper estimation of the mean overall mass transfer coefficient by equation (4). Due to the high oxygen diffusivity in the gas phase compared to those in the liquid and solid phase, the first resistance term in equation (4) results negligible.

The mass transfer coefficient in the liquid phase, k_L, can be evaluated from empirical correlations for laminar flow which relate together dimensionless groups (Péclet, Reynolds and Sherwood numbers). In the developing diffusive concentration profile and for boundary layers which are extremely thin relative to the channel width, the following relation has been proposed:[36]

$$\begin{cases} \frac{k_L h_L}{D} = 1.233\left(\frac{xD}{uh_L^2}\right)^{-1/3}, \frac{xD}{uh_L^2} \le c_1 \\ \frac{k_L h_L}{D} = c_2, \frac{xD}{uh_L^2} > c_1 \end{cases} \quad (6)$$

where D is the oxygen diffusion coefficient in the liquid phase. c_1 and c_2 are constant values that can be evaluated by computationally solving oxygen mass balance equations for the system shows in Fig. 2A.

The numerical solution of the convective-diffusion equation for the fluidic domain and the diffusive equation for the solid domain were obtained with the support of the software COMSOL Multiphysics 3.4 at different operative conditions. Boundary and initial conditions were set as follows: the top of the membrane domain is taken to be at a constant concentration in equilibrium with the adjacent gas phase, whereas oxygen concentration at the bottom surface is equilibrated with that in the fluidic domain. In the inlet section of the fluidic domain it was set a constant concentration, whereas at the outlet section it was considered only a convective flux. The remaining walls were assumed to be impermeable to oxygen. All values for the parameters used for the simulations are listed in Table 1.

Table 1. Summary of physical properties.

Property	U.M.	Valu	Ref.
D, oxygen diffusion in PBS	$m^2\ s^{-1}$	2.1×10^{-9}	37
p, oxygen permeability in PDMS	$(10^{-10}\ cm^3(STP) \times cm/cm^2 \times s \times cmHg)$	800	38
O_2 solubility in PBS at 1 atm and 298K	$mol\ m^{-3}$	1.045	39

Results and discussion

Microfluidic platform validation

Fig. 4A shows the oxygen concentration distribution in the microfluidic channel obtained by computational simulation of oxygen mass balance equations. Boundary conditions were set as follows: inlet oxygen partial pressure, $p_{O_2}^{L,IN}$, was set to 21%, whereas oxygen partial pressure in the gas phase, $p_{O_2}^{G}$, is assumed to be constant at 0%. Oxygen flux through the PDMS membrane is directed from the liquid phase to the gas compartment according to the oxygen partial pressure gradient. Oxygen flux at the membrane interface decreases along the *x*-coordinate due to the progressive reduction of the gradient for 1 mm channel length as shown in Fig. 4B.

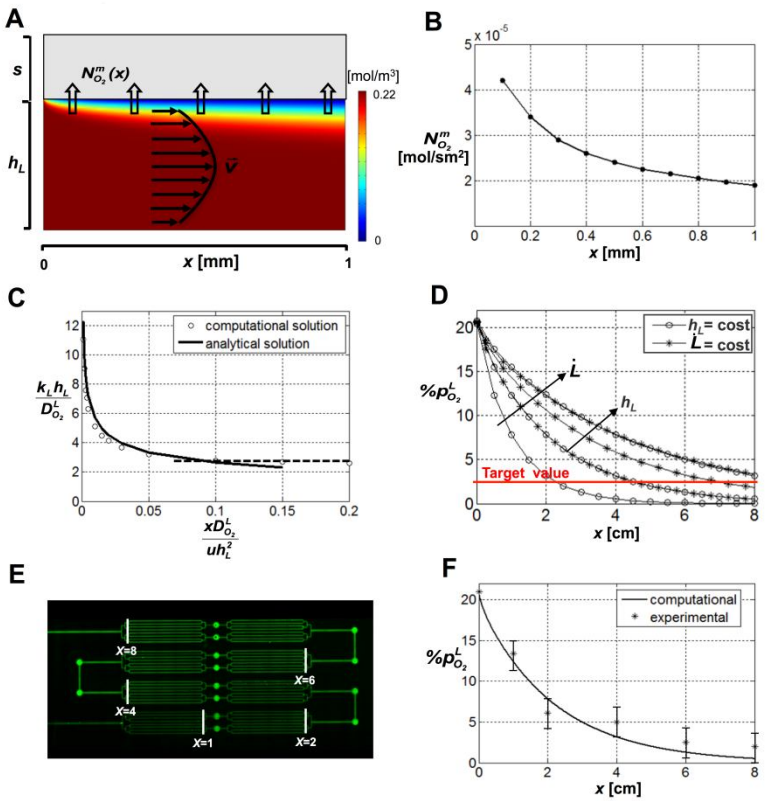

Figure 4. **Mass transport model development and validation**. (A) 2D representation of oxygen

concentration obtained by computational solution of mass balance equations in the microfluidic channel longitudinal cross-section. Empty arrows show oxygen flux directed from liquid phase to the gas one, in which oxygen partial pressure is assumed to be 0%. Full arrows show *y*-direction velocity profile. (B) Profile of the oxygen flux normal to the PDMS membrane interface along *x*-coordinate. (C) Comparison of computational and analytical solution in term of adimensional numbers according to Eq. 6. (D) Oxygen partial pressure profile obtained from analytical solution given by Eq. 5 as a function of *x*-coordinate, parametric in liquid flow rate, $\dot{L}$, and channel height, h_L. Red line shows design target value of 2%. (E) Fluorescence imaging of fluidic layer filled with Ru(ddp) solution, using $\dot{L}$=100 µl/min and h_L=40 µm. White mark shows the region of interest for fluorescence quantification reported in Fig. 4F (values of *x*-coordinate are in cm). (F) Comparison of $p_{O_2}^L$ experimental profile inside the fluidic layer and the analytical solution obtained by Eq. 5.

In order to properly design the gas exchanger, the application of computational simulation to a larger portion or overall microfluidic channel could be time consuming and computational intensive. For this reason a simplified analytical theory to fairly describe mass transport inside the microfluidic device was derived. The mass balance analytical expression (Eq. 5) can describe oxygen profile inside the channel as a function of all operative parameters that affect mass transfer process and of the mean overall mass transfer coefficient (<K_G>) and, in particular, liquid mass transfer coefficient (k_L). In this work, we adopt the model proposed by Vollmer and coworkers [36] to our system using computational results to estimate model parameters. We found out that c_1 and c_2 constant values of Eq 6 are 0.10 and 2.62 respectively. Fig. 4C shows a comparison between computational simulation and modified analytical model (Eq. 6) in terms of adimensional numbers. This analytical model allows to fairly estimate the liquid mass transfer coefficient for several experimental conditions, in particular for different liquid flow rates $(\dot{L})$ and channel heights (h_L).

On the other hand, the minimal channel length for achieving a target $p_{O_2}^L$ reduction using specific liquid flow rate and channel height can be easily estimated by Eq. 5. Fig. 4D shows $p_{O_2}^L$ profiles as a function of *x*-coordinate, obtained by varying both $\dot{L}$ and h_L.

In order to experimentally validate the developed theory we mapped fluorescence intensity of the oxygen sensitive dye in the overall fluidic layer of the oxygen exchanger (Fig. 4E). Fig. 4E shows a fluorescence intensity increase along *x*-coordinate from the inlet to the outlet according to $p_{O_2}^L$. Fig. 4F shows a comparison of experimental $p_{O_2}^L$ measured at different *x*-coordinate values (reported in Fig. 4E) and analytical solution obtained from Eq. 4. Very good agreement between profiles within the experimental uncertainty has been observed. Finally, using the simplified analytical theory, we designed a gas exchanger that is able to perform a $p_{O_2}^L$ reduction of 95% with a steady state flow rate of 100 µl min^{-1}. The gas exchanger configuration consists in 8 exchanger units in series formed by 8 parallel channels with 80 mm total length, 40 µm height and 100 µm width.

Calcium dynamics in hypoxia

The microfluidic cell culture chamber and gas exchanger must preserve cardiomyocytes physiological characteristics while providing fast transient

biochemical stimulation. The cell culture chamber was properly designed to obtain a uniform laminar flow avoiding unpaired velocity profile, back flow and stagnant dead volumes. This ideal condition was experimentally verified by observing the dynamic of a pulse of fluorescein in the cell culture chamber at different flow rates (data not shown). In addition, before each experiment, the culture was maintained in perfusion for 1 hour in normoxic solution while recording calcium dynamics. The cardiomyocytes displayed normal calcium dynamics during electrical stimulation. In order to test the time course of substance delivery to the microfluidic chamber, we injected a 50 µl bolus of 10 mM caffeine solution in the perfusion line. The caffeine stimulated Ca^{2+} release from sarcoplasmic reticulum (SR) had a rapid onset and resulted in the change in fluorescence intensity. Such effect lasted 45 s, after which the calcium transients amplitude returned to normal indicating complete caffeine wash out (Fig. 5A). This time is consistent with the estimated permanence time of caffeine within the microfluidic chamber, as evaluated through fluorescence dye experiments.

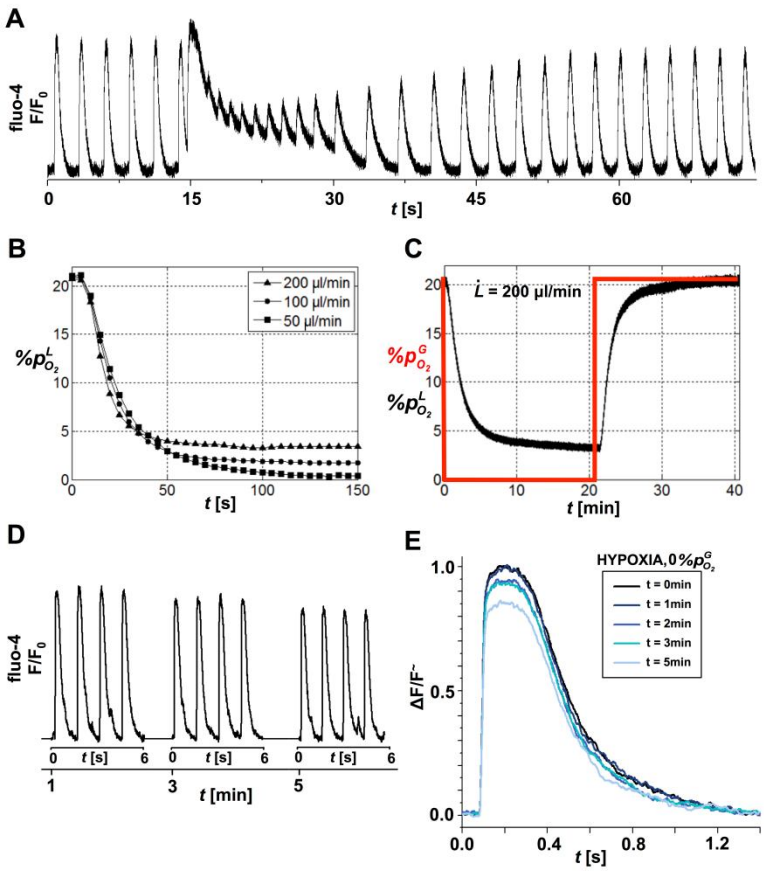

Figure 5. **Effect of hypoxia on calcium transients**. (A) Calcium dynamic in a cardiomyocyte under electrical stimulation revealed through fluo-4 in the microfluidic culture chamber during perfusion of 50 µl of 10 mM caffeine solution; cardiomyocyte displays normal Ca^{2+} transients and response to caffeine with full recovery after wash out. (B,C) Liquid phase oxygen dynamic during step impulse of the oxygen partial pressure in the gas phase monitored by Ru(ddp) with three different flowrates (B) and by optic fiber sensor with $\dot{L}$ = 200 µl min^{-1} (C) at exchanger outlet. (D) Calcium transients sequence at different time points after hypoxic stimulus to the cell culture. (E) Comparison of single normalized calcium transients at different time points after hypoxic stimulus.

In order to analyze the early effect of hypoxic events on cardiac physiology it is fundamental to fully characterize the oxygen partial pressure dynamics after set point variations. For this reasons, oxygen partial pressure at the outlet of the gas exchanger were measured by continuously detecting intensity fluorescence of oxygen sensitive dye during a $p_{O_2}^G$ set point change from 21% to 0% at three different flow rates: 50, 100 and 200 µl min^{-1} (Fig. 5B). The $p_{O_2}^L$ half decay value of 10 s for all different flow rates ensures fast oxygen dynamics. Different hypoxic steady state levels ($p_{O_2}^L$ < 5%) can be achieved by varying medium flow rate (Fig. 5B). In order to exclude gas leakage between the gas exchanger and the culture chamber, oxygen partial pressure values, $p_{O_2}^L$, were continuously monitored at cell culture chamber inlet by fiber optic probe. Fig. 5C shows $p_{O_2}^L$ steady state values (black line) reached after two $p_{O_2}^G$ set point variations (red line): 21% to 0% and 0% to 21%. Consistent measurements reported in Fig. 5B-C confirms an efficient gas insulation.

All together, these results show that the microfluidic experimental set up (as reported in Fig. 1) is able to accurately control oxygen partial pressure on cell culture in terms of steady state levels and rapid set point variations. It is worth to underline that oxygen partial pressure control is achieved without any perturbations on liquid media, allowing long term confocal acquisitions on same region of interest. These technical improvements make possible to perform experimental investigations using the same cell as its own control, continuously acquiring biological data prior and during the hypoxic stimulation.

In order to rationally study the hypoxia-induced effects on calcium handling during excitation-contraction coupling it is important to investigate the duration of hypoxic stimulation that could exert a cell physiological response.

In this context, Fig. 5D shows a sequence of calcium dynamics in response to fast $p_{O_2}^L$ drop as a function of time. A comparison of normalized calcium transient peaks at different time points (Fig. 5E) shows a significant alteration of the fluorescence intensity peak maximum after 5 min from hypoxic stimulus. All other experiments were performed considering this time frame as a minimal value to elicit a hypoxia-induced physiological response.

We then sought to determine the hypoxic level at which hypoxia-induced effects on calcium handling during excitation-contraction coupling can be recorded. A multiple step experiment was designed by setting $p_{O_2}^G$ at 5 different values from 21% to 0% with 5% interval and the resulting $p_{O_2}^L$ step profile is shown in Fig. 6A. Corresponding values of $p_{O_2}^L$ and $p_{O_2}^G$ were correlated to obtain operating curve shown in Fig. 6A insert. Interestingly, the operating curve differs slightly from the equilibrium curve within the accuracy used in the gas exchanger design ($p_{O_2}^L$ = 2% as target value (Fig. 4D), corresponding to 95% reduction from normoxic conditions).

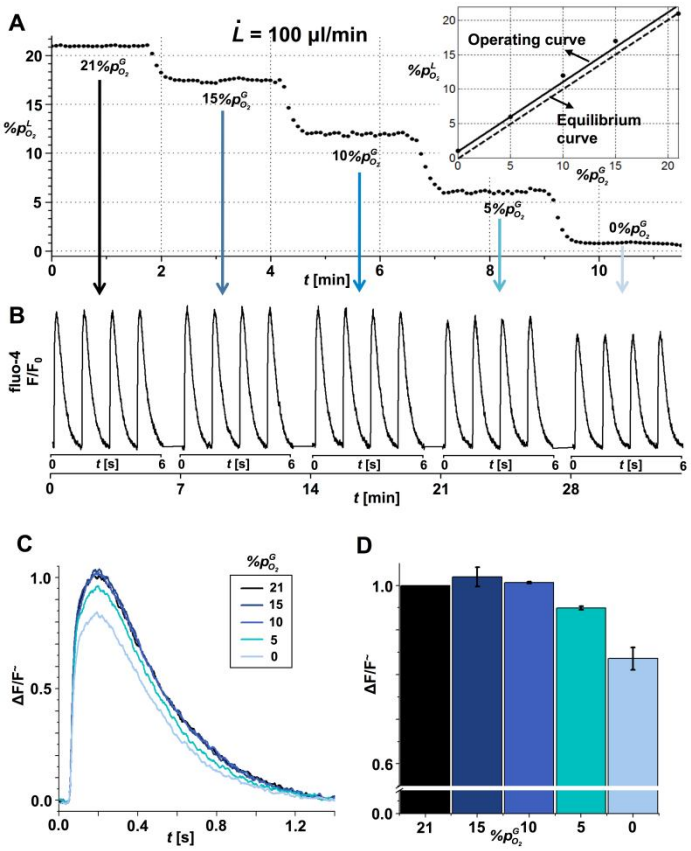

Figure 6. **Oxygen level threshold.** (A) $p^L_{O_2}$ profile for five different $p^G_{O_2}$ with $\dot{L}$ =100 µl min^{-1}. Insert shows equilibrium and operating curve obtained by calibration. (B) Calcium transients sequence at different $p^L_{O_2}$ measured 7 minutes after $p^G_{O_2}$ set-point change. Blue arrows show correspondence between $p^G_{O_2}$ set-point and calcium transient sequence (Fig. 5A). (C) Comparison of single normalized calcium transients at different oxygen partial pressure. (D) Averaged values of normalized calcium transients peak height at different oxygen partial pressure. The histogram is based on 5 replicates of same conditions.

Fig. 6B shows the corresponding sequence of calcium transients acquired for 6 s at different $p^L_{O_2}$ levels measured 7 minutes after the $p^G_{O_2}$ set-point change. Blue arrows show correspondence between $p^G_{O_2}$ set-point values and calcium transients. The baseline fluorescence maintained the same intensity for all the duration of the experiment and the effect of hypoxic stimulation emerged with a decrease of the maximum of the normalized calcium transient peak (Fig. 6C). The analyzed cells did not display calcium cycling alterations for $p^G_{O_2}$ > 5% (n=5). At 5% a poor significant difference (P<0.05, n=5) decrease was observed, whereas at $p^G_{O_2}$ = 0% the alteration of calcium transient was observed with high statistical relevance (P<0.01, n=5) (Fig. 6D). These data show that the observed effect reveals itself only in highly hypoxic nearly anoxic conditions, remaining latent at higher oxygen concentrations.

To test the reversibility of the hypoxia induced Ca^{2+} changes and, concurrently, exclude artifact deriving form long term confocal acquisition such as dye photo-

bleaching, the cardiomyocyte culture was subjected to a fast drop of $p_{O_2}^L$ and maintained in hypoxic conditions for 10 min followed by 10 min of reperfusion with normoxic medium (Fig. 7A).

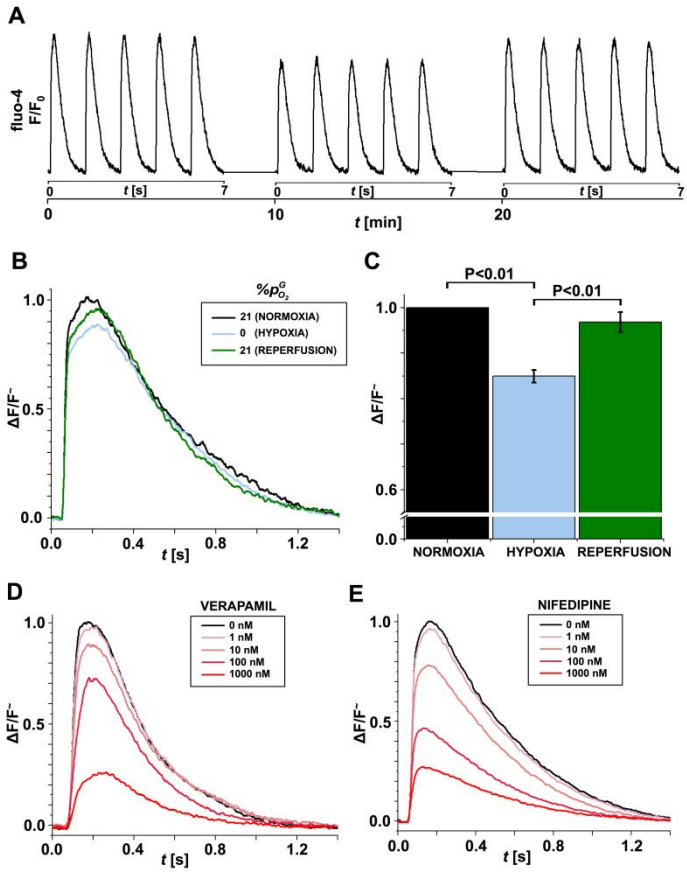

Figure 7. **Reversible effect of hypoxia on calcium cycling.** (A) Calcium transients sequence measured in normoxic, hypoxic ($p_{O_2}^G$ = 0%) and normoxic conditions. (B) Comparison of single normalized calcium transients in normoxic, hypoxic ($p_{O_2}^G$ = 0%) and normoxic condition. (C) Averaged values of normalized calcium transients peak height in normoxic, hypoxic ($p_{O_2}^G$ = 0%) and normoxic condition. The histogram is based on 5 replicates of same conditions. (D,E) Normalized calcium transients for different concentrations of L-type Ca^{2+} channel antagonist Verapamil (D) and Nifedipine (E).

Whole-cell calcium dynamics were acquired every 10 min. In response to hypoxic stress we observed a decrease of the maximum calcium transient peak (Fig. 7B) with no alteration of the baseline fluorescence (n=8). After recovering the normoxic conditions, the cardiomyocytes displayed again the same fluorescence intensity, indicating a recovery of calcium cycling towards basal conditions. By analyzing the variation of fluo-4 fluorescence after 10 minutes of hypoxia and subsequent 10 minutes of reperfusion by means of percentage decrease against normoxic fluorescence intensity, a statistically relevant decrease (~15%, P<0.01) emerged (Fig. 7C). The recovery of normal calcium transients after the return to normoxic conditions highlights the reversibility of the biological effect and excludes the responsibility of dye photo-bleaching from

the observed decrease of fluorescence.

All together, these results show that there is a significant reversible alteration of calcium homeostasis in excitation-contraction coupling during fast hypoxic stimuli. This experimental evidence underlines the ability of the cell to sense oxygen level and rapidly adapt to normoxic/hypoxic/normoxic transitions by regulating either directly or through secondary pathways the molecular machinery involved in cardiac Ca^{2+} homeostasis.[3] In addition to direct channel sensing or specifically target protein modification (such as phosphorylation and cysteine reduction), hypoxia may also alter the regulation of these channels via indirect bulk mechanisms, such as changes in cell redox state by action of ROS.[3] However, all these hypoxia-induced phenomena affect membrane depolarization and concurrently alter of L-type voltage-gated calcium channels (VGCC) function, which provide the main entry pathway for extracellular Ca^{2+} into cardiomyocytes and are a major component of excitation-contraction coupling machinery. L–type VGCCs trigger the calcium-induced calcium release (CICR) process through extracellular calcium influx; calcium entry through VGCCs, which are topologically associated to calcium-release channels (ryanodine receptors) in the sarcoplasmic reticulum (SR) membrane, cause further calcium SR release within cytosol compartment. These secondary calcium dynamics can be easily measured as reported in this study.

In this context, the alterations in excitation-contraction coupling under hypoxia could be related to impaired CICR for hypoxia-dependent desensitization of L-type VGCCs.

In order to explore this hypothesis, experimental investigation of calcium transients upon inhibition of the L-type Ca^{2+} channel with two antagonists was performed. Fig. 7D and 7E show normalized calcium transient at different concentrations of channel blocker ranging from 1 nm to 1000 nM in normoxic conditions. Similar calcium peak reductions recorded for hypoxia below 5% $p_{O_2}^{L}$ were observed with 100nM of Verapamil and 10 nM of Nifedipine Fig. 7D and Fig. 7E, respectively.

These findings confirm that a hypoxia-induced alteration of primary calcium entry through L-type VGCCs could turn in a reduced calcium concentration during excitation-contraction coupling and consequently, in an alteration of the physiological activity of cardiomyocytes.

Our results suggest that a cardioprotective mechanism during early phases of acute ischemia takes place through the reduction of calcium homeostasis in excitation-contraction coupling.

A reversible adaptation of myocardium after short ischemic stress (5 min and 15 min ischemia/reperfusion) *in vivo* was first observed by Heyndrickx and co-workers.[40] They demonstrated that a fully reversible dysfunction of the ischemic heart is prolonged after hypoxic stress, named “myocardial stunning”. The molecular basis behind this physiological behavior is still unclear. Myocardial stunning results from different adaptive mechanisms such as down-regulation of myocardial metabolism, and leads to activation of long-term cardioprotective responses including activation of cell survival pathways resulting in changes in

gene and protein expression.[41]

In this context, we first show that a fully reversible adaptive mechanisms of cardiopreservation might take place during the early events of ischemic stress through fast alteration in ion channel function in response to changes in cellular oxygen.

Conclusions

A microfluidic gas exchanger was designed to accurately and very quickly regulate $p_{O_2}^L$ without perturbing medium flux and consequently on line acquisition. By developing an *ad hoc* mass transfer theory, supported by computational simulations, we were able to predict $p_{O_2}^L$ inside cell culture chamber as a function of operative parameters (liquid flow rate). Experimental validation of $p_{O_2}^L$ profile inside the gas-exchanger microchannels confirmed that both constructive method and analytical model were valid.

With the support of the developed technological system we observed a significant calcium handling alteration in a neonatal rat cardiomyocyte population after an exposure to 5 min of hypoxic conditions. Thanks to accuracy in tuning oxygen level in our system we found a threshold value of 5% $p_{O_2}^L$, above which no significant calcium transients peak decreases were observed.

The recovery of normal calcium transients after the return to normoxic conditions highlights the reversibility of the biological effect and excludes the responsibility of sample damaging phenomena like dye photo-bleaching from the observed decrease of fluorescence.

We also explored the hypothesis that calcium-handling alteration in hypoxia could be affected by the desensitization of voltage gated calcium channels. In order to support our hypothesis we compared calcium transients peak obtained during a hypoxic stimulus and those obtained under effect of L-type calcium antagonist, Verapamil and Nifedipine.

Rational understanding of how the cardiomyocyte adapts to acute ischemic stress and sustains its survival represents an important challenge because it might help in finding novel strategies to enhance cardiomyocytes survival in patients.

References

1. S. Allender, C. Foster, L. Hutchinson and C. Arambepola, J. Urban Health, 2008, 85, 938–951.

2. R. J. Diaz and G. J. Wilson, Cardiovasc. Res., 2006, 70, 286–296.

3. L. A. Shimoda and J. Polak, Am. J. Physiol.: Cell Physiol., 2010, 300, C951–C967.

4. A. L. Russ, K. M. Haberstroh and A. E. Rundell, Exp. Mol. Pathol., 2007, 83, 143–159.

5. D. A. Saint, Br. J. Pharmacol., 2009, 153, 1133–1142.

6. Y. K. Ju, D. A. Saint and P. W. Gage, J. Physiol., 1996, 497, 337–347.

7. W. P. Wang, J. H. Ma, P. H. Zhang and A. T. Luo, Pfluegers Arch., 2007, 454, 461–475.

8. L. C. Hool, J. Physiol., 2004, 554, 743–754.

9. I. M. Fearon, A. C. V. Palmer, A. J. Balmforth, S. G. Ball, G. Mikala, A. Schwartz and C. Peers, J. Physiol. (London), 1997, 500, 551–556.
10. L. C. Hool, Circ. Res., 2000, 87, 1164–1171.
11. N. Gaur, Y. Rudy and L. Hool, Circ. Res., 2009, 105, 1196–1203.
12. I. M. Fearon, G. Varadi, S. Koch, I. Isaacsohn, S. G. Ball and C. Peers, Circ. Res., 2000, 87, 537–539.
13. S. Movafagh and M. Morad, Ann. N. Y. Acad. Sci., 2010, 1188, 153–158.
14. L. C. Hool, C. A. Di Maria, H. M. Viola and P. G. Arthur, Cardiovasc. Res., 2005, 67, 624–635.
15. T. J. Kamp and J. W. Hell, Circ. Res., 2000, 87, 1095–1102.
16. P. Kaplan, E. Babusikova, J. Lehotsky and D. Dobrota, Mol. Cell. Biochem., 2003, 248, 41-47.
17. L. Guerra, E. Cerbai, S. Gessi, P. A. Borea and A. Mugelli, Br. J. Pharmacol., 1996, 118, 1278–1284.
18. J. W. Allen and S. N. Bhatia, Biotechnol. Bioeng., 2002, 82, 253–262.
19. C. B. Allen, B. K. Schneider and C. W. White, Am. J. Physiol.: Lung Cell. Mol. Physiol., 2001, 281, L1021–L1027.
20. D. E. Powers, J. R. Millman, S. Bonner-Weir, M. J. Rappel and C. K. Colton, Biotechnol. Prog., 2010, 26, 805–818.
21. L. Kim, Y. Toh, J. Voldman and H. Yu, Lab Chip, 2007, 7, 681–694.
22. D. J. Beebe, G. A. Mensing and G. M. Walker, Annu. Rev. Biomed. Eng., 2002, 4, 261–286.
23. D. N. Breslauer, P. J. Lee and L. P. Lee, Mol. BioSyst., 2006, 2, 97–112.
24. Z. Y. Zhang, P. Boccazzi, H. G. Choi, G. Perozziello, A. J. Sinskey and K. F. Jensen, Lab Chip, 2006, 6, 906–913.
25. A. Groisman, C. Lobo, H. J. Cho, J. K. Campbell, Y. S. Dufour, A. M. Stevens and A. Levchenko, Nat. Methods, 2005, 2, 685–689.
26. E. Leclerc, Y. Sakay and T. Fujii, Biotechnol. Prog., 2004, 20, 750–755.
27. R. Gomez-Sjoberg, A. A. Leyrat, D. M. Pirone, C. S. Chen and S. R. Quake, Anal. Chem., 2007, 79, 8557–8563.
28. M. Polinkovsky, E. Gutierrez, A. Levchenko and A. Groisman, Lab Chip, 2009, 9, 1073–1084.
29. M. Adler, M. Polinkovsky, E. Gutierrez and A. Groisman, Lab Chip, 2010, 10, 388–391.
30. R. H. W. Lam, M. C. Kim and T. Thorsen, Anal. Chem., 2009, 81, 5918–5924.
31. S. C. Oppegard, K. H. Nam, J. R. Carr, S. C. Skaalure and T. Eddington, PLoS One, 2009, 4, e6891.
32. P. Abbyad, P. L. Tharaux, J. L. Martin, C. N. Baroud and A. Alexandrou, Lab Chip, 2010, 10, 2505–2512.
33. J. E. Baumgardner and C. M. Otto, Respir. Physiol. Neurobiol., 2003, 136, 131–139.
34. E. Figallo, C. Cannizzaro, S. Gerecht, J. A. Burdick, R. Langer, N. Elvassore and G. Vunjak-Novakovic, Lab Chip, 2007, 7, 710–719.
35. R. B. Bird, W. E. Stewart and E. N. Lightfoot, Transport Phenomena, 2nd edn, John Wiley & Sons, 2001.
36. A. P. Vollmer, R. F. Probstein, R. Gilbert and T. Thorsen, Lab Chip, 2005, 5, 1059–1066.
37. H. Shiku, T. Saito, C. C. Wu, T. Yasukawa, M. Yokoo, H. Abe, T. Matsue and H. Yamada, Chem. Lett., 2006, 234–235.
38. T. C. Merkel, V. I. Bondar, K. Nagai, B. D. Freeman and I. Pinnau, J. Polym. Sci., Part B: Polym. Phys., 1999, 38, 415–434.
39. S. A. M. van Stroe-Biezen, A. P. M. Janssen and L. J. J. Janssen, Anal. Chim. Acta, 1993, 280, 217–222.
40. G. R. Heyndrickx, R. W. Millard, R. J. McRitchie, P. R. Maroko and S. F. Vatner, J. Clin. Invest.,

1975, 56, 978–985.

41. C. Depre and S. F. Vatner, Heart Failure Rev., 2007, 12, 307–317.

Annex 3

Integrated multi-stage tissue on a chip generation from human pluripotent stem cells

Giovanni G. Giobbe[1,2,*], Federica Michielin[1,2,*], Sebastian Martewicz[1,2], Stefano Giulitti[1,2], Camilla Luni[1,2], Sirio Dupont[3], Annarosa Floreani[4], Nicola Elvassore[1,2]

[1] Department of Industrial Engineering (DII), University of Padova, Via Marzolo 9, 35131 Padova, Italy

[2] Venetian Institute of Molecular Medicine (VIMM), Via Orus 2, 35129 Padova, Italy

[3] Department of Molecular Medicine, University of Padova School of Medicine, Viale Colombo 3, 35131 Padova, Italy.

[4] Department of Surgery, Oncology and Gastroenterology (DiSCOG), University of Padova, Via Giustiniani 2, 35124 Padova, Italy

* These authors contributed equally to the work

Under final revision
Nature Methods
2015

Abstract

Micro-engineering human tissues and “organs-on-chips” remains an open challenge from both scientific and technological points of view. Here, we described a robust and efficient microfluidic-based approach for the differentiation of human pluripotent stem cells into functional cells. Specific frequency of periodic medium perfusion enhances the selectiveness of early germ layer differentiation and cell commitment through extrinsic signal microfluidic modulation. Human cardiomyocytes and hepatocytes generated on chip from human pluripotent stem cells through multi-stage approach show functional differentiation and proper response to drug pharmaco-kinetics, which opens a new perspective for multi-parametric and large scale human cell-based screening assays.

The development of human organs-on-chips, in which the microscale engineering technologies are combined with cultured human cells to recapitulate the whole living organ microenvironment, offers a unique opportunity to study human physiology and pathophysiology in an organ-specific context[1,2,3]. This technological perspective could provide an effective solution to the limitations of conventional cell culture models that fail to recapitulate complex, organ-level disease processes in humans and it could overcome the use of costly and time-consuming animal testing, which often shows poor predictive power of human biology and physiology. Moreover, the scientific community, the major pharmaceutical companies and the government agencies are recognizing the paramount importance of developing new technologies, which allow to perform cost-effective and multi-parametric assay for *ad hoc* studies in development, disease and pathogenesis, or for screening specific therapeutic strategies.

Recently, successful examples of organs-on-chips development have been provided[4,5,6,7], however, they were obtained from primary animal cells and, in few cases, from primary human cells. The possibility of developing direct organogenesis-on-chip from human pluripotent stem cells (hPSCs) could overcome the limited availability of human primary cells, such as human hepatocytes or cardiomyocytes. Human embryonic stem cells (hESCs) and induced pluripotent stem cells (hiPSCs) grown in culture have the potential to give rise to any fetal and adult cell type. Furthermore, they show intrinsic and unexpected levels of emergent self-organization for generating highly ordered structures and tissues[8,9,10], thus opening a wide perspective for multi-organ generation on a chip.

Biomimetic scale-down of multi-stage developmental process (from germ layer specification and phenotypic differentiation to tissue morphogenesis) could take advantage of the intrinsic properties of micro-technologies and microfluidics that allow accurate control of cell culture microenvironment, of temporal evolution of chemical gradients and of mechanical features, which support specific tissue differentiation[11,12,13]. Few studies reported on mouse embryonic stem cell cultures using microfluidic systems and highlighted the importance of accurate soluble microenvironment regulation to maintain pluripotency and self-renewal[14,15,16]. We reported for the first time on hESCs culture on a chip[17] and few other works dealt with hESCs modulating flow perfusion, mainly for maintaining pluripotency[18,19]. Integrated functional hPSCs differentiation on a chip, which certainly requires step-by-step control of hPSCs programming for resembling early stages of tissue morphogenesis, has not been developed yet.

Here, we explored whether we can control stem cell expansion, selective germ layer commitment and derivation of functional tissue-specific cells on a chip from both hESCs and hiPSCs through a multi-stage microfluidic-based technology. The different developmental stages required cell niche specification in terms of accurate balance between extrinsic and intrinsic cell signaling. The identification of the essential role of autocrine-paracrine factors in pluripotency, self-renewal, and germ layer commitment[20], suggests a synergic mechanism of specific extrinsic exogenous and endogenous factors in controlling transcriptional activity as schematized in **Fig. 1a**.

The extrinsic factors modulation requires an optimal *in vitro* delivery of exogenous factors and removal of endogenous cell-secreted factors, in principle either providing continuous perfusion or periodic delivery of medium change. However, continuous microfluidic flow perfusion generates soluble factors spatial gradients[14] and, consequently, heterogeneous up/downstream hESC culture conditions (**Fig. S1**). On the other hand, discontinuous periodic medium delivery allows proper factors supply, while avoiding up/downstream effects throughout the channels, in terms of colony size, cell density and pluripotency markers expression of both hESCs and hiPSCs (**Fig. S1 and S2**).

We hypothesized that a discontinuous periodic medium delivery with stage-dependent frequency (number of cycles of medium change per day) is an effective method for modulating soluble microenvironments and, consequently, stem cell niche specification *in vitro*, according to scheme in **Fig. 1a**. Intuitively, low frequencies allow endogenous factors accumulation within the channel. Conversely, high frequencies promote sustained exogenous factors supply, but lead to continuous wash-out of endogenous secreted factors. As also qualitatively described by a simplified computational model (see **Supplementary Methods** for model details and **Fig. S3**), the frequency of medium delivery, *f*, strongly impacts on the balance between extrinsic exogenous and endogenous factors (**Fig. 1b**).

Thus, we investigated the optimal frequency for both hESCs and hiPSCs expansion in microfluidic channels to maintain high stemness and homogeneous morphology among colonies at different regions along the channels. HPSCs were injected into multiple microfluidic platforms, each containing 10 independent channels and connected to a multi-port syringe pump (**Fig. 1c**), and cultured with different frequencies for up to 6 days (**Fig. 1d**). Both hESCs (hES2) and hiPSCs (ADHF#1) homogeneously express pluripotency markers such as OCT4, SOX2, TRA-1-60 and TRA-1-81, as revealed by immunofluorescence staining (**Fig. 1e**). A frequency-dependent expression level of pluripotency markers OCT4, NANOG and DNMT3B was observed in hES2 cells after 6 days of culture (**Fig. 1f**). Statistically significant differences were observed among frequencies for OCT4 and NANOG. Specifically, a significantly higher OCT4 expression was observed for f=2d^{-1}, compared to all other frequencies and continuous perfusion (CP), and a higher NANOG expression for f=2d^{-1}, compared to other frequencies and CP. DNMT3B results highly expressed for all the investigated frequecies and highly reduced only in f=1d^{-1}, f=4d^{-1}, f=8d^{-1} and CP. Overall this result shows that f=2d^{-1} is the optimal frequency for pluripotency maintenance, with OCT4, NANOG and DNMT3B expressions comparable to the standard static condition (Petri dish), used as positive control.

To further demonstrate that this optimal low-frequency culture conditions (f=2d^{-1}) is strongly related to an appropriate balance of exogenous molecules and endogenous cell-secreted factors, we designed an *ad hoc* experiment where HES2-conditioned medium collected in f=2d^{-1} experiment was used to culture HES2 cells at higher frequency. **Fig. 1g** shows statistically significant 3-fold increase in OCT4 expression when conditioned medium is used at f=8d^{-1} compared to fresh medium at the same frequency. Expression levels

comaparable with f=2d^{-1} were achieved, providing evidences that microfludic-conditioned media could potentially alter cell fate.

We first verified that this behavior is not strictly related to the medium alterations derived by nutrients depletion (glucose) and waste-products accumulation (ammonia and lactate) in microfluidic channels (**Fig. S4**). On the other hand, as TGFβ/Activin/Nodal pathway greatly contributes to pluripotency and self-renewal in hPSCs[21,22], we further investigated whether the observed frequency-dependent differences were correlated to the levels of endogenous TGFβ/Activin/Nodal ligands released by the cells into the conditioned medium. To quantify these factors we used a functional read-out, namely their ability to activate SMAD2/3 transcriptional activity, measured through the established synthetic CAGA12-luciferase reporter in HaCaT cells[23,24]. HES2 cells were first adapted to feeder-free culture conditions using defined Essential 8 (E8) medium; then, they were plated in microfluidic channels or in Petri dish and cultured in the absence of exogenous TGFβ1, by using E7 medium. Conditioned media were then collected from Petri dish and microfluidic channels in two different conditions, i.e. f=8d^{-1} and f=2d^{-1}, and used to treat HaCaT cells (**Fig. S5** and **Supplementary Methods**). As shown in **Fig. 1h**, conditioned medium with f=2d^{-1} contained higher levels of TGFβ ligands when compared to both f=8d^{-1} and static condition. In line with these results, the expression levels of NANOG, a known direct transcriptional target of SMAD2/3 in hESCs[25], was up-regulated in f=2d^{-1} conditions when compared to both lower frequency and static condition (**Fig. 1i**). Together, these data suggest that the endogenous TGBβ/Activin/Nodal ligands are released or accumulated in a frequency-dependent manner, thus promoting pluripotency.

We next investigated whether the frequency of periodic perfusion could also be used for directing early germ layer commitment according to microfluidic modulation of extrinsic endogenous and exogenous factors (**Fig. 2a**). HESCs were expanded for 3 days and differentiated for 4 days at different frequencies in spontaneous differentiation conditions (**Supplementary Methods**). Expression levels of early germ layers markers were analyzed through qRT-PCR analysis of β-III TUBULIN and OTX2 (ectoderm), BRACHYURY-T, GATA4 and αSMA (mesoderm), alpha-fetoprotein (AFP), EOMES and FOXA2 (endoderm). Under these conditions, static culture showed higher ectoderm but not mesoderm and endoderm marker expression. On the other hand, frequency-dependent germ layer commitment was observed in microfluidic culture. Ectoderm markers result highly expressed at lower frequencies (f=1d^{-1} and f=2d^{-1}) and completely down regulated at higher frequency (f=8d^{-1}), whereas mesoderm and endoderm expression are enhanced at higher frequency (f=8d^{-1}). We also showed that conditioned medium from f=1d^{-1} up-regulates OTX2 expression and down-regulates BRACHYURY-T when delivered at high frequency, i.e. f=8d^{-1} (**Supplementary Fig. S6**). These experimental observations are consistent with the hypothesis that high accumulation of extrinsic endogenous factors promotes ectoderm differentiation, while inhibiting meso-endoderm specification[14,20].

To verify whether an efficient and selective induction of the three germ layers could be achieved, hPSCs were induced to ectoderm, mesoderm and endoderm by specific differentiation media and with *ad hoc* frequency (**Fig. 2b**). Particularly, consistent with previous results, f=4d^{-1} was used for endoderm, f=3d^{-1} for mesoderm and f=1d^{-1} for ectoderm specification. Selective germ layers commitment was successfully obtained as reported by qRT-PCR analysis, which showed high expression of germ layer-specific genes for each differentiation protocol. Interestingly, endoderm is significantly more highly expressed in microfluidic condition compared to conventional static differentiation. As previously demonstrated for pluripotency maintenance, it seems that microfluidic environment effectively washed out endogenous factors, which could inhibit endoderm differentiation, and efficiently delivered exogenous pro-endoderm factors. Immunofluorescence analyses (**Fig. 2c**) confirmed that highly selective commitment for all germ layers, with low level of contaminations by other ones, can be achieved also at protein level in each specific differentiation protocol. Next, we examined if perfusion frequency can be further adjusted for optimizing germ layer microfluidic induction when specific differentiation protocols are used. As proof of concept, results in **Fig. 2d** show how selective induction of mesoderm was achieved by adjusting frequency of periodic perfusion. In particular, 3-fold higher BRACHYURY-T expression was observed at f=2-3d^{-1}, compared to f=1d^{-1} and almost null expression at f=12d^{-1}. High homogeneity within the channels was maintained also during hPSCs early commitment and differentiation (**Fig. S7**).

Collectively, our findings indicate that frequency of periodic perfusion is an additional parameter to enhance robustness and efficiency of early germ layer specification, also when specific protocols are adopted.

To further prove that microfluidic cell culture with periodic perfusion could potentially yield to greater efficacy than conventional protocols in Petri dish, we provided a screening of different media developed for endoderm specification. It is worth to underline that endoderm differentiation simultaneously requires large quantities of exogenous compounds (Activin-A) while washing out of endogenous inhibiting factors, which is almost unachievable in conventional Petri dish. As expected, intermittent perfusion with optimal frequency (f=4d^{-1}) yielded to significant higher cell viability (in 5 over 6 conditions) and to significant 3-fold increase in SOX17^{+}/FOXA2^{+} cells (in 3 over 6 conditions) compared to Petri dish culture (**Fig. S8**).

We then demonstrated how functional tissue-specific cell generation on chip could be achieved. We focused on cardiac and hepatic cells derived from mesoderm and endoderm germ layers, respectively, which are extremely relevant for tissue-on-a-chip applications. Cell differentiation was achieved by combining *ad hoc* hPSCs differentiation stages, germ layer specification and mature differentiation, with proper frequencies of periodic perfusion and chemical regulation of soluble microenvironment. Cardiac and hepatic differentiation protocols are described in **Supplementary Methods**.

First we showed how cardiac cells on chip were derived after 15 days of frequency-dependent multi-stage differentiation protocol (**Fig. 3a**), consisting on

Wnt-dependent mesoderm induction, early cardiac commitment (by Wnt inhibition) and functional cardiac maturation (by pro-cardiac factors supply). Typically 5 to 10 thousands cardiac cells per channel were obtained. We robustly achieved spontaneous contractile activity from both HES2 and ADHF#1-derived cardiomyocytes (**Supplementary Videos 1**, **2** and **3**), and 65.4 ± 11.9% of cardiac troponin-T positive cells showing defined cardiac sarcomeric organization (**Fig. 3b**). HPSC-derived cardiomyocytes show spontaneous calcium transients and excitation-contraction coupling. In the line scan magnification in **Fig. 3c** both calcium transients and spark-like spontaneous activity are presented. Analyzing calcium handling of hPSC-cardiomyocytes in microchannels, we observed cardiomyocyte functional response to 0.5 µM Verapamil with reduced calcium release after L-type channel inhibition, and response to 10 mM caffeine with cytosolic calcium increase after ryanodine channel activation. We successfully showed that it is possible to generate functional cardiac cells on chip and to directly perform dynamic biochemical stimulations taking advantage of the microfluidic environment, which allows robust, accurate, fast, and cost-effective spatio-temporal control of cell microenvironment[11].

We next applied our methodology to derive hepatocytes on chip, consistently with the previously endoderm-optimized conditions, which showed higher efficiency in endoderm differentiation than conventional cell culture ("+ B27 + NaB" medium in **Fig. S8**). Hepatic cells were robustly obtained from hESCs and hiPSCs by early endoderm commitment, definitive endoderm specification and hepatocyte-like cell maturation steps, driven by specific periodic medium delivery (**Fig. 3d**). Characteristic polygonal-shaped hepatocyte-like cells were obtained, with presence of bi-nucleate cells at the late stage, showing high expression of the specific hepatic markers albumin and cytochrome CYP450-3A (**Fig. 3e**). The hepatic cells show functional activity by high glycogen storage capacity (75.0 ± 7.5%) and indocyanine green uptake and clearance (**Fig. 3f**). Compared to static conditions, we obtained a shortening of the time required for differentiation (from 16d to 14d) and 40% greater albumin secretion rate on the last day of maturation (**Fig. 3g**). Similar results were obtained by applying our method to other hiPSC lines derived with non-integrating methods: SEN#1, derived with non-integrating Sendai viruses, mRNA#1 and mRNA#2, derived with mRNA technology (**Supplementary methods** and **Fig. S9**). An albumin production rate comparable with hESC-derived hepatocytes was obtained with the different hiPSC lines, confirming the robustness of the method. Quantification of immunofluorescence of late stage albumin and CYP450-3A in HES2 shows higher expression in microfluidic differentiated cells compared to static differentiation control (**Fig. 3h** and **Fig. S10**).

To prove how this system could be used for monitoring cell drug response and pharmacokinetics, we performed a series of experiments on hepatocyte drug cytotoxicity. Acetaminophen was chosen for its widely used applications, its fundamental hepatic metabolism and its toxicity on hepatic cells at high doses. A first experiment was performed on HepG2 cells exposed to different drug concentrations for 24h. Cell death caused by drug cytotoxicity was comparable between static control and microfluidic culture conditions (**Fig. S11 and**

Supplementary Methods). Higher cytotoxicity in microfluidic cells clearly correlated with nuclear area reduction, compared to lower correlation in the static control. Next, hESC-derived hepatocyte-like cells were exposed to acetaminophen in static culture, and at f=2d^{-1} in microfluidic culture for 24h (**Fig. 3i**). A 25 mM concentration of acetaminophen caused 75% of dead cells in micro-channels compared to 20% in the static control, although the overall amount of acetaminophen per cell was 10 times lower in microfluidics. This result is consistent with a higher level of differentiation of microfluidic hepatocyte-like cells which show well developed CYP450-3A-mediated drug metabolism[26] compared to less functionally cells differentiated in static condition (**Fig. 3h**). Drug cytotoxicity also affected cell morphology and membrane integrity. An acetaminophen concentration of 25 mM caused abnormal cell morphology (**Fig. S12**).

The tight temporal control of medium delivery achievable by microfluidic technology makes it particularly suitable to test not only drug concentration cytotoxicity but also different posologies of acetaminophen administration to hESC-derived hepatic cells in a 24 h timespan (**Fig. 3j**). Results show that, even at low dose, repeated drug administration (4 times per day for 3 h each) has a significantly higher cytotoxic impact than a one-shot at high dosage, regardless of the higher overall amount of drug in the single-administration case. This is consistent with literature data of serum alanine aminotransferase (ALT) elevation after repeated administration of low doses of acetaminophen in healthy young adults[27]. However, this chronic cytotoxic effect is not linearly dependent on drug concentration. Taken together, these results show that the microfluidic environment together with optimized periodic perfusion frequency provides an effective methodology for generating hepatic-like tissues on a chip with remarkable functional differentiation suitable for high-throughput drug testing in terms of drug concentration and posology.

In conclusion, we derived functional tissue-specific cells on a chip through a robust multi-stage microfluidic technology, which allows accurate spatio-temporal control of cell soluble microenvironment through regulation of periodic perfusion frequencies. Moreover, functionally differentiated cells derived in the microfluidic channels can be directly used for dynamic multi-parametric large-scale drug screening or for developing micro-engineered human organ models. This technology opens a new perspective in generating organs-on-chips from hPSCs overcoming the issues related to the limited availability of human primary cell sources. This last aspect will require strong scientific and technological efforts for further mimicking the organogenesis *in vitro*.

Methods

Computational Model

Mathematical model of signaling pathway, describing gene transcriptional activity promoted by synergic positive effect of extrinsic exogenous and endogenous factors is shown in **Fig. 1a**. The model takes into account only

relevant phenomena to highlight the effect of dynamic changes in extrinsic factors modulated by medium delivery frequency, *f*, on a hypothetic transcriptional activity. Black arrows in **Fig. 1a** indicate chemical reactions involved in the pathway. In particular, reactions (1) and (2) describe the coupling of exogenous, *Ex*, and endogenous, *En*, factors to specific membrane receptors, which promotes the activation of transcriptional factor, *Tr*. In addition, *Tr* is activated at a basal level through reaction (3) and induces expression of pluripotency-associated genes through reaction (4). Gene transcripts, *Gt*, in turn, produce newly *En*, as indicated by reaction (5). The model consists of four ordinary differential equations describing dynamic mass balance equation for the involved species *Ex*, *En*, *Tr* and *Gt*:

$$\begin{cases} \frac{d\tilde{c}_{Ex}}{dt} = \dot{N}_{Ex}^{IN} - \dot{N}_{Ex}^{OUT} - V_1 \\ \frac{d\tilde{c}_{En}}{dt} = -\dot{N}_{En}^{OUT} - V_2 + V_5 \\ \frac{d\tilde{c}_{Tf}}{dt} = V_1 V_2 + V_3 \\ \frac{d\tilde{c}_{Gt}}{dt} = V_4 - V_5 \end{cases} \quad (1)$$

c are concentrations of species involved in the pathway (*Ex*, *En*, *Tr* and *Gt)*; ~ symbol indicates adimensional concentration normalized for the initial concentration value c^0. *N* is the molar flux, given from the product between the medium flow rate and the concentration of each species, at the inlet and outlet of the microfluidic channel. Exogenous inlet flux is constant, as exogenous factors are continuously supplied with medium, whereas outlet fluxes are time-dependent. All chemical reaction rates are assumed first order kinetics as follows:

$$V_1 = k_1 \tilde{c}_{Ex}$$

$$V_2 = k_2 \tilde{c}_{En}$$

$$V_3 = k_3$$

(2)

$$V_4 = k_4 \tilde{c}_{Tf}$$

$$V_5 = k_5 \tilde{c}_{Gt},$$

where k_i are constant of reaction with arbitrary value and dimension [t^{-1}]. As an intermittent medium delivery is used, system of equations (1) can be solved throughout an interval time equivalent to the reciprocal of the frequency, 1/*f*, and for a defined number of cycles, N_{tot}. Consequently, null inlet and outlet fluxes and opportune initial periodic conditions were set. Time for medium change in the microfluidic channel was assumed negligible and periodic concentration values of *Ex* and *En* were set equal to 1 and 0 respectively after every time period (1/*f*). The system was solved for different values of *f* with periodic initial conditions written as follows:

$$\begin{cases} \dfrac{d\tilde{c}_{Ex}}{dt} = -k_1\tilde{c}_{Ex} & \tilde{c}_{Ex}(t=\dfrac{i}{f})=1 \\ \dfrac{d\tilde{c}_{En}}{dt} = -k_2\tilde{c}_{En}+k_5\tilde{c}_{Gt} & \tilde{c}_{En}(t=\dfrac{i}{f})=0 \\ \dfrac{d\tilde{c}_{Tf}}{dt} = k_1k_2\tilde{c}_{Ex}\tilde{c}_{En}+k_3 & \tilde{c}_{Tf}(t=0)=0.1 \\ \dfrac{d\tilde{c}_{Gt}}{dt} = k_4\tilde{c}_{Tf}-k_5\tilde{c}_{Gt} & \tilde{c}_{Gt}(t=0)=0.1 \\ & i=0,1,...,N \end{cases} \quad (3)$$

System of ordinary equations (3) was computationally solved with MATLAB, by using *ode15s function*. Constant rates k_1, k_2, k_4 and k_5 were arbitrarily set equal to 1, whereas k_3 was taken equal to 0.1. N_{tot} was chosen in order to achieve a pseudo-stationary of all species concentrations.

Microfluidic device fabrication and functionalization

Each microfluidic device, containing 10 independent channels 18 mm long and 1.5 mm wide, was fabricated by standard soft-lithographic techniques[9]. The master was photo-lithographically patterned through SU8-2100 negative photoresist (MicroChem, Newton, MA) to obtain a final thickness of 200 μm, according to manufacturer's indications. A premixed 10:1 ratio of polydimethylsiloxane, PDMS, pre-polymer and curing agent solution (Sylgard 184 kit; Dow Corning, Midland, MI) was casted on the silicon wafer and cured at 70 C° for 2 h. The PDMS mold was cut, peeled off, and punched with a 21G stainless steel needle (Small Part Inc., Logansport, IN) to obtain inlet/outlet holes. The PDMS mold was assembled and sealed to a 50×75 mm cleaned glass slide by plasma bonding. 10 independent medium reservoirs (with 70 μL capacity), one for each channel, were obtained by sealing an additional PDMS block to the top of the device by plasma bonding. The assembled device was cleaned with isopropanol (Sigma-Aldrich-Aldrich, St. Louis, MO) and sterilized in autoclave. Microfluidic channels were filled with 20% Matrigel Reduced Factor, MRF (BD) and incubated overnight at 4°C. Before cell seeding, protein solution was aspirated and microfluidic device was incubated at 37°C and 5% CO_2 atmosphere for 1 h.

Cellular reprogramming

Send#1 hiPSCs were derived through Sendai viruses-mediated reprogramming. Human fibroblasts derived from skin-biopsy were plated and cultured in a 24-well plate and cultured to 70% confluence in fibroblast medium (DMEM supplemented with 10% FBS). CytoTune iPS Sendai Reprogramming Kit (Life Technologies) based on replication incompetent Sendai virus was used to deliver the four transcription factors Oct4, Sox2, Klf4 and c-Myc and induce reprogramming to iPSc, according to manufacturer instructions. After 24h transduction, cells were fed every other day for 7 days. Transduced cells were then transferred onto inactivated MEF feeder cells at a density of 1 x 10^4 cells on a 6-well plate and expanded as reported below. mRNA#1 and mRNA#2 hiPSCs were generated through mRNA-mediated reprogramming following the protocol reported in Warren et al (2010)[10]. Briefly, inactivated human newborn foreskin

fibroblast feeders (NuFF-RQ, AMS Biotechnology) were seeded in 6-well tissue culture plates, coated with gelatin 0.2%, at a density of 260 cell/mm^2, and cultured in Dulbecco's modified Eagle medium (DMEM, Life Tecnologies) supplemented with 10% fetal bovine serum, FBS (Life Tecnologies). After 24 h, human foreskin BJ fibroblasts (Miltenyi Biotec) were seeded at 10 cell/mm^2 and cultured in Eagle's minimal essential medium (EMEM, Life Tecnologies) with 10% FBS. After another 24 h, medium was switched to Pluriton reprogramming medium (Miltenyi Biotec) supplemented with B18R interferon inhibitor (Prodotti Gianni) at a final concentration of 200 ng/mL, and transfections using mmRNA (Miltenyi Biotec) were started and repeated for 18 days, 4 hours prior to daily medium changes. The transfection mix was prepared pooling two solutions: the first obtained diluting 5X 100 ng/µL mmRNA of Oct4, Sox2, Klf4, c-Myc, Nanog, Lin28, and nuclear GFP in OptiMEM (Life Technologies), and the second diluting 10X lipofectamine RNAiMAX (Life Technologies) in Opti-MEM. After mixing, the final solution was incubated for 15 min and then added to the culture medium. At day 6 after the first transfection, Pluriton reprogramming medium was replaced with B18R-supplemented NuFF-conditioned Pluriton medium, which was produced culturing in parallel NuFF cells in T75 flasks with Pluriton medium supplemented with bFGF (Peprotech) at 4 ng/mL. Two days after the last transfection, iPS colonies were picked and passaged to MEF-coated 12-well plates and expanded as reported below.

HPSCs culture and integration in microfluidic devices

HiPSCs ADHF#1 (obtained from Center for iPS Cell Research and Application, iCeMS, Kyoto University), Send#1, mRNA#1 and mRNA#2 and hESCs HES2 (from National Stem Cell Bank, Madison, WI) were cultured in gelatin-coated multiwells with mitomycin C-treated mouse embryonic fibroblasts (MEF; Chemicon) co-culture, in DMEM F-12 (Life Technologies) supplemented with 20% KO serum (Life Technologies), 10% MEF conditioned medium (only for hES2), 20 ng/mL or 10 ng/mL of basic fibroblast growth factor, bFGF (Life Technologies) for hESCs and hiPSCs respectively, 0.1 mM β-mercaptoethanol (Life Technologies), 1% non-essential amino acid (Life Technologies) and 1% Pen/Strep (Life Technologies). HPSCs were passaged to new feeder using CTK solution (trypsin 0.25% - collagenase IV - Ca^{2+}) for hiPSCs or trypsin 0.25% for hESCs (Life Technologies). HES2 cells were also adapted in feeder-free culture conditions using Essential 8, E8, medium (Stemcell Technologies). Celle were cultured in 50% Matrigel Reduced Factor, MRF, coated multiwall plates and passaged through EDTA 0.5mM (Life Technologies). HPSCs were integrated within microfluidic devices by injecting cells suspension into each channel and incubating devices overnight at 37°C and 5% CO_2 atmosphere without perfusion, to allow cell adhesion. We used proper cell seeding concentration to achieve 70% confluence cell culture at 24 h after seeding. A 11-port pump (Cavro® XLP pump, TECAN, San Jose, CA) was used to independently deliver the medium from the reservoirs into each microfluidic channels. 0.5 ID Tygon tubings (Cole-Parmer, Vernon Hills, IL) and 21G stainless-steel needles with a polypropylene luer (Microtest, Taipei, Taiwan) were used to connect the microfluidic chip to the pump. Discontinuous medium delivery with defined temporal frequencies was achieved by automatically controlling the

multi-channel syringe pump through LabView 8.2 (National Instruments, Austin, TX). Every medium change was performed using a flowrate of 6 μL min^{-1} for 2 min, which corresponds to perfuse the twice the equivalent of channel volume. For pluripotency maintenance, hPSCs were cultured with f=2d^{-1}.

HPSCs differentiation into germ layers

For spontaneous differentiation, no exogenous factors and cytokines were used. Basal medium was composed of KnockOut DMEM, FBS 20%, NEAA 1%, L-glutamine 0,5% and P/S 1% (all from Life Technologies). Ectoderm differentiation was induced with DMEM F-12 and Neurobasal medium (both from Life Technologies), 1:1 ratio, supplemented with 1% B27 (Life Technologies), 1% N2 (Life Technologies) and β-met 0.1 mM[11,12]. Mesoderm differentiation was induced with StemPro-34 (Life Technologies) supplemented with 2 mM L-glutamine (Life Technologies), transferrin 200 ng/mL, 0.5 mM ascorbic acid (Sigma-Aldrich), Activin-A 0.3 ng/mL (R&D) and BMP-4 3 ng/mL (R&D)[13]. Endoderm differentiation was induced with RPMI1640 containing 1% B27 (both from Life Technologies), 1mM sodium butyrate, NaB (Sigma-Aldrich), 100 ng/ml Activin-A (Peprotech) and 50 ng/mL Wnt3a (R&D)[14] for the first 2 days. The second endoderm medium was KO DMEM with KO serum 20%, L-glutamine 1 mM, NEAA 1%, DMSO 1%, β-met 0.1 mM, P/S 1% for other 2 days. HPSCs specification was induced for 4 days in all three germ layers.

Cardiac and hepatic specification

For cardiac differentiation cells were cultured with in RPMI/B27 w/o insulin. After 24 h, the medium was changed to RPMI/B27 w/o insulin supplemented with 5 ng/mL BMP4 (R&D) for another 4 days. At day 5, the medium was changed to RPMI/B27 w/o insulin. At day 7 the cells were transferred to RPMI/B27 complete and cultured for other 10 days[15]. From day 12-15 cells start contracting spontaneously. Endoderm differentiation was induced with RPMI1640 containing 1X B27 (both from Life Technologies), 1 mM sodium butyrate (Sigma-Aldrich), 100 ng/ml ActivinA (Peprotech), 50 ng/mL (R&D) Wnt3a and 1% P/S for 1 day, then changed to the same medium with reduced 0.5 mM sodium butyrate for 2 days. Medium was changed to KO-DMEM, 20%SR (both from Life Technologies), 1 mM L-glutamine, 1% NEAA, 0.1 mM β-met, 1% DMSO (Sigma-Aldrich) and 1% P/S for 6 days. Hepatic-like cells were maturated with L15 medium (Sigma-Aldrich) supplemented with 8.3% FBS, 8.3% tryptose phosphate broth, 10 μM hydrocortisone 21-hemisuccinate, 1 μM insulin (all from Sigma-Aldrich) and 2 mM L-glutamine containing 10 ng/ml hepatocyte growth factor and 20 ng/ml oncostatin M (both from R&D) and 1% P/S for 6 days[6]. For adult specification and maturation, cells were cultured with f=2d^{-1} maturation medium change. The functional differentiation of cardiac and hepatic cells was performed in 30 and 50 independent microfluidic experiments, respectively.

HepG2 cell culture

HepG2 cells were cultured in 0.6% gelatin-coated glass slides in 24-well plates for static culture and gelatin-coated micro-channels for microfluidic culture. Cells were expanded in DMEM 88%, FBS heat inactivated 10%, NEAA 1% and P/S 1%.

Glucose and metabolites analysis

Media glucose concentration was measured with FreeStyle Lite glucometer and stripes (Abbott). Enzimatic detection of ammonia and L(+)-Lactate concentrations in exhaust media were performed through Ammonia assay kit (AA0100, Sigma-Aldrich) and Lactate assay kit (MAK064, Sigma-Aldrich), respectively, following manufacturer's instructions.

Functional tests

HPSCs-derived cardiomyocytes were analyzed at confocal microscopy (Leica SP5) for calcium transient during caffeine and verapamil treatments[16]. HPSCs-derived hepatocyte-like cells were stained with PAS staining (Sigma-Aldrich) according to manufacturer's instructions, for glycogen storage analysis. Indocyanine green test, ICG, (Sigma-Aldrich) was performed by incubating living cells for 15 min with dye solution, according to manufacturer's instructions. Green cells retaining ICG were photographed. After 6 hours, same fields were photographed in order to see complete clearance of ICG by functional hepatocyte-like cells. Albumin production and secretion was assessed by collection of spent medium (10 μL from each micro-channel) and performing enzyme linked immune-sorbent ELISA assay (Immunology Consultants Laboratory, Inc.) following manufacturer's instructions. Albumin levels were detected at 450 nm by using plate reader Infinite F2000 PRO (Tecan). Cytotoxicity experiments were performed using hepatotoxic acetaminophen drug, on HepG2 cells and hESC-derived hepatocyte-like cells. Acetaminophen BioXtra ≥99.0% (Sigma-Aldrich) was dissolved in DMSO to a 5 M starting solution. Following dilutions of 50, 25, 12.5, 10, 5, 1, 0.5 mM were done on HepG2 culture medium, and hepatic maturation medium for hepatocyte-like cells. As controls, untreated cells were cultured in their media, and control cells were treated with only DMSO 1% diluted in media. Cells were treated for 24h at $f=2d^{-1}$ or with multiple 3h administrations using a multiple-port microfluidic switch[17]. For nuclear area calculation, treated cells were fixed and stained with Hoechst, and fluorescence images were taken at 80X magnification. For cytotoxic effects on cell morphology and integrity, treated cells were fixed and stained with phalloidin for f-actin and albumin. Live and dead assay (Life Technologies) was performed on living cells after 24h, for dead cells quantification. Cell were washed with PBS and incubated with 4 μM ethidium homodimer-1 (stains red dead cells), 4 μM calcein AM (stains green live cells) and 4 μM Hoechst (stains blue cell nuclei) for 45 min at room temperature. Cells were then washed with PBS and analyzed at fluorescence microscopy. Cytotoxicity was expressed as fraction of dead cells over total cells per 20X image.

Luciferase assay

CAGA12 SMAD2/3 reporter HaCaT cell line were obtained form Stefano Piccolo's Lab (Department of Molecular Medicine, University of Padova) cultured in DMEM supplemented with 10% FBS[18,19]. For luciferase assay cells were plated in 12-well plates at 70% confluency and incubated overnight in DMEM without serum and then treated with media containing recombinant Tgfβ1 (Peprotech) or Tgfβ receptor inhibitor SB431542 (Peprotech) or to conditioned medium for 8 h. In the last case media were heat-treated for 5 min at 95°C. Luiferase expression

was detected as described in Inui et al.[19]. Data were normalized on total protein content, determined through Bradford assay.

Immunofluorescence

Immunofluorescence analyses were performed on paraformaldehyde 4% fixed cells for 15 min. Blocking and permeabilization was performed with 5% heat inactivated bovine fetal serum, TritonX-100 (Sigma-Aldrich) 0.1% for 1h. Cells were stained using primary antibodies in blocking buffer 1 h room T, or overnight 4°C, depending on the antibody: Oct4 1:200 (sc-5279 Santa Cruz), Sox-2 1:200 (AB5603 Millipore), Tra-1-60 1:200 (MAB4360 Millipore), Tra-1-81 1:200 (MAB4381 Millipore), β-III tubulin 1:500 (T3952 Sigma-Aldrich), α-fetoprotein 1:250 (A8452 Sigma-Aldrich), Brachyury 1:100 (ab20680 Abcam), cardiac troponin T 1:100 (MS-295-P Thermo Scientific), albumin 1:100 (MAB1455 R&D), CYP-3A 1:150 (GTX117120 Genetex), cytokeratin-18 1:150 (GTX105624S Genetex). For SOX17 (AF1924, R&D) and FOXA2/HNF3b (D56D6, Cell Sgnaling) staining, cells were incubated in 5% horse serum in 0.3% TritonX-100 blocking solution for 1h at room temperature. Primary antibodies were diluted 1:400 and 1:20 respectively and incubated in 1% BSA in 0.3% TritonX-100 overnight at 4°C. Immuno-staining was done with secondary antibodies Alexa Fluor 488, 594 (Life Technologies) and Cy3 (Jackson ImmunoLab) and DAPI nuclear staining incubation for 1 h at 37°C. Pictures were taken on Leica DMI 6000 B.

Gene expression analysis

For RNA extraction, cells were lysed with 0.5 mL of TRIzol (Life Technologies) per replicate and incubated with 0.1 mL of chloroform (Sigma-Aldrich) for 3 min. Cells were centrifuged at 12500 g for 15 min at 4°C. Aqueous supernatant was collected and diluted 1:1 with 70% ethanol. Total RNA was then extracted from solution using RNeasy Mini Kit (Qiagen), following manufacturer's instructions. RNA was quantified using NanoDrop spectrophotometer and quality for each extraction was assessed. RNA was used with A(260/280)nm = 2.0 $\pm$ 0.1, A(260/230)nm = 2.0 $\pm$ 0.1 and A(320)nm $\approx$ 0.05. RNA retro-transcription was performed using the High-Capacity cDNA Reverse Transcription Kit (Life Technologies), according to manufacturer's instructions. The qRT-PCR was performed with TaqMan gene expression assay probes (Life Technologies) according to manufactures instructions. Following genes were used: GAPDH (glyceraldehyde 3-phosphate dehydrogenase), POU5F1 (OCT4), NANOG (homeobox protein NANOG), DNMT3B (DNA cytosine-5-methyltransferase 3 beta), TUBB3 (beta-III tubulin), OTX2 (orthodenticle homeobox 2), T (BRACHYURY-T), GATA4, ACTA2 (alpha-smooth muscle actin), AFP (alpha-fetoprotein), EOMES, FOXA2 probe sets (all from TaqMan Life Technologies). Reactions were performed on ABI Prism 7000 machine and results were analyzed with ABI Prism 7000 SDS software. GAPDH expression was used to normalize Ct values of gene expression, and data were shown as relative fold change to control cells, using the delta-delta Ct method.

Statistical analysis

For statistical analyses, single pairwise comparisons were analyzed using Student's t-test with $P < 0.05$ (*) or $P < 0.01$ (**) indicating significance. Multiple

comparisons were performed by one-way ANOVA with Tukey post-test, with $P < 0.05$ (*) or $P < 0.01$ (**) indicating significance. The number *n* used throughout the text indicates the number of independent biological replicates, referred to experiments performed on different chips (with different passages of cells) and on different independent channels within the same chip (with same passages of cells).

Acknowledgements

This research was supported by Progetti di Eccellenza CARIPARO and Progetti di Eccellenza Giovani Ricercatori of Ministero della Salute. We acknowledge Miltenyi Biotec for kindly providing mmRNA reprogramming kit.

Author contribution

G.G.G., F.M. and N.E. designed the research; G.G.G. and F.M. performed the experiments; S.M. performed cardiac functional tests; S.G. helped in microfluidic platform set-up and microfluidic cell culture; S.G. and C.L performed reprogramming experiments; S.D. helped in TGFβ experiments; A.F. supervised hepatic differentiation experiments; N.E. coordinated the project; G.G.G., F.M. and N.E. wrote the manuscript.

References

1. Huh, D., Torisawa, Y., Hamilton, G. A., Kim, H. J. & Ingber, D. E. Microengineered physiological biomimicry: Organs-on-Chips. Lab. Chip 12, 2156–2164 (2012).
2. Huh, D. et al. A Human Disease Model of Drug Toxicity–Induced Pulmonary Edema in a Lung-on-a-Chip Microdevice. Sci. Transl. Med. 4, 159ra147–159ra147 (2012).
3. Ghaemmaghami, A. M., Hancock, M. J., Harrington, H., Kaji, H. & Khademhosseini, A. Biomimetic tissues on a chip for drug discovery. Drug Discov. Today 17, 173–181 (2012).
4. Huh, D. et al. Reconstituting organ-level lung functions on a chip. Science 328, 1662–1668 (2010).
5. Lee, S.-A. et al. Spheroid-based three-dimensional liver-on-a-chip to investigate hepatocyte–hepatic stellate cell interactions and flow effects. Lab. Chip (2013). doi:10.1039/C3LC50197C
6. Jang, K.-J. et al. Human kidney proximal tubule-on-a-chip for drug transport and nephrotoxicity assessment. Integr. Biol. Quant. Biosci. Nano Macro (2013). doi:10.1039/c3ib40049b
7. Grosberg, A., Alford, P. W., McCain, M. L. & Parker, K. K. Ensembles of engineered cardiac tissues for physiological and pharmacological study: Heart on a chip. Lab. Chip 11, 4165–4173 (2011).
8. Sasai, Y. Cytosystems dynamics in self-organization of tissue architecture. Nature 493, 318–326 (2013).
9. Eiraku, M. et al. Self-organizing optic-cup morphogenesis in three-dimensional culture. Nature 472, 51–56 (2011).
10. Eiraku, M. et al. Self-Organized Formation of Polarized Cortical Tissues from ESCs and Its Active Manipulation by Extrinsic Signals. Cell Stem Cell 3, 519–532 (2008).
11. Discher, D. E., Mooney, D. J. & Zandstra, P. W. Growth Factors, Matrices, and Forces Combine and Control Stem Cells. Science 324, 1673–1677 (2009).
12. Dupont, S. et al. Role of YAP/TAZ in mechanotransduction. Nature 474, 179–183 (2011).

13. Wan, C., Chung, S. & Kamm, R. D. Differentiation of Embryonic Stem Cells into Cardiomyocytes in a Compliant Microfluidic System. Ann. Biomed. Eng. 39, 1840–1847 (2011).

14. Przybyla, L. M. & Voldman, J. Attenuation of extrinsic signaling reveals the importance of matrix remodeling on maintenance of embryonic stem cell self-renewal. Proc. Natl. Acad. Sci. 109, 835–840 (2012).

15. Przybyla, L. & Voldman, J. Probing embryonic stem cell autocrine and paracrine signaling using microfluidics. Annu. Rev. Anal. Chem. Palo Alto Calif 5, 293–315 (2012).

16. Moledina, F. et al. Predictive microfluidic control of regulatory ligand trajectories in individual pluripotent cells. Proc. Natl. Acad. Sci. 109, 3264–3269 (2012).

17. Figallo, E. et al. Micro-bioreactor array for controlling cellular microenvironments. Lab. Chip 7, 710–719 (2007).

18. Korin, N., Bransky, A., Dinnar, U. & Levenberg, S. The culture of human embryonic stem cells in microchannel perfusion bioreactors. 64160N–64160N (2006). doi:10.1117/12.695558

19. Villa-Diaz, L. G. et al. Microfluidic culture of single human embryonic stem cell colonies. Lab. Chip 9, 1749 (2009).

20. Giobbe, G. G. et al. Confined 3D microenvironment regulates early differentiation in human pluripotent stem cells. Biotechnol. Bioeng. 109, 3119–3132 (2012).

21. James, D., Levine, A. J., Besser, D. & Hemmati-Brivanlou, A. TGFβ/activin/nodal signaling is necessary for the maintenance of pluripotency in human embryonic stem cells. Development 132, 1273–1282 (2005).

22. Singh, A. M. et al. Signaling Network Crosstalk in Human Pluripotent Cells: A Smad2/3-Regulated Switch that Controls the Balance between Self-Renewal and Differentiation. Cell Stem Cell 10, 312–326 (2012).

23. Inui, M. et al. USP15 is a deubiquitylating enzyme for receptor-activated SMADs. Nat. Cell Biol. 13, 1368–1375 (2011).

24. Levy, L. et al. Arkadia Activates Smad3/Smad4-Dependent Transcription by Triggering Signal-Induced SnoN Degradation. Mol. Cell. Biol. 27, 6068–6083 (2007).

25. Xu, R.-H. et al. NANOG is a direct target of TGFbeta/activin-mediated SMAD signaling in human ESCs. Cell Stem Cell 3, 196–206 (2008).

26. Manyike, P. T., Kharasch, E. D., Kalhorn, T. F. & Slattery, J. T. Contribution of CYP2E1 and CYP3A to acetaminophen reactive metabolite formation. Clin. Pharmacol. Ther. 67, 275–282 (2000).

27. Watkins, P. B. et al. Aminotransferase elevations in healthy adults receiving 4 grams of acetaminophen daily: a randomized controlled trial. JAMA J. Am. Med. Assoc. 296, 87–93 (2006).

28. Slager, H. G., Freund, E., Buiting, A. M. J., Feijen, A. & Mummery, C. L. Secretion of transforming growth factor-β isoforms by embryonic stem cells: Isoform and latency are dependent on direction of differentiation. J. Cell. Physiol. 156, 247–256 (1993).

Supplementary citations

1. Provin, C. & Fujii, T. Reaction-diffusion phenomena in a PDMS matrix can modify its topography. Lab. Chip 11, 2948–2954 (2011).

2. Brown, P. D., Wakefield, L. M., Levinson, A. D. & Sporn, M. B. Physicochemical activation of recombinant latent transforming growth factor-beta's 1, 2, and 3. Growth Factors Chur Switz. 3, 35–43 (1990).

3. Gleizes, P.-E. et al. TGF-β Latency: Biological Significance and Mechanisms of Activation. STEM CELLS 15, 190–197 (1997).

4. Slager, H. G., Freund, E., Buiting, A. M. J., Feijen, A. & Mummery, C. L. Secretion of transforming growth factor-β isoforms by embryonic stem cells: Isoform and latency are dependent on direction of differentiation. J. Cell. Physiol. 156, 247–256 (1993).

5. Lyons, R. M., Keski-Oja, J. & Moses, H. L. Proteolytic activation of latent transforming growth factor-beta from fibroblast-conditioned medium. J. Cell Biol. 106, 1659–1665 (1988).

6. Hay, D. C. et al. Efficient Differentiation of Hepatocytes from Human Embryonic Stem Cells Exhibiting Markers Recapitulating Liver Development In Vivo. STEM CELLS 26, 894–902 (2008).

7. Sui, L., Bouwens, L. & Mfopou, J. K. Signaling pathways during maintenance and definitive endoderm differentiation of embryonic stem cells. Int. J. Dev. Biol. 57, 1–12 (2013).

8. McLean, A. B. et al. Activin a efficiently specifies definitive endoderm from human embryonic stem cells only when phosphatidylinositol 3-kinase signaling is suppressed. Stem Cells Dayt. Ohio 25, 29–38 (2007).

9. Luni, C., Michielin, F., Barzon, L., Calabrò, V. & Elvassore, N. Stochastic Model-Assisted Development of Efficient Low-Dose Viral Transduction in Microfluidics. Biophys. J. 104, 934–942 (2013).

10. Warren, L. et al. Highly Efficient Reprogramming to Pluripotency and Directed Differentiation of Human Cells with Synthetic Modified mRNA. Cell Stem Cell 7, 618–630 (2010).

11. Chambers, S. M. et al. Highly efficient neural conversion of human ES and iPS cells by dual inhibition of SMAD signaling. Nat. Biotechnol. 27, 275–280 (2009).

12. Camnasio, S. et al. The first reported generation of several induced pluripotent stem cell lines from homozygous and heterozygous Huntington's disease patients demonstrates mutation related enhanced lysosomal activity. Neurobiol. Dis. 46, 41–51 (2012).

13. Kouskoff, V., Lacaud, G., Schwantz, S., Fehling, H. J. & Keller, G. Sequential development of hematopoietic and cardiac mesoderm during embryonic stem cell differentiation. Proc. Natl. Acad. Sci. U. S. A. 102, 13170–13175 (2005).

14. Hay, D. C. et al. Highly efficient differentiation of hESCs to functional hepatic endoderm requires ActivinA and Wnt3a signaling. Proc. Natl. Acad. Sci. U. S. A. 105, 12301–12306 (2008).

15. Lian, X. et al. Robust cardiomyocyte differentiation from human pluripotent stem cells via temporal modulation of canonical Wnt signaling. Proc. Natl. Acad. Sci. 109, E1848–E1857 (2012).

16. Martewicz, S. et al. Reversible alteration of calcium dynamics in cardiomyocytes during acute hypoxia transient in a microfluidic platform. Integr. Biol. Quant. Biosci. Nano Macro 4, 153–164 (2012).

17. Zambon, A., Zoso, A., Luni, C., Frommer, W. B. & Elvassore, N. Determination of glucose flux in live myoblasts by microfluidic nanosensing and mathematical modeling. Integr. Biol. Quant. Biosci. Nano Macro 6, 277–288 (2014).

18. Levy, L. et al. Arkadia Activates Smad3/Smad4-Dependent Transcription by Triggering Signal-Induced SnoN Degradation. Mol. Cell. Biol. 27, 6068–6083 (2007).

19. Inui, M. et al. USP15 is a deubiquitylating enzyme for receptor-activated SMADs. Nat. Cell Biol. 13, 1368–1375 (2011).

Main figures

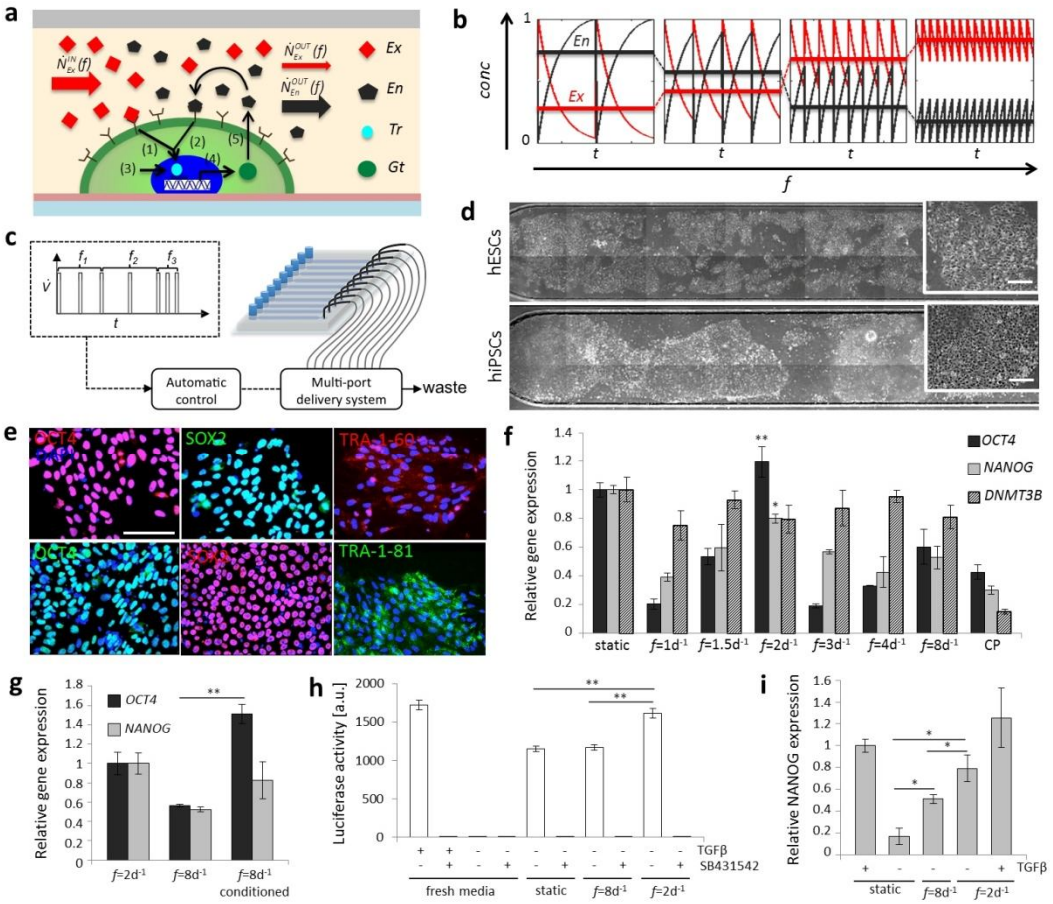

Figure 1 | Culture of human pluripotent stem cell on a chip. (**a**) Hypothetic pluripotency-aasociated signaling model in microfluidic stem cell culture. Both exogenous (*Ex*) and endogenous (*En*) factors, with frequency-dependent concentration, contribute to transcriptional activity of pluripotency genes through activation of target transcription factors (*Tr*). Black arrows indicate chemical reactions involved in the pathway. Reactions (1) and (2) describe the coupling of exogenous, *Ex*, and endogenous, *En*, factors to specific membrane receptors, which promote the activation of transcriptional factor, *Tr*. *Tr* is also activated at a basal level through reaction (3) and induces expression of pluripotency-associated genes through reaction (4). Gene transcripts, *Gt*, produce newly *En*, as indicated by reaction (5). (**b**) Temporal profiles of normalized *Ex* and *En* factors concentrations in the microfluidic channel at increasing frequencies. Low frequencies promote endogenous factors accumulation and depletion of exogenous factors, compared to higher frequencies, which allow sustained exogenous factors supply, but continuous endogenous factors wash out, leading to different level of mean concentration values over time (straight lines). (**c**) Experimental set-up. Medium delivery in microfluidic platform is controlled by a multi-port delivery system with 10 independent operating channels and 1 single discharge channel. Flow rate, frequency of medium delivery, temporal delay between cycles and total number of cycles are set independently in every channel and automatically controlled through Labview software. (**d**) HESCs and hiPSCs were integrated within microfluidic channels and expanded up to 6 days with f=2d^{-1}. Insets show maintenance of typical stem cells colonies morphology. Scale bar 100 μm. (**e**) HESCs and hiPSCs immunofluorescence analysis of pluripotency markers OCT4, SOX2, TRA-1-60 and TRA-1-81 after 6 days in microfluidic channels. Scale bar 50 μm. (**f**) Frequency-dependent qRT-PCR analysis of pluripotency markers OCT4, NANOG and DNMT3B expression after 6 days of hES2 cells culture. An optimal frequency of 2d^{-1} has been observed, which allows the highest OCT4, NANOG and DNMT3B expression levels comparable to standard static conditions. Data are normalized on GAPDH expression. A statistical higher OCT4 expression for

f=2d^{-1}, compared to all other frequencies and continuous perfusion (CP), and NANOG expression for f=2d^{-1}, compared to f=1d^{-1} f=4d^{-1} f=8d^{-1}, and CP, was observed. Data are shown as mean ± s.e. (n=6). ((**g**) HES2 cells were first seeded in microfluidic channels and cultured with f=2d^{-1}. Exhaust medium was collected from at least 4 micro-channels (8μL per channel) every 12h for 5 days and stored at 4°C. This conditioned medium was subsequently used to culture HES2 cells with f=8d^{-1}. HES2 cells cultured in non-optimal frequency conditions, i.e. f=8d^{-1}, with conditioned medium (f=8d^{-1} conditioned) collected from HES2 cutured in optimal condition (f=2d^{-1}) display a significant 3-fold OCT4 expression increase and a higher but not significant NANOG expression increase compared to cells cultured with fresh medium (f=8d^{-1}). Data are normalized on GAPDH expression. Data are shown as mean ± s.e. (n=6) (**h**) Luciferase assay based on the CAGA12 SMAD2/3 reporter HaCaT cell line. HES2 cells were adapted in feeder-free culture conditions using defined Essential 8 (E8) medium, plated in microfluidic channels or in Petri dish and cultured in E7 medium, which has the same composition of E8 medium but without addition of exogenous recombinant TGFβ1. Conditioned media were collected from Petri dish and microfluidic culture in two different conditions, i.e. f=8d^{-1} and f=2d^{-1}, and heat-treated to induce latent TGFβ activation[28]. The amount of the TGFβ/Activin/Nodal ligands was indirectly quantified by exposing CAGA12-luciferase HaCaT cells to the collected media. f=2d^{-1} medium contained higher amounts of TGFβ ligands compared to both f=8d^{-1} and Petri dish. Fresh E8 and E7 media (with no TGFβ1) were used as positive and negative controls. Addition of the small-molecule TGFβ receptor inhibitor SB431542 confirms that the inductions are caused by extracellular factors in the medium. Data are normalized on total protein content, determined through Bradford assay. See Supplementary Fig. S3 for controls of the heat-activation procedure. Data are shown as mean ± s.e. (n=6). (**i**) QRT-PCR analysis of NANOG expression of hES2 cells cultured in feeder-free conditions with E8 medium or E7 medium (in absence of TGFβ) in microfluidic channels and in Petri dish. Compared to standard conditions a significant higher NANOG expression was achieved in microfluidic culture compared to static conditions and by using f=2d^{-1} compared to f=8d^{-1}. NANOG expression in f=2d^{-1} conditions using E8 medium confirmed the result shown in Fig. 1f, in which standard non-defined medium was used. Data are shown as mean ± s.e. (n=6).

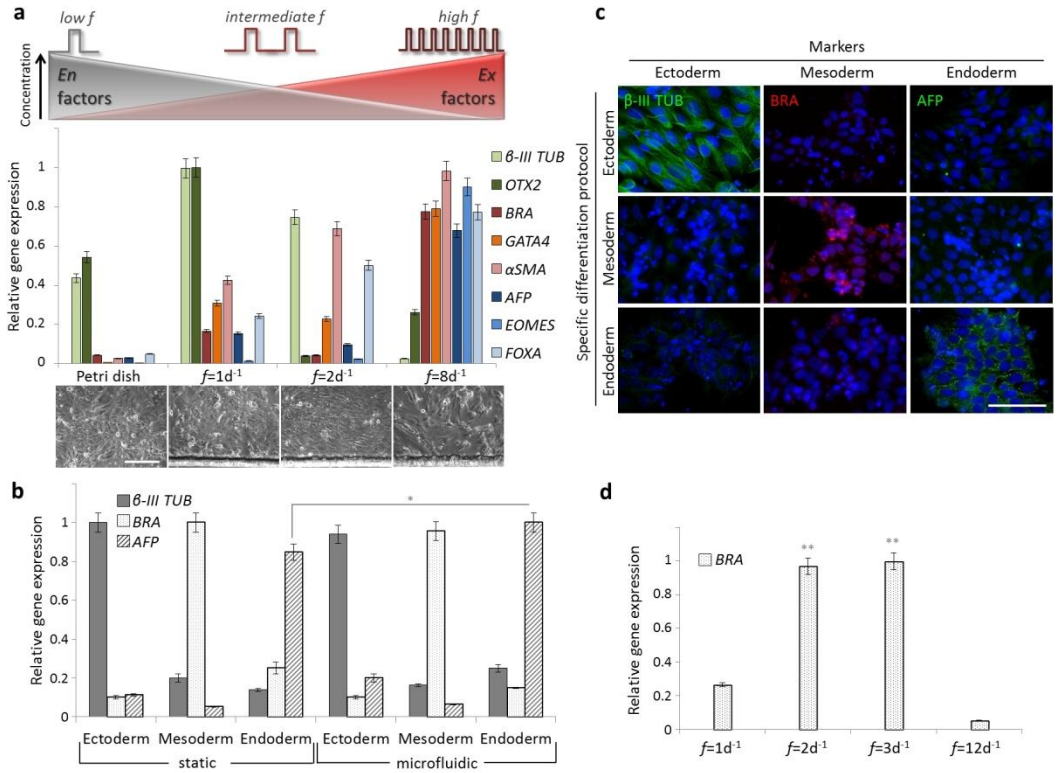

Figure 2 | Early germ layer induction of hESC on-a-chip. (**a**) Frequency-dependent differentiation. Schematic of frequency, *f*, relation to *En* and *Ex* factors balance (up). The qRT-PCR analysis (gene expression normalized on GAPDH) of β-III tubulin and OTX2 for ectoderm, brachyury T, GATA4 and alpha-smooth muscle actin for mesoderm, alpha-fetoprotein, EOMES and FOXA2 for endoderm in hESC spontaneous differentiation on chip, under different *f*. Cell morphology in phase contrast for each differentiation condition. Scale bar 50 µm. Data are shown as mean ± s.d. (*n*=6). (**b**) Early germ layer induction with specific media. QRT-PCR analysis of β-III tubulin, BRACHYURY-T and AFP, and comparison between standard static control and microfluidic condition. Data are shown as mean ± s.d. (*n*=6). (**c**) Specific differentiation markers expression. Differentiation protocols applied on hESC line cultured on micro-channels. Immunofluorescence analysis of each differentiation protocol, with expression of β-III tubulin in ectoderm, BRACHYURY-T in mesoderm and AFP in endoderm. Scale bar 50 µm. (**d**) Mesoderm microfluidic optimization. QRT-PCR analysis of BRACHYRY-T expression at different frequencies of medium change for germ layer commitment optimization. BRACHYRY-T expression is comparable between f=2d^{-1} and f=3d^{-1}, while there is a significantly lower expression at higher and lower frequencies. Data are shown as mean ± s.d. (*n*=6).

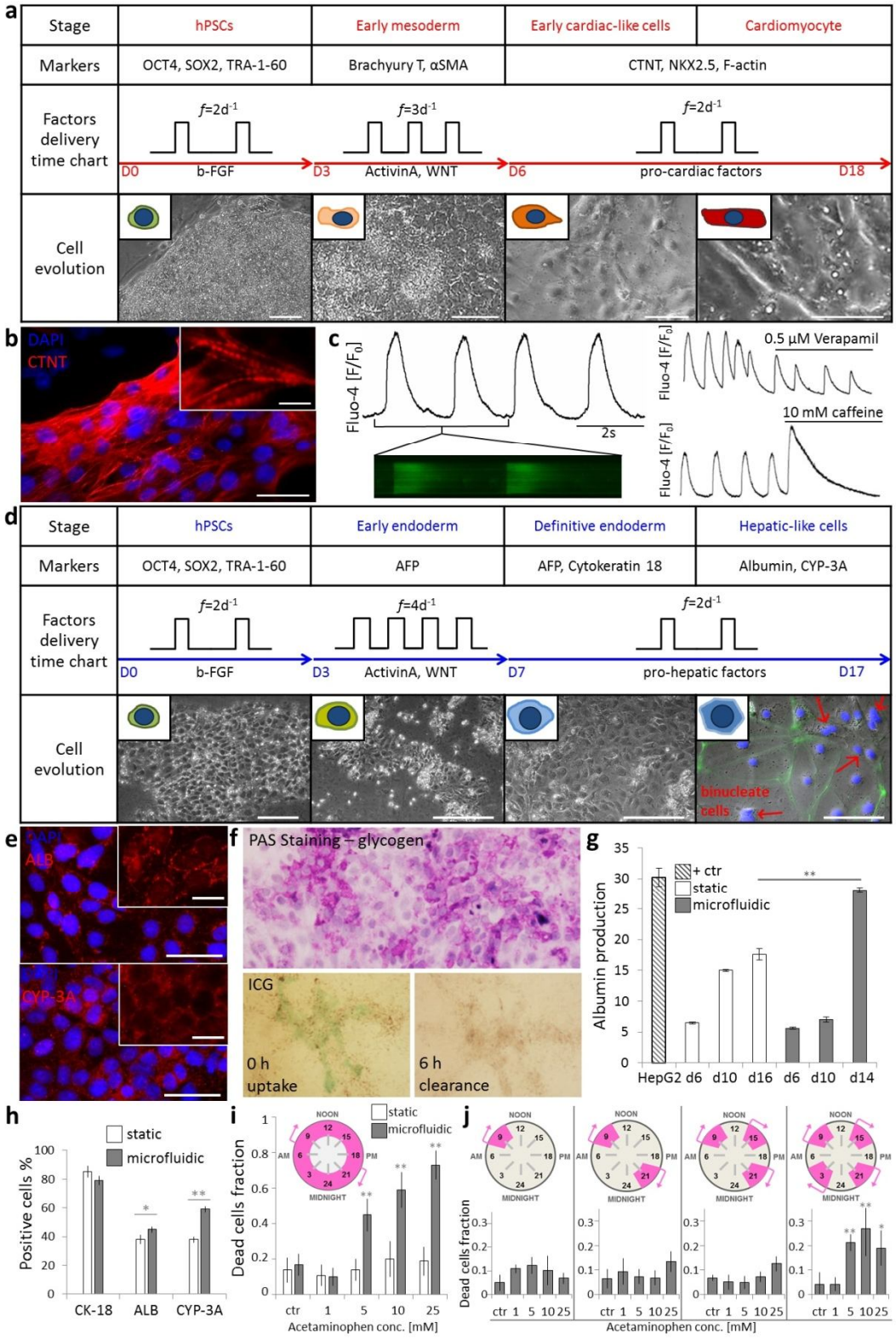

Figure 3 | Cardiac and hepatic functional differentiation on-a-chip. (**a**) Microfluidic cardiomyocyte differentiation protocol and morphology changes from pluripotent state to differentiated cell type. Scale bars 200 μm. (**b**) Immunofluorescence of hES-derived CM showing cardiac troponin T organization (scale bars 20 μm). CTNT positive cells immunofluorescence quantification results in 65.4 ± 11.9% (s.d. n=6). (**c**) Microfluidic calcium dynamics. Spontaneous calcium transients in hESC-cardiomyocytes recorded with Fluo-4 indicator. Functional cardiomyocytes response to 0.5

μM verapamil with reduction in calcium release, and to 10 mM caffeine with increase in cytosolic calcium. (**d**) Hepatic differentiation protocol and cell change in morphology up to hepatocyte-like cells. Red arrows indicate bi-nucleated cells in late stages. Scale bars 200 μm. (**e**) Immunofluorescence stain for hepatocyte-like markers albumin and cytochrome P450-3A. Scale bars 20 μm. (**f**) Periodic acid-Schiff stain of hepatic cells derived on chip; nuclei are stained in blue, pink-violet colored cells show glycogen storage. Indocyanine green staining (ICG) of live hepatic cells. Colorant is absorbed and metabolized in 6 h by functional hepatocyte-like cells. (**g**) ELISA albumin secretion quantification [ng/mL/day/2x10^5 cells]. Microfluidic-derived hepatocyte-like cells secrete 40% more albumin, than in static control at the last day of differentiation. Data are shown as mean ± s.d. (*n*=6). (**h**) Quantification of immunofluorescence markers. Microfluidic hepatic cells show significant higher expression of ALB and CYP-3A compared to static control. Data are shown as mean ± s.d. (*n*=10). (**i**) Concentration-dependent cytotoxicity of acetaminophen in hepatocyte-like cells. Higher degree of maturation is shown by microfluidic-cultured cells, which respond linearly to drug concentration compared to static culture, when exposed to constant 24 h treatment at f=2d^{-1}. Data are shown as mean ± s.d. (*n*=6). (**j**) Microfluidics allows multiple administrations in the 24 h for dose-dependent cytotoxicity of acetaminophen in hepatic cultures. Four administrations per day result in higher concentration-dependent cytotoxicity compared to reduced (3, 2, 1) administrations. According to 2-way ANOVA test, group 4 results significantly different from the other 3 groups (P<0.01). In group 4, data at 5, 10 and 25 mM are significantly different from control and 1 mM. Data are shown as mean ± s.d. (*n*=6).

Supplementary figures

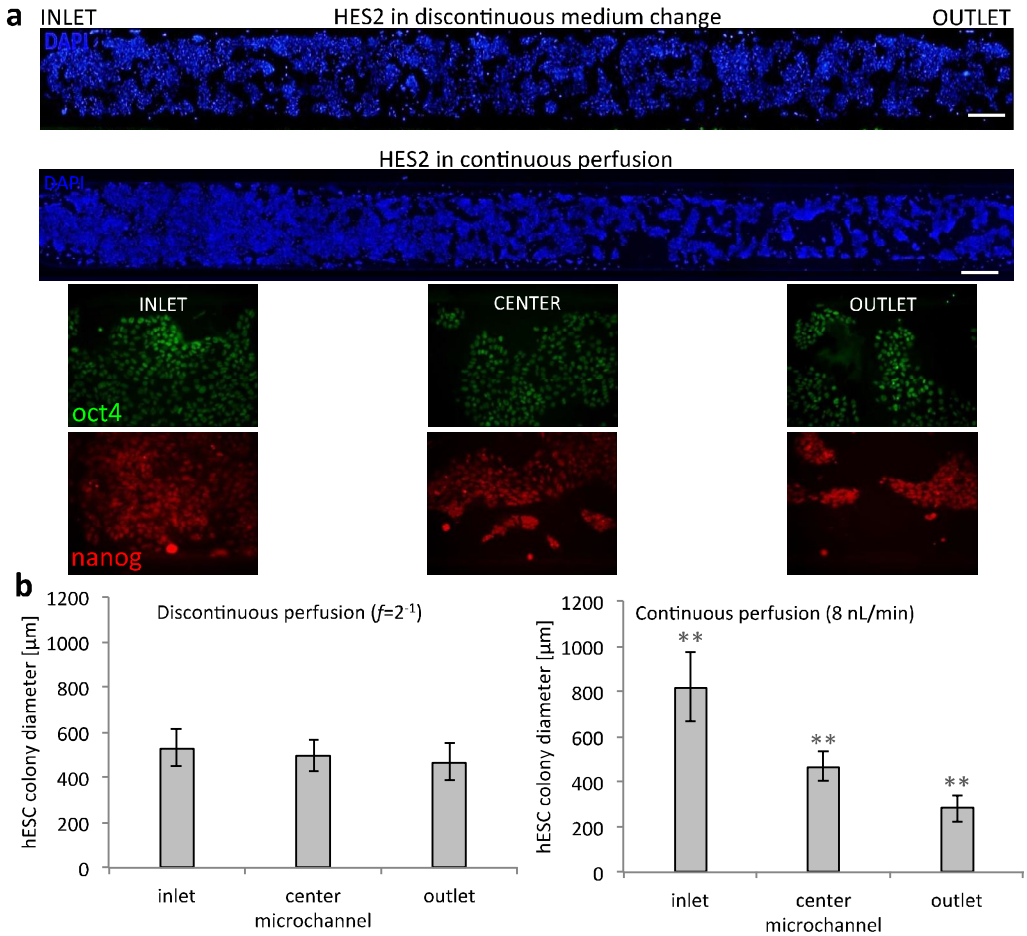

Fig. S1 | Discontinuous vs. continuous perfusion culture in microfluidic channel. (**a**) Cell colonies morphology and nuclei distribution of hES2 cells cultured with continuous perfusion (flowrate 8nL/min) and discontinuous flow (f=2d^{-1}) for 72h. In order to make a fair comparison between

the two conditions, we used in both experiments the same overall amount of medium (12µL per day). By using continuous perfusion, HES2 cell line shows OCT4 and NANOG expression, but high inhomogeneity of cell growth is present along the channel, with higher growth at the inlet compared to the outlet. Scale bars 100 µm. (**b**) Graphs showing measurement of HES2 colonies diameters at inlet, center and outlet of micro-channels, after continuous perfusion and discontinuous medium change for 72 h. Colonies in continuous perfusion show high inhomogeneity, with statistically significant differences between each paired conditions. Data are shown as mean ± s.d. (n=12).

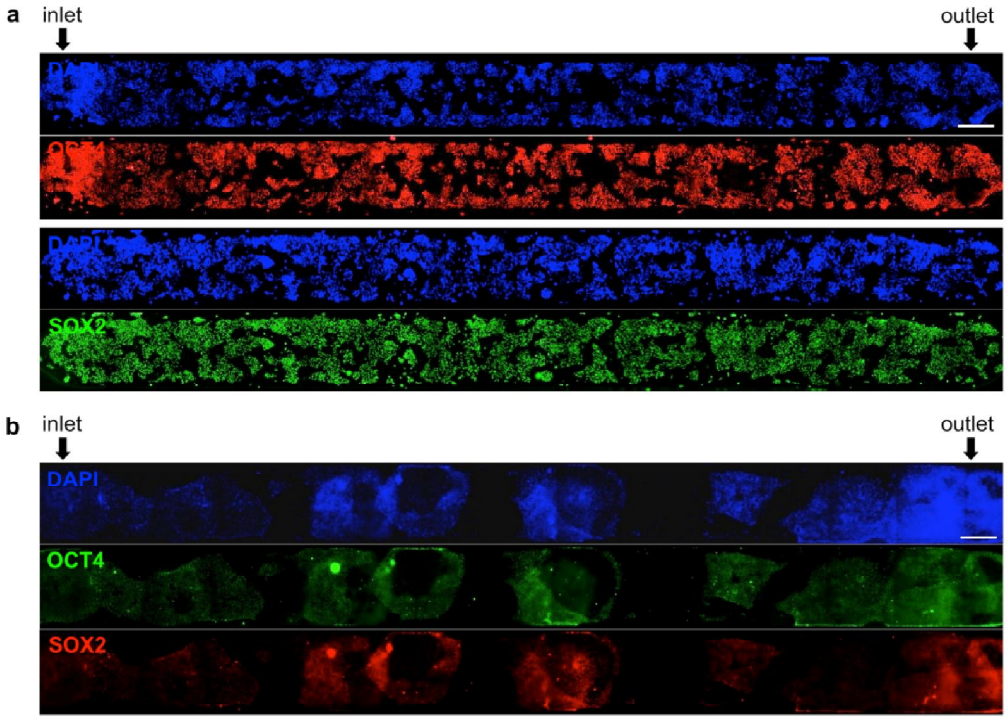

Fig. S2 | Pluripotency marker expression in human pluripotent stem cells cultured in micro-channels with f=2d^{-1}. (**a**) HES2 cells showing OCT4 and SOX2 expression. (**b**) ADHF#1 hiPS cell line showing OCT4 and SOX2 expression. High homogeneity in markers expression is shown along the micro-channels with no upstream and downstream effects (quantitative analysis of OCT4 and SOX2 mean fluorescence intensity between inlet and outlet show differences smaller than 10%). Scale bars 100 µm.

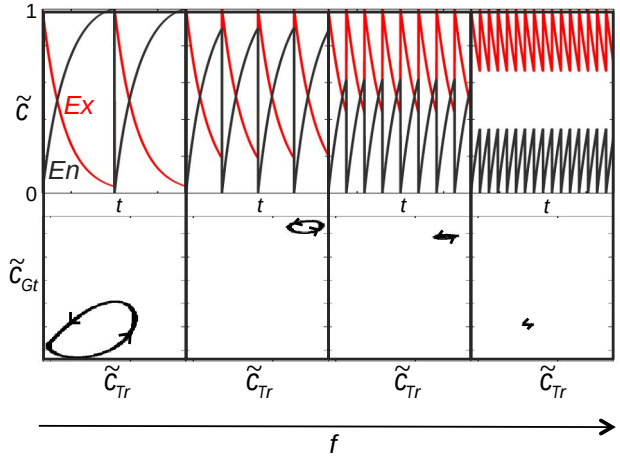

Fig. S3 | Signaling model output. Temporal profiles of normalized *Ex* and *En* factor concentrations in the microfluidic channel at increasing frequencies (top). Gene transcript (*Gt*) concentration profile plotted versus corresponding Transcription factor (*Tr*) variation during a single medium perfusion at increasing frequencies. C tilde represents normalized concentration.

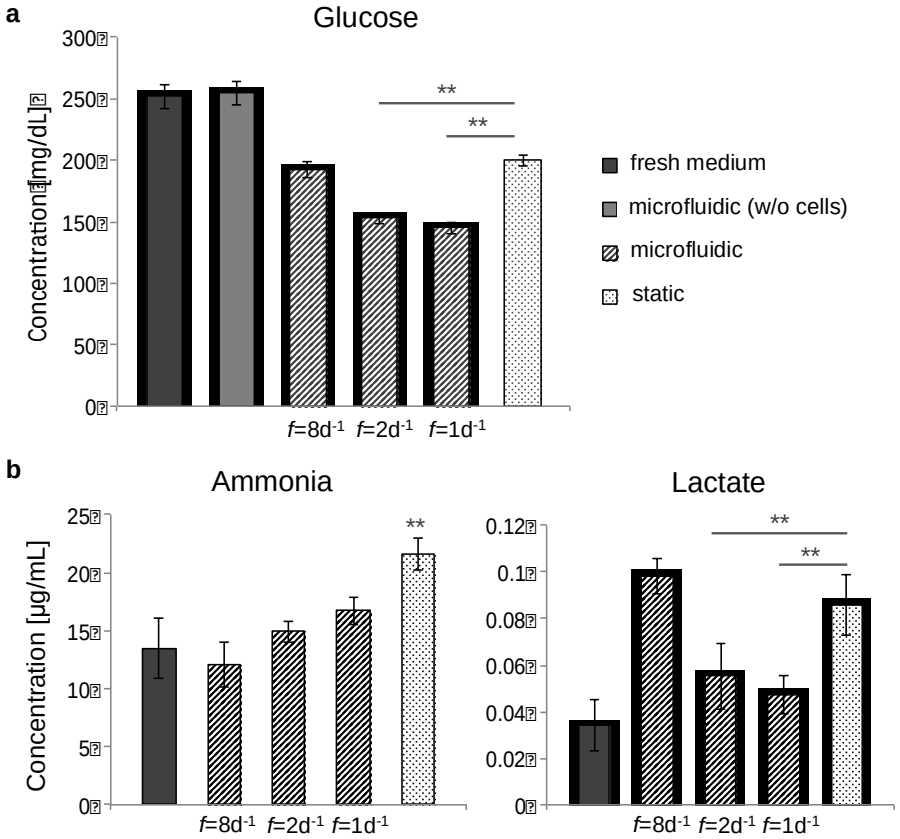

Fig. S4 | Glucose and metabolites (ammonia and lactate) analyses of conditioned media collected from hESCs cultured in microfluidic channels, compared to static culture in Petri dish. HES2 cells were plated into microfluidic platforms and in standard Petri dish with same cell density and cultured up to 5 days. Conditioned media were sampled from Petri dish after 24h every day and from microfluidic channels after every perfusion cycle. Specifically, 8 μL exhaust medium were collected from each channel every 3, 12 or 24h corresponding to f=8, 2, 1d^{-1} for 5 days from cells seeding. Fresh medium was used as positive (for glucose) or negative (for ammonia and lactate) control. (**a**) Glucose concentration of medium inside a microfluidic channel (with no cells seeded) is equivalent to fresh medium. Glucose concentration of medium in microfluidic channel collected at the end of the cycle of perfusion is reported for three different frequencies of medium change. Interestingly only a 25% statistical decrease of glucose concentration was observed for low frequencies f=2d^{-1} and f=1d^{-1}, compared to standard condition in Petri Dish. (**b**) Ammonia and lactate concentrations result equal or lower than those measured in static culture for every condition analyzed. Surprisingly, ammonia concentration (left) results statistically lower in media collected from micro-channels than that collected in static condition. This is probably due to the high ammonia diffusion through in PDMS[1], which causes ammonia depletion from micro-channels. Lactate concentration (right) in exhaust medium of micro-channels is comparable or lower than the one observed in standard Petri dish. Data are shown as mean ± s.d. (n=6).

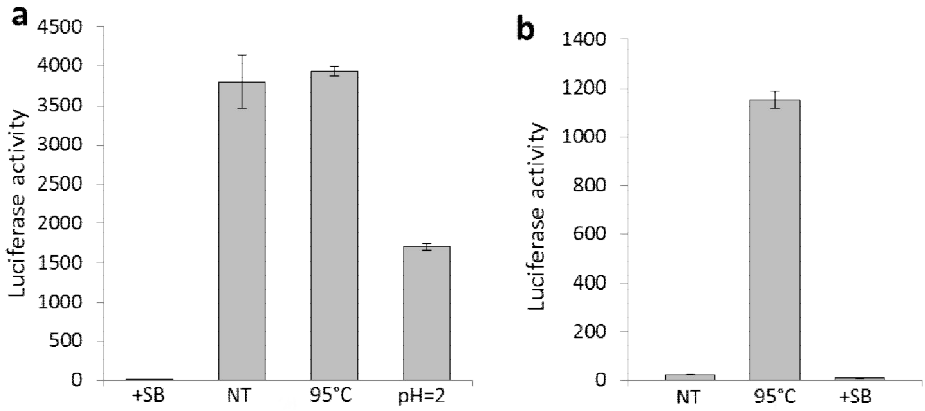

Fig. S5 | Determination of the optimal conditions to detect Tgfβ ligands present in conditioned media. Tgfβ ligands are secreted from cells in a latent form that is not able to bind and activate Tgfβ receptors. To measure its biological activity, it is thus necessary to release Tgfβ ligands from the latency-associated peptide (LAP), either by heat treatment or medium acidification[2,3,4,5]. (**a**) We first checked which method was less detrimental for the activity of recombinant Tgfβ1 (i.e. of the ligand in absence of LAP), by using active recombinant Tgfβ1 (1ng/mL), either untreated (NT) or treated (95°C or acid pH). Media were then added to HaCaT cells bearing the stable SMAD2/3 CAGA12-luciferase reporter. Addition of the Tgfβ receptor inhibitor SB431542 (10μM, +SB) to untreated medium sets the reporter background in absence of any SMAD activation. Acid treatment was detrimental for exogenous recombinant Tgfβ activity and excluded from further analyses. (**b**) E7 medium without exogenous Tgfβ1 was conditioned by hES2 cells, cultured in standard Petri Dish in feeder-free conditions, and used to treat HaCaT CAGA12-luciferase cells for 8h. Untreated conditioned medium (E7) was barely active; heat-treatment of the same medium (95°C) instead released latent Tgfβ ligands and caused a strong activation of the SMAD2/3 reporter; addition of the Tgfβ receptor inhibitor to the heat-activated medium (+SB) ensures that luciferase activation depends on extracellular factors. Data are normalized on total protein content, determined through Bradford assay. Data are shown as mean ± s.d. (n=3).

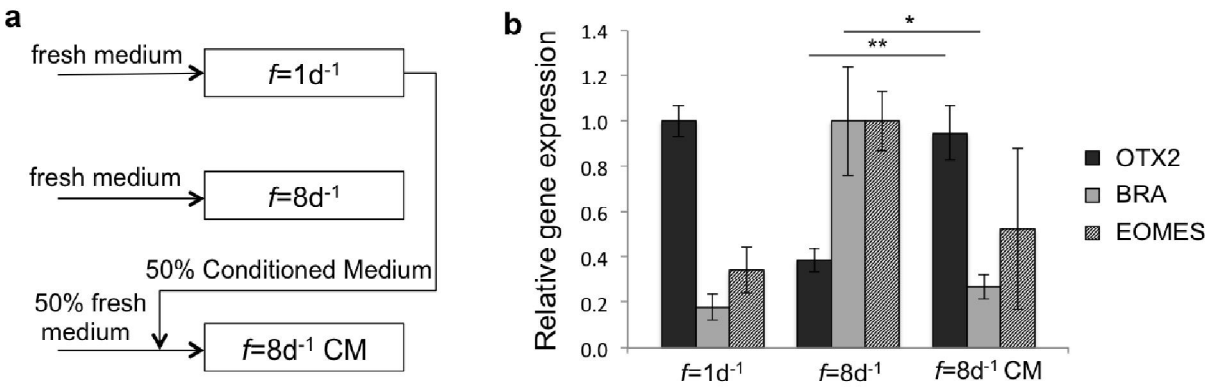

Fig. S6 | Germ layer specification with conditioned media in microfluidics. (**a**) Experimental design. HES2 cells were plated in microfluidic chips, cultured for 3 days and induced to differentiate into early germ-layers under spontaneous differentiation conditions for 4 days as reported in experiment of **Fig.2a**. During spontaneous differentiation, fresh medium was perfused with f=1d^{-1} and f=8d^{-1}. Conditioned medium was collected from the f=1d^{-1} experiment, diluted with 1:1 ratio with fresh medium and used to differentiate same cells with f=8d^{-1} as schematically shown. (**b**) Expression of representative genes for each germ layer (OTX2 for ectoderm, BRACHYURY-T and EOMES for meso-endoderm) measured through realtime PCR analysis. Consistently with data reported in **Fig.2a**, OTX2 results more expressed at low frequency. Conversely, higher frequency promotes BRACHYURY-T and EOMES markers

expression. By using conditioned medium, a significant 2.5-fold OTX2 expression increase and a 3-fold BRACHYURY-T decrease were observed. These data support the hypothesis that conditioned medium containing higher accumulation of cell-secreted endogenous factors induces cell fate switch between ectoderm and meso-endoderm commitment even at high frequency. Data are shown as mean ± s.e. (n=6).

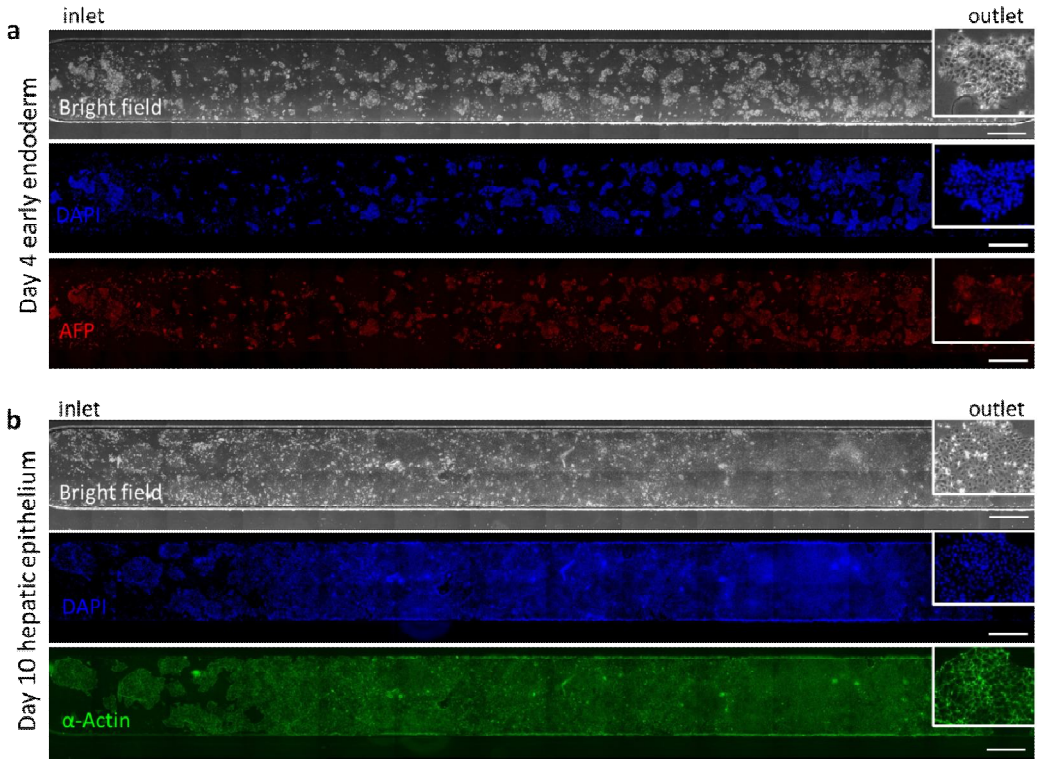

Fig. S7 | Cell homogeneity during differentiation in endodermal differentiating hESCs. (**a**) Differentiation at f=4d^{-1} in micro-channels at day 4 of early endoderm. Cells show high and homogenous expression of alpha-fetoprotein (quantitative analysis of AFP mean fluorescence intensity between inlet and outlet show differences smaller than 15%, which is within experimental variability). (**b**) Day 10 of definitive endoderm commitment. Cells show polygonal epithelial shape at day 10 along microfluidic channel, and homogenous cell distribution. Scale bars 100 µm.

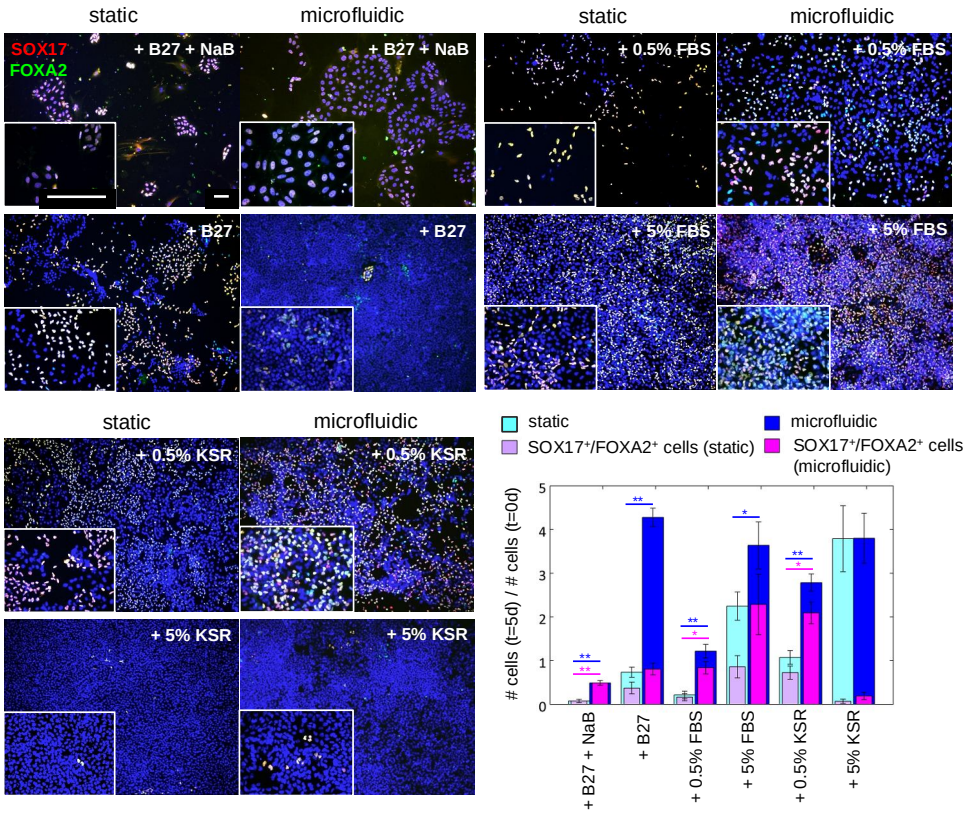

Fig. S8 | Endoderm differentiation in static vs. microfluidic culture condition. HES2 cells were seeded in 24-well plates or microfluidic channels and induced to differentiate into endoderm after 3 days. Six different differentiation protocols were tested in order to demonstrate possible advantages of microfluidic environment in terms of cells vitality (final number of cells/initial number of cells) and efficiency of 5-days endoderm specification. Basal medium for endoderm commitment contain high concentration of Activin-A (100ng/mL) and Wnt3a (50ng/mL) for the first 2 days and Activin-A (100ng/mL) for the following 3 days. A frequency of $4d^{-1}$ was used for microfluidic differentiation. Different basal medium supplementations include B27-supplement, FBS (not chemically defined) and KSR at two different concentrations, i.e. 0.5 and 5%. Efficiency of endoderm specification after 5 days was determined by double immuno-staining with endoderm-specific markers SOX17 and FOXA2. B27-supplement with sodium buthyrate (NaB) was previously used for specific endoderm commitment (**Fig.2c**), ensuring high efficiency near 100% both in static and microfluidic condition. However, addition of NaB, which is recognized to promote homogeneous hepatocyte differentiation and, if combined with Activin-A, an efficient definitive endoderm commitment[6], causes dramatic cell death upon treatment both in static and microfluidic condition, whereas NaB removal allows increased cell survival and reduced efficiency. Nevertheless, a statistical significant 4-fold increase of $SOX17^+/FOXA2^+$ cells was observed in microfluidic channels compared to standard Petri dish. Low concentration FBS-supplemented medium is widely employed for endoderm commitment, as higher concentrations inhibit endoderm commitment, even though promoting cell survival[7]. Consistently, increasing FBS concentration promotes cell survival and proliferation, whereas reducing efficiency in static condition. Surprisingly, intermittent perfusion allows increased proliferation compared to Petri dish and efficiency comparable with that obtained in low serum condition. Particularly, a significant 4-fold increase of $SOX17^+/FOXA2^+$ cells in microfluidic compared to static condition was observed, when 0.5% FBS supplementation is used. Knock out serum replacement (KSR) is also recognized to inhibit hESCs differentiation and promote self-renewal, by means of PI3K signaling activation[8]. Again, a significant 3-fold increase of $SOX17^+/FOXA2^+$ cells in microfluidic compared to static condition was observed, with 0.5% KSR supplementation. No significant

differences were observed with higher concentration of KSR. Scale bars 100μm. Data are shown as mean ± s.e. (n=6).

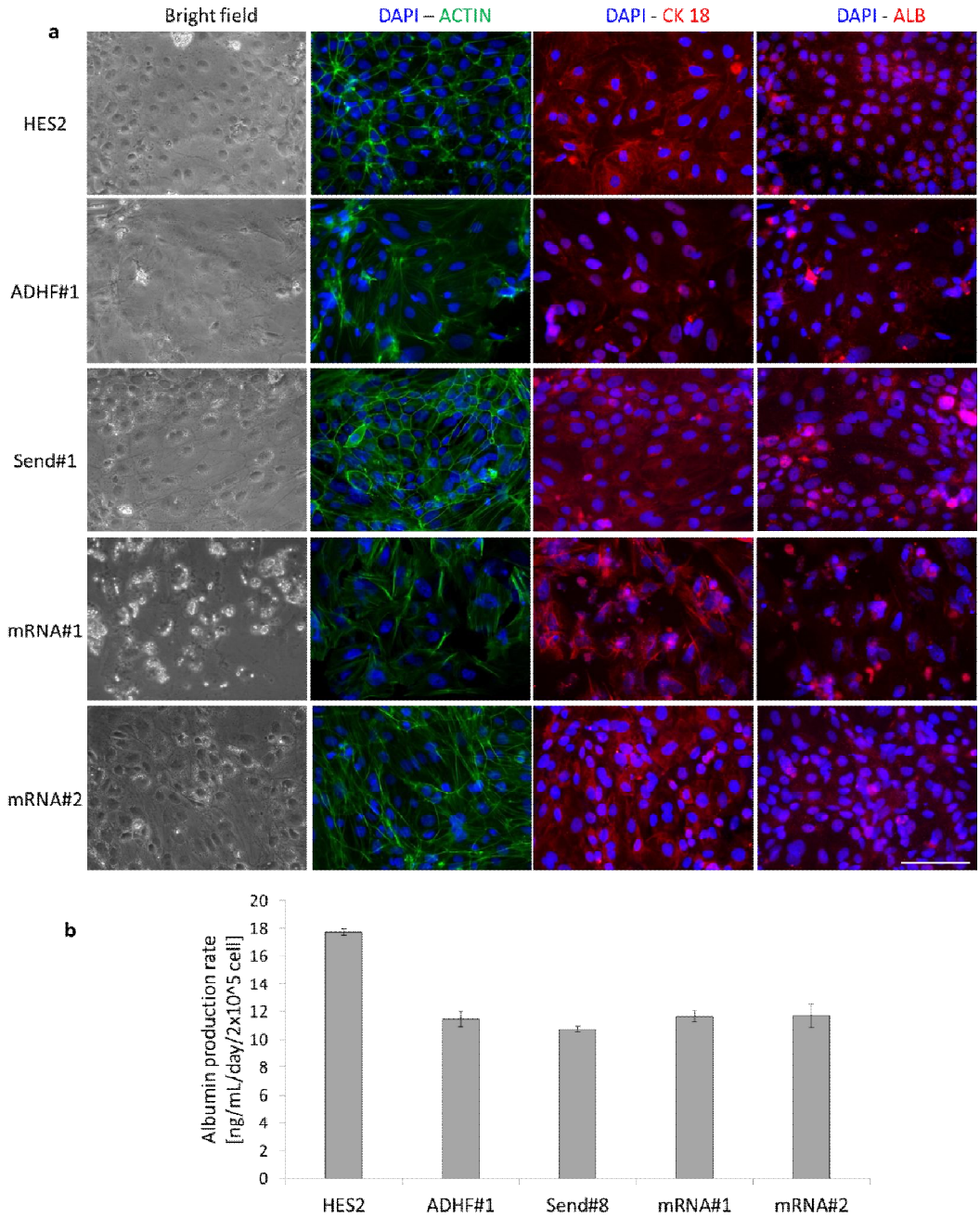

Fig. S9 | Comparison between different cell lines differentiated in hepatocyte-like cell through microfluidic technology. (**a**) Immunofluorescence panel shows cell morphology in bright field and F-ACTIN (green) staining, and hepatic markers (red) CYTOKERATIN-18 and ALBUMIN. Differentiated cell lines are HES2 (human embryonic stem cell line) and human induced pluripotent stem cell lines ADHF#1 (adenovirus-derived), Send#1 (Sendai virus-derived), mRNA#1-2 (modified mRNAs-derived). (**b**) Graph shows ELISA quantification of secreted human albumin for the different cell lines at day 16 of differentiation. Scale bar 75 μm. Data are shown as mean ± s.d. (n=6).

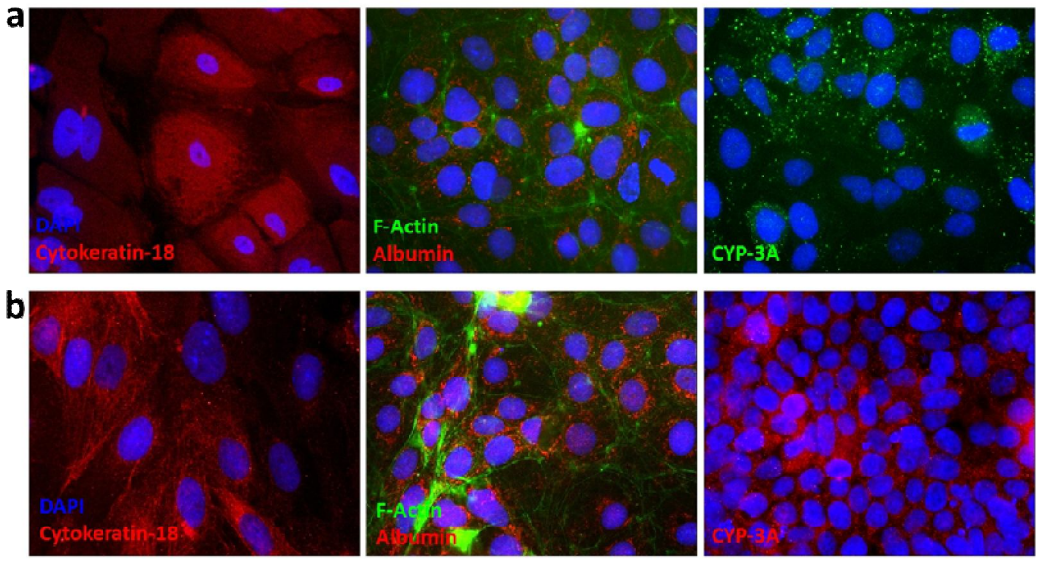

Fig. S10 | Comparison between standard static (**a**) and microfluidic (**b**) hepatocyte-like cells. HESC-derived hepatocyte-like cells differentiated in standard Petri dish condition cells show similar expression of CK-18 hepatic endoderm marker compared to microfluidic condition. Microfluidic hepatocyte-like cells show higher expression of albumin and CYP-3A compared to standard static differentiated cells.

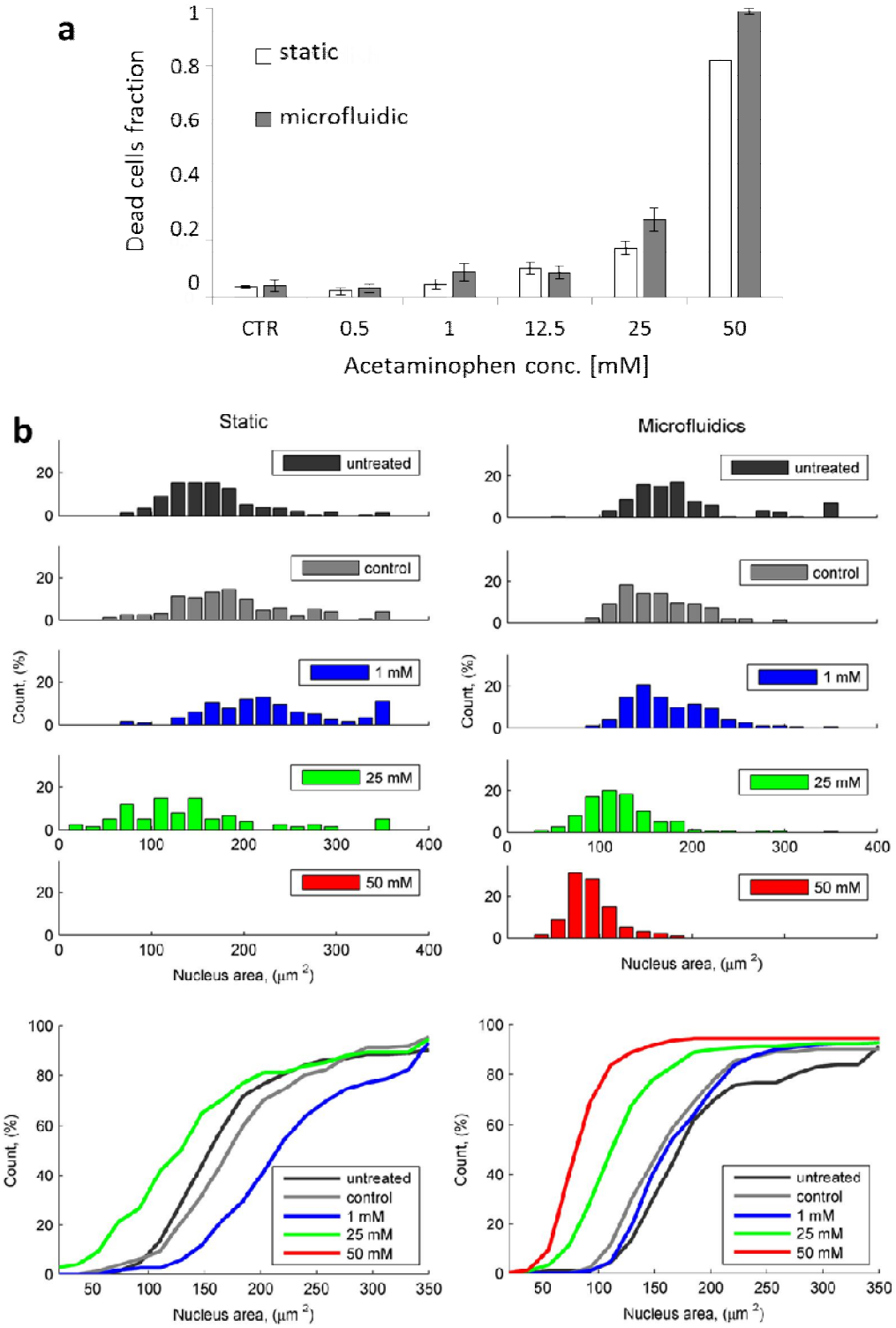

Fig. S11 | HepG2 cell line drug treatment. (**a**) Graph showing cell death in response to acetaminophen cytotoxicity in HepG2 cell line after 24 h treatment. Control cells (CTR) were cultured in medium with DMSO 1% (drug solvent), while treated cells were cultured with growing acetaminophen concentrations (0.5, 1, 12.5, 25, 50 mM). After live and dead assay calculation, no notable differences in dead cell fraction are found between static control cells and microfluidic cultured cells (at f=2d^{-1}). (**b**) HepG2 treated with different hepatotoxic acetaminophen drug concentrations for 24 h. Untreated cells were cultured in standard culture medium, control cells were cultured in medium with DMSO 1% and treated cells were cultured with growing acetaminophen concentrations (1, 25, 50 mM). Nuclei areas of static control cells and

microfluidic cultured cells were calculated and represented as probability density function (top) and cumulative density function (bottom). Cell nuclei area diminishes at higher acetaminophen concentrations in response to growing cell cytotoxicity (50 mM static data is missing because of cell detachment). The reduction in nuclear area at growing drug concentrations is more appreciable and clean in microfluidic cultured cells, compared to static control cells.

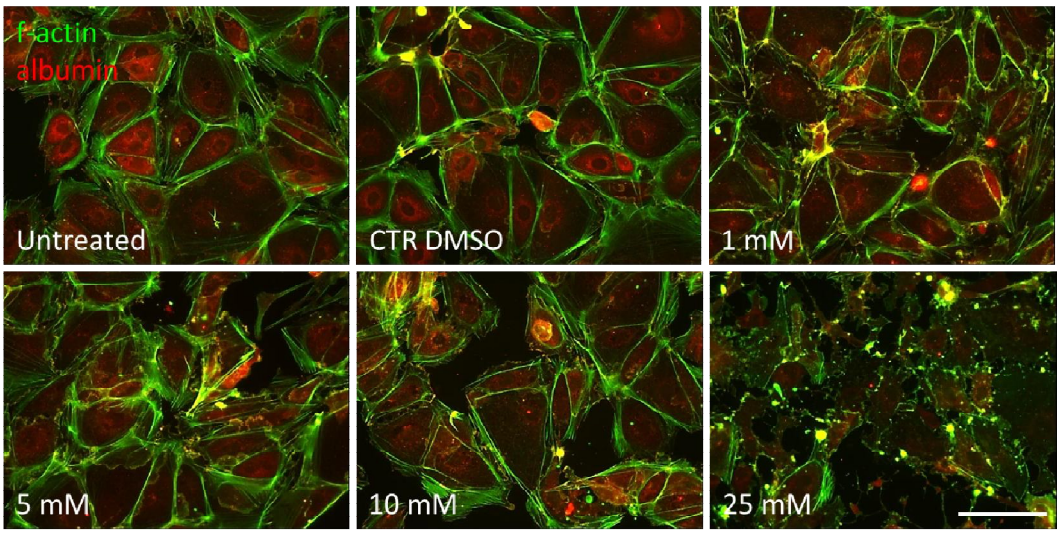

Fig. S12 | Drug treatment of HESC-derived hepatocyte-like cells in microfluidic condition. Immunofluorescence panel shows f-actin staining for cell morphology (green) and albumin (red) in cells treated with different acetaminophen concentrations at day 22 of differentiation, for 24 h at f=2d^{-1}. At growing drug concentrations cell morphology is disrupted, in response to acetaminophen cytotoxicity, especially at 25 mM with almost complete loss of cell structure and function. Scale bar 30 µm.

Annex 4

Complete restoration of multiple dystrophin isoforms in genetically corrected Duchenne muscular dystrophy patient–derived cardiomyocytes

Susi Zatti[1,2], Sebastian Martewicz[1,2], Elena Serena[1,2], Narumi Uno[3], Giovanni Giobbe[1,2], Yasuhiro Kazuki[3], Mitsuo Oshimura[3] and Nicola Elvassore[1,2]

[1] Department of Industrial Engineering, University of Padova, Padova, Italy;

[2] Venetian Institute of Molecular Medicine (VIMM), Padova, Italy;

[3]Department of Biomedical Science, Institute of Regenerative Medicine and Biofunction, Graduate School of Medical Science, Tottori University, Yonago, Japan.

Molecular Therapy — Methods & Clinical Development
Volume 1, article 1
doi:10.1038/mtm.2013.1

Abstract

Duchenne muscular dystrophy (DMD)–associated cardiac diseases are emerging as a major cause of morbidity and mortality in DMD patients, and many therapies targeted to skeletal muscle failed to improve cardiac function. The reprogramming of patients' somatic cells into pluripotent stem cells, combined with technologies for correcting the genetic defect, possesses great potential for the development of new treatments for genetic diseases. In this study, we obtained human cardiomyocytes from DMD patient– derived, induced pluripotent stem cells genetically corrected with a human artificial chromosome carrying the whole dystrophin genomic sequence. Stimulation of cytokines was combined with cell culturing on hydrogel with physiological stiffness, allowing an adhesion-dependent maturation and a proper dystrophin expression. The obtained cardiomyocytes showed remarkable sarcomeric organization of cardiac troponin T and α-actinin, expressed cardiac-specific markers, and displayed electrically induced calcium transients lasting less than 1 second. We demonstrated that human artificial chromosome carrying the whole dystrophin genomic sequence is stably maintained throughout the cardiac differentiation process and that multiple promoters of the dystrophin gene are properly activated, driving expression of different isoforms. These dystrophic cardiomyocytes can be a valuable source for in vitro modeling of DMD-associated cardiac disease. Furthermore, the derivation of genetically corrected, patient-specific cardiomyocytes represents a step toward the development of innovative cell and gene therapy approaches for DMD.

Introduction

Duchenne muscular dystrophy (DMD) is one of the most common and severe inherited neuromuscular disorders, affecting 1 in 3,500 newborn males. DMD is caused by mutations in the dystrophin gene encoding a key structural protein of the dystrophin glycoprotein complex, which connects the contracting cytoskeletal machinery of skeletal and cardiac muscle fibers to the extracellular matrix scaffold.1 The absence of dystrophin in DMD patients causes a broad spectrum of physical consequences, eventually leading to a premature death.2 Approximately 20% of deaths are the result of cardiomyopathies and/or cardiac conduction abnormalities. The increased life span of patients affected by DMD allowed by the improvements in treatments of respiratory muscle disease made cardiomyopathies (present in ~90% of patients) emerge as a major cause of morbidity and mortality.3 In addition, many experimental therapies have mainly focused on skeletal muscle, aiming at the restoration of dystrophin expression in myofibers, and have failed to improve cardiac function.4 Derivation of DMD patient–specific cardiomyocytes (CMs) and the correction of their genetic defect could provide a valuable cell source for in vitro modeling and for studying DMD-related cardiac dysfunctions, in addition to potentially representing a significant advancement toward an effective therapy for DMD-associated cardiomyopathies. The efficient reprogramming technology pioneered by Yamanaka and colleagues5 opened the perspective of deriving large numbers of disease-specific human cells in vitro. Human induced pluripotent stem (hiPS) cells are recently emerging as an ideal cell source for the generation of clinically relevant cardiac disease models.6 Several recent studies demonstrate how hiPS cell–derived CMs can be used for modeling the pathological phenotype of inherited cardiac disorders, such as the LEOPARD syndrome,7 type 1 and 2 long QT syndrome, 8–10 catecholaminergic polymorphic ventricular tachycardia, 11 arrhythmogenic right ventricular dysplasia/cardiomyopathy,12 and the dilated cardiomyopathy.13 However, to our knowledge, CMs from DMD patient–derived hiPS cells have never been obtained so far. Moreover, disease-specific hiPS cell–derived cells could represent a platform for studying in vitro the pathological dystrophic phenotype and for testing and validating the therapeutic approaches and their efficiency in restoring the normal phenotype.14 In addition, it has been recently demonstrated that hiPS cell–derived CMs can efficiently integrate in injured hearts of a guinea pig,15 providing a proof of principle for the application of these cells in regenerative medicine aiming at the treatment of cardiac dysfunctions. In the perspective of a therapeutic application, the genetic defect of CMs derived from inherited disease–specific hiPS cells should be corrected before these cells are reengrafted in the patient. DMD is among the most difficult genetic diseases to treat, and the dystrophin gene is the largest gene described in the human genome. Promising results have been obtained in rodent models of Duchenne cardiomyopathy using adeno-associated viruses carrying minimized synthetic dystrophin genes (mini- and microdystrophin).16 These approaches do not allow the insertion of a complete functional version of the dystrophin gene. On the other hand, exon-skipping approaches,17 which redirect

the gene processing bypassing the mutation, can be applied only to defined ranges of patients, based on their specific mutations. Several studies suggest that utrophin may help in the preservation of heart function in young adult mdx mice and heterozygous mdx mice.18,19 However, similar to dystrophin, the large size of the utrophin gene also presents a significant challenge to gene delivery.16 Other approaches for the treatment of Duchenne cardiomyopathy include the forced expression of sarcoendoplasmic reticulum calcium-ATPase via adeno-associated virus gene transfer, aimed at restoring calcium homeostasis and improving cardiac contractility,20 without correction of the genetic defect. A highly promising gene delivery tool for the correction of the DMD gene is represented by human artificial chromosomes (HACs). HAC is an artificially created exogenous minichromosome having the ability to replicate and segregate autonomously in target human cells and to be stably maintained at episomal level, without integration into the host genome. In addition, HACs have the capacity to carry large genomic loci with all their regulatory elements.21 An HAC vector carrying, for the first time, the whole dystrophin genomic locus including the associated regulatory elements (DYSHAC) was developed by Hoshiya et al.22 Furthermore, Kazuki et al.23 have demonstrated the complete correction of hiPS cells derived from a DMD patient, using the DYS-HAC, pioneering an innovative and promising therapeutic approach for the treatment of DMD and DMD-associated cardiac diseases. The first preclinical proof of safety and efficacy of DYS-HAC– mediated therapy has been provided by Tedesco et al.24 In this study, the authors showed a significantly ameliorated phenotype in the mdx dystrophic mouse model after the transplantation of mdx

mesoangioblasts genetically corrected with the DYS-HAC. In addition, the same group recently reported the differentiation in mesoangioblast- like stem/progenitor cells from DMD patient–derived hiPS cells, carrying the genetic correction with the DYS-HAC.25

In this article, we aim to differentiate DMD patient–derived, genetically corrected hiPS cells into CMs with a mature phenotype and to assess the maintenance of the DYS-HAC during the differentiation of hiPS cells. In particular, we aim at investigating the correct activation, at HAC level, of the complex mechanisms regulating dystrophin expression, such as multiple promoter activities, which should be finely regulated in a development- and tissue-specific way.

An ad hoc cardiac differentiation procedure, combining the delivery of cytokines with mechanical stimulation, by culturing cells on hydrogel with physiological stiffness, has been designed to allow full CM maturation. DYS-HAC–mediated dystrophin expression restoration has been assessed at different stages of the differentiation process. The dystrophic CMs established in this work could potentially represent a valuable cell source to be used for in vitro modeling of DMD-associated cardiomyopathies, and at the same time, the genetically corrected dystrophic CMs possess a promising therapeutic potential for the treatment of DMD.

Results

Differentiation of hiPS cells toward the cardiac lineage

To obtain DMD-specific CMs, their genetic correction, and a positive control of dystrophin expression, the hiPS following cell lines that differentiated toward the cardiac lineage were used: (i) hiPS cells derived from a DMD patient with deletion of exons 4–43 of the muscle isoform Dp427m (DMD hiPS cells); (ii) DMD patient–specific hiPS cells genetically corrected by an HAC carrying the full-length genomic dystrophin sequence (DYS-HAC hiPS cells); and (iii) hiPS cells derived from a healthy individual (healthy hiPS cells), carrying a normal genotype with a wild-type copy of the dystrophin gene. First, DMD, DYS-HAC, and healthy hiPS cell lines were cultured and expanded in their undifferentiated state for up to 10 passages. During expansion, hiPS cell colonies maintained the expression of pluripotency markers such as Oct4, Sox2, c-Myc, Tra-1-60, and Tra-1-81, as evaluated by immunofluorescence (see Supplementary Figure S1a). In addition, DYS-HAC hiPS cells were monitored for the expression of the enhanced green fluorescent protein, a marker contained in the DYS-HAC (see Supplementary Figure S1b). The expanded colonies were then used for embryoid body (EB) generation. DMD, DYS-HAC, and healthy hiPS cell–derived EBs were differentiated toward the cardiac lineage through an ad hoc optimized procedure. Overall outline of this procedure is shown in Figure 1a. Remarkably, the enhanced green fluorescent protein gene, driven by a CAG promoter contained in the DYS-HAC,23 was expressed during all the stages of the differentiation procedure, in DYS-HAC hiPS cells (Figure 1b), in DYS-HAC hiPS cell–derived EBs (Figure 1c), and in cultured cells after EB adhesion (Figure 1d), indicating the stable maintenance of the DYS-HAC. During the first 16 days of the differentiation procedure, EBs were cultured in suspension and subjected to a staged protocol, adapted from the one developed by Kattman et al.,26 based on the addition of specific cytokines known to play a key role in cardiogenesis during embryonic development to the culture medium. This 16-day differentiation procedure resulted in a relevant percentage of spontaneously contracting EBs (see Supplementary Videos S1 and S2), ranging from a minimum of 14% for DMD hiPS cell–derived EBs to a maximum of 44% for healthy hiPS cell– derived EBs (Table 1).

Table 1. Percentage of spontaneously contracting EBs and cTnT-positive cells obtained for each cell line used

hiPS cell lines	*Contracting EBs obtained (% ± SD): day16*	*cTnT-positive cells (% ± SD): day 24*
DMD hiPS cells	14 ± 4	7,6 ± 0,7
DYS-HAC hiPS cells	19 ± 5	8,2 ± 1,5
Healthy hiPS cells	44 ± 2	9,8 ± 4,6

cTnT, cardiac troponin T; DMD, Duchenne muscular dystrophy; DYS-HAC, human artificial chromosome carrying the whole dystrophin genomic sequence; EBs, embryoid bodies; hiPS cells, human induced pluripotent stem cells; SD, standard deviation calculated on data obtained from 5 independent analyses.

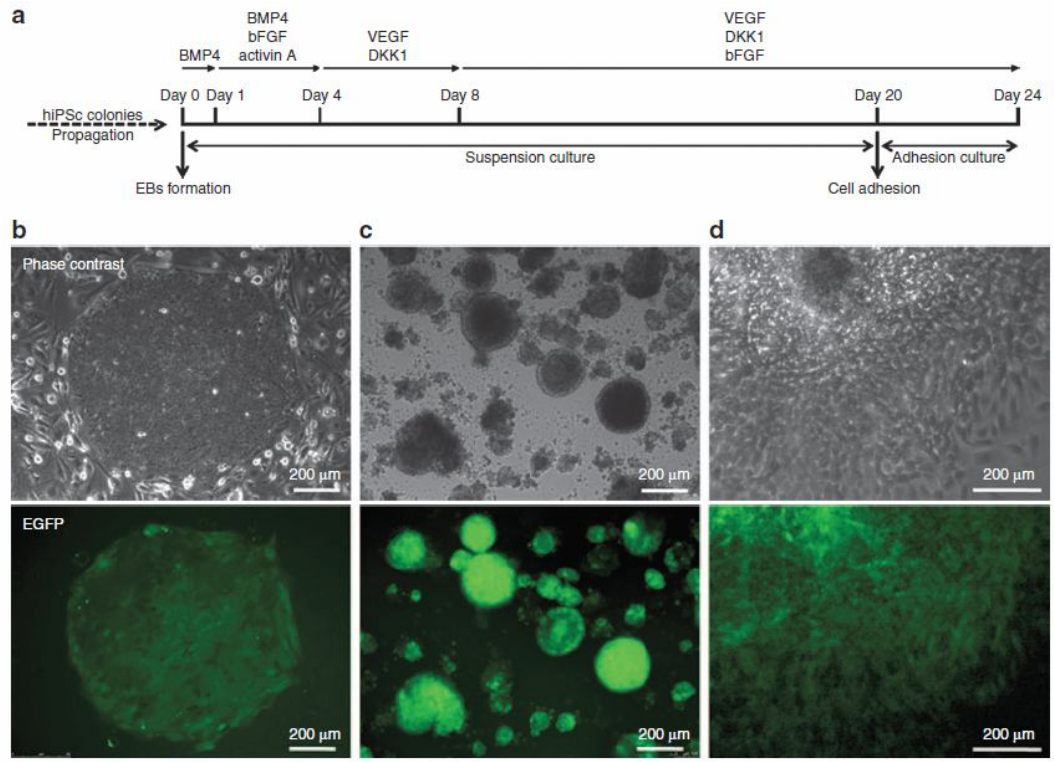

Figure 1. Differentiation of hiPS cells. (a) Schematic representation of the differentiation procedure. (b) Undifferentiated colonies of DYS-HAC hiPS cells cultured on murine embryonic fibroblast feeder cells. (c) EBs generated from DYS-HAC hiPS cell colonies on day 4 of the differentiation procedure. (d) Cultured cells 2 days after EB adhesion. Epifluorescence images show the expression of EGFP in each condition, indicating the presence of the DYSHAC. BMP4, bone morphogenetic protein 4; DYS-HAC, human artificial chromosome carrying the whole dystrophin genomic sequence; EBs, embryoid bodies; EGFP, enhanced green fluorescent protein; hiPS cells, human induced pluripotent stem cells; VEGF, vascular endothelial growth factor; bFGF, basic fibroblast growth factor.

Our recent data demonstrated that a proper cardiac differentiation requires cell–substrate interactions to promote functional and structural maturation of hiPS cell–derived CMs.36 For this reason, contracting EBs were cultured in suspension up to day 20 and then seeded on hydrogel substrate with a physiological stiffness for additional 4 days. Following adhesion, a remarkable maturation of CMs was observed in terms of both cytoskeletal architecture and cardiac marker expression (Figure 2). CMs obtained on day 24 were characterized by a remarkable sarcomeric organization, as revealed by immunofluorescence of α-actinin, cardiac troponin T (cTnT), and F-actin, and GAP junction formation, as revealed by immunofluorescence of connexin 43 (Figure 2a). The percentage of cTnT-positive CMs obtained on the overall population was ~10% (Table 1). The same percentage increased to 44 ± 2% when only contracting EBs were selected. Expression of sarcomeric cardiac-specific proteins, in particular cTnT and ventricular myosin light chain, in adhered CMs, was also confirmed by reverse transcription–polymerase chain reaction (RT-PCR) (Figure 2b). For DMD hiPS cell–derived CMs, expression of ML2v, a marker of terminally differentiated ventricular CMs, was not observed before CM adhesion but was observed only

after adhesion. Mesoderm- and cardiac-specific transcription factors GATA4 and NKX2.5 were also expressed in all conditions tested, as revealed by RT-PCR (Figure 2b) and immunofluorescence (Figure 2a), respectively. CMs cultured in adhesion displayed both spontaneous and electrically induced calcium transients lasting less than 1 second, typical of calcium cycling during contraction (Figure 2c), together with a diffuse intracellular distribution of cardiac-specific sarcoendoplasmic reticulum calcium-ATPase (Figure 2a), a key element of the calcium handling machinery needed for calcium reuptake after contraction.

Taken together, these results show that functionally differentiated CMs were derived from DMD, DYS-HAC, and healthy hiPS cells. The observed differences in terms of percentage of spontaneously contracting EBs and cTnT-positive CMs on the overall population (Table 1) can be due to the intrinsic variability related to the use of different hiPS cell lines and the efficiency of the cardiogenic protocol itself. HAC-driven expression of dystrophin sequences originally deleted in the DMD patient We then focused on the genetically corrected CMs, testing the restoration of HAC-mediated dystrophin expression. DYS-HAC is the first vector carrying the whole dystrophin genomic locus, including all the associated regulatory elements.22 This potentially allows proper activation of the complex mechanism regulating dystrophin expression, for instance, the activities of seven different promoters driving transcription of tissue-specific isoforms and exon-skipping and exon-scrambling events, which are finely regulated in both development- and tissue-specific manner.1 The possibility to restore dystrophin expression in a tissue-specific manner, following native regulation mechanisms, makes DYS-HAC a promising tool for the treatment of DMD also at cardiac muscle level.

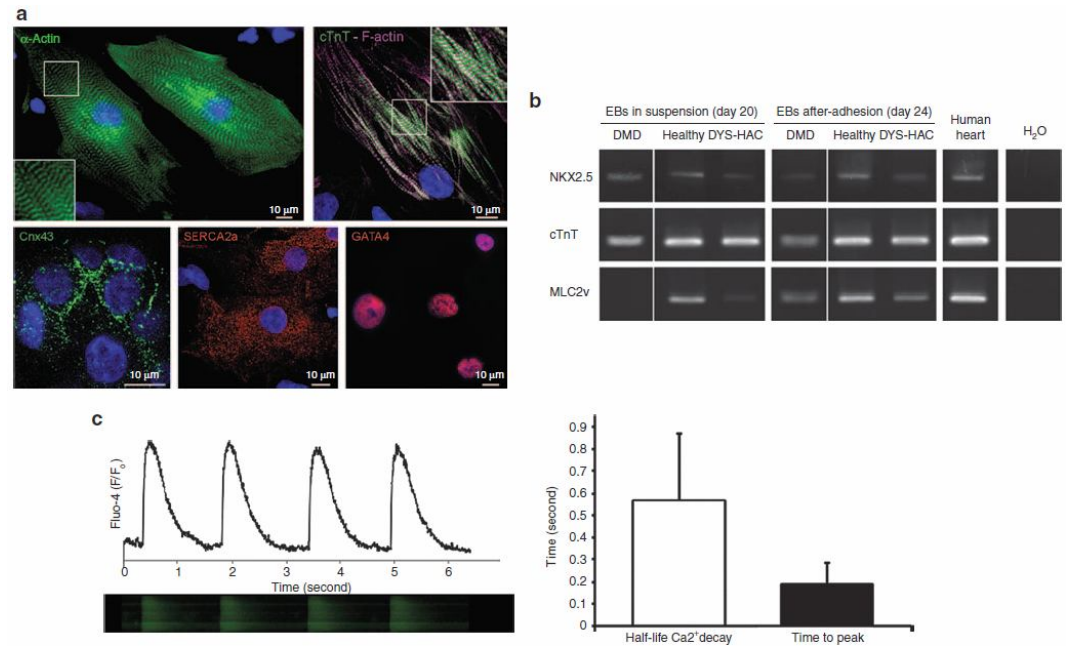

Figure 2. Characterization of hiPS cell–derived CMs. (a) Immunofluorescence of α-actinin; cardiac troponin T (cTnT) and F-actin; connexin 43 (Cnx43); sarcoendoplasmic reticulum calcium-ATPase (SERCA2a); and GATA4 in adhered CMs on day 24 of the differentiation procedure. Nuclei are counterstained with DAPI. (b) RT-PCR shows the expression of NKX2.5, cTnT, and MLC2v in EBs obtained from DMD, healthy, and DYS-HAC hiPS cells cultured in suspension (on day 20) and

on the EB-derived adhered cells on day 24 of the differentiation procedure. (c) Typical calcium transients displayed by hiPS cell–derived CMs on day 24 of the differentiation procedure. The histogram reports quantitative evaluation of calcium reuptake rate by the half-life of calcium decay and the calcium release phase as the time to peak. Data are presented as SD. CMs, cardiomyocytes; DAPI, 4′,6-diamidino-2-phenylindole; DMD, Duchenne muscular dystrophy; DYS-HAC, human artificial chromosome carrying the whole dystrophin genomic sequence; hiPS cells, human induced pluripotent stem cells; MLC2v, ventricular myosin light chain; RT-PCR, reverse transcription–polymerase chain reaction.

First, dystrophin expression was analyzed on healthy, DMD, and genetically corrected DYS-HAC hiPS cells during the cardiac differentiation procedure, by RT-PCR using specific primers designed to span exon–exon junctions localized inside the deleted genomic sequence of the DMD patient (from exon 4 to 43 of the muscle dystrophin isoform) (Figure 3a). mRNA from human heart and skeletal muscle was used as positive control. As expected, healthy hiPS cell–derived EBs displayed dystrophin expression both when cultured in suspension and after adhesion, whereas, as expected, in DMD hiPS cell–derived EBs, no dystrophin expression was observed in any condition (Figure 3b). In DYS-HAC hiPS cell–derived EBs, dystrophin expression was restored both when cultured in suspension and after adhesion. A positive result was obtained for each of the five exon junctions checked, distributed on the whole deleted genomic region. HAC-driven expression of multiple dystrophin isoforms In vivo, CMs are known to express the full-length muscle dystrophin isoform (Dp427m), together with other isoforms, such as the Dp260 (ref. 27) and Dp71, the smallest but multifunctional product of the DMD gene expressed in many tissues, including cardiac muscle. Dp71 has been shown to contribute to the proper clustering and anchoring of structural and signaling proteins to the plasma membrane and of nuclear envelope proteins to the inner nuclear membrane.28

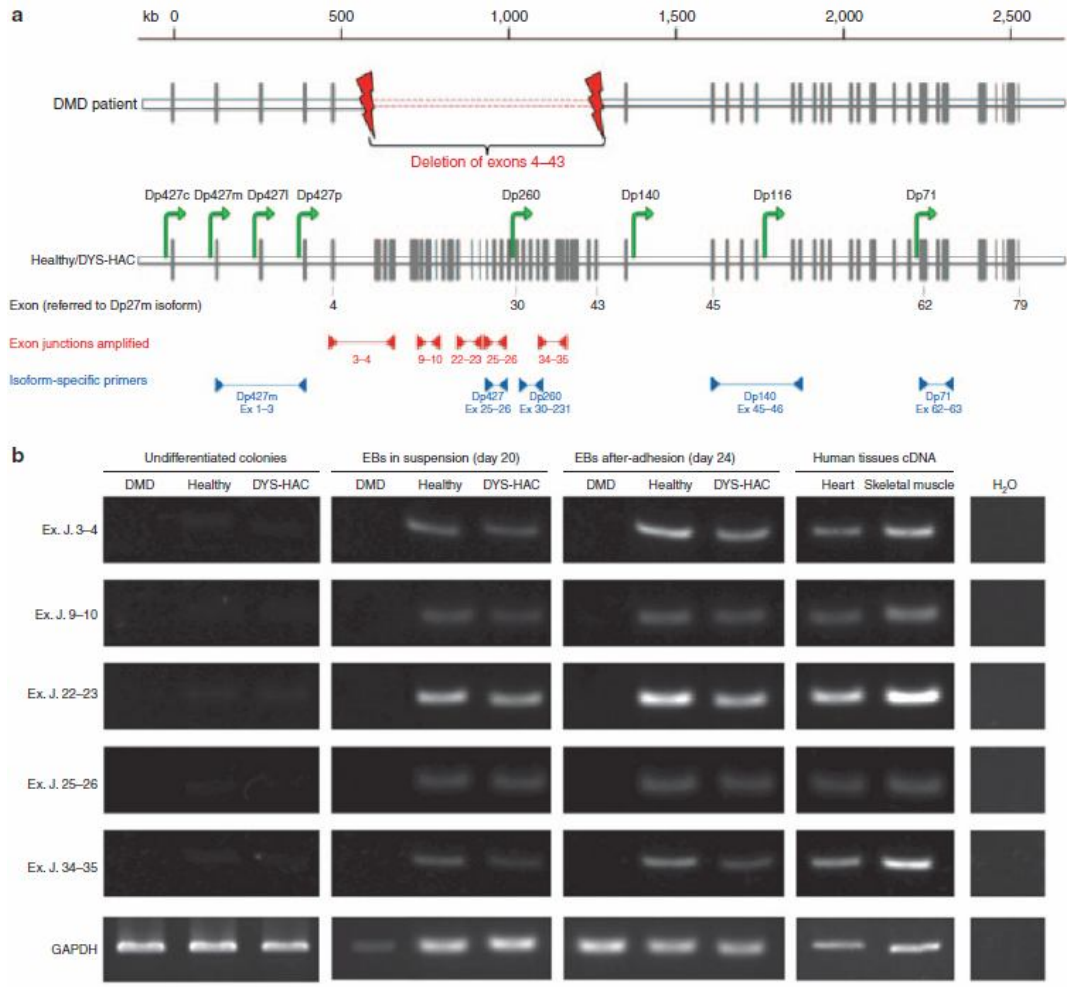

Figure 3. HAC-driven expression of dystrophin sequences originally deleted in DMD patients. (a) The genomic organization of the dystrophin gene: the gray vertical bars represent the exons; the green arrows indicate the promoters driving the expression of the different dystrophin isoforms within the gene1,2; primer pairs used to amplify exon–exon junctions inside the deleted region are indicated by red arrowheads, and those used to amplify specific isoforms are indicated by blue arrowheads. Exon number is referred to exons composing the muscle dystrophin isoform Dp427m. (b) RT-PCR of specific dystrophin sequences localized inside the patient with deletion of exons (Ex) 4–43. Primers were constructed to spam five different exon–exon junctions (Ex. J.). cDNA from human heart and skeletal muscle was used as positive control. Analyses were performed at three different stages of the differentiation process: undifferentiated colonies, differentiated EBs cultured in suspension (day 20), and adhered cells (day 24), for each hiPS cell lines (DMD, healthy, and DYS-HAC hiPS cells). cDNA from human tissues was used as positive control. cDNA, complementary DNA; DMD, Duchenne muscular dystrophy; DYS-HAC, human artificial chromosome carrying the whole dystrophin genomic sequence; EBs, embryoid bodies; HAC, human artificial chromosome; hiPS cells, human induced pluripotent stem cells; RT-PCR, reverse transcription–polymerase chain reaction.

The expression of different dystrophin isoforms such as Dp427m, Dp260, Dp140, and Dp71 was analyzed by RT-PCR during the cardiac differentiation procedure on healthy, DMD, and DYS-HAC hiPS cells (Figure 4a). mRNA from human tissues was used as positive control. As expected, healthy hiPS cell–derived EBs (both in suspension and after adhesion) displayed the expression of all the four different dystrophin isoforms. The expression of isoform Dp140 indicates the presence of

other cell types in addition to CMs, which are expected in this type of differentiation procedures.29 In DMD hiPS cell–derived EBs, the expression of the Dp260 isoform, the promoter of which stands within the large genomic deletion (exons 4–43), was not observed, whereas isoforms Dp140 and Dp71 were still detectable as their promoters are downstream of the deleted area (intron 44 and intron 62, respectively). The amplicon relative to isoform Dp427m is still present, as the primers specific for this isoform are designed on the first transcribed exons (exons 1–3), upstream of the deletion, testifying a proper initiation of dystrophin transcription. On DYS-HAC hiPS cell–derived EBs (both in suspension and after adhesion), expression of all isoforms can be observed, notably with the restoration of Dp260 isoform transcript. To assess the efficiency of HAC-driven recovery of dystrophin mRNA levels, we performed RT-PCR experiments targeted at the isoforms expressed in the cardiac tissue (Figure 4b). A set of primers targeting exons 25–26 identifying all Dp427 isoforms was used in addition to the Dp427m-specific one to assess the relative expression of Dp427 transcripts inside the deleted genomic region. Confirming the previous results of the RT-PCR, DMD hiPS cell–derived EBs did not display at all the expression of transcripts from inside the deleted genomic region, both in regard to Dp427

isoforms, the transcription of which is truncated after exon 4, and in regard to Dp260 isoform, the transcription of which cannot be initiated. The expression of the truncated Dp427m isoform and the short Dp71 isoform was variable among the different experiments, not reaching statistical significance (n = 3). Differentiated healthy and DYS-HAC hiPS cell–derived CMs displayed similar amounts of all transcripts tested, highlighting the proper function of the HAC in driving and regulating the transcription of different dystrophin isoforms.

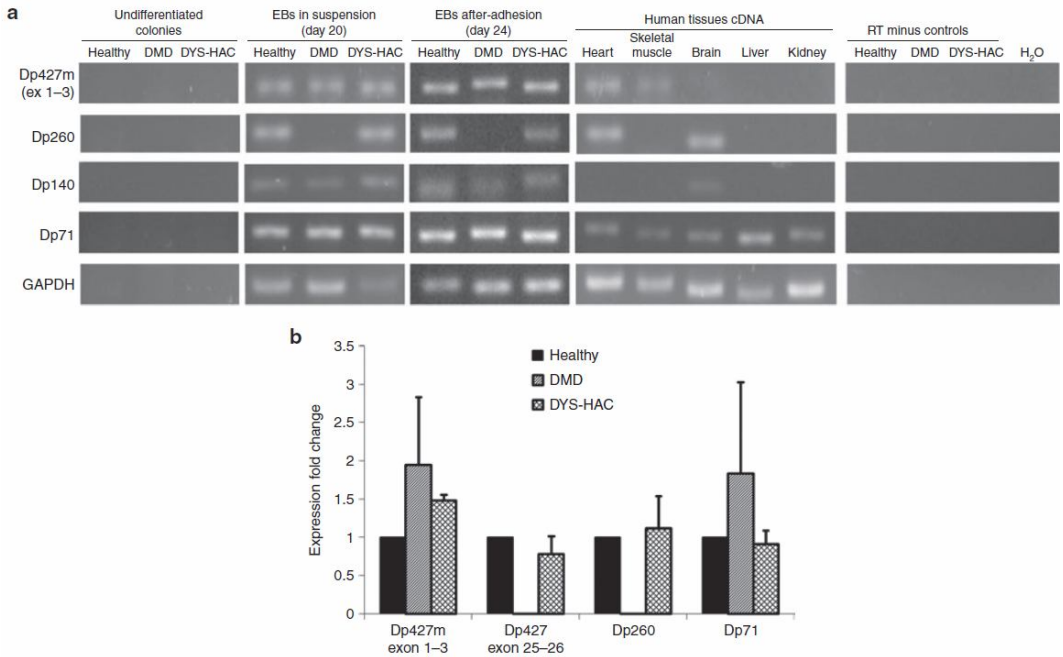

Figure 4. HAC-driven expression of multiple dystrophin isoforms. (a) RT-PCR of dystrophin isoforms Dp427m, Dp260, Dp140, and Dp71 at three different stages of the differentiation process: undifferentiated colonies, differentiated EBs cultured in suspension (day 20), and

adhered cells (day 24), for each hiPS cell lines (DMD, healthy, and DYS-HAC hiPS cells). cDNA from human tissues was used as positive control. (b) Realtime PCR for dystrophin isoforms present in cardiac tissue. Muscle-specific Dp427m is double checked with Dp427m-specific primer set spanning exons 1–3 and an all Dp427 isoform-specific primer set spanning exons 25–26. Data are presented as mean ± SD. cDNA, complementary DNA; DYS-HAC, human artificial chromosome carrying the whole dystrophin genomic sequence; EBs, embryoid bodies; HAC, human artificial chromosome; hiPS cells, human induced pluripotent stem cells; RT-PCR, reverse transcription–polymerase chain reaction; DMD, Duchenne muscular dystrophy.

Taken together, these analyses on mRNA transcripts show that, during the cardiac differentiation protocol, dystrophin expression is correctly restored by the DYS-HAC and multiple dystrophin isoforms are expressed.

HAC-mediated restoration of dystrophin protein expression and correct subcellular localization In vivo, in physiological conditions, dystrophin is a key structural protein creating a bridge across the sarcolemma, which provides a flexible connection between the basal lamina of the extracellular matrix and the inner cytoskeleton. For this important role, dystrophin should be correctly folded and localized under the plasma

membrane of skeletal and cardiac muscle cells. For this reason, we verified the proper restoration of dystrophin expression at protein level and its subcellular localization by immunofluorescence and confocal microscopy. Analyses were performed 4 days after EB adhesion on substrate with a physiological stiffness

of 15 kPa (Figure 5a). DYS-HAC hiPS cell–derived EBs displayed a clear dystrophin expression at membrane localization, drawing the boundaries of cTnT-positive CMs. A similar dystrophin staining was observed in healthy hiPS cell–derived EBs. On the other hand, as expected, in DMD hiPS cell–derived EBs, any dystrophin staining was observed. These results were confirmed by western blot analysis, in which full-length dystrophin was not observed in DMD hiPS cell– derived CMs, whereas its expression was perfectly restored in CMs corrected with the DYS-HAC (Figure 5b). Although much less abundant, other dystrophin isoforms were also detectable in the DYS-HAC–corrected cells (see Supplementary Figure S2). These results demonstrate that the DYS-HAC restores the expression of dystrophin at protein level, which can correctly localize at membrane localization in genetically corrected, hiPS cell–derived CMs.

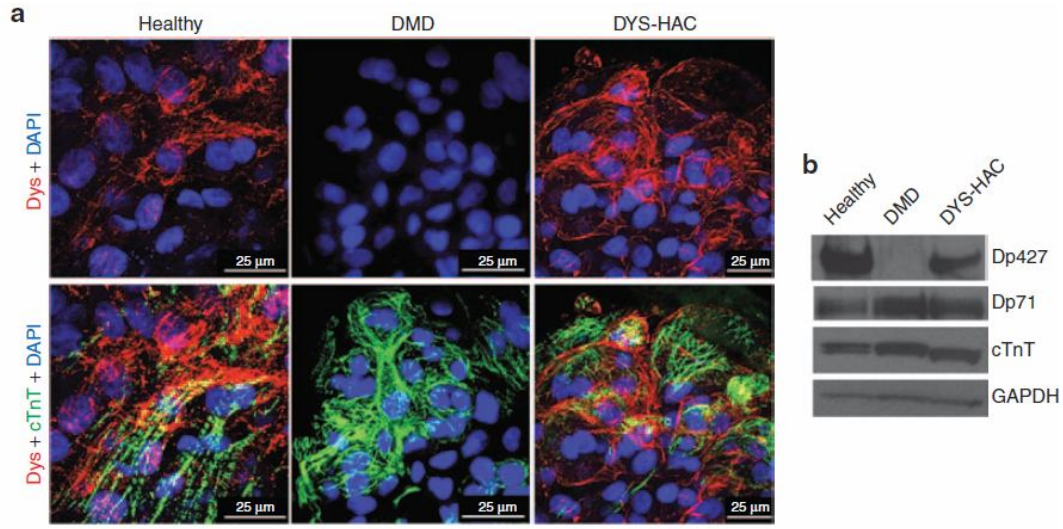

Figure 5. HAC-mediated restoration of dystrophin protein expression and correct subcellular localization. (a) Confocal microscopic analysis of dystrophin and cardiac troponin T expression on CMs obtained on day 24 of the differentiation procedure from DMD, healthy, and DYS-HAC hiPS cells. Nuclei are counterstained with DAPI. (b) Western blot analysis for dystrophin isoforms with a polyclonal antibody and for cardiac marker troponin T detected in two isoforms in the samples from human hiPS cell–derived cardiomyocytes. CMs, cardiomyocytes; DAPI, 4′,6-diamidino-2-phenylindole; DMD, Duchenne muscular dystrophy; DYS-HAC, human artificial chromosome carrying the whole dystrophin genomic sequence; HAC, human artificial chromosome; hiPS cells, human induced pluripotent stem cells.

Discussion

The derivation of genetically corrected, patient-specific hiPS cells has been recently shown to be a promising strategy for modeling genetic diseases. In particular, An et al.30 reported the derivation of hiPS cells from Huntington's disease patients' fibroblasts that were genetically corrected by an homologous recombination approach and differentiated into DARPP-32–positive neurons. Tedesco et al.25 reprogrammed fibroblasts and myoblasts from limb-girdle muscular dystrophy patients in hiPS cells and developed a protocol for the derivation of mesoangioblast-like cells that were genetically corrected in vitro with a lentiviral vector carrying the human α-sarcoglycan gene. The huge potential of hiPS cell technology has also been demonstrated in modeling human cardiovascular diseases. Some pioneering proof-of-concept studies on patients with inherited arrhythmogenic diseases, most notably different subtypes of long QT syndrome, reported the derivation of hiPS cell–derived cardiac cells to reproduce the clinical phenotype "in the petri dish."14,31 In this work we derived, for the first time to our knowledge, human CMs (hCMs) from DMD patient–specific hiPS cells and genetically corrected hCMs from DYS-HAC–containing hiPS cells. Different procedures for the cardiac differentiation of pluripotent stem cells have been reported in literature, mainly reproducing in vitro the processes of embryonic development through the stimulation of soluble cytokines, driving pluripotent stem cells toward early mesoderm specification until the derivation of cardiac progenitor cells.26,32,33 However, the major

drawback of their application, both in vitro and in vivo, is their immature phenotype. To study the restoration of dystrophin expression and its correct localization in cardiac cells, the derivation of hCMs characterized by a functionally and structurally mature phenotype is of paramount importance. We developed an ad hoc optimized differentiation procedure integrating a cytokine-based EB differentiation with a subsequent step of adhesion-dependent maturation. Increasing evidence demonstrate that adhesion and substrate sensing are key requirements for the process of muscle cell functional differentiation. In our previous work, we have shown that the development of sarcomeric structures of human striated muscles is influenced by the substrate on which the cells are cultured.34 Furthermore, in our group, it has been recently demonstrated that adhesion on substrate with a physiological stiffness promotes functional maturation of hCMs, allowing a shortening of calcium transients.36 Using the procedure developed, we derived hCMs presenting expression of cardiac-specific markers, a defined sarcomeric organization, and calcium transients lasting less than 1 second. In these conditions, dystrophin has been observed to correctly localize at membrane level on both healthy and genetically corrected hCMs. Certain variability has been observed in the expression of cardiac muscle markers along the differentiation process, for the different hiPS cell lines. This could be explained since, as widely reported in literature, hiPS cell lines derived from different cells and different clones can have a different ability to differentiate toward the cardiac lineage. In addition, it has been recently demonstrated that in vitro cultured DMD skeletal muscle cells display a delay in the appearance of typical myogenic markers.35 Similarly, we observed a delay in the expression of the late cardiac differentiation marker ventricular myosin light chain in DMD-derived cardiac cells, compared with the healthy and genetically corrected (DYS-HAC) ones. Further analyses could be performed to specifically address this issue in cardiac muscle. hiPS cell–derived CMs represent a unique platform for testing in vitro the efficiency of the DYS-HAC in restoring a proper dystrophin expression at cardiac level, in a patient-specific manner. DYS-HAC is a potential tool for use in DMD gene correction, and its ability to properly restore dystrophin expression on differentiated human cells has been recently reported.25 However, its efficiency in restoring different isoforms' expression on differentiated hCMs has not been extensively investigated so far. For the first time, we demonstrated that DYS-HAC (i) does not hinder and is stably maintained during cardiac differentiation of hiPS cells; (ii) allows a proper dystrophin expression restoration during the cardiac differentiation procedure of hiPS cells (in particular, the expression of specific sequences deleted in the patient was observed); (iii) drives the transcription of multiple dystrophin isoforms in CMs at similar expression levels compared with healthy hiPS cell–derived CMs, in particular, the full-length muscle isoform Dp427m and the cardiac isoform Dp260, which are not expressed in the DMD patient with deletion of exons 4–43; and (iv) allows the recovery of full-length dystrophin protein that localizes properly at the cell membrane. These results highlight DYS-HAC as a potential tool for use in gene correction of DMD patient cells.

Finally, the coupling of DMD CMs with specific technologies for testing cardiac functionality, such as measurement of force generation or performance under stressed condition, will provide a unique platform for studying in vitro the pathogenesis of DMD-associated cardiac disease and its correction.

Methods

hiPS cell culturing and cardiac differentiation

hiPS cells, obtained as previously reported,23 were cultured on a feeder layer of mitomycin-C–inactivated murine embryonic fibroblasts. Composition of the culture medium was as follows: Dulbecco's modified Eagle medium/F12 (Life Technologies) containing 20% knockout serum (Life Technologies), 2 mmol/l of l-glutamine (Life Technologies), 0.1 mmol/l of nonessential amino acids (Life Technologies), 0.1 mmol/l of 2-mercaptoethanol (Life Technologies), 50 units and 50 mg/ml of penicillin and streptomycin (Life Technologies), and 4 ng/ml of basic fibroblast growth factor (Peprotech). To maintain the pluripotent state for a high number of passages and avoid chromosomal aberrations, the colonies were passed as described

below—usually once a week. hiPS cells were washed with phosphate-buffered saline (PBS) and treated with 1 ml of CTK solution for 30 seconds. CTK solution was prepared as follows: 5 ml of 2.5% trypsin (Life Technologies), 5 ml of 1 mg/ml collagenase IV (Sigma-Aldrich), 0.5 ml of 0.1 mol/l CaCl2 (Sigma-Aldrich), and 10 ml of knockout serum were all added to 30 ml of distilled water. The mechanical separation of colonies was performed with the use of a stereomicroscope to dissect the undifferentiated colonies into several pieces using a cutting pipette. These selected pieces were then replated for expansion onto dishes containing fresh murine embryonic fibroblast feeders or moved to ultralow adhesion plates to be cultured in suspension for EB generation. The obtained EBs were differentiated in suspension using a protocol adapted from Kattman et al.26 Briefly, for EB formation, the detached and separated colonies were maintained for 24 hours in basal medium (StemPRO-34; Life Technologies), 2 mmol/l of l-glutamine (Life Technologies), 150 µg/ml of transferrin (Roche), 50 µg/ml of ascorbic acid (Sigma-Aldrich), 0.4 mmol/l of monothioglycerol (Sigma-Aldrich), 50 units and 50 mg/ml of penicillin and streptomycin (Life Technologies) supplemented with 10 ng/ml of human bone morphogenetic protein 4 (R&D). From day 1 to day 4, EBs were cultured in basal medium with 10 ng/ml of human bone morphogenetic protein 4, 5 ng/ml of human basic fibroblast growth factor (R&D), and 6 ng/ml of hActivin A (R&D). From day 4 to day 8, the EB culture medium consisted of basal medium and 10 ng/ml of human vascular endothelial growth factor (R&D) and 150 ng/ml of hDKK (R&D). Finally, from day 8 to day 14, the EB culture medium consisted of basal medium and 10 ng/ml of human vascular endothelial growth factor and 5 ng/ml of human basic fibroblast growth factor. Cultures were maintained in a 5% CO2, 5% O2, and 90% N2 environment for the first 16 days and then transferred to a 5% CO2 air environment. The obtained EBs were maintained in suspension using the last medium described

until day 20 and then seeded on hydrogel substrates with a physiological stiffness of 15 kPa (prepared as previously described)34,36,37, functionalized with 100 µg/ml of laminin (BD), and cultured in these conditions for additional 4 days.

Immunofluorescence

A standard immunohistochemistry protocol was used. Briefly, cells were fixed with PBS containing 2% paraformaldehyde (Sigma-Aldrich) for 7 minutes, permeabilized with PBS containing 0.5% Triton X-100 (Sigma-Aldrich), and blocked in PBS containing 2% horse serum for 45 minutes, at room temperature. Primary antibodies were applied for 1 hour at 37 °C. Cells were washed in PBS (Life Technologies) and incubated with fluorescence-conjugated secondary antibodies against mouse, rabbit, or goat, depending on primary antibody used, for 45 minutes at 37 °C. Finally, nuclei were counterstained with 4□,6-diamidino-2-phenylindole (Sigma-Aldrich), and samples were mounted with Elvanol and viewed under Leica TCS SP5 fluorescence confocal microscope (Leica). Primary antibodies used were the following: mouse monoclonal

anti-cTnT (Thermo Scientific; #MS-295-P; 1:100 dilution), mouse monoclonal anti-α-actinin (Sigma-Aldrich; #A7811; 1:100 dilution), rabbit polyclonal antidystrophin (Abcam; #ab15277; 1:200 dilution), mouse monoclonal anti-Cx43 (Millipore; #MAB3067; 1:100 dilution), goat polyclonal anti-SERCA2a (Santa Cruz; #SC 8094; 1:200 dilution), and goat polyclonal anti-GATA4 (Santa Cruz; #SC 1237; 1:200 dilution). Secondary antibodies used were the following: goat anti-mouse (Invitrogen; #A11005 and #A11001; 1:200 dilution), goat anti-rabbit (Invitrogen; #A11012 and A1108; 1:200 dilution), and donkey antigoat (Jackson ImmunoLab; #705-165-003; 1:300 dilution). All antibodies were diluted in 3% bovine serum albumin (Sigma-Aldrich).

Calcium measurements

Confocal calcium measurements were performed as previously reported in Martewicz et al.38 Briefly, CMs were loaded in serum-free 25 mmol/l HEPES Dulbecco's modified Eagle medium (Life Technologies) supplemented with 2,5 mmol/l of fluorescent calcium dye Fluo-4 AM (Life Technologies) for 20 minutes at 37 °C in the presence of 2 mmol/l of Pluronic F-127 (Life Technologies) and 20 mmol/l of sulfinpyrazone (Sigma-Aldrich), then incubated for additional 10 minutes at 37 °C without Fluo-4 AM, and added with 0.2 mmol/l of di-8-ANEPPS (Life Technologies). Cell dynamics were obtained in recording solution: NaCl, 125 mmol/l; KCl, 5 mmol/l; Na3PO4, 1 mmol/l; MgSO4, 1 mmol/l; HEPES, 20 mmol/l; CaCl2, 2 mmol/l; and glucose, 5.5 mmol/l, to pH 7.4 with NaOH. Line scans were acquired with a Leica TCS SP5 fluorescence confocal microscope using a 63× oil immersion objective, with 488-nm Ar laser line as an excitation source and 400-Hz acquisition frequency. Line scans were then analyzed using ImageJ software (version number 1.46) to obtain calcium transient profile. For evaluating the calcium reuptake rate after contraction, the half-life of the calcium decay was considered. Half-life of the calcium decay was calculated by fitting a first-order exponential decay to the calcium reuptake phase of the calcium transient profile. For the calcium release phase, the time to peak value was calculated considering

the time from baseline to a minimum of the second derivative of the calcium transient. All numerical data were manipulated with Origin 8.1 software.

Reverse transcription–polymerase chain reaction.

Total RNA from hiPS cell colonies and differentiated EBs was purified with RNeasy Mini Kit (Qiagen), in accordance with the manufacturer's instructions, or with TRIzol reagent (Invitrogen) and treated using a Turbo DNA-free kit (Applied Biosystems) to remove genomic DNA contamination. For the cardiac marker analyses, first strand complementary DNA (cDNA) synthesis was performed using an oligo- (dT)20 primer and the cDNA Reverse Transcription Kit (Applied Biosystems). PCR was performed with cDNA using AmpliTaq Gold (Applied Biosystems). Amplifications were performed with an annealing temperature of 55 or 58 °C for 30–35 cycles. For the dystrophin isoform analyses, cDNA retrotranscription was carried out with High Capacity cDNA Reverse Transcription Kit (Invitrogen), followed by RT-PCR using Platinum Taq Polymerase (Invitrogen) with annealing temperature of 60 °C for 35 cycles. All the amplicons were resolved by electrophoresis on a 2% agarose gel, followed by staining with SYBR Safe Gel. Primer sequences are given in Table 2.

Real-time PCR

Real-time PCR on cDNA retrotranscribed with High Capacity cDNA Reverse Transcription Kit was carried out with Power SYBR Green PCR Master Mix (Applied Biosystems) in a 7000 System thermal cycler platform (Applied Biosystems). Annealing temperature for all primer sets was 60 °C (sequences reported in Table 2). Relative amount of transcripts was calculated with PfaffI method relative to healthy hiPS cell–derived EB expression levels. Amplification efficiency for all primer sets was >1.9.

Western blot analyses

Detection of dystrophin (antibody 1:500; o/n + 4 °C; Abcam; #ab15277), cTnT (antibody 1:500; 60 minutes at room temperature; Thermoscientific #MS-295-P), and GAPDH (antibody 1:2,000; 60 minutes at room temperature; Abcam; #ab8245) was carried out after protein lysates were resolved in a NuPAGE 3–8% Tris-acetate polyacrylamide gel (Invitrogen) and transferred for 6 hours at 4°C on a polyvinylidene difluoride membrane (Invitrogen) with a BioRad cassette. Detection was performed with Novex ECL Kit (Invitrogen). Anti-rabbit (Invitrogen) and anti-mouse (BioRad) secondary horseradish peroxidase–conjugated antibodies were used.

Acknowledgments

This work was supported by Fondazione Ing. Aldo Gini, Fondazione CaRiPaRo, and Fondazione Citta della Speranza. We thank Motonobu Katoh (Department of Biomedical Science, Institute of Regenerative Medicine and Biofunction, Tottori University, Yonago, Japan) for helping with experimental work.

References

1 Muntoni, F, Torelli, S and Ferlini, A (2003). Dystrophin and mutations: one gene, several proteins, multiple phenotypes. Lancet Neurol 2: 731–740.

2 Blake, DJ, Weir, A, Newey, SE and Davies, KE (2002). Function and genetics of dystrophin and dystrophin-related proteins in muscle. Physiol Rev 82: 291–329.

3 Spurney, CF (2011). Cardiomyopathy of Duchenne muscular dystrophy: current understanding and future directions. Muscle Nerve 44: 8–19.

4 Fayssoil, A, Nardi, O, Orlikowski, D and Annane, D (2010). Cardiomyopathy in Duchenne muscular dystrophy: pathogenesis and therapeutics. Heart Fail Rev 15: 103–107.

5 Takahashi, K, Tanabe, K, Ohnuki, M, Narita, M, Ichisaka, T, Tomoda, K et al. (2007). Induction of pluripotent stem cells from adult human fibroblasts by defined factors. Cell 131: 861–872.

6 Robinton, DA and Daley, GQ (2012). The promise of induced pluripotent stem cells in research and therapy. Nature 481: 295–305.

7 Carvajal-Vergara, X, Sevilla, A, D'Souza, SL, Ang, YS, Schaniel, C, Lee, DF et al. (2010). Patient-specific induced pluripotent stem-cell-derived models of LEOPARD syndrome. Nature 465: 808–812.

8 Moretti, A, Bellin, M, Welling, A, Jung, CB, Lam, JT, Bott-Flügel, L et al. (2010). Patientspecific induced pluripotent stem-cell models for long-QT syndrome. N Engl J Med 363: 1397–1409.

9 Itzhaki, I, Maizels, L, Huber, I, Zwi-Dantsis, L, Caspi, O, Winterstern, A et al. (2011). Modelling the long QT syndrome with induced pluripotent stem cells. Nature 471: 225– 229.

10 Matsa, E, Rajamohan, D, Dick, E, Young, L, Mellor, I, Staniforth, A et al. (2011). Drug evaluation in cardiomyocytes derived from human induced pluripotent stem cells carrying a long QT syndrome type 2 mutation. Eur Heart J 32: 952–962.

11 Novak, A, Barad, L, Zeevi-Levin, N, Shick, R, Shtrichman, R, Lorber, A et al. (2012). Cardiomyocytes generated from CPVTD307H patients are arrhythmogenic in response to ß-adrenergic stimulation. J Cell Mol Med 16: 468–482.

12 Ma, D, Wei, H, Lu, J, Ho, S, Zhang, G, Sun, X et al. (2013). Generation of patient-specific induced pluripotent stem cell-derived cardiomyocytes as a cellular model of arrhythmogenic right ventricular cardiomyopathy. Eur Heart J 34: 1122–1133.

13 Sun, N, Yazawa, M, Liu, J, Han, L, Sanchez-Freire, V, Abilez, OJ et al. (2012). Patient-specific induced pluripotent stem cells as a model for familial dilated cardiomyopathy. Sci Transl Med 4: 130ra47.

14 Zeevi-Levin, N, Itskovitz-Eldor, J and Binah, O (2012). Cardiomyocytes derived from human pluripotent stem cells for drug screening. Pharmacol Ther 134: 180–188.

15 Shiba, Y, Fernandes, S, Zhu, WZ, Filice, D, Muskheli, V, Kim, J et al. (2012). Human ES-cellderived cardiomyocytes electrically couple and suppress arrhythmias in injured hearts. Nature 489: 322–325.

16 Lai, Y and Duan, D (2012). Progress in gene therapy of dystrophic heart disease. Gene Ther 19: 678–685.

17 Lu, QL, Yokota, T, Takeda, S, Garcia, L, Muntoni, F and Partridge, T (2011). The status of exon skipping as a therapeutic approach to duchenne muscular dystrophy. Mol Ther 19: 9–15.

18 Bostick, B, Yue, Y, Long, C and Duan, D (2008). Prevention of dystrophin-deficient cardiomyopathy in twenty-one-month-old carrier mice by mosaic dystrophin expression or complementary dystrophin/utrophin expression. Circ Res 102: 121– 130.

19 Janssen, PM, Hiranandani, N, Mays, TA and Rafael-Fortney, JA (2005). Utrophin deficiency worsens cardiac contractile dysfunction present in dystrophin-deficient mdx mice. Am J Physiol Heart Circ Physiol 289: H2373–H2378.

20 Shin, JH, Bostick, B, Yue, Y, Hajjar, R and Duan, D (2011). SERCA2a gene transfer improves electrocardiographic performance in aged mdx mice. J Transl Med 9: 132.

21 Kazuki, Y, Hoshiya, H, Takiguchi, M, Abe, S, Iida, Y, Osaki, M et al. (2011). Refined human artificial chromosome vectors for gene therapy and animal transgenesis. Gene Ther 18: 384–393.

22 Hoshiya, H, Kazuki, Y, Abe, S, Takiguchi, M, Kajitani, N, Watanabe, Y et al. (2009). A highly stable and nonintegrated human artificial chromosome (HAC) containing the 2.4 Mb entire human dystrophin gene. Mol Ther 17: 309–317.

23 Kazuki, Y, Hiratsuka, M, Takiguchi, M, Osaki, M, Kajitani, N, Hoshiya, H et al. (2010). Complete genetic correction of ips cells from Duchenne muscular dystrophy. Mol Ther 18: 386–393.

24 Tedesco, FS, Hoshiya, H, D'Antona, G, Gerli, MF, Messina, G, Antonini, S et al. (2011). Stem cell-mediated transfer of a human artificial chromosome ameliorates muscular dystrophy. Sci Transl Med 3: 96ra78.

25 Tedesco, FS, Gerli, MF, Perani, L, Benedetti, S, Ungaro, F, Cassano, M et al. (2012). Transplantation of genetically corrected human iPSC-derived progenitors in mice with limb-girdle muscular dystrophy. Sci Transl Med 4: 140ra89.

26 Kattman, SJ, Witty, AD, Gagliardi, M, Dubois, NC, Niapour, M, Hotta, A et al. (2011). Stage-specific optimization of activin/nodal and BMP signaling promotes cardiac differentiation of mouse and human pluripotent stem cell lines. Cell Stem Cell 8: 228–240.

27 D'Souza, VN, Nguyen, TM, Morris, GE, Karges, W, Pillers, DA and Ray, PN (1995). A novel dystrophin isoform is required for normal retinal electrophysiology. Hum Mol Genet 4: 837–842.

28 Tadayoni, R, Rendon, A, Soria-Jasso, LE and Cisneros, B (2012). Dystrophin Dp71: the smallest but multifunctional product of the Duchenne muscular dystrophy gene. Mol Neurobiol 45: 43–60.

29 Shiba, Y, Hauch, KD and Laflamme, MA (2009). Cardiac applications for human pluripotent stem cells. Curr Pharm Des 15: 2791–2806.

30 An, MC, Zhang, N, Scott, G, Montoro, D, Wittkop, T, Mooney, S et al. (2012). Genetic correction of Huntington's disease phenotypes in induced pluripotent stem cells. Cell Stem Cell 11: 253–263.

31 Oh, Y, Wei, H, Ma, D, Sun, X and Liew, R (2012). Clinical applications of patient-specific induced pluripotent stem cells in cardiovascular medicine. Heart 98: 443–449.

32 Mummery, C, Ward-van Oostwaard, D, Doevendans, P, Spijker, R, van den Brink, S, Hassink, R et al. (2003). Differentiation of human embryonic stem cells to cardiomyocytes: role of coculture with visceral endoderm-like cells. Circulation 107: 2733–2740.

33 Laflamme, MA, Chen, KY, Naumova, AV, Muskheli, V, Fugate, JA, Dupras, SK et al. (2007). Cardiomyocytes derived from human embryonic stem cells in pro-survival factors enhance function of infarcted rat hearts. Nat Biotechnol 25: 1015–1024.

34 Serena, E, Zatti, S, Reghelin, E, Pasut, A, Cimetta, E and Elvassore, N (2010). Soft substrates drive optimal differentiation of human healthy and dystrophic myotubes. Integr Biol (Camb) 2: 193–201.

35 Martone, J, De Angelis, FG and Bozzoni, I (2012). U1 snRNA as an effective vector for stable expression of antisense molecules and for the inhibition of the splicing reaction. Methods Mol Biol 867: 239–257.

36 Serena, E, Cimetta, E, Zatti, S, Zaglia, T, Zagallo, M, Keller, G et al. (2012). Micro-arrayed human embryonic stem cells-derived cardiomyocytes for in vitro functional assay. PLoS ONE 7: e48483.

37 Zatti, S, Zoso, A, Serena, E, Luni, C, Cimetta, E and Elvassore, N (2012). Micropatterning topology on soft substrates affects myoblast proliferation and differentiation. Langmuir 28: 2718–2726.

38 Martewicz, S, Michielin, F, Serena, E, Zambon, A, Mongillo, M and Elvassore, N (2012). Reversible alteration of calcium dynamics in cardiomyocytes during acute hypoxia transient in a microfluidic platform. Integr Biol (Camb) 4: 153–164.